



ScuDo

Scuola di Dottorato ~ Doctoral School
WHAT YOU ARE, TAKES YOU FAR



Doctoral Dissertation
Doctoral Program in Mechanical Engineering (33rd Cycle)

Structural Health Monitoring based on Piezoelectric transducers: a Carbon Fiber Automotive Component Application case

by

Ing. Lorenzo Sisca

* * * * *

Supervisor

Prof. Massimiliana Carello

Doctoral Examination Committee:

Prof. Monica Tiboni, Referee, Università di Brescia

Prof. Roger Serra, Referee, INSA

Prof. Massimo Violante, Co-examiner, Politecnico di Torino

Prof. Stefano Mauro, Co-examiner, Politecnico di Torino

Prof. Pierluigi Rea, Co-examiner, Università degli Studi di Cassino e del Lazio
Meridionale

Politecnico di Torino

May 5, 2021

Declaration

I hereby declare that the contents and organization of this dissertation constitute my own original work and does not compromise in any way the rights of third parties, including those relating to the security of personal data.

Ing. Lorenzo Sisca
Torino, May 5, 2021

Summary

In the recent years, the materials composing the structure of Aircraft, such as steel and aluminum, are being progressively replaced with lower density materials, as the Reinforced Plastics. The same trend is found in the Automotive field to achieve the reduction of fuel consumption and CO₂ emission. It is known that polymer composites have outstanding properties of specific modulus and strength respect to their low density but suffer more than metals from damage generation and propagation. Furthermore, defects can be included in the material during manufacturing and work as crack initiators for catastrophic delamination.

The maintenance on composite structure is therefore based on finding the defects or damages, thanks to several Non-Destructive Techniques (NDT). To optimize the maintenance on aircrafts, a variety of on-board systems has been applied for on-line Structural Health Monitoring (SHM). SHM systems based on piezoelectric transducers earned a particularly high interest for continuous monitoring on metallic and composite structures. The application of this system in the automotive sector could enhance passenger safety, through the monitoring of the vehicle structure health status.

The principle behind the system is the propagation of ultrasonic Lamb waves inside the material between a couple of piezoelectric patches that act as actuator and sensor. A difference in the vibrational behavior in time is an indicative of damage or a defect in the structure. The validation of the SHM system - composed of sensors, electronic devices and algorithms - is commonly conducted using sections of the structure or specimens with same materials and simple geometry.

In this Thesis, six mathematical models for evaluating the electrical response of piezoelectric sensors were implemented, with the aim of selecting the most effective model for damage identification. Two specific programs have been created for Off-line and On-line monitoring of the composite structures.

The preliminary tests for the system validation were carried out on three types of simple specimens of different geometries made of different materials (steel, aluminum and carbon fiber). The “beam” and “plate” specimens allowed the study the phenomenon of free propagation of the guided Lamb waves in the frequency

range 1-100 kHz both in unidirectional and on the plane, evaluating their interference with superficial and volume damages. The “simulacrum” specimen was subjected to vibrational test at different loading steps, using 4-point bending test equipment.

The specimens’ configurations were necessary for the evaluation of the overall behavior of ultrasonic waves on the structures. The developed methodology was created to identify any damage generated in the bending loading on an innovative Automotive component, a carbon fiber leaf spring suspension. The types of damage and the geometries studied in the Thesis are depicted in Figure 0.1.



Figure 0.1 – Damage types and geometries studied in the Thesis

A correlation study has been carried on the virtual simulation of the vibrations generated by the piezoelectric transducers for the evaluated geometries, in order to support the positioning of sensors on the component to be monitored.

The proposed numerical-experimental methodology is an essential foundation for the monitoring systems based on piezoelectric transducers in the Automotive sector.

Acknowledgment

This Thesis has been my greatest technical project, it brought me to abandon the comfort zone of the chemistry and materials science to investigate a particular mechatronic problem.

Firstly, I want to thank *Prof. Massimiliana Carello* that has always believed in me although my huge defects. The supervision of *Andrea Airale* and *Alessandro Ferraris* has not only made me grow by the technical point of view but was an example for me to understand that I can change the world only with determination and hard work.

The people I met in *Politecnico di Torino*, *Team H2politO*, *IEHV Research group*, *BeonD* have become my family and I thank them for the moments spent with me. It is not possible to list all of them, I would certainly forget someone. An incomplete and disordered list is: *Alessandro M.*, *Enrico*, *Christian*, *Nithin*, *Shuang*, *Pietro*, *Patrizio*, *Maria*, *William*, *Gruppo Testing*, *Gruppo CAE*, *Gruppo Progettazione*, *Gruppo Elettronica/Batterie*, *Area IT*, *Eva*, *Mauro*, *Matteo*, *Raffaele*, *Raffaella*, *Daniele*, *Tecnici e Personale Amministrativo del DIMEAS*, *Professors that I have known in Politecnico di Torino and in my travels for Conferences*.

In particular, I sincerely thank *Simone Re.*, *Thibault*, *Arthur*, *Victor*, *Giulia*, *Simone Ra.* and *Ing. Gianluca Poli* for their support in the realization of this Research work.

The vicinity of my *friends and housemates* has been very important for the survival at Torino and the relaxing days at Cuneo.

Nothing could have been possible without *my grandparents*, *my parents*, *my brother and sister*, *my aunts and uncles*, *my cousins*, and *Paola e Chiara*, *Beppe e Grazia*, that always were presence and glad to celebrate my successes.

Last but not least, I thank *Federica - my love* - the girl that I got close to me facing up to the bad moments and sharing the most important of my life.

Finally, I want to remember my grandparents *Nonno Berto e Nonna Giovanna*, who taught me every day how to be happy with a few stuff and arrange with anything. I think that the transmission of knowledge between old and new generations is one of the best things that humans can make and for this reason the PhD research course has realized me so much.

Alla mia famiglia

Contents

Summary	ii
Acknowledgment	iv
Contents	vii
List of Tables	x
List of Figures	xi
Nomenclature	xix
1. State of the Art	1
1.1. Smart Materials and SHM for Automotive	2
1.2. Guided waves	6
1.3. SHM System Components	10
1.3.1. Piezoelectric Transducers	11
1.3.2. Network Disposition	12
1.3.3. Laboratory Equipment	14
1.3.4. Specimens Characteristics	15
1.3.5. Environmental Operating Conditions	18
1.3.6. Data Processing	21
2. Case study definition	25
2.1. Aim of the thesis	26
2.2. Experimental Methodology	27
2.2.1. Beam specimen	28
2.2.2. Plate specimen	28
2.2.3. Simulacrum specimen	29
2.2.4. Leaf Spring Component	30
2.2.5. Damage Definition	31
3. System Setup	33
3.1. Hardware	34
3.1.1. Piezoelectric transducers	34
3.1.2. Electrical connections	35
3.1.3. Data logger	36
3.2. Software	37
3.2.1. LabVIEW Program	37

3.2.2.	MatLab Program.....	38
3.3.	Mechanical Test Bench	39
3.3.1.	Dynamometer	39
3.3.2.	Fixture for Leaf Spring Bending.....	41
3.3.3.	Strain Gauge Amplifier	42
4.	Data Analysis.....	43
4.1.	Data Acquisition.....	43
4.1.1.	Single Frequency	43
4.1.2.	Multiple Frequency.....	45
4.2.	Data Processing	46
4.2.1.	Damage Index Algorithms.....	47
4.2.2.	Off-line Monitoring	50
4.2.3.	On-line Monitoring.....	51
5.	Experimental Results	54
5.1.	Preliminary Tests.....	54
5.1.1.	Bending Tests on Simulacrum.....	54
5.1.2.	Bending Tests on Leaf Spring	55
5.2.	SHM Off-line Tests	56
5.2.1.	Beam specimen.....	57
5.2.2.	Plate specimen	59
5.2.3.	Simulacrum specimen.....	61
5.2.4.	Leaf Spring component	64
5.3.	SHM On-line Tests.....	66
5.3.1.	Leaf Spring in Static condition	67
5.3.2.	Leaf Spring in Dynamic condition	69
6.	Virtual Simulations.....	76
6.1.	Virtual Methodology	77
6.1.1.	FEA Models.....	77
6.1.2.	Electro-Mechanical Coupling	81
6.2.	SHM Virtual Results	84
6.2.1.	Beam Specimen	85
6.2.2.	Plate Specimen	87
6.2.3.	Simulacrum Specimen.....	89
6.2.4.	Leaf Spring Component.....	91
7.	Conclusions	95
	References.....	99
	Appendix A.....	104
	SHM Off-line Data & Results	104
	Beam specimen	104

Plate specimen.....	107
Simulacrum specimen	111
Leaf Spring component.....	115
Appendix B.....	126
SHM Virtual Results & Correlation	126
Beam Specimen.....	126
Plate Specimen.....	128
Simulacrum Specimen	131
Leaf Spring Component	133
Own Publications	135
Curriculum Vitae	138

List of Tables

Table 1.1 – Comparison of strengths, limitations and SHM potential for different sensing systems [7]	6
Table 1.2 – List of the most used Damage Index formulations converted in MatLab language [37].....	23
Table 2.1 – Stacking Sequence of the Leaf Spring	27
Table 2.2 – Case studies for this research work.....	27
Table 3.1 – Technical specifications of NI USB-6259 device.....	37
Table 4.1 – Damage Index Formulations used in this thesis [37].....	48
Table 4.2 – Off-line and On-line programs.....	49
Table 6.1 – List of specimens, materials, geometries, number of piezo simulated with FEA models	77
Table 6.2 – Methods used to model beam, piezo patches, glue and export keywords.....	78

List of Figures

Figure 0.1 – Damage types and geometries studied in the Thesis	iii
Figure 1.1 – Evolution of the materials with functionalities and complexity [1]	2
Figure 1.2 – Scheme of the mechanoreceptors in the human skin [2]	3
Figure 1.3 – Reasons for aircraft industry’s interest in SHM [3].....	3
Figure 1.4 – Maintenance strategies from the oldest to the innovative perspectives [5].....	4
Figure 1.5 – Evolution of the on-board system “OnStar” [6]	4
Figure 1.6 – Geographical distribution of deposited patents, keyword "Structural Health monitoring"	5
Figure 1.7 – Scheme of the particle motion for a) longitudinal and b) transversal modes, the transversal waves can behave as c) symmetric modes (S) or d) anti-symmetric modes [10]	7
Figure 1.8 – Configurations of piezoelectric patches in a) “pulse-echo” and b) “pitch-catch” [11]	7
Figure 1.9 – a) Signal Shape and b) central frequency of burst for SHM [12], c) normalized input and output signals with S0 and A0 group waves [13]	8
Figure 1.10 – Experimental measures of the Amplitude of A0 and S0 Lamb modes for a) 1,6 mm Aluminum plate and b) 2 mm CFRP plate [13]	8
Figure 1.11 – a) Principle of the Scanning Laser Vibrometer, b) measures of piezo actuator disc at different frequencies [14].....	9
Figure 1.12 – Scanning Laser Vibrometer measures of measures of quasi-isotropic (left) and orthotropic (right) CFRP laminates [14].....	9
Figure 1.13 – LS-DYNA models of a) piezo actuator, b) piezo sensor, c) stiffened CFRP structure [17].....	10
Figure 1.14 – ABAQUS model of a plate with a defect: a) A0 and b) S0 modes responses [18]	10
Figure 1.15 – a) ABAQUS model for the piezoelectric simulation and b) fitting of the experimental and virtual signals [19]	10
Figure 1.16 – Acellent solutions for SHM on rotorcrafts [20].....	11

Figure 1.17 – Schemes of principle for a) direct and b) inverse piezoelectric effects [21]	11
Figure 1.18 – Piezoelectric discs for SHM application: a) soldering technique and available formats [22], b) electrical connection with cables and printed circuit [25], c) network of DuraAct™ [24].....	12
Figure 1.19 – SMART Layer™ a) embedded in composite panel [26], b) glued on surface [24]	12
Figure 1.20 – Disposition of piezo network: a) square [17], b) circular [17], c) hexagonal [31]	13
Figure 1.21 - Disposition of piezo network in case of a) notch [18] and b) fatigue crack [34].....	13
Figure 1.22 – Disposition of piezo network in case of stiffener: a) glued [36], b) co-laminated [37], c) welded [35]	13
Figure 1.23 – Disposition of piezo network on a) relevant panel of aircraft wing, b) detail [17].....	14
Figure 1.24 – System components for laboratory tests: a) scheme [41] and b) real setup [13]	15
Figure 1.25 – Customized piezo amplifier for special SHM applications [23]	15
Figure 1.26 – Adhesive used for piezo: a) scheme of shear stress [11], b) efficiency of joining [45]	16
Figure 1.27 – SHM response in case of piezo debonding: a) test setup and b) results [32]	16
Figure 1.28 – Types of simulated damage: a) impact damage, b) glued-on mass, c) hole cavity [13].....	17
Figure 1.29 – Damage artificially introduced on a rivet hole [40].....	17
Figure 1.30 – Damage on composite panels: a) quasi-static crush [13], b) cumulative impacts [30].....	17
Figure 1.31 – Impact on CFRP panels: a) drop-dart tower, b) S-scan and c) C-scan ultrasonic tests [17].....	18
Figure 1.32 – Peak amplitude reduction during conditioning for a) A0 and b) S0 Lamb modes [41].....	18
Figure 1.33 – Thermal fatigue: a) cycle description and b) effect on the wave velocity [47].....	19
Figure 1.34 – Effect of low-frequency disturbs on SHM response: a) shaker setup, b) signal result [48].....	19
Figure 1.35 – Effect of uniaxial loads on the piezoelectric response signal for an aluminum plate [46]	19

Figure 1.36 – Effect of different temperatures: a) group velocity, b) response signal amplitude [12]	20
Figure 1.37 – a) Synchronous signals, b) correct scatter, c) asynchronous signals, d) false scatter [49]	20
Figure 1.38 – Typical signals of piezoelectric sensors [24].....	20
Figure 1.39 – a) Decision methodology for data processing [37], b) schematic definition of decision threshold value [50]	21
Figure 1.40 – a) Original signal, b) normalized envelope of the signal, c) positive envelope, d) time-frequency plot [52].....	22
Figure 1.41 – Spectrogram visualization: a) actuator signal, b) sensor signal in damaged condition, c) scatter of damaged respect to undamaged condition [51].	22
Figure 1.42 – Time of Flight calculation from actuator (red) and sensor signal (blue) [53]	22
Figure 1.43 – Localization algorithms based on a) cross-correlation (RAPID) [40] and b) ToF [53]	24
Figure 1.44 – Scheme of principle for the Time Reversal Method [44]	24
Figure 2.1 – Scheme of the main goals of the thesis.....	25
Figure 2.2 – Functions integration on the Innovative Leaf Spring Automotive Suspension [58].....	26
Figure 2.3 – Component dimensions and points of interface with vehicle [58]	26
Figure 2.4 – a) Scheme of beam specimen, b) Beam specimens made of three materials.....	28
Figure 2.5 – Test configurations for the Beam specimen: a) Appended, b) Clamped.....	28
Figure 2.6 – Test configuration for the Plate specimen	29
Figure 2.7 – a) Scheme of plate specimen, b) Real plate specimens made of three materials.....	29
Figure 2.8 – Test configuration for the Simulacrum specimen: bending load	29
Figure 2.9 – a) Scheme of simulacrum specimen, b) Real simulacrum specimens made of three materials	30
Figure 2.10 – Test configuration for the Leaf Spring component: Bending load	30
Figure 2.11 – a) Scheme of half part of Leaf Spring with sensors, b) real Leaf Spring.....	31
Figure 2.12 – Scheme of piezoelectric patches (PZT) and Strain gauges (SG) on the Leaf Spring: a) top and b) bottom face	31

Figure 2.13 – Piezoelectric patches and Strain gauges on the Leaf Spring: a) top and b) bottom face	31
Figure 2.14 – Detail of Piezoelectric patches and Strain gauges on the Leaf Spring a) top and b) bottom face	31
Figure 2.15 –Scheme of a) Damage 1 and b) Damage 2, Images of Beam specimens with c) Damage 1 and d) Damage 2.....	32
Figure 2.16 – Detail of the manual clamp applied in the case of Leaf Spring component.....	32
Figure 3.1 – Scheme of the measurement chain.....	33
Figure 3.2 – Scheme of the DuraAct™ Piezoelectric transducer [28].....	34
Figure 3.3 – Available geometries of Kapton covered piezoelectric: a) rectangular and circular shapes, b) multi-element films [28]	35
Figure 3.4 – DuraAct™ P-876K025: a) dimensions [28], b) application on specimens.....	35
Figure 3.5 – a) Soldering of piezo patches, b) detail of the short cables, c) detail of the shielded cable	36
Figure 3.6 – a) National Instruments Multifunction DAQ NI USB-6259 with PC control by MatLab, b) scheme of channels on the spring terminals	36
Figure 3.7 – a) Front Panel and b) Block Diagram developed for the SHM system on LabVIEW.....	38
Figure 3.8 – a) MatLab code and b) interactive Menu developed for the SHM system	39
Figure 3.9 – MatLab customized graph representing the actuation and response signals	39
Figure 3.10 – Universal Testing machine Shimadzu AG-X Plus 300 kN.....	40
Figure 3.11 –Non-contact Biaxial Video-extensometer used in Tensile test on a) metallic and b) composite specimens	41
Figure 3.12 – a) Equipment of Four-point Bending test, b) detail of support with 5 mm radius head.....	41
Figure 3.13 – Special fixture for Bending test of Leaf Spring mounted on Shimadzu dynamometer	41
Figure 3.14 – a) Detail of the IPE beams with the linear guide, b) alignment process using a laser pointer	42
Figure 3.15 – a) HBK 350 Ω strain gauge, b) HBK QuantumX MX1615B data acquisition module, c) connector for a single strain gauge measurement	42
Figure 4.1 – Nomenclature for piezo patches: Piezo 1 is the actuator, Piezo 2 is the sensor	43

Figure 4.2 – a) Actuation signal shape (blue) and real output (red), b) methodology for data acquisition	44
Figure 4.3 – Series of 10 overlapped piezo responses at 50 kHz: a) detrended, b) low-pass filtered	45
Figure 4.4 – Spectrogram of Actuation signal from piezo 1	45
Figure 4.5 – Spectrograms of a) Baseline and b) Test signals from Piezo 2 ..	46
Figure 4.6 – Max and min Voltage peaks for an example of Baseline, Test1 and Test2 configurations	47
Figure 4.7 – Spectrograms of Standard Deviation between a) Test1 and Baseline, b) Test2 and Baseline	47
Figure 4.8 – Example of data series (blue line), upper (red line) and lower envelope (yellow line), global maximum of the data series (blue dot), global maximum of the difference envelope (red dot)	48
Figure 4.9 – a) Choice of frequency from Off-line program results, b) time reference of the structural change from On-line program results	49
Figure 4.10 – Data saving format of .txt file for Off-line program	50
Figure 4.11 – User visualization of each Damage Index of Test 1 and Test 2 configurations respect to the Baseline for the Off-line program	50
Figure 4.12 – Percentage change of the Damage Index of the Test 2 respect to the Test 1	51
Figure 4.13 – Data saving format of .txt file for On-line program: a) signals, b) Damage Index	51
Figure 4.14 – User visualization of the On-line program a) Baseline and b) Test signals for each piezo couple	52
Figure 4.15 – User visualization of the On-line program Realtime signals for each piezo couple	53
Figure 4.16 – User visualization of the On-line program Damage Index for each piezo couple	53
Figure 5.1 – a) Sensors' network on Simulacrum specimen, b) Four-point Bending configuration	54
Figure 5.2 – Experimental results of the Bending tests on Simulacrum specimens: a) Force vs. Displacement, b) Force vs. Strain	55
Figure 5.3 – Leaf Spring with the top and bottom faces of the half part with sensors	55
Figure 5.4 – Experimental results of the Bending tests on Leaf Spring component: a) Force vs. Displacement, b) Force vs. Strain	56
Figure 5.5 – Progression of Bending test on Leaf Spring at 1, 2, 3 and 4 kN.	56

Figure 5.6 – Piezo couple PZT 1-2 studied for the influence of Damage on the Beam specimen	57
Figure 5.7 – SHM Off-line Test results for the Beam specimens made of a) Aluminum, b) Steel, c) Carbon Fiber	58
Figure 5.8 – Piezo couples PZT 1-2 and PZT 1-3 studied for the influence of Damage on the Plate specimen	59
Figure 5.9 – SHM Off-line Test results for the Plate specimens made of a) Aluminum, b) Steel, c) Carbon Fiber	60
Figure 5.10 – Piezo couple PZT 1-2 studied for the influence of Damage and Bending load on the Simulacrum specimen	61
Figure 5.11 – SHM Off-line Test results for the Simulacrum specimens made of a) Aluminum, b) Steel, c) Carbon Fiber for the PZT 1-2 piezo couple.....	62
Figure 5.12 – SHM Off-line Test results for the Simulacrum specimens made of a) Aluminum, b) Steel, c) Carbon Fiber for the PZT 1-3 piezo couple.....	63
Figure 5.13 – Half part of Leaf Spring component with Piezoelectric patches and Strain gauges	64
Figure 5.14 – SHM Off-line Test results for each piezo couple on the Leaf Spring.....	65
Figure 5.15 – SHM Off-line Test results for a) PZT 1-2 and b) PZT 1-4 on the Leaf Spring	66
Figure 5.16 – Piezo couples PZT 1-2 and PZT 1-5 studied for the influence of Clamp and Bending load on the Leaf Spring component.....	67
Figure 5.17 – SHM On-line Test results for the Leaf Spring in static condition with clamp.....	69
Figure 5.18 – a) Experimental system for the SHM of the Leaf Spring component in Bending configuration, b) detail of the upper bending support.....	70
Figure 5.19 – Test cycle in terms of Force vs. Time.....	71
Figure 5.20 – Strain gauges measures during the bending cyclic test on Leaf Spring.....	71
Figure 5.21 – SHM On-line Test results for the Leaf Spring in dynamic condition without clamp	72
Figure 5.22 – SHM On-line Test results for the Leaf Spring in dynamic condition without clamp	73
Figure 5.23 – SHM On-line Test results for the Leaf Spring in dynamic condition without (left column) and with clamp (right column) – part 1	74
Figure 5.24 – SHM On-line Test results for the Leaf Spring in dynamic condition without (left column) and with clamp (right column) – part 2.....	75

Figure 6.1 – CAD models of a) Beam, b) Plate, c) Simulacrum, d) Leaf Spring	77
Figure 6.2 – Methods a) 1, b) 2, c) 3, d) 4 used to model beam, glue, piezo actuator.....	78
Figure 6.3 – Methods a) 1, b) 2, c) 3, d) 4 used to model beam, glue, piezo sensor	78
Figure 6.4 – a) Mesh of beam specimen with shell 2D and piezo with solid 3D, b) selection of piezo nodes on bottom (green) and top surfaces (red).....	79
Figure 6.5 – a) Selection of the set of nodes on bottom surface of piezo actuator, b) Displacement signal at 50 kHz imposed using the keyword *BOUNDARY_PRESCRIBED_MOTION_SET	79
Figure 6.6 – a) Selection of the center nodes on bottom surface for piezo actuator and sensor, b) Example of Displacement for piezo actuator (red) and piezo sensor (green) exported using the keyword *DATABASE_NODOUT	80
Figure 6.7 – a) Selection of the bottom surface for piezo actuator and sensor, b) Example of Interface Force for piezo actuator and c) piezo sensor exported using the keyword *DATABASE_RCFORC	80
Figure 6.8 – a) Conventions for piezoelectric disks, b) types of oscillation and c) electro-mechanical coupling of inverse and direct piezoelectric effects [28] ...	82
Figure 6.9 – a) Method developed to calculate Voltage from Displacement, b) correlation with real data	83
Figure 6.10 – Scale Factors (SF) for a) Beam, b) Plate and c) Simulacrum specimens at 25, 50, 75 kHz	84
Figure 6.11 – Scheme of the special test, b) detail picture of the piezo joining	84
Figure 6.12 – Sensor responses from the special test at frequencies of a) 25 kHz, b) 50 kHz, c) 75 kHz.....	84
Figure 6.13 – Evolution of the wave propagation on the Beam specimen at 25 kHz, in terms of z-Displacement at different simulation time.....	86
Figure 6.14 – Results at 25, 50 and 75 kHz for Beam specimen made of CFRP: a) virtual Displacement of piezo actuator 1 and sensor 2, b) correlation between virtual and real Voltage signals of piezo sensor 2	87
Figure 6.15 – Evolution of the wave propagation on the Plate specimen at 25 kHz, in terms of z-Displacement at different simulation time.....	88
Figure 6.16 – Results at 25, 50 and 75 kHz for Plate specimen made of CFRP: a) virtual Displacement of piezo actuator 1 and sensors 2, 3, 4, correlation between virtual and real Voltage signals of b) piezo sensor 2 and c) piezo sensor 3	89

Figure 6.17 – Evolution of the wave propagation on the Simulacrum specimen at 25 kHz, in terms of z-Displacement at different simulation time.....	90
Figure 6.18 – Results at 25, 50, 75 kHz for Simulacrum specimen made of CFRP: a) virtual Displacement of piezo actuator 1 and sensor 2, b) correlation between virtual and real Voltage signals of piezo 2	91
Figure 6.19 – Evolution of the wave propagation on the Leaf Spring at 25 kHz, in terms of 1 st Principal Stress at different simulation time.....	92
Figure 6.20 – Results at 25 kHz for Leaf Spring: a) virtual Displacement of piezo actuator 1 and sensors 2, 3, 4, 5, correlation between virtual and real Voltage signals of b) piezo sensor 2, c) piezo sensor 3, d) piezo sensor 4, e) piezo sensor 5	93

Nomenclature

Acronyms/Abbreviation

<i>SHM</i>	Structural Health Monitoring
<i>CFRP</i>	Carbon Fiber Reinforced Plastic
<i>PIEZO</i>	Piezoelectric Transducer
<i>PZT</i>	Piezoelectric Transducer
<i>ToF</i>	Time of Flight
<i>ToA</i>	Time of Arrival
<i>DI</i>	Damage Index
<i>CCA</i>	Damage Index based on Maximum of the correlation
<i>CC0</i>	Damage Index based on Zero-lag correlation
<i>CRC</i>	Damage Index based on Correlation coefficient
<i>NRE</i>	Damage Index based on Normalized residual energy
<i>MA</i>	Damage Index based on Maximum amplitude of the difference
<i>ENV</i>	Damage Index based on Maximum envelope of the difference
<i>FEM</i>	Finite Element Method
<i>FEA</i>	Finite Element Analysis
<i>IEHV</i>	Innovative Electric and Hybrid Vehicles
<i>EOCs</i>	Environmental Operating Conditions
<i>RAPID</i>	Reconstruction Algorithm for Probabilistic Inspection of Defects
<i>BASELINE</i>	Experimental condition of specimen for initial data acquisition
<i>TEST</i>	Experimental condition of specimen for current data acquisition
<i>BEND</i>	Experimental condition of specimen in bending loading

Chapter 1

State of the Art

The aim of this Chapter is to introduce the topic of the Structural Health Monitoring (SHM), explaining the reasons of the application in the aircraft industry and trying to find the potential for implementing in the future automobiles. The theme of Smart materials and Smart structures is crucial for the development of sensor networks able to give the users information about the health of components avoiding the traditional inspection techniques.

The principle of SHM based on piezoelectric transducers (PZT) is the propagation of ultrasonic waves inside the material between a couple of piezo that act as actuator and sensor. The generation of a damage or a defect on the structure in time is therefore related to a difference in the vibration behavior, resulting in the damage detection and localization if the sensor network is used for triangulation. Simulation tools can support the understanding of the waves' propagation and correlation with the real data.

Piezoelectric elements are customized in geometry and power with respect to the final application conditions, structure dimension and material. An electronic system is needed to generate the excitation waves - at the selected frequencies with a proper reliability - and collect the response signal. The data processing is fundamental to observe changes in the vibrational behavior and correctly detect the presence of damage.

The validation of the SHM system composed by sensors, electronic devices and algorithms is commonly made using sections of the structure or specimens with same materials and simple geometry. The capacity to detect small damages is tested introducing artificial imperfections, such as drilled holes, glued masses, induced delamination. The external variables, as temperature, humidity, static and dynamic loads, are considered conducting specific experimental tests in order to verify the sensitivity of the system in Environmental Operating Conditions.

1.1. Smart Materials and SHM for Automotive

In the last decades, the materials used in the engineered structures have followed the evolution trend represented in Figure 1.1, increasing the functionalities but also the complexity of the systems [1]. The possibility of designing a material defining a priori its final properties allowed the construction of composite materials, that combine the best properties of different materials, for example Carbon Fiber Reinforced Plastics (CFRP).

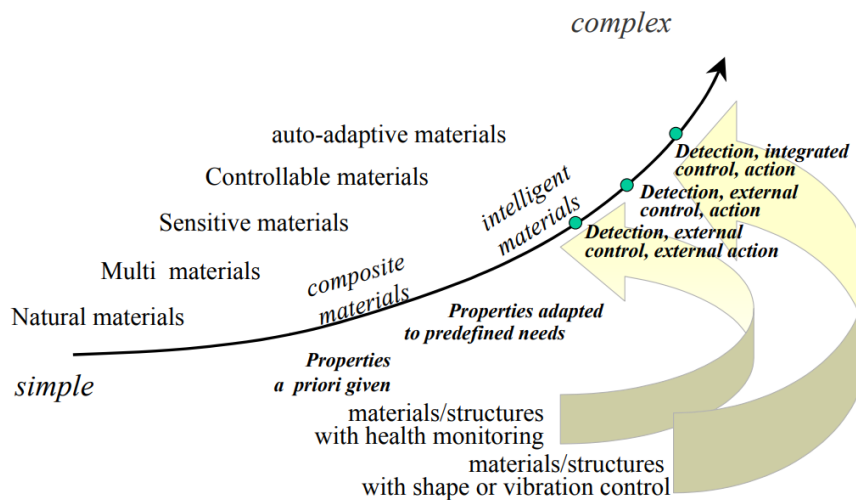


Figure 1.1 – Evolution of the materials with functionalities and complexity [1]

Nowadays in all application fields, the evolution about the materials regards the integration of several sensors to continuously assess the conditions of the structure. The so-called Smart Structures can send the users information, that opportunely manipulated give an objective response of the health status of the system.

An interesting analogy is the human body, which has in the inside a large number of sensors. For example, the “mechanoreceptors” present in the human skin, visible in Figure 1.2, are able to detect pressure, strain, vibrations [2]. Without those, the human body would not be able to identify the phenomena from the surrounding and the skin would be only an inert material. Each of the human receptors work at a specific frequency, similarly to the sensors on a smart structure, that are able to collect different samples.

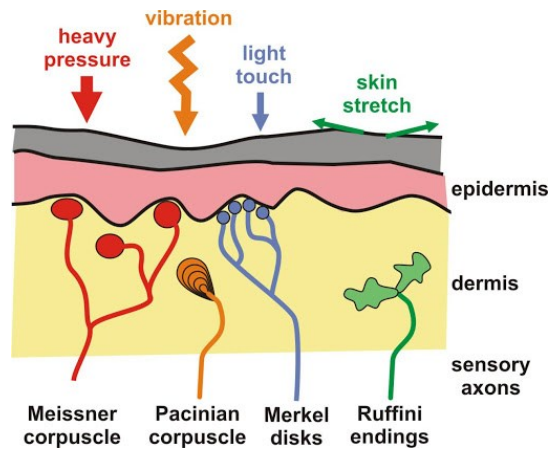


Figure 1.2 – Scheme of the mechanoreceptors in the human skin [2]

The need of knowledge about the health condition of a structure is reasonable, proportionally to the safety and reliability requirements to be assessed. Some examples of the first applications of smart structures are civil engineering and commercial aircrafts [3].

The technical names to describe the verification of the smart structures are “Structural Health Monitoring (SHM)”, “Condition Monitoring” or “Fault Detection”. It is possible to explain the reasons of the increasing interest about this technology observing Figure 1.3 and concern the reduction of operating activity for programmed maintenance and use of Non-Destructive Techniques (NDT) for flaws detection and monitoring [3]. The values in the histogram represent the answers of aircraft industry when inquired about their interest in SHM systems on board.

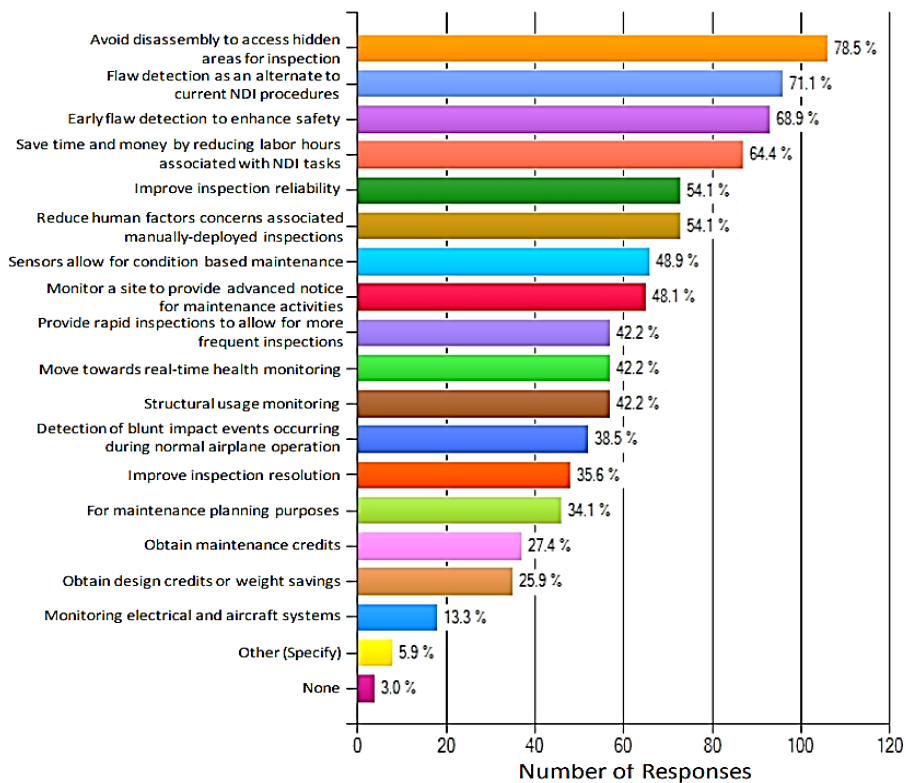


Figure 1.3 – Reasons for aircraft industry’s interest in SHM [3]

The first reports about the technological advancements on SHM in aircrafts has been presented at the Conferences IWSHM (International Workshop on SHM) and

EWSHM (European Workshop on SHM) founded in 1997 and 2002 respectively. Successively, in 2004 the Structural Health Monitoring International Journal was the first specialized journal on this topic. Fu-Kuo Chang, Professor at the Stanford University and Founder of IWSHM, declared in 2011 that SHM technology enables the transition from traditional Schedule-Driven Maintenance to Condition-Based Maintenance [4].

The Maintenance strategies for the structure functionality are depicted in Figure 1.4. The Reactive type - with replacement when a part is damaged - and Preventive - programming the substitution - are not capable to estimate the real duration of the component. The sensors application on smart structures permits the Predictive and Prescriptive Maintenance, using algorithms based on sensor response and Artificial Intelligence [5].

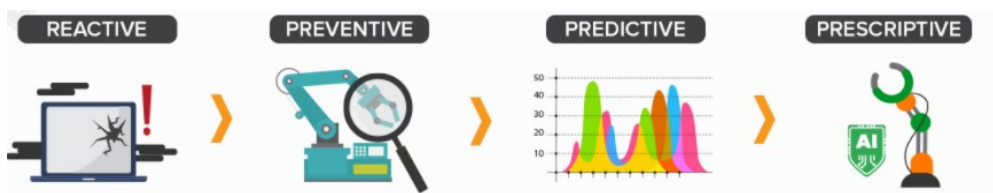


Figure 1.4 – Maintenance strategies from the oldest to the innovative perspectives [5]

In the Automotive industry, carmakers are interested in applying an advanced maintenance strategy to offer diagnostics and predictive prognostics to the car owners with warnings and health reports. In fact, the first communication system was “OnStar”, developed in 1996 by General Motors with Motorola Automotive and applied on Cadillac (DeVille, Seville and Eldorado). The system has acquired in time functionalities for electronic system checkup, as reported in Figure 1.5 [6].



Figure 1.5 – Evolution of the on-board system “OnStar” [6]

Although the SHM presents itself as mature and widespread in many sectors, the structural applications related to the automotive field are not. The presence of SHM is still timid and limited to niche and very specific cases, not reaching the market in relevant levels. This is clearly mirrored to the availability of patents and IP protection related to this field. The general analysis of the IP scenario related to the keyword “Structural Health Monitoring” is presented in Figure 1.6. The

geographical distribution of the applications, as usual, has a big concentration in terms of number of patents in China, followed by the US and other developed countries such as Korea, UK, Japan and Germany.

Another relevant analysis can be performed in terms of relevance of the keyword in the last couple of decades. The number of new patents filled a year from 2001 to 2019 has a growing trend, correlated with the relevance of the field.

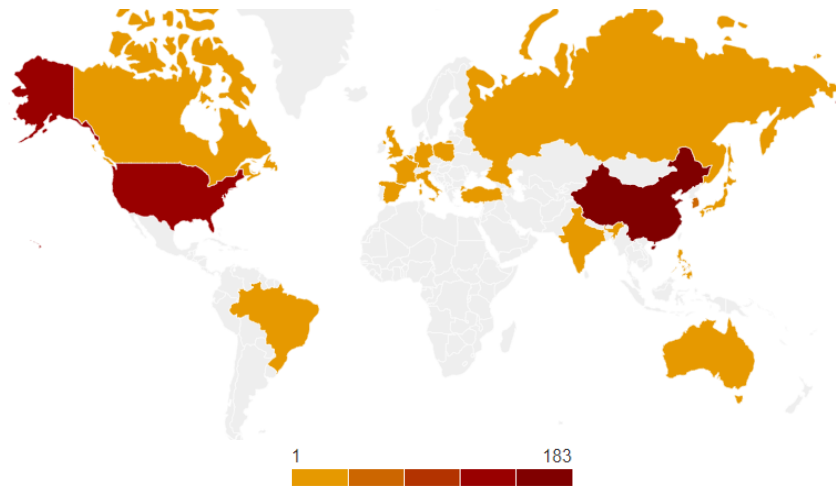


Figure 1.6 – Geographical distribution of deposited patents, keyword "Structural Health monitoring"

Within the most relevant patent applicants of the last 20 years are present some Chinese Universities, the American companies Boeing Co. and Acellent Technologies Inc. and the Brazilian Embraer S.A., this indicates a good balance between industry and academia product development.

The materials applied on the aircrafts are mainly the traditional metals, steel, aluminum, but in recent years they are progressively replaced with lower density materials, as the Reinforced Plastics. The same trend has highlighted in the Automotive field to assess the reduction of fuel consumption and CO₂ emission. It is known that the polymer composites have outstanding properties of specific modulus and strength respect to the low density but suffer more than metals from damage generation and propagation. Furthermore, during the manufacturing some defects can be included in the material and work as crack initiator for catastrophic delamination. The maintenance on composite structure is therefore based on finding the defects or damages, thanks to several techniques with different fields of application.

Table 1.1 presents the most important methods for detecting the Structural Health, with a particular attention to the SHM potential application [7].

Method	Strengths	Limitations	SHM Potential
Visual	Inexpensive equipment Inexpensive to implement No data analysis Portable Simple procedure	Only surface damage Only large damage Human interpretation Can be time consuming	Currently none
X-radiography	Penetrates surface Small defects with penetrant No data analysis Permanent record of results Simple procedure	Expensive equipment Expensive to implement Human interpretation Can be time consuming Require access to both sides Safety hazard	Currently none
Strain Gauge	Portable Embeddable Surface mountable Simple procedure Low data rates	Expensive equipment Expensive to implement Data analysis required Localized results	Lightweight Conformable Can be deposited Very low power draw Results for small area
Optical fibers	Inexpensive equipment Embeddable Quick scan of large area	Expensive to implement Data analysis required High data rates Accuracy in question	Lightweight Large area coverage Must be embedded Requires laser
Ultrasonic	Inexpensive to implement Portable Sensitive to small damage Quick scan of large area	Very expensive equipment Complex results Specialized software High data rates Couplant required Require access to both sides	Currently none
Eddy current	Inexpensive to implement Portable Surface mountable Sensitive to small damage	Expensive equipment Very complex results Specialized software Safety hazard Conductive material only	Lightweight Conformable Can be deposited Very high power draw Results for small area
Acoustic emission	Inexpensive equipment Inexpensive to implement Surface mountable Portable Quick scan of large area Sensitive to small events	Very complex results Very high data rates Specialized software	Lightweight Conformable Can be deposited No power required Results for large area Triangulation capable
Modal analysis	Inexpensive equipment Inexpensive to implement Surface mountable Portable Simple procedure Quick scan of large area	Complex results High data rates Specialized software Results are global	Lightweight Conformable Can be deposited Multi-purpose sensors Low power required Results for small area
Lamb waves	Inexpensive equipment Inexpensive to implement Surface mountable Portable Sensitive to small damage Quick scan of linear space	Very complex results Very high data rates Specialized software	Lightweight Conformable Can be deposited Medium power draw Linear scan results Triangulation possible

Table 1.1 – Comparison of strengths, limitations and SHM potential for different sensing systems [7]

Since not all techniques are applicable on a structure for continuous monitoring and some of them are not suitable for composite materials, the best candidates for lightweight, conformability and large area covered are Optical Fibers, Acoustic Emission and Lamb Waves [7]. The Lamb Waves method is based on piezoelectric transducers that work as actuators and sensors in the acousto-ultrasonic regime. They give the possibility to monitor the condition of specific areas of the structure, positioning the transducers only on the most safety-critical positions [8]. The principle of this technique is the focus of this research work and it is explained in the next section.

1.2. Guided waves

The SHM based on guided waves takes advantage of the propagation behavior of particular waves inside the materials. While the traditional Ultrasonic Non-Destructive Testing study the bulk section of the structure, the Guided waves are able to inspect large area thanks to surface propagation [9]. Within the several types of Guided waves, the most common are Lamb waves, that propagates on the surface of thin plates and shells in the frequency range 10÷500 kHz. The piezoelectric transducers, due to the possibility to act as actuators and sensors, are used to excite

the structure at this frequency regime and measure the vibrational response of the structure. The presence of a defect or a damage is found comparing the final response with the initial baseline of the electrical signal measured by the sensors, repeating the same excitation signal from the actuator piezo.

The excitation of structure results in the propagation of waves with different behavior. The longitudinal and transversal modes shown in Figure 1.7 are both present and the second one is normally more intense. The transversal mode, with particle motion perpendicular to the plane, can have symmetric modes (S) or anti-symmetric modes (A) respect to the section midplane [10].

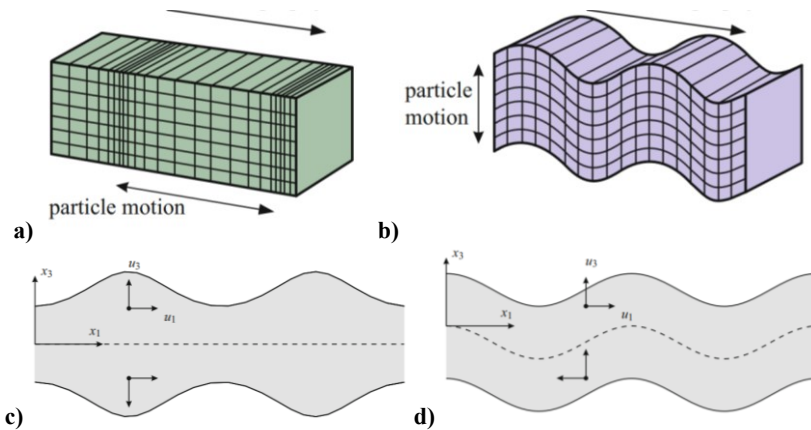


Figure 1.7 – Scheme of the particle motion for a) longitudinal and b) transversal modes, the transversal waves can behave as c) symmetric modes (S) or d) anti-symmetric modes [10]

Basically, the stimulation of the structure, called interrogation, is produced by an electrical excitation of the piezo actuator. The technique is called “pulse-echo” if the response signal is read by the same piezo, or “pitch-catch” if it is used a second piezo, as represented in Figure 1.8 [11]. The first requires a more accurate processing and cannot cover large areas of structures, while the second is widely use due to the possibility to connect the piezo elements in networks.

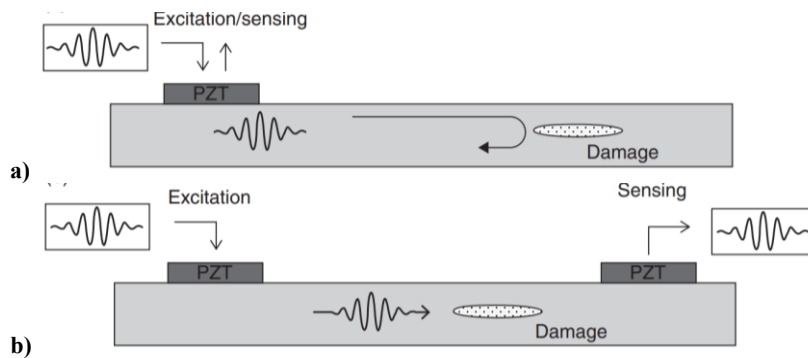


Figure 1.8 – Configurations of piezoelectric patches in a) “pulse-echo” and b) “pitch-catch” [11]

The common signal for SHM applications is a 5 sines burst with a Hanning modulation, with the shape shown in Figure 1.9 a) at the central frequency of Figure 1.9 b) [12]. An example of the response signal is represented in Figure 1.9 c), where the transversal symmetric and anti-symmetric modes have been sensed at the same frequency of input signal but at different times [13].

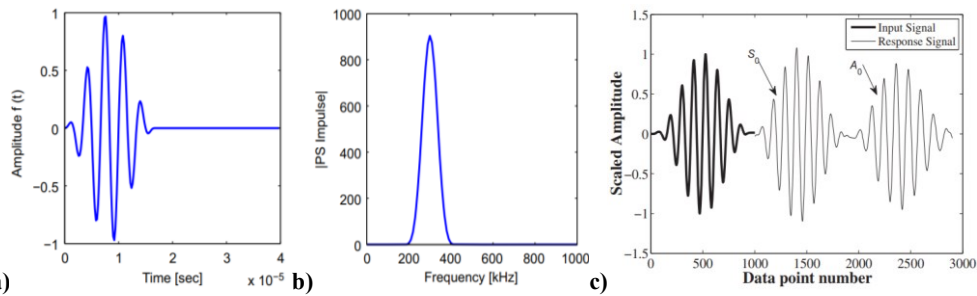


Figure 1.9 – a) Signal Shape and b) central frequency of burst for SHM [12], c) normalized input and output signals with S_0 and A_0 group waves [13]

The typical modes of Lamb waves can be distinguished in the output signal of a piezo sensor with different group and phase velocities respect to the frequency of the input signal [9]. Their amplitudes change with material type, as the example of Figure 1.10 for Aluminum and CFRP, where the A_0 mode is more present at lower frequencies [13].

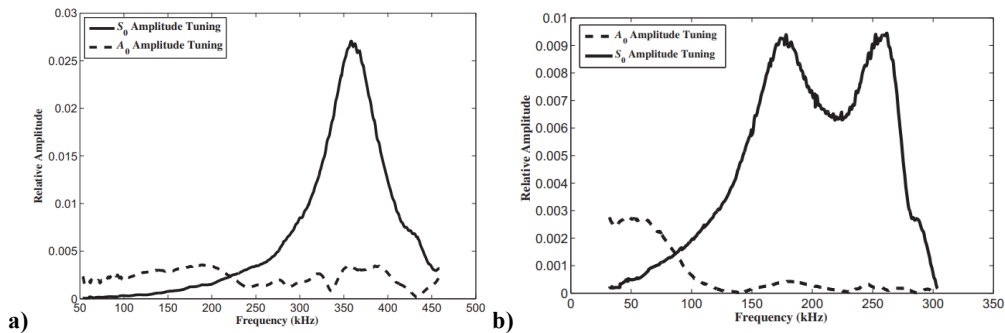


Figure 1.10 – Experimental measures of the Amplitude of A_0 and S_0 Lamb modes for a) 1,6 mm Aluminum plate and b) 2 mm CFRP plate [13]

The dynamic behavior of piezo actuator and structure can be measure with extremely precision with the scanning laser vibrometer [14,15]. In Figure 1.11 are reported the principle of the technique and the analysis of the surface motion of a piezoelectric disc at different excitation frequencies. The propagation of S and A Lamb wave modes can be studied on different composite stacking sequences, as visible in Figure 1.12. For the balanced quasi-isotropic composites the propagation is circular, while for orthotropic composites there is a preferred direction along the fibers.

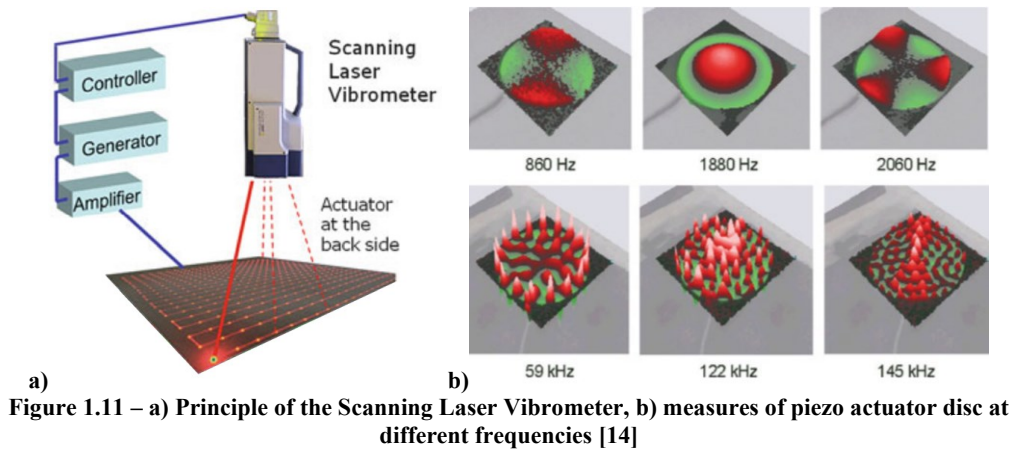


Figure 1.11 – a) Principle of the Scanning Laser Vibrometer, b) measures of piezo actuator disc at different frequencies [14]

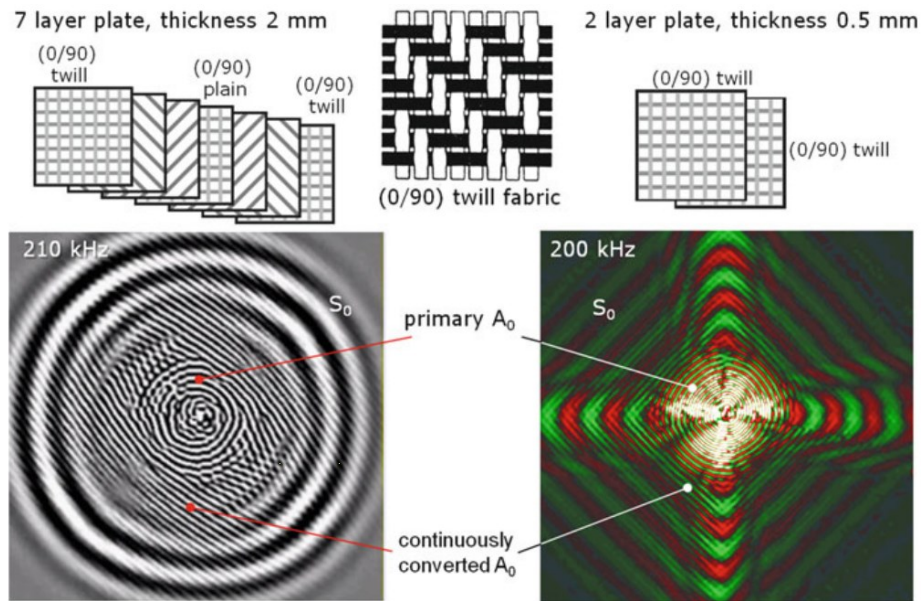


Figure 1.12 – Scanning Laser Vibrometer measures of measures of quasi-isotropic (left) and orthotropic (right) CFRP laminates [14]

Since a laser vibrometer analysis is not common, the structure vibration at the regime of Lamb waves is also studied using simulation tools, in order to understand better the results of the pitch-catch testing with piezoelectric elements. Theoretical formulations are able to numerically simulate the possible wave modes generated on a specific structure [16] and some commercial tools allow to represent the piezoelectric elements with different methodologies.

Boffa [17] simulated the waves propagation on a carbon fiber structure using LS-DYNA to evaluate the waves interaction with the stiffener. As shown in Figure 1.13, the piezo actuator has been modelled applying in plane orthogonal forces to 8 nodes along a circle of 10 mm diameter and the response signal is virtually measured with nodal displacement sampling.

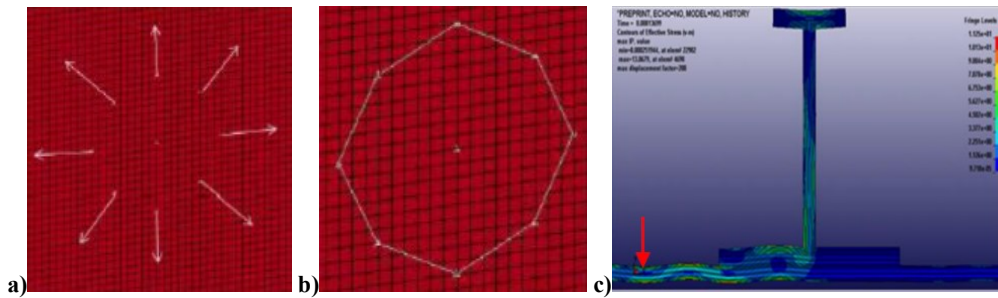


Figure 1.13 – LS-DYNA models of a) piezo actuator, b) piezo sensor, c) stiffened CFRP structure [17]

This simplified method based on a mechanical approximation has been also used on ABAQUS to represent the interaction of the separated A_0 and S_0 modes with a virtual defect on a plate, as visible in Figure 1.14 [18].

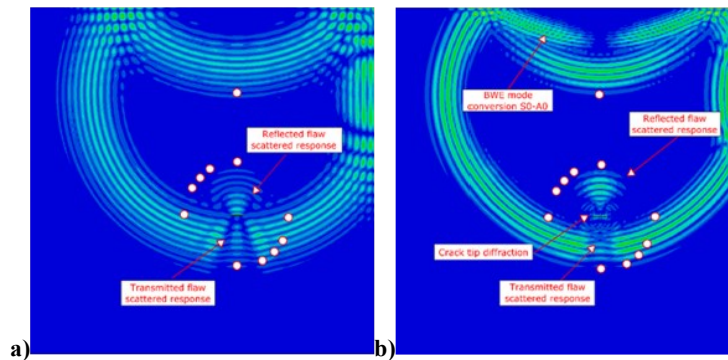


Figure 1.14 – ABAQUS model of a plate with a defect: a) A_0 and b) S_0 modes responses [18]

Recently, material cards specific for piezoelectric simulation have been introduced on ABAQUS, able to reproduce the electro-mechanical coupling with the structure and the electrical potential load for piezo actuators [19]. These functions allow to model the system more in detail, as seen in Figure 1.15, with the benefits of good fitting with the experimental signals, but increasing the computational time.

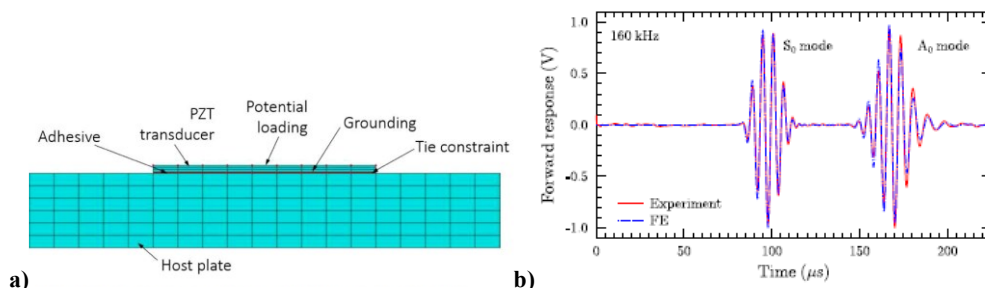


Figure 1.15 – a) ABAQUS model for the piezoelectric simulation and b) fitting of the experimental and virtual signals [19]

1.3. SHM System Components

The Guided wave method require a reliable apparatus both to generate Lamb waves and to collect response signals using piezoelectric sensors. Some commercial products are available for SHM on rotorcraft structures, developed by the American company Acellent, as can be seen in Figure 1.16 [20]. Thanks to the relative simplicity of the system and the relevant interest at the academic level, it is possible

to find in literature a huge quantity of reference about laboratory prototypes, cited below in the text.

This section describes the actual scenario of system setup, with detail on the sub-components and system validation.

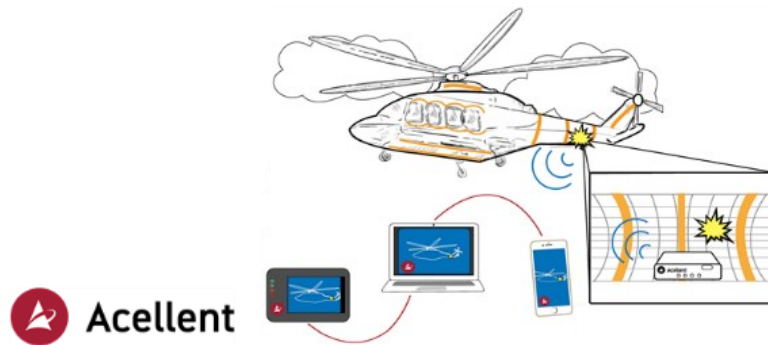


Figure 1.16 – Acelent solutions for SHM on rotorcrafts [20]

1.3.1. Piezoelectric Transducers

The Piezoelectric elements are the core of the system for generating and sensing the Lamb waves on structure. The piezo actuators and sensors are based respectively on the inverse and direct piezoelectric effects, schematized in Figure 1.17 [21].

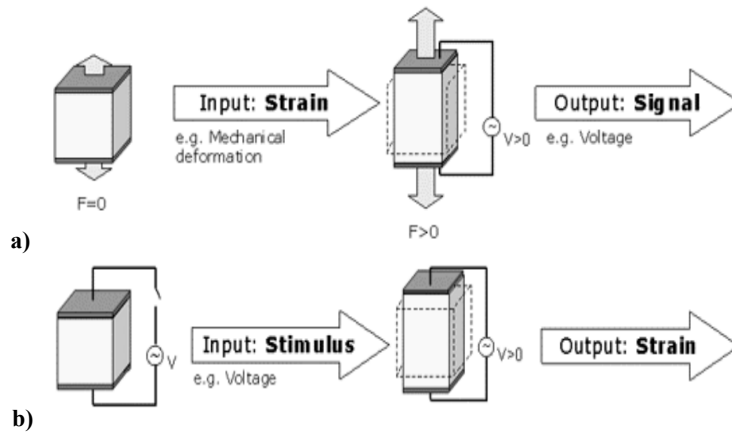


Figure 1.17 – Schemes of principle for a) direct and b) inverse piezoelectric effects [21]

For SHM application, the most common format of the piezoelectric transducers is the disc shape [22], although some rectangular formats are also known [23]. The Figure 1.18 a) and b) report piezoelectric discs with diameter of about 10 mm and thickness of 0,2 mm, that need to be manually soldered on the faces for working. To avoid this critical phase, some commercial solutions are available, called DuraAct™ [24,17] and SMART Layer™ [25-27].

The DuraAct™ are commercialized by Physik Instrumente (PI) as piezoelectric elements covered with Kapton film, applied on the surface of structures to monitor (Figure 1.18 c)). The polymer coating simultaneously serves as a mechanical preload as well as an electrical insulation, which makes the DuraAct bendable [28,29].

The SMART Layer™, called also diagnostic film, has been designed by Stanford University to be embedded in composite panels during manufacturing and easily introduce the piezoelectric elements inside complex structures. They consist in extended layers of EPDM film with custom shape that integrate piezo transducers and flexible printed circuit. Two examples are depicted in Figure 1.19.

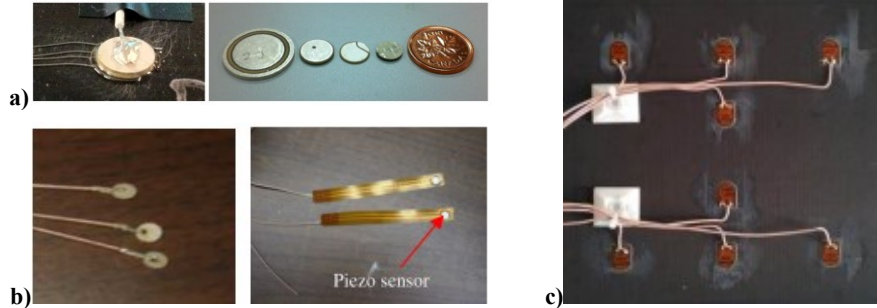


Figure 1.18 – Piezoelectric discs for SHM application: a) soldering technique and available formats [22], b) electrical connection with cables and printed circuit [25], c) network of DuraAct™ [24]

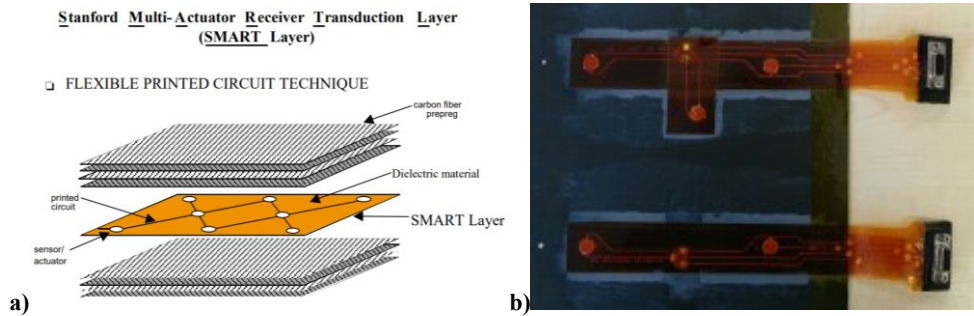


Figure 1.19 – SMART Layer™ a) embedded in composite panel [26], b) glued on surface [24]

1.3.2. Network Disposition

The disposition of piezoelectric actuators and sensors on the structure is a critical issue. There is not a preferred network shape, each operator applies in a different method according to the scope and the available number of piezo elements.

Regarding the actuators, generally one piezo at time is used, but in particular cases with high attenuation of the structure, two piezo are glued closely and excited in phase to amplify the waves [30]. The other piezo are used in the sensor configuration for a series of measurements and then changed the actuation-sensor pair using a switching device. In case of large plates, the geometrical disposition of piezo can be square, circular or hexagonal, as reported in Figure 1.20 [17,31-33].

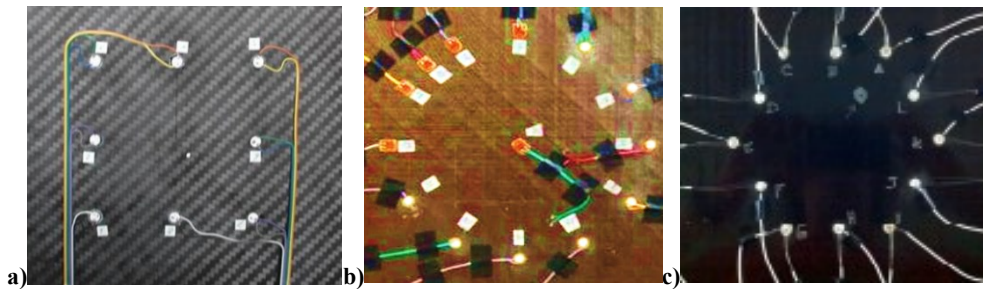


Figure 1.20 – Disposition of piezo network: a) square [17], b) circular [17], c) hexagonal [31]

These configurations are suitable for the investigation of the propagation behavior of Lamb waves on the structure in different directions, especially for composite materials. The interaction with an artificial damage is analyzed, when the damage is introduced in the center of piezoelectric network as a notch [18] or a growing fatigue crack [34], as the configurations reported in Figure 1.21.

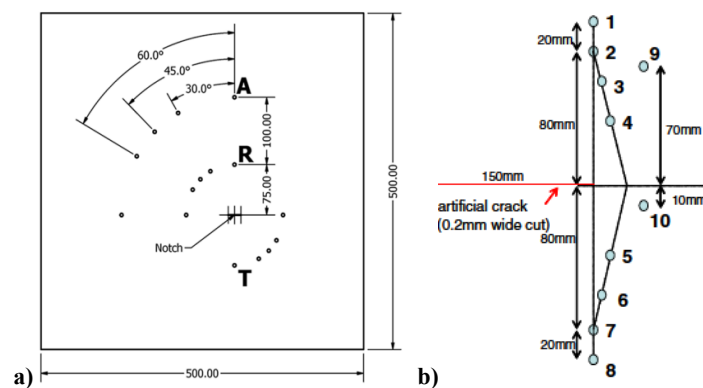


Figure 1.21 - Disposition of piezo network in case of a) notch [18] and b) fatigue crack [34]

In case of complex structures to monitor, a representative section is studied at the laboratory scale. An example is the stiffened plate widely applied in aircrafts, where the piezoelectric transducers are positioned in several ways, as shown in Figure 1.22. The zone around the stiffener has to be monitored because of the possible crack initiation, due to welding [35], layer co-lamination [8,36-39] or riveting [40].

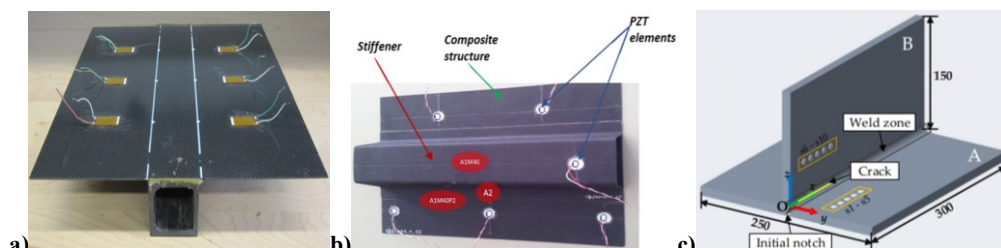


Figure 1.22 – Disposition of piezo network in case of stiffener: a) glued [36], b) co-laminated [37], c) welded [35]

The validation of monitoring systems passes through prototypes near to application scale, as shown in Figure 1.23 for a part of aircraft wing [17].

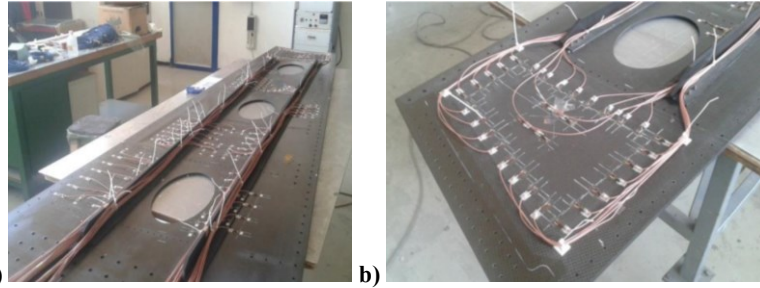


Figure 1.23 – Disposition of piezo network on a) relevant panel of aircraft wing, b) detail [17]

1.3.3. Laboratory Equipment

The essential instrumentation to develop a SHM system with piezoelectric transducers is composed by a voltage generator for the actuators and a digital oscilloscope for the sensors, as shown in Figure 1.24. The ultrasonic Lamb waves are produced with a 5 cycles Hanning tone-burst with central frequency in the range 10÷500 kHz [41].

The sensor response needs a proper sampling rate to be collected without loss of signal. Generally, a sample rate of 2 MSamples/s is used [17], in case of particular investigations it can arrive at 72 MS/s [19]. For each configuration of piezo actuator and sensor a series of identical measures is conducted for statistical processing, in some cases up to 100 repetitions [38]. If the signal has a low amplitude its conditioning requires an external high-voltage commercial amplifier [16,18] or customized amplifier, as reported in Figure 1.25 [23]. The quality of the signal depends on the cabling technique, it is preferred the use of 1 to 3 meter shielded coaxial cables [17].

Actually, the measurement is made using digital oscilloscopes that store the results or pass them to PC, as Agilent [16-18,38], Tektronix [13,39,42], MATEC [40] or Quazar [19]. The series of products developed by National Instruments offer the possibility to control the device from PC, as for CompactDAQ [23] and Multifunction Data Acquisition (DAQ) [17], or using an integrated FPGA controller, as for NI-PXIE [24,31]. The Acellent SMART Suitcase [25] and ScanGenie [35] are commercial products able to produce the burst specific for SHM and acquire data in the range of Lamb waves with a proper sampling rate.

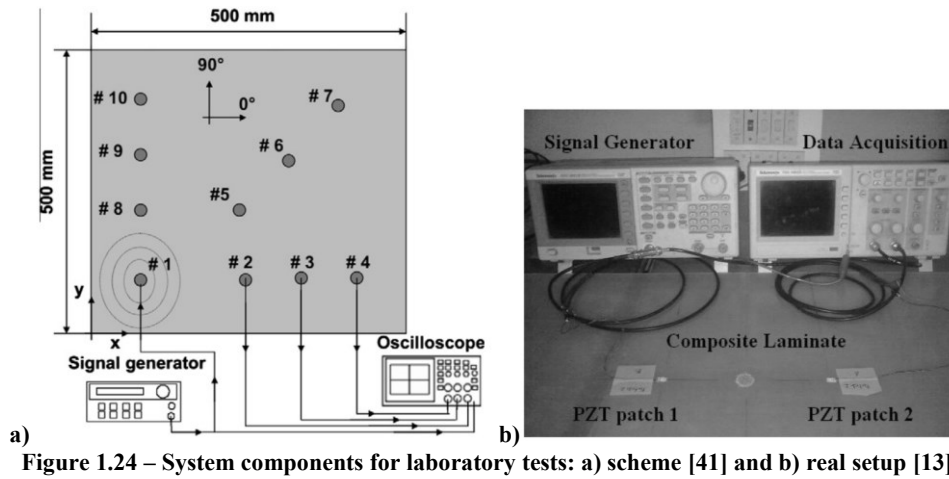


Figure 1.24 – System components for laboratory tests: a) scheme [41] and b) real setup [13]



Figure 1.25 – Customized piezo amplifier for special SHM applications [23]

1.3.4. Specimens Characteristics

The materials more commonly investigated for SHM trials are steel [38], aluminum [18,19,34,39] and composite materials, more based on Carbon Fiber [16,17,24,31,33,37,41-44] than Glass Fiber [13] both in unidirectional and balanced stacking sequence. The sandwich structures are less studied [23] because of the difficulty of propagation of Lamb waves inside the different materials. The typical dimensions of the plate specimens are 300x300x4 mm or in larger size of 1000x400x5 mm.

The adhesive used to apply the piezoelectric elements on the host structure must resist to shear stress resulting from normal strain of the structure and vibration of the piezo actuator, as seen in Figure 1.26 [11]. The most common adhesive is an epoxy resin, that is preferred over a thermo-bonded glue for the higher efficiency in the electro-mechanical coupling [45].

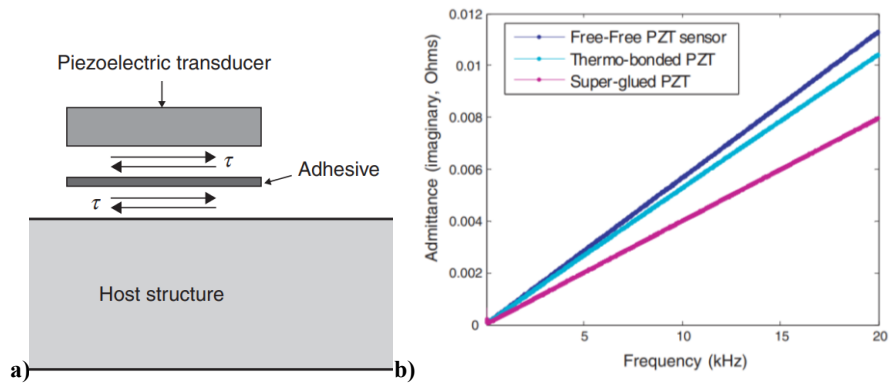


Figure 1.26 – Adhesive used for piezo: a) scheme of shear stress [11], b) efficiency of joining [45]

The partial debonding of the adhesive in the application of a piezoelectric disc has been studied [32] and the results are reported in Figure 1.27. The sensor response signal is strongly influenced both from the sensor debonding and the actuator debonding, therefore particular attention to this phase must be paid.

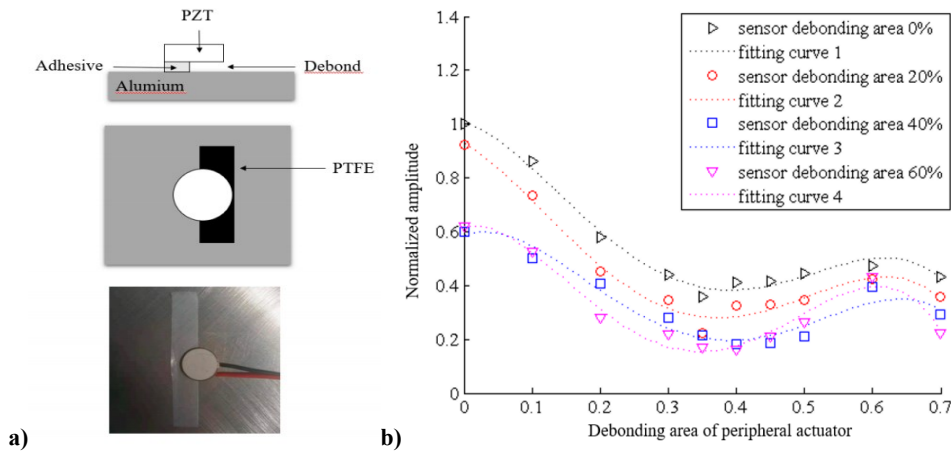


Figure 1.27 – SHM response in case of piezo debonding: a) test setup and b) results [32]

Depending on the material type, specimens are subjected to several artificial damages in order to reproduce the real phenomenon of structural degradation. In composite materials a delamination is usually introduced using a Teflon film of 50 μm thickness during manufacturing [43]. For durability analysis a specimen with a 0.2 mm wide notch cut is stressed to monitor the crack propagation [34]. The drilled holes are commonly executed into the panels for easiness and repeatability [31]. Some research works compare different types of damage, as Neodymium magnets with delamination [37] and damages with cavities and glued-on mass, as shown in Figure 1.28 [13]. The added mass can be a metal cylinder [13,46] or a fire clay to simulate a high-damping zone [44].

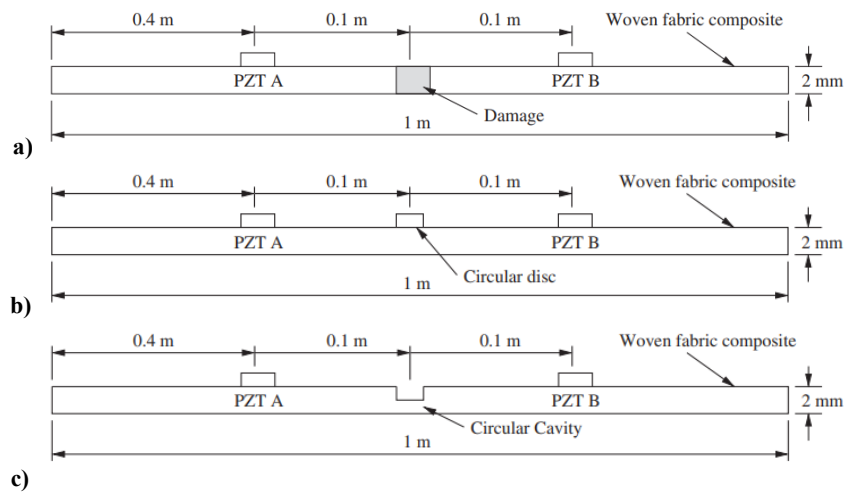


Figure 1.28 – Types of simulated damage: a) impact damage, b) glued-on mass, c) hole cavity [13]

The already mentioned rivets are fundamental for the integrity of a metallic structure. In Figure 1.29 is reported the progressive damage introduced on the rivet hole for detection and monitoring [40].

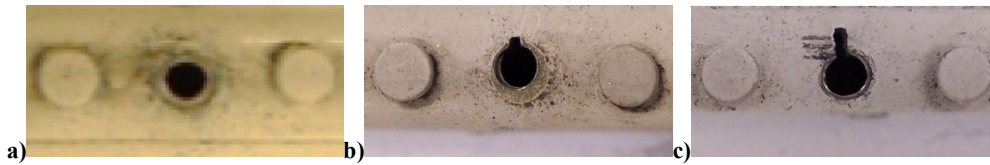


Figure 1.29 – Damage artificially introduced on a rivet hole [40]

The quasi-static crush [13] and the low velocity impact [30,17], reported in Figure 1.30 and Figure 1.31 for composite material laminates, are the laboratory tests that best replicate the damages on large panels. The indentation and consequent delamination are observed during the maintenance stages using Ultrasonic C-Scan devices, that is able to quantify the damage size but not to assess a continuous monitoring.

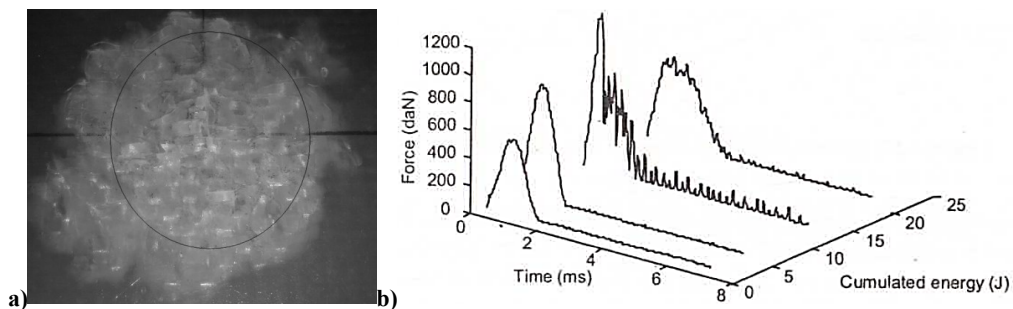


Figure 1.30 – Damage on composite panels: a) quasi-static crush [13], b) cumulative impacts [30]

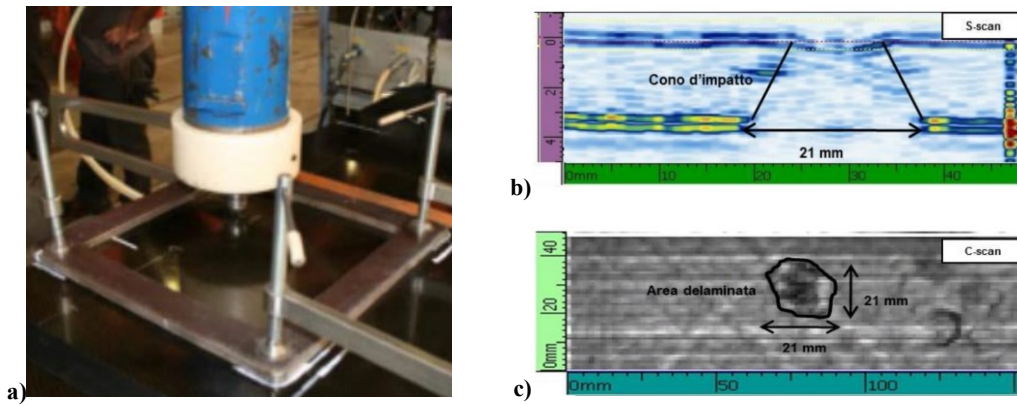


Figure 1.31 – Impact on CFRP panels: a) drop-dart tower, b) S-scan and c) C-scan ultrasonic tests [17]

1.3.5. Environmental Operating Conditions

The monitored structure in real application can be subjected to dynamic conditions that differ from the laboratory conditions. The main variations are operational and environmental conditions, respectively the structural loading and temperature/humidity [8,9,38]. The SHM may detect false positives related to ambient variable change instead of real damage. The laboratory specimen has, therefore, to reproduce the external conditions to analyze the response of the SHM system in the Environmental Operating Conditions (EOCs). In the following, are reported some experimental results from specific conditioning.

A CFRP plate exposed to hot/wet conditions (70°C, 85% humidity) for 2 month shows a reduction on peak amplitude both for A₀ and S₀ Lamb wave modes, as seen in Figure 1.32 [41].

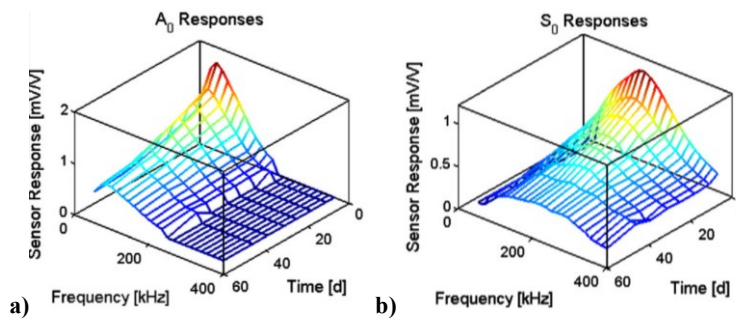


Figure 1.32 – Peak amplitude reduction during conditioning for a) A₀ and b) S₀ Lamb modes [41]

The variation of temperature with the cyclic profile of Figure 1.33 is called thermal fatigue and promotes the moisture absorption in the CFRP laminates with a coupled effect of influence on the wave propagation velocity [47].

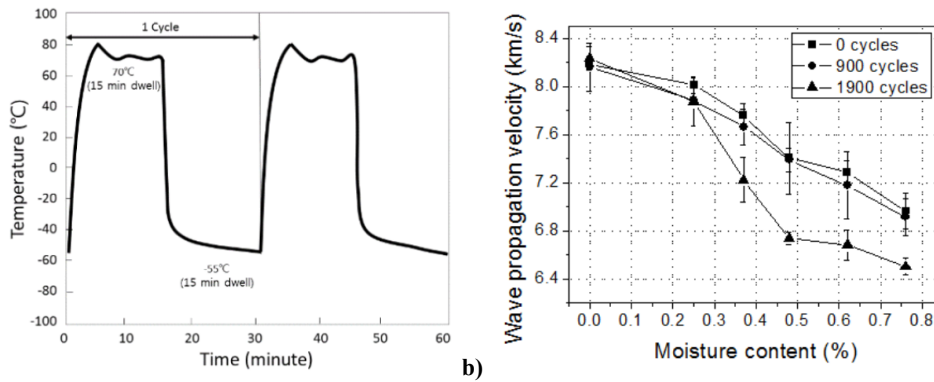


Figure 1.33 – Thermal fatigue: a) cycle description and b) effect on the wave velocity [47]

The structures in operative conditions are subjected to external vibrations, therefore the SHM system based on ultrasonic waves can be affected. In the Figure 1.34 it is shown the influence of a continuous low frequency excitation produced by a shaker on an aluminum plate, in terms of offset and trend changes of the response signal [48].

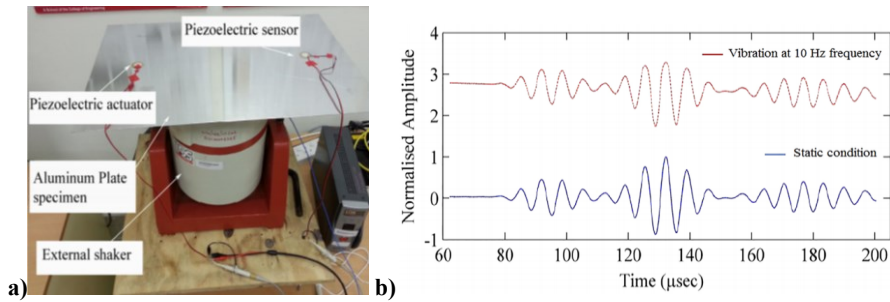


Figure 1.34 – Effect of low-frequency disturbs on SHM response: a) shaker setup, b) signal result [48]

The influence of uniaxial loads on an aluminum plate at different loading steps is reported in Figure 1.35 in terms of signal scatter from the baseline condition [46].

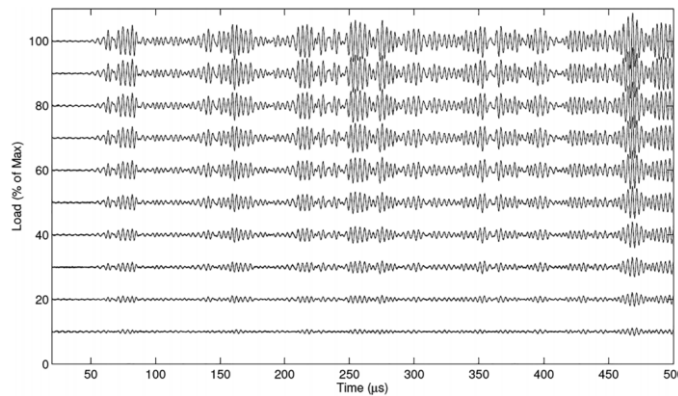
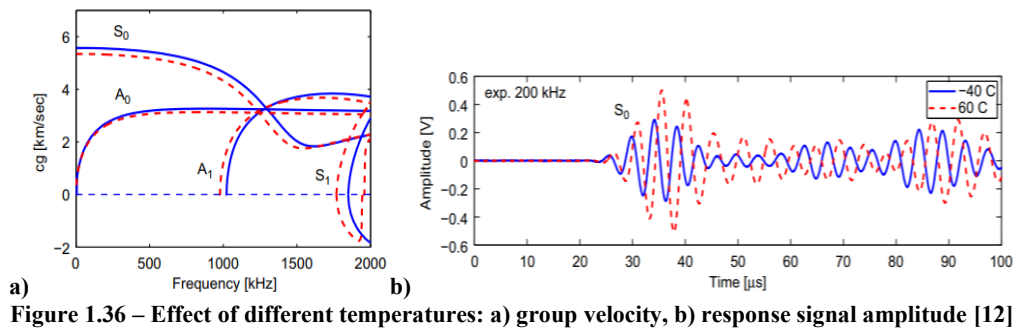
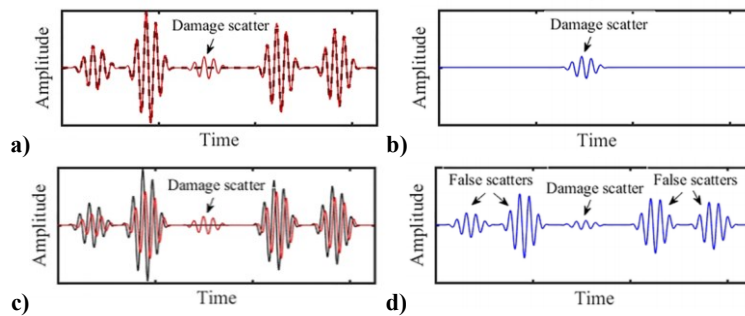


Figure 1.35 – Effect of uniaxial loads on the piezoelectric response signal for an aluminum plate [46]

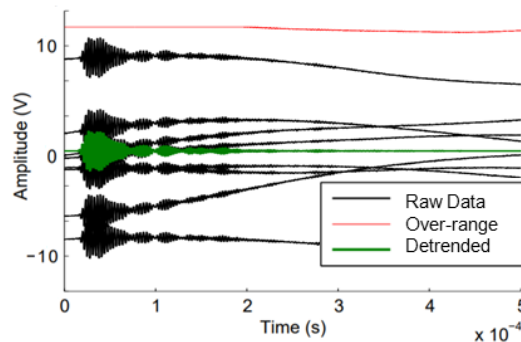
In Figure 1.36 it is shown how the temperature affects the propagation of anti-symmetric and symmetric Lamb wave modes, changing both the group velocity and the amplitude [12].



For external reasons, a time delay of the response signal can happen. In Figure 1.37 is schematized the influence of imperfect synchronization on the signal scatter between the test response and the initial baseline [49]. The scatter due to damage presence can reduce, while the scatter of intense peaks leads to false positives with high amplitude.



The black lines in Figure 1.38 represent a series of 8 acquired signals with the typical behavior of piezoelectric sensors [24]. The information of dynamic response due to the excitation burst is added on a drifting baseline. Furthermore, the offset at time zero is not null and can vary from negative to positive values in the entire input range. If the signal offset is over the range, as the red line, the measurement is considered not valid. The signal drift is caused by several factors, for example the presence of parasite interferences with lower frequency and higher amplitude, like the power supply of the electronic device or the actuator cable proximity to the sensor cable. The drift can be digitally corrected, offsetting the signal to zero and removing the baseline oscillation, resulting in the green line.



1.3.6. Data Processing

The aim of data processing in SHM systems is the conversion of complex signals to a simple quantitative variable, that allows the users to understand the health condition of the structure [9]. The system setup and the methodology for damage detection assessed in the training phase on specimens in laboratory have to be validated in the testing phase on the real structure in unknown state, as proposed in Figure 1.39 [37]. In the training phase a specimen is artificially damaged, building a specific data processing technique to calibrate the system and calculate a “Damage Index” (DI) value incremental with damage size. The information of damaged structure is computed after an accurate selection of the decision threshold, that is a DI value obtained statistically to avoid false alarms and noise interaction [50]. The DI formulation and the value of decision threshold are matter of study.

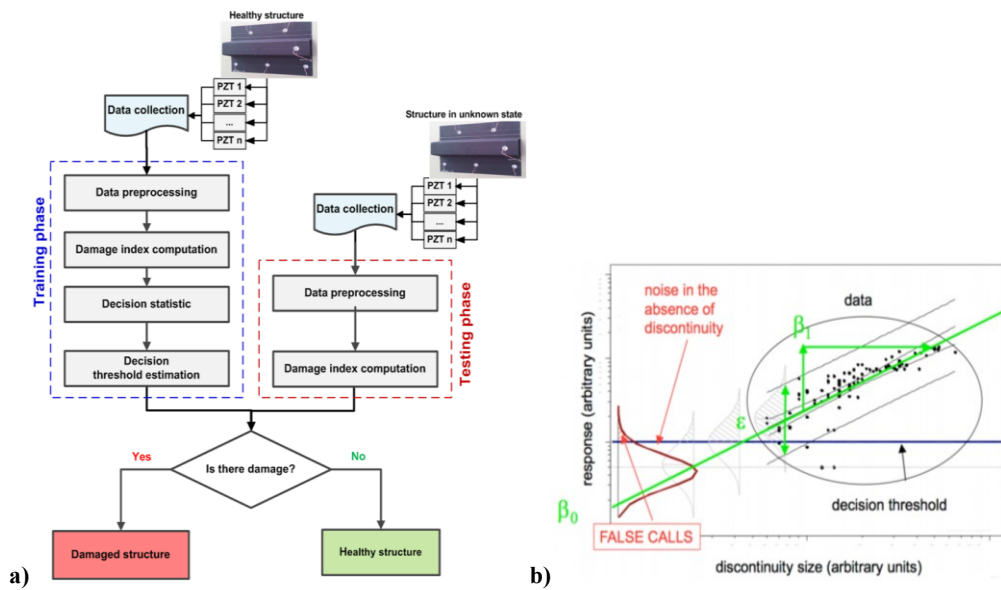


Figure 1.39 – a) Decision methodology for data processing [37], b) schematic definition of decision threshold value [50]

Furthermore, the location of damages on the structure can be obtained from triangulation techniques based on the different piezo couples' positions and the calculated Damage Index.

The presence of damages or changes in the structure can be detected also observing the response signal of the piezoelectric sensor. Since SHM data are very complex, the visualization proposed by Stanford University is widely used [30,34,51,52]. The methodology for data processing is described in the Figure 1.40. The Voltage-Time signal is acquired, then the envelope of the group waves is applied. The envelope line obtained at the specific frequency is then plot on the entire frequency range, using a Time-Frequency-Amplitude spectrogram.

The scattering of each point on the spectrogram is used to observe variations between two measurements executed at different time or health conditions, as reported in Figure 1.41. The final curve is not containing information about the entity or location of the damage, but it is useful to evaluate the ranges of frequency

more sensitive to damage presence and consequently reduce the number of experimental tests.

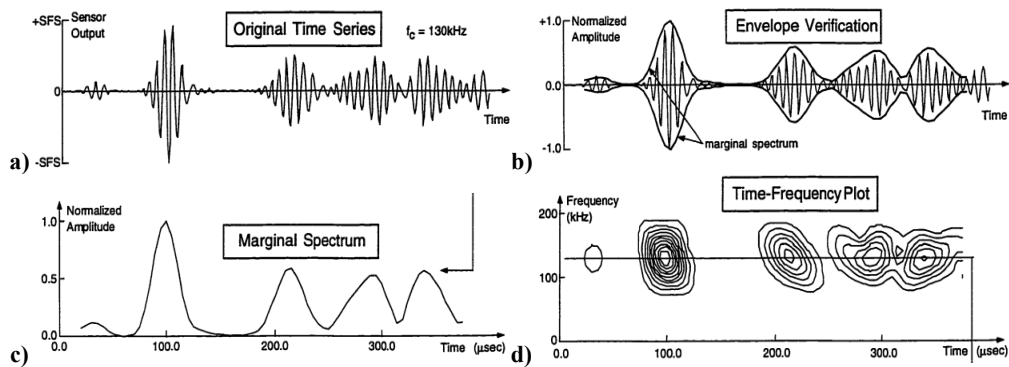


Figure 1.40 – a) Original signal, b) normalized envelope of the signal, c) positive envelope, d) time-frequency plot [52]

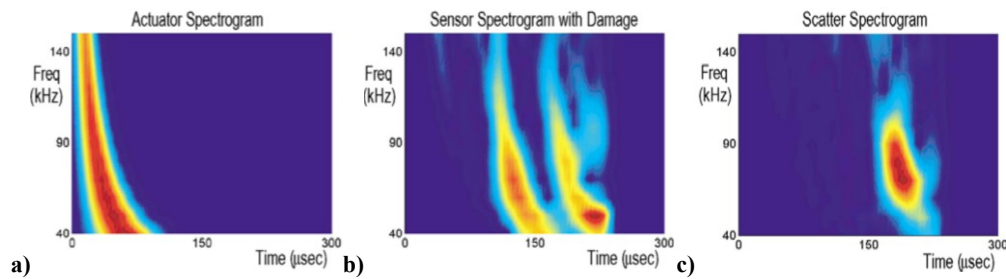


Figure 1.41 – Spectrogram visualization: a) actuator signal, b) sensor signal in damaged condition, c) scatter of damaged respect to undamaged condition [51]

The simplest Algorithm that analyzes the response signal is based on Time of Flight (ToF), also called Time of Arrival (ToA) [17,34,53-56]. This time value is calculated between the envelop peaks of group waves sent from the actuator and received from sensor, as represented in Figure 1.42. The variation of the ToF value in test configuration respect to the baseline acquisition is evaluated for damage detection.

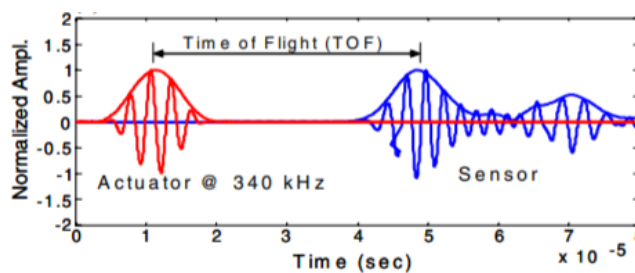


Figure 1.42 – Time of Flight calculation from actuator (red) and sensor signal (blue) [53]

In Table 1.2 a list of complex Algorithms based on the cross-correlation analysis, Fourier Transform and signal difference is reported [37]. They are the most used Damage Index formulations converted in MatLab language for easy implementation on the processing software.

DI name	Comments	Definition
CCA	MATLAB based implementation of the maximum of the correlation	$1 - \max(xcorr[x_{ij}(t), y_{ij}(t)])$
CCO	MATLAB based implementation of the zero-lag correlation	$1 - xcorr[x_{ij}(t), y_{ij}(t)](0)$
CRC	MATLAB-based implementation of the correlation coefficient	$1 - corrcoeff[x_{ij}(t), y_{ij}(t)]$
NRE	Normalized residual energy	$\int_0^T (x_{ij}(t) - y_{ij}(t))^2 dt$
MA	Maximum amplitude of the difference	$\max[x_{ij}(t) - y_{ij}(t)]$
FFT	FFT of the difference signal at f_0	$\max[x_{ij}(t) - y_{ij}(t)]$
ENV	Maximum envelope of the difference	$\max[ENV(x_{ij}(t) - y_{ij}(t))]$

Table 1.2 – List of the most used Damage Index formulations converted in MatLab language [37]

The CCA Damage Index is the basic formulation of the RAPID Algorithm (Reconstruction Algorithm for Probabilistic Inspection of Defects) for localization of damages on the structure [31,40,57]. The DI value for RAPID is calculated in terms of Signal Difference Coefficient (SDC), as described in Equation (1). The Equation (2) explains the formulation of the cross-correlation coefficient, deriving from covariance and standard deviation of the test signal D respect to the baseline signal B.

$$SDC_{ij} = 1 - \rho_{ij}, \quad i, j = 1, \dots, n_e, \quad i \neq j \quad (1)$$

$$\rho_{ij} = \frac{Cov(B_{ij}, D_{ij})}{\sigma(B_{ij}) \cdot \sigma(D_{ij})} \quad (2)$$

where:

- SDC is the Damage Index value of the piezo couple ij,
- i, j are the indices corresponding to the piezo actuator and sensor,
- ρ is the cross-correlation coefficient,
- Cov is the covariance function,
- B, D are the Baseline signal and Test signal.

The decision threshold (t_{SDC}) of Damage Index based on the SDC value is calculated after a series of experimental tests with undamaged and damaged specimens. The decision about the structural health is made comparing the processed SDC with the threshold, as in Equation (3). The triangulation for damage localization assigns an elliptical area to each piezo couple of actuator and sensor, that cumulatively superposes the final SDC after comparison with the decision threshold. The result is the Damage map in Figure 1.43.

$$SDC_{ij} = \begin{cases} 0 & \text{if } SDC_{ij} < t_{SDC} \\ SDC_{ij} & \text{if } SDC_{ij} \geq t_{SDC} \end{cases} \quad (3)$$

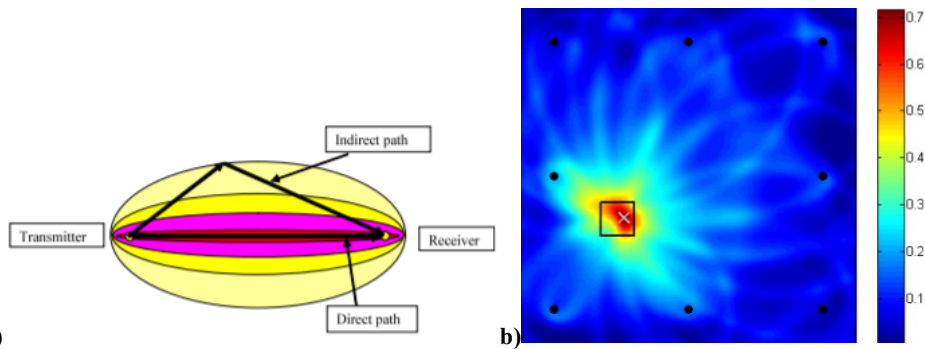


Figure 1.43 – Localization algorithms based on a) cross-correlation (RAPID) [40] and b) ToF [53]

Recently has been developed the Time Reversal Method (TRM) that aims to avoid false alarms based on environmental and operating conditions changes [9,19,44]. This procedure is quite interesting because it does not require a baseline signal for damage detection. It is based on the time reversibility of Lamb waves on the materials, represented in the Figure 1.44. The principle is that on healthy structures the burst signal sent in forward direction from piezo actuator to piezo sensor is aligned with the time reversed signal sent in backward direction. The change in the received time reversed wave is brought by the presence of damages.

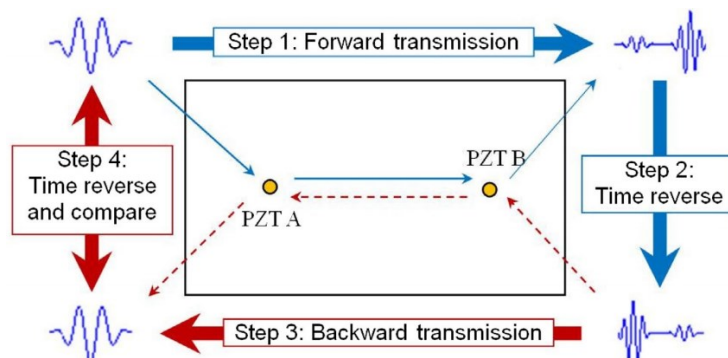


Figure 1.44 – Scheme of principle for the Time Reversal Method [44]

Chapter 2

Case study definition

Considering the schema of Figure 2.1, the main goals of this thesis are:

- **Sector change** – effective applicability for automotive applications from aerospace industry
- **Materials investigation** – SHM adaptation on different materials used in automotive
- **Application component** – methodology applied to an automotive component case (suspension system) starting from properly designed specimens
- **Influence of loading conditions** – evaluation in both free and bending configurations
- **Damage Index selection** – Processing algorithm definition for damage detection
- **Indication for Sensor Positioning via Simulation** – Virtual methodology to design a-priori the Sensor Network

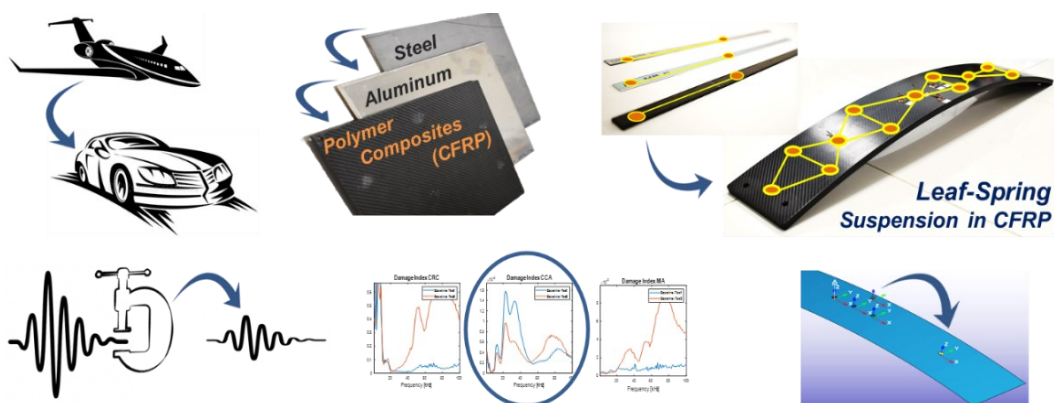


Figure 2.1 – Scheme of the main goals of the thesis

2.1. Aim of the thesis

The methodology defined in this thesis to assess SHM has been applied to an automotive component prototype, a CFRP leaf spring developed by the IEHV research group of Politecnico di Torino [58]. It is a technology demonstrator of a suspension system that integrates functionalities of spring, anti-roll bar and lower/longitudinal control arm, as described in Figure 2.2. It is integrally made of carbon fiber epoxy composite, with layers stacking sequence properly designed to replace the traditional automotive suspension system. In Figure 2.3 are reported the overall dimensions of the prototype, with the vehicle interfaces.

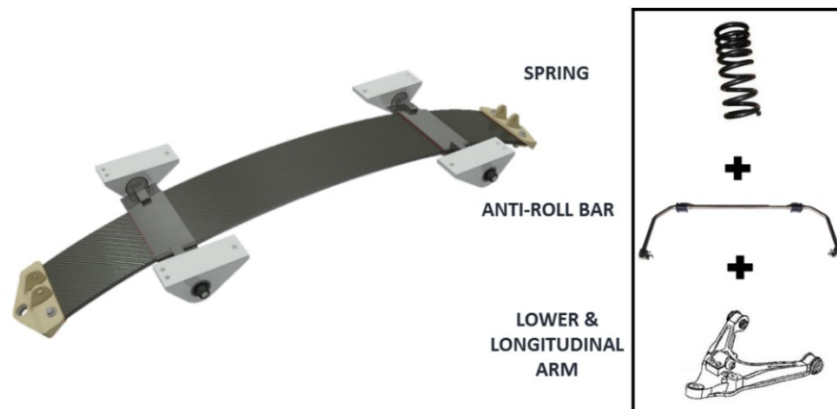


Figure 2.2 – Functions integration on the Innovative Leaf Spring Automotive Suspension [58]

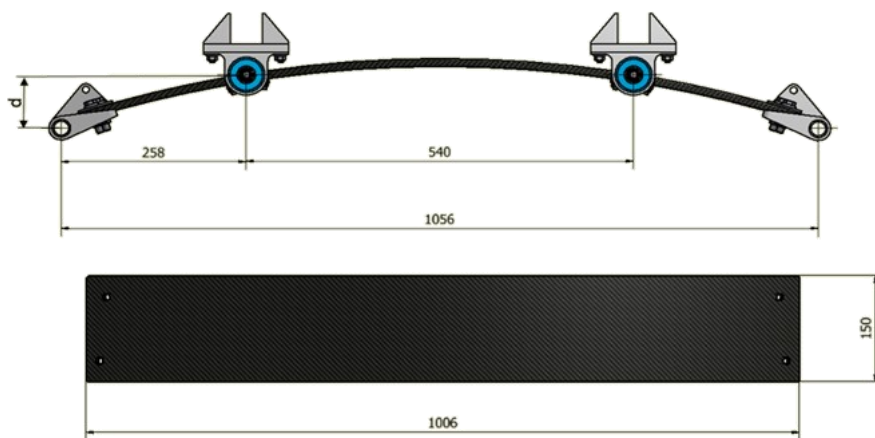


Figure 2.3 – Component dimensions and points of interface with vehicle [58]

The Leaf Spring is made of Carbon Fiber reinforcing Epoxy Resin. The commercial name of the material is GG245T and it consists of prepreg balanced woven layers (245 g/m^2) with the same thickness (0,25 mm). The production of the component passes through the obtaining of the resin mold, the cut of prepreg plies, the manual overlap of plies into the mold, the closure in a vacuum bag, the thermal cure under pressure and the refinement.

The final component is designed with a specific shape and a precise stacking sequence, that takes into account the mechanical performance of the structure and the surface skin for the aesthetic refinement. The Stacking Sequence of the Leaf Spring is composed by 55 layers, stacked as reported in Table 2.1.

#Ply	Thickness [mm]	Angle [°]	#Ply	Thickness [mm]	Angle [°]
1	0.25	0	...		
2	0.25	0	50	0.25	0
3	0.25	45	51	0.25	45
4	0.25	0	52	0.25	0
5	0.25	45	53	0.25	45
6	0.25	0	54	0.25	0
...			55	0.25	0

Table 2.1 – Stacking Sequence of the Leaf Spring

2.2. Experimental Methodology

Focusing on the goal of this research work, the Leaf Spring has the role of safety component in the suspension system of the vehicle. The integrity of this structure is a priority and a proper methodology to monitor constantly the health status has to be developed and adapted to its particular shape and advanced material.

As found in the Chapter 1, the SHM systems based on piezoelectric transducers are good candidates to meet this requirement. The actual applications in aerospace industry with much different loading conditions constricts to a completely new validation of the SHM system for an automotive component as the leaf spring passing through simple case studies, in order to understand better the phenomena.

The proposed methodology is based on testing the specimens described in Table 2.2 made of three materials: carbon fiber composite, aluminum, steel. The different geometries, number of piezoelectric transducers used, combination of test configurations and loading cases are considered with customized specimens increasing in complexity to reach the wider knowledge of the system response for the final tests on Leaf Spring component. As explained in the following Chapters, the SHM methodology bases on the verification of some Damage Index algorithms for damage detection on the described specimens and leaf spring component.

Type	Material	Geometry	Dimension [mm]	N. Piezo	Test Conditions
Specimen BEAM	Composite Aluminum Steel	Rectangular	300 x 12	2	Appended Clamped On Table
Specimen PLATE	Composite Aluminum Steel	Square	250 x 250	4	On Table
Specimen SIMULACRUM	Composite Aluminum Steel	Rectangular	250 x 70	3	Bending Step 0-1-2
Component LEAF-SPRING	Composite	Rectangular curved	1000 x 150	6	Bending Step 0-1-2-3-4

Table 2.2 – Case studies for this research work

2.2.1. Beam specimen

The beams realized in three materials allow the propagation of the wave in a thin and narrow plate, where the guided waves are constrained to move from the source in the longitudinal direction.

It is possible that the waves reflect at the edges coming backward. For this reason, the piezoelectric actuator and sensors positioning is important in order to correctly evaluate the signal acquired in time.

The artificial damage is placed in the center between actuator and sensor, as represented in Figure 2.4. The configurations tested are presented in Figure 2.5: appended to test the specimen in free mode and clamped at one edge to reduce the free path of the waves.

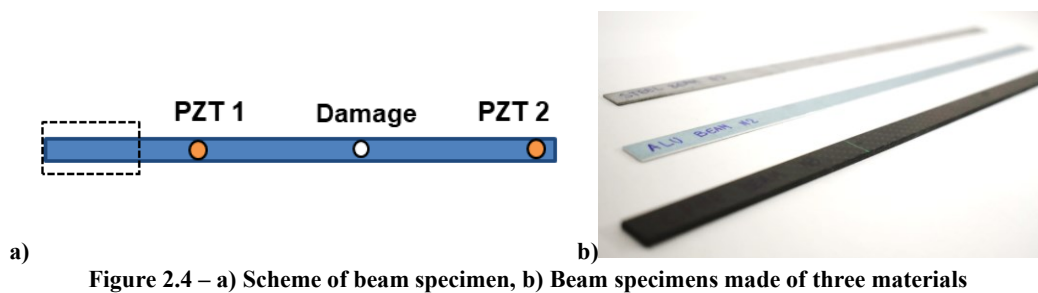


Figure 2.4 – a) Scheme of beam specimen, b) Beam specimens made of three materials

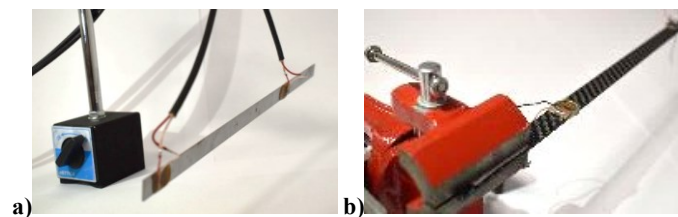


Figure 2.5 – Test configurations for the Beam specimen: a) Appended, b) Clamped

2.2.2. Plate specimen

The plate has been designed to be square, planar and thicker than the beam. As presented in Figure 2.6, the tested configuration for three materials is only positioned on the table to avoid issues of appending or clamping. The Figure 2.7 illustrates that four piezoelectric patches are placed in the middle of each side forming a symmetrical network. The artificial damage is placed in the quadrant of PZT 1 and PZT 2 on the diagonal.

The reasons for these choices are the following: Firstly, the plate is the validation of the SHM results on beam; Secondly, the variation in thickness induces a variation in fraction of symmetrical and anti-symmetrical lamb wave modes to be evaluated; Lastly, the damage and all the configurations can be evaluated in symmetry thanks to the piezoelectric patches on the sides.



Figure 2.6 – Test configuration for the Plate specimen

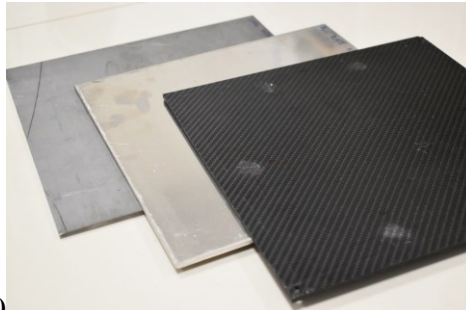
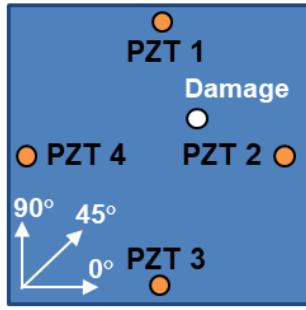


Figure 2.7 – a) Scheme of plate specimen, b) Real plate specimens made of three materials

2.2.3. Simulacrum specimen

The simulacrum is the required specimen to pass from a non-stressed specimen to the leaf spring component, that is designed to be continuously under bending load. Because the leaf spring works in elastic condition, also the simulacrum specimens in all the materials have been tested in the elastic bending zone. Furthermore, the bending of a plate is the preferred loading configuration for the validation of prototypal systems, as crack monitoring with piezoelectric elements [59] and optical fibers comparisons with strain gauges [43]. For the present specimens, the range of load is defined using two longitudinal strain gauges on the bottom face, one is placed in the center and one under the support. The evaluation of SHM system is made both in the unloaded and loaded static conditions, with the fixture reported in Figure 2.8.

As presented in Figure 2.9, the piezoelectric actuator is placed in the center of the top face, the 1st sensor is on the same face but over the upper support, in order to study the attenuation under loading. The 2nd sensor is mounted on the bottom face exactly under the actuator, to evaluate the waves propagation in the thickness.

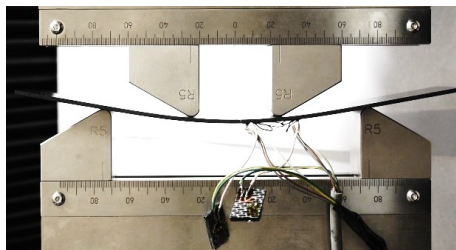


Figure 2.8 – Test configuration for the Simulacrum specimen: bending load

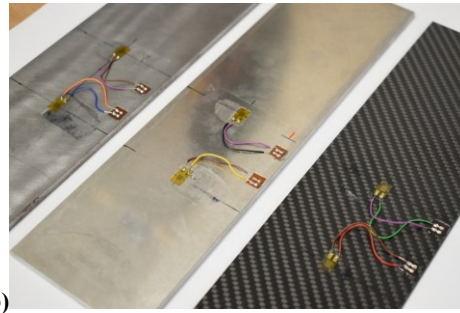
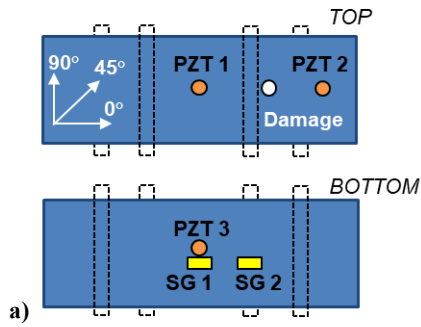


Figure 2.9 – a) Scheme of simulacrum specimen, b) Real simulacrum specimens made of three materials

2.2.4. Leaf Spring Component

The Leaf Spring is tested in bending loading configuration (Figure 2.10). As for the simulacrum, the loading range is evaluated using one strain gauge longitudinal in the center position on each face, as showed in Figure 2.11.

The piezoelectric patches are placed in a network similar to the simulacrum, as designed in Figure 2.12 and realized in Figure 2.13 and Figure 2.14. The actuator (PZT 1) is on the top center and the sensors are installed only to one half of the leaf spring thanks to the symmetry. The distance of the actuator to the 1st sensor (PZT 2) is half of the distance to the 2nd sensor (PZT 3), to evaluate the attenuation of waves doubling the path. The 3rd sensor (PZT 4) is away from the center of leaf spring over the bending support. The 4th sensor (PZT 5) is at 45° crossing the composite woven to understand the matrix attenuation influence. The 5th sensor (PZT 6) is placed on the bottom face exactly under the actuator.



Figure 2.10 – Test configuration for the Leaf Spring component: Bending load

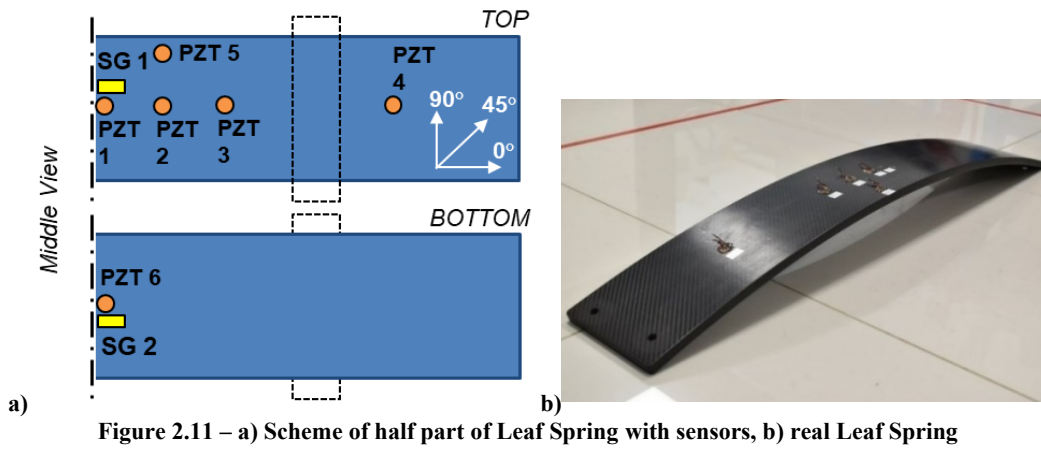


Figure 2.11 – a) Scheme of half part of Leaf Spring with sensors, b) real Leaf Spring

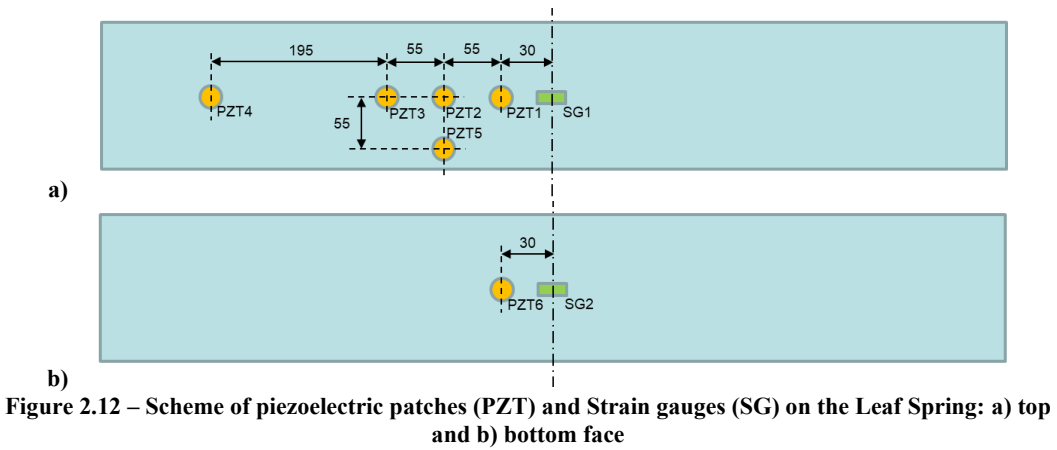


Figure 2.12 – Scheme of piezoelectric patches (PZT) and Strain gauges (SG) on the Leaf Spring: a) top and b) bottom face

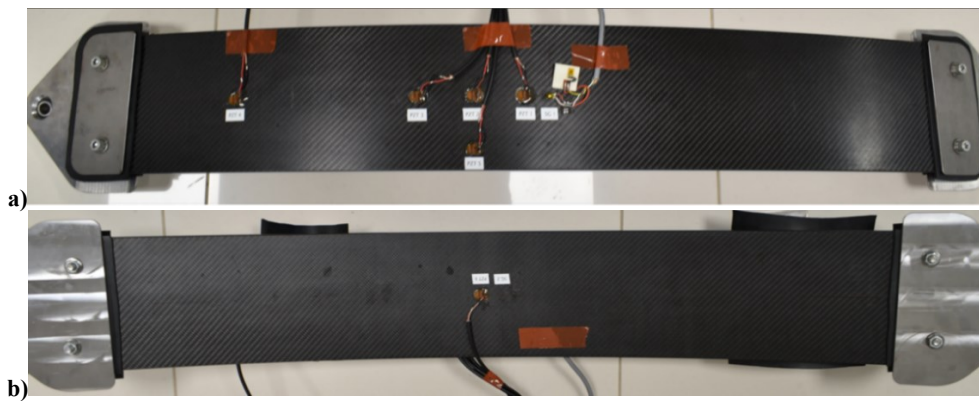


Figure 2.13 – Piezoelectric patches and Strain gauges on the Leaf Spring: a) top and b) bottom face

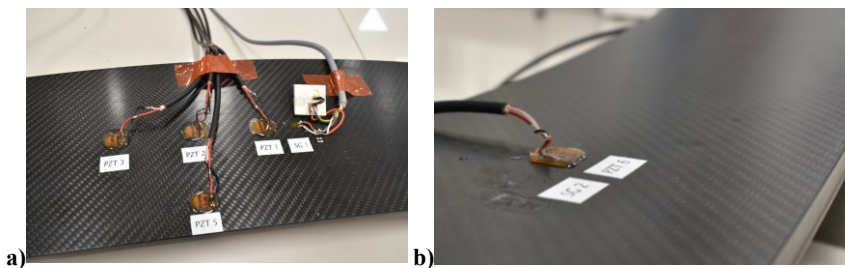


Figure 2.14 – Detail of Piezoelectric patches and Strain gauges on the Leaf Spring a) top and b) bottom face

2.2.5. Damage Definition

Two different artificial damages have been produced on specimens using a 4 mm drill bit on a bench pillar drill, obtaining the profiles showed in Figure 2.15.

The first damage is a non-passing indentation of 2 mm diameter on the surface of specimen, representing a surface defect on the structure. The second damage is a passing hole of 4 mm, representing a volume defect in the structure.

These damages have been chosen according to [31] to obtain two different configurations of damage and ensure high repeatability between different specimens and geometries. In fact, the main evaluation of this Thesis is about the data processing of piezoelectric sensors signals, therefore the geometrical difference between damage configuration respect to the undamaged one on the same specimen has to be as constant as possible.

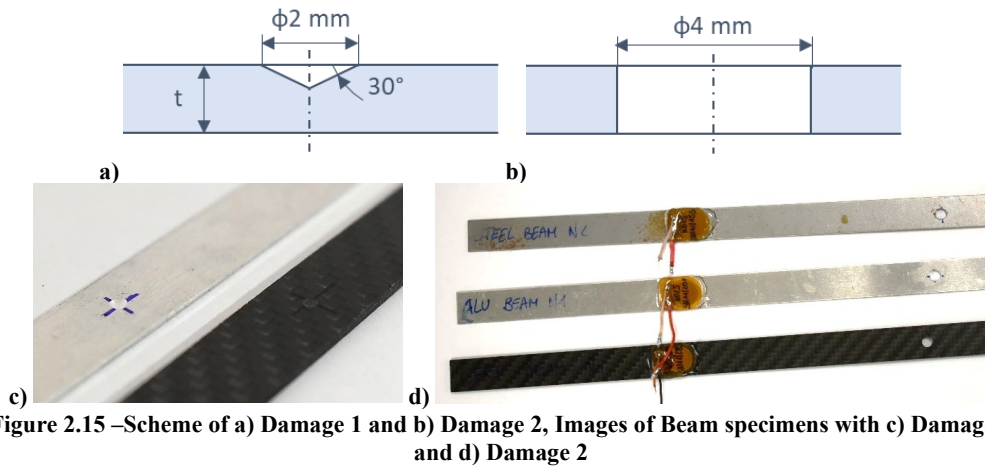


Figure 2.15 –Scheme of a) Damage 1 and b) Damage 2, Images of Beam specimens with c) Damage 1 and d) Damage 2

Since the Leaf Spring component is a unique prototype, it is not possible to introduce any damage. For this reason, a damage has been simulated applying a manual clamp, as in Figure 2.16, that locally increases the stiffness of Leaf Spring.



Figure 2.16 – Detail of the manual clamp applied in the case of Leaf Spring component

Chapter 3

System Setup

The present Chapter describes the development of the experimental setup for the Structural Health Monitoring (SHM) system applied on the considered case studies (see Chapter 2). The definition of the system is original and started from a blank sheet for the experimental campaign that has been carried on the specimens and automotive component for the SHM evaluation.

The choices made and reported in this Chapter are the result of an evaluation between hardware/software availability in the Laboratory of Politecnico di Torino and the financial resources dedicated to this Research activity. The instrumentations used is suitable for Laboratory analysis and the global cost is not aligned with the automotive sector, since the objective of the Research is to identify a methodology for damage monitoring and not to develop a final product ready to sell.

The measurement chain of the system, made of hardware components and software codes, is reported in Figure 3.1.

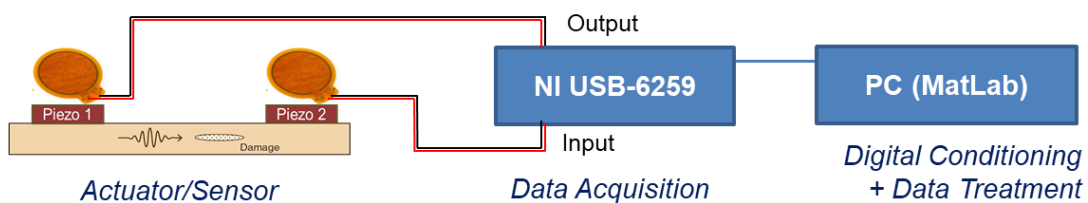


Figure 3.1 – Scheme of the measurement chain

The hardware components are specific piezoelectric transducers, suitable shielded cables and connections, a National Instruments electronic device for analog control of piezoelectric patches and data logging.

The program has been developed using the commercial software MatLab, able to control the National Instruments hardware and to acquire efficiently the raw data for the data processing.

The final results expected from the system is the indication of the Health status as a numerical value, called Damage Index, for the objective monitoring of the

structure. In particular, a series of six Algorithms that calculate a different Damage Index are applied to raw data acquired in this thesis, in order to identify the best in terms of sensitivity to the particular conditions of the specimens and component under test.

The research presented has the aim to combine the electronic validation of the SHM system with the exposure of specimens to loading configurations, in order to investigate the influence of that on the Damage Index calculation. The hardware used to create a repeatable condition of stress on the studied structures is an Universal Testing machine, equipped with a standard bending fixture for the specimens and a customized fixture for the Leaf Spring suspension testing. The stress analysis is carried on measuring the local strain adopting HBK resistive strain gauges and relative amplifier.

3.1. Hardware

3.1.1. Piezoelectric transducers

The Piezoelectric transducers used for Structural Health Monitoring need to have several requirements:

- Repeatability of vibration generation (inverse effect)
- Repeatability of vibration acquisition (direct effect)
- Resistance to the environmental conditions
- Flexibility to resist with the deformation of structure
- Good interaction with adhesives for bonding on structure
- Simplicity of electrical connection

All of these specifications have been found in the piezoelectric transducers of PI Physik Instrument GmbH, already applied, for example, in actuation control and energy harvesting. The particularity of the DuraAct™ piezo transducers, reported in Figure 3.2, is the protection of the Piezoelectric ceramic layer and electrodes with a special skin of polyimide Kapton film [28]. The polymeric cover gives flexibility to the entire component and ensures the resistance to environmental effects as hygrothermal degradation.

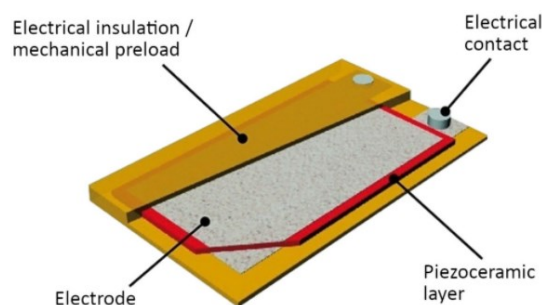


Figure 3.2 – Scheme of the DuraAct™ Piezoelectric transducer [28]

The available geometries of DuraAct™ are reported in Figure 3.3. The rectangular patches are indicated to produce the effect of dilatation and contraction of the structure, both for static actuation at low excitation frequency and dynamic control at higher frequencies. The phenomenon is amplified with parallel transducers designed in a printed circuit. The circular patches are not effective in static condition and are used for dynamic generation of waves at high frequencies.

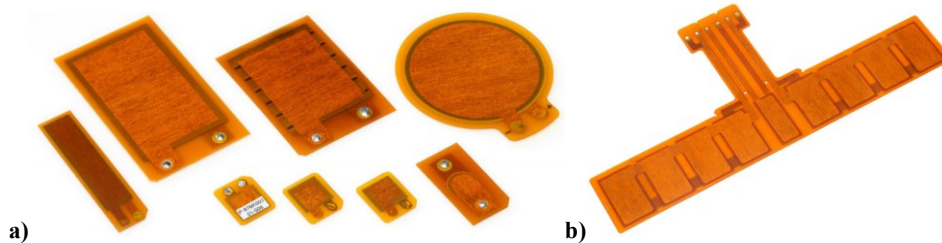


Figure 3.3 – Available geometries of Kapton covered piezoelectric: a) rectangular and circular shapes, b) multi-element films [28]

In particular, for SHM, the preferred geometry changes from the structure and the material, but the circular is the most common, because of the circular waves produced. In this research, the circular Piezoelectric transducer PI DuraAct™ P-876K025 has been used with material PIC255 (modified Lead Zirconate-Lead Titanate), Piezoceramic disk $\phi 10$ mm and thickness 0,2 mm, total thickness of 0,5 mm. The dimensions of the chosen patch and an example of application on the specimens are reported in Figure 3.4. The glue used is a transparent two-components epoxy resin with a curing at room temperature.

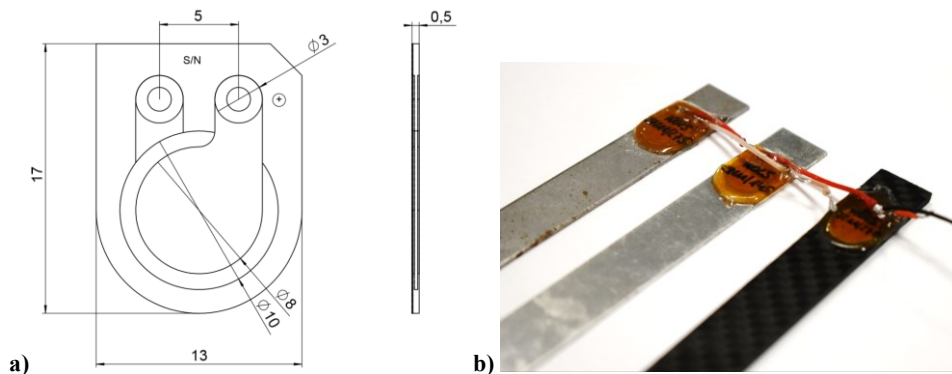


Figure 3.4 – DuraAct™ P-876K025: a) dimensions [28], b) application on specimens

3.1.2. Electrical connections

The Piezoelectric transducers are used in the SHM system as actuators, when excited from a voltage signal converting it to a mechanical deformation, and as sensors, when the movement of the structure is transformed in voltage signal. In both cases, they are connected to the electronic system using a proper connection.

The right contact of the DuraAct™ corresponds to the upper electrode with the positive sign, the left contact to the lower electrode with negative sign. For convention, in this thesis, the red cable has been associated to negative contact and the white/black cable to the positive.

To facilitate the change of specimen under test and eliminate all the electrical disturbs due to the manipulation of the cables, two short cables of 20 mm and 40 mm have been soldered and glued to the Piezo patch, remaining together the structure. The length is different to avoid the contact between the two phases. The short cables are soldered to the 3-meter shielded cable visible in Figure 3.5, that connect the transducer to the control device. In order to reduce the interferences and avoid electromagnetic parasite loops, the shielding is connected in “star” shape to the control device, not to piezoelectric transducer.

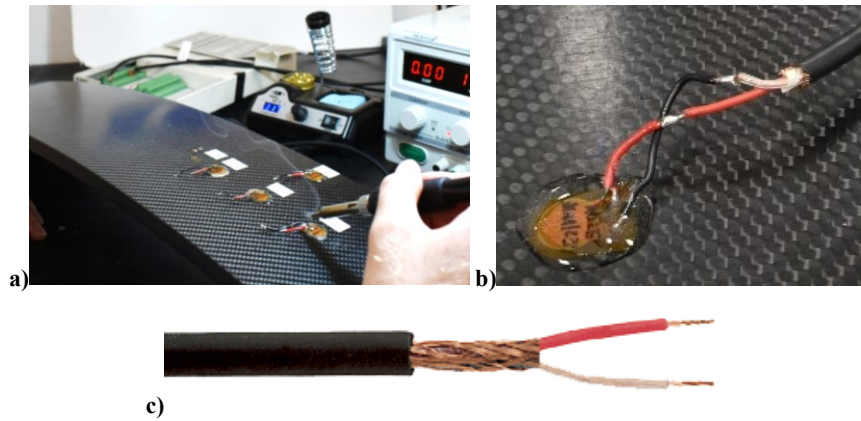


Figure 3.5 – a) Soldering of piezo patches, b) detail of the short cables, c) detail of the shielded cable

3.1.3. Data logger

The control of Piezoelectric transducers, working as actuators or sensors, has been properly made using the National Instruments Multifunction DAQ NI USB-6259. This is a compact device that offers high speed for analog data output and input, remaining at laboratory scale for the component testing. As can be seen in Figure 3.6, the electronic device can be used on table near the computer and connected using a USB 2.0 cable.

Cables of piezo actuator are connected to AO channels, for example white cable (positive) to AO 0 and red (negative) to AO GND. Cables of piezo sensors are connected in single-ended configuration to AI channels, for example white cable (positive) to AI 1 and red (negative) to AI GND. The shielding of each cable is always connected to the nearest GND channel.

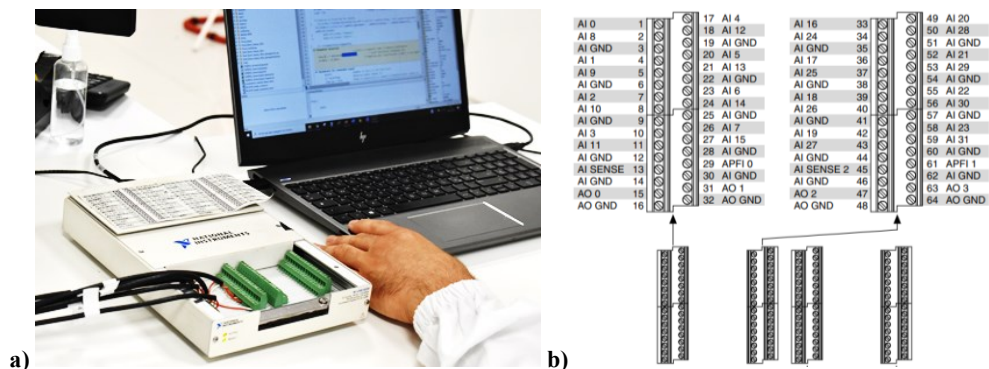


Figure 3.6 – a) National Instruments Multifunction DAQ NI USB-6259 with PC control by MatLab, b) scheme of channels on the spring terminals

The specifications of NI USB-6259 device relevant for the SHM system development are summarized in Table 3.1. There are 32 single-ended Analog Input (AI) channels available, with the possibility to connect 32 piezo sensors. The Sample rate limited to 1 MS/s using USB 2.0 cable is enough to read a periodic signal of 100 kHz, following the rule of Nyquist-Shannon. The Analog-to-Digital Converter (ADC) has 16 bits, about 65 k levels, to read the Voltage signal. Due to these levels, the Multifunction device is able to assess different Absolute Accuracy and Sensitivity in relation to the Input range selected by Software. In this work, the Input range of ± 10 V has been used with 1920 μ V of accuracy and 112 μ V of sensitivity. The signal bandwidth shows the typical knee behavior, with a breakpoint of 1.5 MHz at -3 dB, confirming the good reading of frequencies under 100 kHz.

Regarding the Analog Output (AO), there are 4 channels available, with the possibility to connect 4 piezo actuators. The Digital-to-Analog Converter (DAC) with 16 bits allows the variation of Absolute accuracy changing the Output range. In this work, the Output range of ± 10 V has been used with 2080 μ V of accuracy. The Analog Output channels can supply a maximum current of ± 5 mA, compatible with the current needed by the piezo actuators around 1.5 mA.

Analog Input (AI)	Number of Channels	16 differential or 32 single-ended
	Sample Rate	1 MS/s (USB 2.0)
	ADC Resolution	16 bits
	Input Range	± 0.1 V, ... , ± 10 V
	Absolute Accuracy	52 μ V (at ± 0.1 V), ... , 1920 μ V (at ± 10 V)
	Sensitivity	6 μ V (at ± 0.1 V), ... , 112 μ V (at ± 10 V)
	Breakpoint Frequency	1.5 MHz
Analog Output (AO)	Number of Channels	4
	Update Rate	1 MS/s (USB 2.0)
	DAC Resolution	16 bits
	Output Range	± 5 V, ± 10 V
	Absolute Accuracy	1045 μ V (at ± 5 V), 2080 μ V (at ± 10 V)
	Output Current	± 5 mA

Table 3.1 – Technical specifications of NI USB-6259 device

3.2. Software

3.2.1. LabVIEW Program

The solution to control the National Instruments devices is the NI LabVIEW suite, that uses the graphical language called G to control the hardware and the software functions. A program can be developed on LabVIEW in two parallel spaces: Block Diagram, that contains the graphical code with functional blocks connected by virtual wires; Front Panel, that is the user interface thanks to that the user visualizes the good working of the program when it is running. In Figure 3.7

are reported the Front Panel and the Block Diagram properly developed for the SHM system on LabVIEW.

The program has been tested and validated with NI USB-6259 device for SHM purpose, the interface was user-friendly, but the complexity of the data from piezo sensors required the substitution of the LabVIEW program with a MatLab code for the entire processing and visualization.

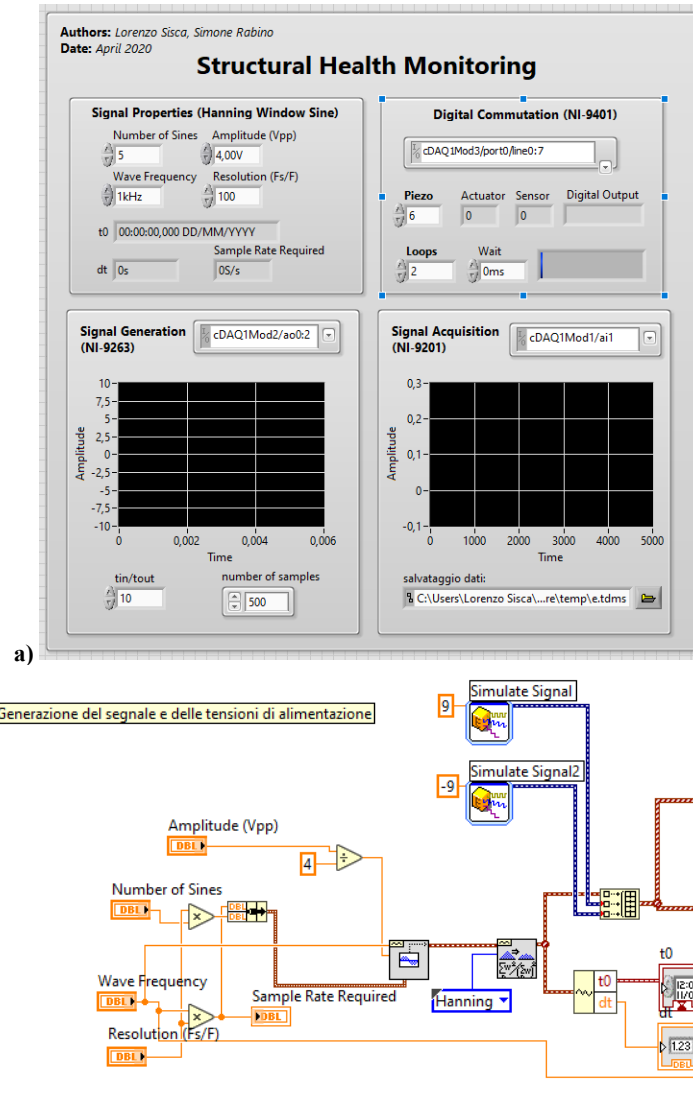


Figure 3.7 – a) Front Panel and b) Block Diagram developed for the SHM system on LabVIEW

3.2.2. MatLab Program

The NI USB-6259 hardware, connected to the PC through a USB 2.0 cable, has been controlled with a properly made MatLab code. Before any measurement, a menu of choice has been implemented to let the user select the test configuration and save the consequent files in a folder named with test and date to avoid overwriting. The MatLab window and the Menu are reported in Figure 3.8.

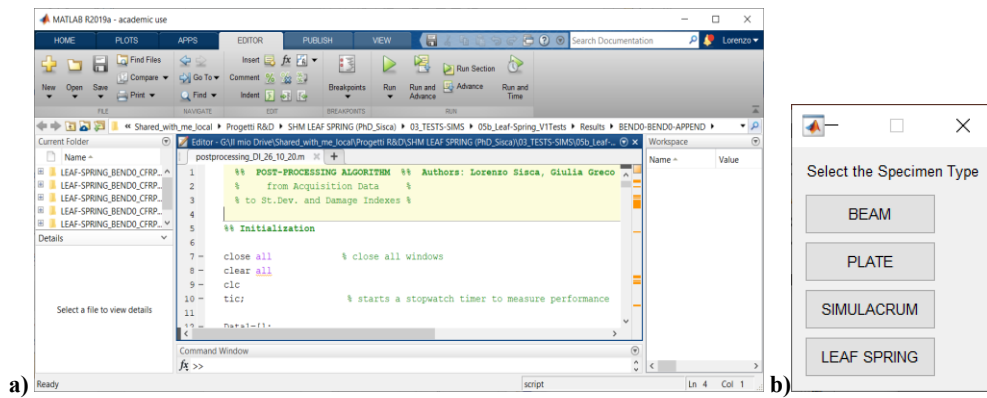


Figure 3.8 – a) MatLab code and b) interactive Menu developed for the SHM system

The excitation signal for actuators and the data acquired from piezo sensors have been stored in .txt files for the analysis and visualized on graphics saved in .fig and .jpg format. An example of graph generated by the program from a SHM test is reported in Figure 3.9. This graphical panel has been generated for each material, specimen, configuration, piezo couple and frequency tested in the experimental activity.

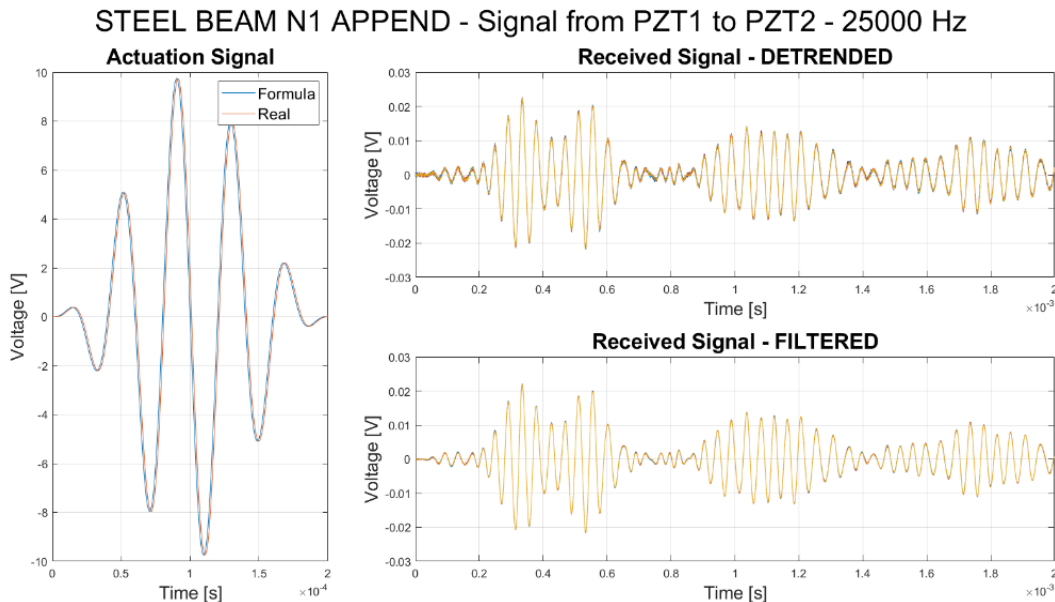


Figure 3.9 – MatLab customized graph representing the actuation and response signals

3.3. Mechanical Test Bench

3.3.1. Dynamometer

The mechanical tests have been executed on the universal testing machine Shimadzu AG-X Plus reported in Figure 3.10.

The main specifications of the machine are:

- Loading Method: Electro-mechanical ball-screw drive
- Load Measurement: Strain-gauge Load Cell 20kN, 300kN

- Load Cell precision: $\pm 1\%$ at 1/1000 of Max. capacity
- Crosshead Position Measurement: Optical encoder
- Crosshead Position Precision: $\pm 0.1\%$, but ± 0.01 mm below 10 mm
- Crosshead Speed Range: 0,0005 ÷ 400 mm/min $\pm 0.1\%$
- Strain Measurement: Non-contact Biaxial Video-extensometer
- Frame Rigidity: 400 kN/mm
- Crosshead Extension: Max. 1000 mm (400 mm with Tensile grips)
- Effective Test Width: Max. 600 mm
- Data Capture Rate: up to 5000 Hz (0,2 msec)
- Data Sampling Rate: 300 kHz
- Compact pneumatic wedge type grips
- Digital display, Operator protections, Led lamps
- Testing software: Trapezium X

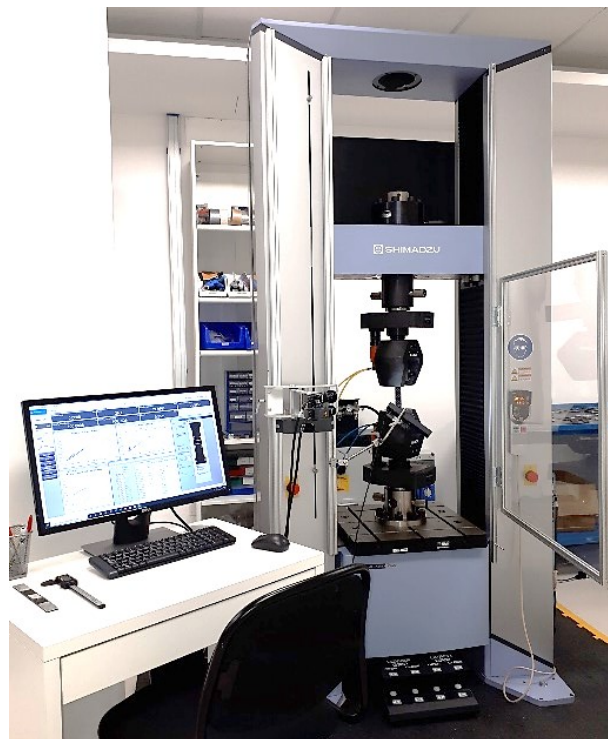


Figure 3.10 – Universal Testing machine Shimadzu AG-X Plus 300 kN

The materials have been characterized with tensile tests using the pneumatic wedge type grips mounting the File-teeth grips for flat samples.

Both metallic and composite specimens have been measured in elongation during the tensile test with the Non-contact Biaxial Video-extensometer, as showed in Figure 3.11. It is placed perpendicularly to the plane of the specimens and is able to monitor during the tensile test the movement of tracking points.

The specifications of the CCD camera are: Lens focal 12,5 mm, Field-of-view 240 mm, Class 0.5, Precision $\pm 1,5$ μm , Sampling rate 100 Hz.

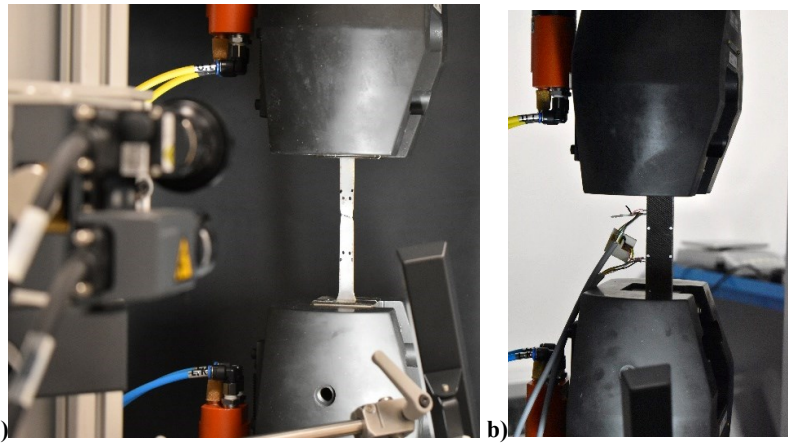


Figure 3.11 –Non-contact Biaxial Video-extensometer used in Tensile test on a) metallic and b) composite specimens

The four-point bending test has been realized with four supports of 5 mm radius head. The fixture, reported in Figure 3.12, is suitable for tests of metals and composite, ensuring the alignment of the supports and avoiding the sliding typical of cylinder supports.

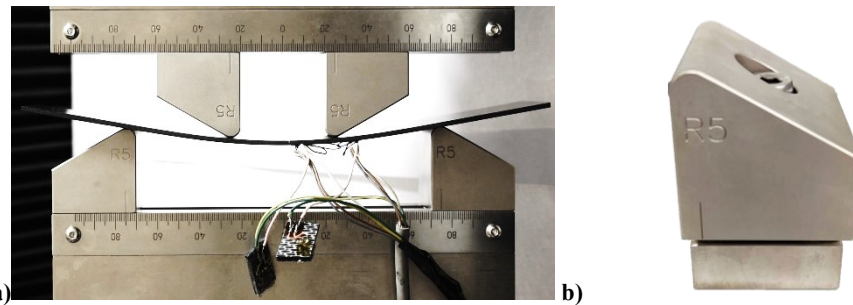


Figure 3.12 – a) Equipment of Four-point Bending test, b) detail of support with 5 mm radius head

3.3.2. Fixture for Leaf Spring Bending

The Leaf Spring component has been tested in bending configuration using a special fixture, as presented in Figure 3.13.



Figure 3.13 – Special fixture for Bending test of Leaf Spring mounted on Shimadzu dynamometer

The equipment reported in Figure 3.14 is composed by two steel IPE beams to give proper rigidity to the bended component. On the lower one, a linear guide provides the sliding of the leaf spring clamps. On the upper one, two cylinders are mounted at a distance of 540 mm in order to realize the four-point bending configuration. The interface with the testing machine is given by four T-slot clamps to the T-slot steel floor and by a cylindrical jig to the load cell. The reciprocal alignment of the beams during the mounting phase is realized using a laser pointer both in the front and lateral side.

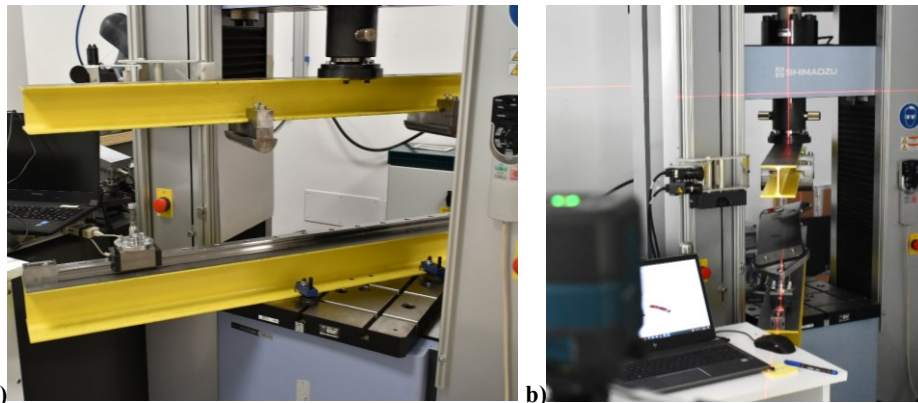


Figure 3.14 – a) Detail of the IPE beams with the linear guide, b) alignment process using a laser pointer

3.3.3. Strain Gauge Amplifier

The deformation on the simulacrum specimens and on the leaf spring component has been measured using the HBK 350 Ω strain gauges illustrated in Figure 3.15. The signal from Wheatstone quarter bridge type II has been amplified with the HBK QuantumX MX1615B data acquisition module at 10 Hz of sampling rate. The system is able to perform both dynamic and static measurements with 16 individually configurable inputs, suitable for reading strain gauges in full, half or quarter bridge (120 or 350 Ω) with data rates up to 20 kS/s per channel. The software used for the measurements is HBK Catman Easy.

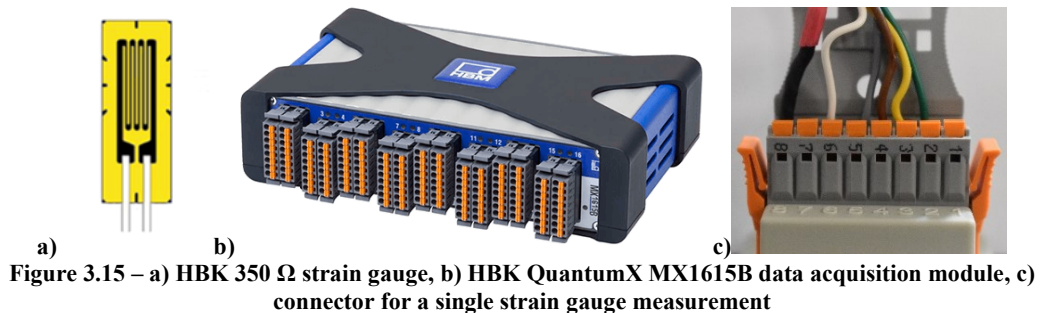


Figure 3.15 – a) HBK 350 Ω strain gauge, b) HBK QuantumX MX1615B data acquisition module, c) connector for a single strain gauge measurement

Chapter 4

Data Analysis

This Chapter explains the original methodology developed to analyze the data acquired from the experimental tests on specimens and leaf spring component, with particular focus on MatLab codes that assess the functionality of the SHM system.

As seen in Chapter 3, the National Instruments hardware is controlled using MatLab for the piezoelectric network management. The code has been properly developed to post-process the acquired data and compare the different conditions of loading, damage and geometry.

The proposed method involves the repetition of ten measurements executed at the same frequency on the same specimen to give a statistical relevance to the results. The average signals of different configurations are compared using specific Damage Index Algorithms that permit to evaluate the significant variation of signals from the calibration phase (Baseline condition) to the testing phase.

4.1. Data Acquisition

4.1.1. Single Frequency

Considering Figure 4.1, the transducer Piezo 1 is the actuator and the Piezo 2 is the sensor, the vibrational wave on their path contains the information about the structural integrity of the component.

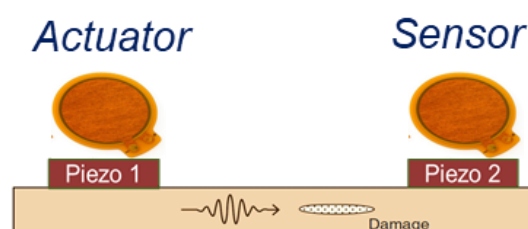


Figure 4.1 – Nomenclature for piezo patches: Piezo 1 is the actuator, Piezo 2 is the sensor

The response signal of the sensor is highly dependent from the type of the excitation signal chosen for the actuator. As reported in the Chapter 1, the most common shape for the burst in the SHM system is a 5 sines Hanning-windowed modulated signal. The Voltage Amplitude chosen for this works is $20 V_{pp}$, as can be seen in the Figure 4.2 a) for the frequency 50 kHz.

The output signal at the chosen frequency is a vector of Voltage values with time intervals of $1 \mu s$, corresponding to 1 MS/s of Update rate. In order to verify the correct generation of the signal from the electronic device, a control output channel has been connected with a control input channel and for each test the real output (red line) is compared with the theoretical values (blue line). The shape is perfectly replicated, only a delay of $1 \mu s$ is found.

As reported in Figure 4.2 b), the excitation of the structure with the burst signal on the piezo actuator is followed by the data acquisition from piezo sensor. The data vector of Voltage values is acquired with time intervals of $1 \mu s$, because of sample rate 1 MS/s, starting from the same instant of burst generation. In this way the output to Piezo 1 and the input from Piezo 2 are synchronous and some evaluations can be made for time comparison of the acquired signals.

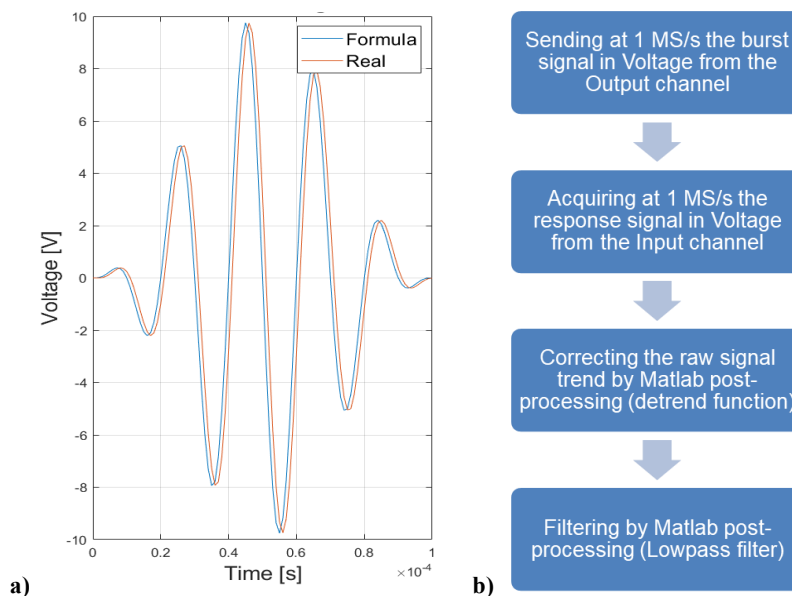


Figure 4.2 – a) Actuation signal shape (blue) and real output (red), b) methodology for data acquisition

The SHM system developed is based on the data acquisition from one sensor each time, avoiding the reduction of the sample rate due to synchronous input channels from different piezo sensors. The total time of acquisition is 10 times longer than the time of burst, that depends on the frequency. The acquisition with the same piezo couple is repeated 10 times for statistical analysis.

The drift of the piezoelectric signal is digitally corrected using a MatLab function called “detrrend” (as explained in Chapter 1). After the detrrend, a low-pass filter is applied on the signal and the cut frequency is the same of the actuation signal. In Figure 4.3 it can be seen the effect of filtering on 10 overlapped piezo responses at 50 kHz, especially in the range of 0,1-0,2 ms.

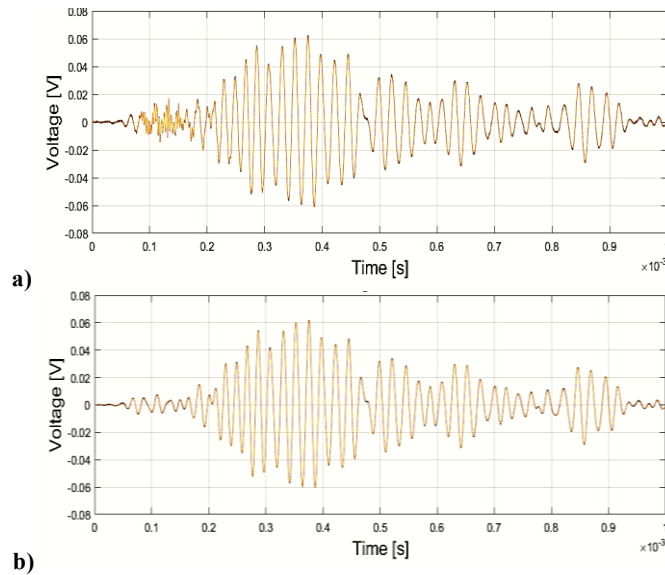


Figure 4.3 – Series of 10 overlapped piezo responses at 50 kHz: a) detrended, b) low-pass filtered

4.1.2. Multiple Frequency

Since the SHM uses a property of Lamb waves to interact with damages in the structure, it is not possible to select a priori the best frequency for specific specimens, geometries, materials and piezo disposition. For this reason, it has been individuated the range of frequencies 1÷100 kHz with step of 1 kHz and for each frequency the procedure explained in the previous paragraph has been applied.

The evaluation of the results at the 100 frequencies is possible with the visualization on spectrogram, in particular the frequency vs. time as a function of voltage (color scale) [51]. Figure 4.4 reports the visualization of the excitation signal from piezo 1 in the entire frequency range. It can be noted that the graph section at 50 kHz is the same of Figure 4.3.

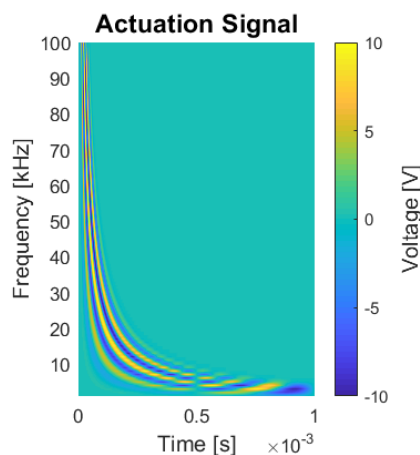


Figure 4.4 – Spectrogram of Actuation signal from piezo 1

In this thesis, the test configuration of the structure “as it is” without defects and damages is called “Baseline”, while the configuration to compare with the Baseline is called “Test” and can be damaged or stressed, according to the specific investigation. The Figure 4.5 reports the example of the Baseline acquisition and

Test acquisition, in particular the values correspond to the average at each frequency between 10 signals acquired from piezo 2.

The thicker yellow and blue lines refer respectively to the positive and negative peaks of Voltage signal over a zero baseline in light blue. The general behavior is due to the velocity increasing with frequency for some groups of waves (according to the basics explained in the Chapter 1). As can be seen, the graphs are very similar and it is impossible to have an information of variations from Baseline to Test configuration without the data post-processing in the entire range of frequencies, as described in the next section.

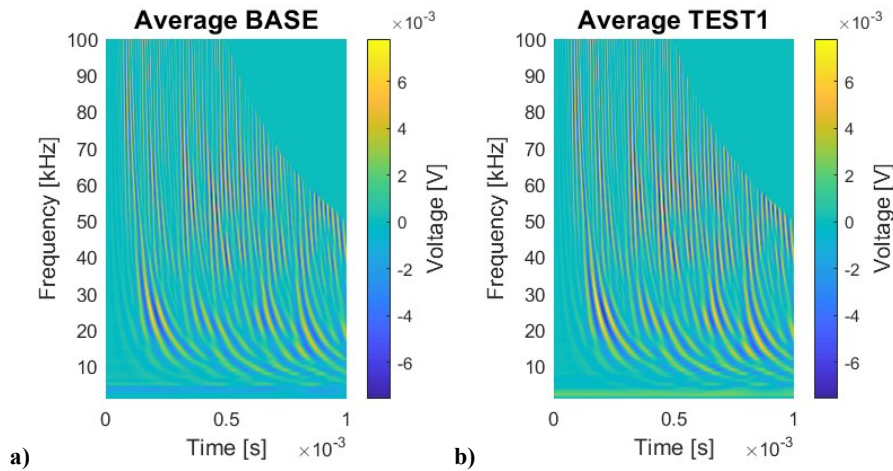


Figure 4.5 – Spectrograms of a) Baseline and b) Test signals from Piezo 2

4.2. Data Processing

The post-processing of data acquired from Piezo 2 in the range of 1÷100 kHz has been carried on in two ways:

- Analyzing the maximum positive and minimum negative peaks at each frequency;
- Comparing each value of the Test configuration with the Baseline using the standard deviation.

The first analysis is useful to understand the trend of the signal amplitude along the frequency range, although it is evaluated the local maximum of the signal. In Figure 4.6 are reported the curves of maximum and minimum Voltage peaks for: Baseline, Test1 and Test2 configurations. From these trends it is possible to evaluate a change in the piezo response looking at a line instead of the spectrogram. The lines at the middle of the graph represent the maximum standard deviation calculated between the 10 signals at each frequency. This value contains the instrumental error for subsequent acquisitions of the same configuration. In fact, it can be noted that under 15 kHz the value of standard deviation is higher than the absolute maximum amplitude of the signal, concluding that in the range 1÷15 kHz the signals are not reliable for the SHM system development.

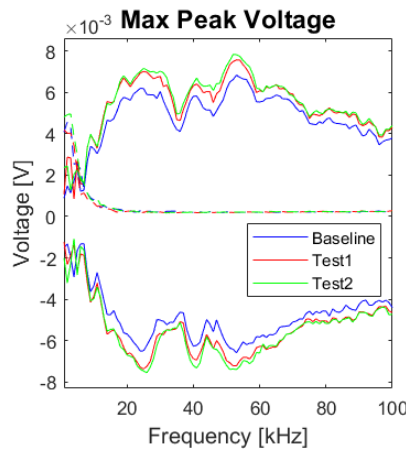


Figure 4.6 – Max and min Voltage peaks for an example of Baseline, Test1 and Test2 configurations

The second analysis is the comparison of the absolute Voltage values for each Test configuration with the Baseline. The Figure 4.7 shows the three-dimensional graphs for an example of standard deviations used for two comparisons Test1 with Baseline and Test2 with Baseline. This type of representation allows to visualize the zones in Frequency and Time domains where the signals acquired in the Test configuration has changed most from the Baseline. In this specific case, the Test2 is related to a damage condition greater than the Test1, in fact there is a wider presence of zones with increased deviation of signal.

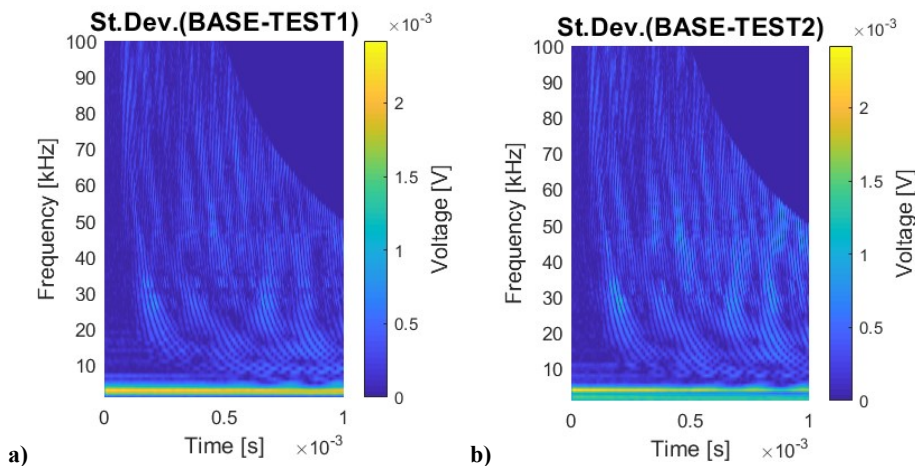


Figure 4.7 – Spectrograms of Standard Deviation between a) Test1 and Baseline, b) Test2 and Baseline

4.2.1. Damage Index Algorithms

The main objective of the SHM system is to identify a variable that can be used to express the state of integrity of the structure. In case of critical damages or working over the design limits, the value of this variable must increase over a threshold leading to an alarm for the user.

In Chapter 1 many theories have been reported to be used in SHM systems. In this thesis the algorithms developed by [37] have been applied to the experimental data of specimens and component testing, since they are an interesting selection of literature algorithms based on cross-correlation and energy comparison between two signals. In Table 4.1 are described the six algorithms used in this Thesis to calculate Damage Index (DI) expressed with the related MatLab functions.

DI Name	Description	MatLab functions
CCA	Maximum of the correlation	$1 - \max(\mathbf{xcorr}[x_{ij}(t), y_{ij}(t)])$
CC0	Zero-lag correlation	$1 - \mathbf{xcorr}[x_{ij}(t), y_{ij}(t)](0)$
CRC	Correlation coefficient	$1 - \mathbf{corrcoef}[x_{ij}(t), y_{ij}(t)]$
NRE	Normalized residual energy	$\int_0^T (x_{ij}(t) - y_{ij}(t))^2 dt$
MA	Maximum amplitude of the difference	$\max[x_{ij}(t) - y_{ij}(t)]$
ENV	Maximum envelope of the difference	$\max[\mathbf{env}(x_{ij}(t) - y_{ij}(t))]$

Table 4.1 – Damage Index Formulations used in this thesis [37]

The algorithms CCA, CC0, CRC are based on the cross-correlation between two series of signals. In particular, the MatLab functions used are:

- *xcorr* that returns the similarity between the first signal and the shifted (lagged) copies of the second signal as a function of the lag,
- *corrcoef* that returns the correlation coefficient between the two series.

The algorithms NRE, MA e ENV are based on the evaluation of amplitude difference between two series of signals. The square difference, in case of NRE, amplify the gap between the signals at the same time of acquisition. The MA consider the global maximum difference that is not the same of the global maximum of the difference envelope, as can be seen in the example of Figure 4.8.

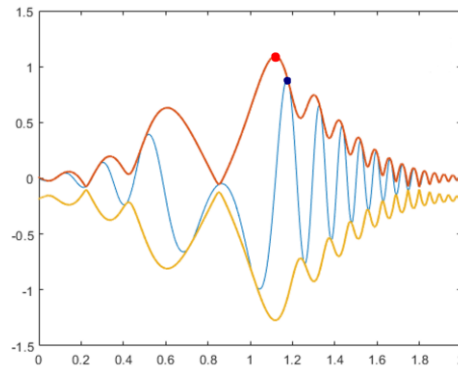


Figure 4.8 – Example of data series (blue line), upper (red line) and lower envelope (yellow line), global maximum of the data series (blue dot), global maximum of the difference envelope (red dot)

The six Damage Index algorithms have been applied for the processing analysis of the two different programs, which functionalities are schematized in Table 4.2.

The first is the “Off-line” program developed to post-process the experimental data in a second time respect to the acquisition. It has been used for the specimens and component testing data, comparing the Baseline configuration with two progressive modifications (damage or stress) in Test1 and Test2 configurations. The range of frequency for the actuation signal was 1-100 kHz and only 1 piezo sensor each time could be analyzed. The second is the “On-line” program developed only for the component testing to post-process the experimental data exactly after they

are acquired. The possibility to calculate the Damage Indices in Real-Time opposes to the scan of the entire frequency range. In this case, only one frequency has been used for the actuation signal and the five piezo sensors have been analyzed subsequently.

Off-line Processing	On-line Processing (Real-Time)
Specimens and Leaf Spring	Leaf Spring
Baseline vs. Test1/Test2	Baseline vs. Real-Time Data
100 Frequencies (1-100 kHz)	1 constant Frequency (X kHz)
1 Piezo couple	5 Piezo couples
6 Damage Index	6 Damage Index
Max. Voltage and St. Dev.	Max. Voltage and St. Dev.

Table 4.2 – Off-line and On-line programs

The Figure 4.9 reports an example of the graphs resulting from the Off-line and On-line programs for data processing. Thanks to the Off-line processing it is possible to visualize a graph for one piezo couple each Damage Index calculated with the data of the configurations Test 1 and Test 2 respect to the Baseline on the range 1-100 kHz. The frequency that expresses the greatest sensitivity, as the increase of Damage Index with the increase of the structure modification (damage or stress), is selected on the Off-line program and used for the On-line program validation. The real-time graph of each Damage Index type monitors all the piezo couples from the starting time of the test. It permits to evaluate the time at which a phenomenon has occurred to the structure and allows to understand the sensitivity of the different Damage Indices.

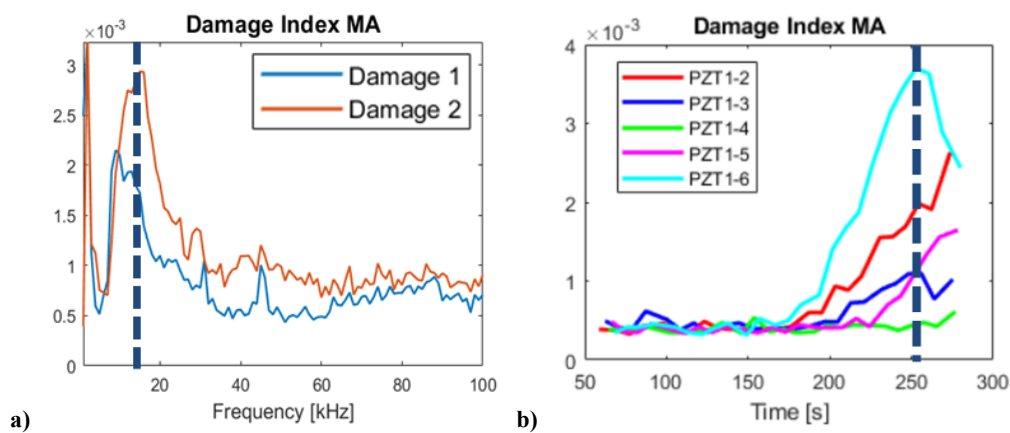


Figure 4.9 – a) Choice of frequency from Off-line program results, b) time reference of the structural change from On-line program results

4.2.2. Off-line Monitoring

The specific format of .txt file (Figure 4.10) has been developed for data saving of acquisition signals. In the first column it is collected the Relative Time in seconds, where the zero corresponds to the starting of the excitation with Piezo 1 and the incremental step is 1 μ s due to the sample rate of 1 MS/s. The second column contains the actuation signal in Volts, that has a 5 sines Hanning-windowed modulation in the range -10 to 10 V. The other columns collect the acquired signals repeated 10 times with the same sensor. The first six rows specify the date of test and the Absolute Time in seconds from the start of test. A single .txt file is related to specific piezo couple actuator-sensor because signals from different piezo couples are not comparable.

Figure 4.11 represents the complete user visualization of each Damage Index calculation of Test 1 and Test 2 configurations respect to the Baseline on the range 1÷100 kHz after the Off-line data processing for a single piezo couple.

1	2020.000000	0.000000	2020.000000	2020.000000	2020.000000	2020.000000	20:
2	11.000000	0.000000	11.000000	11.000000	11.000000	11.000000	11
3	11.000000	0.000000	11.000000	11.000000	11.000000	11.000000	11
4	18.000000	0.000000	18.000000	18.000000	18.000000	18.000000	18
5	9.000000	0.000000	9.000000	9.000000	9.000000	9.000000	9.1
6	10.5		12.354000	14.079000	15.429000		
7	0.00		1.821662	3.551448	4.901513		
8	0.000000	-0.000176	-0.000078	0.000017	0.000013	0.000038	0.1
9	0.000001	0.000470	-0.000064	0.000003	0.000008	0.000053	0.1
10	0.000002	-0.000821	-0.000045	-0.000016	0.000000	0.000069	0.1
11	0.000003	0.002729	-0.000020	-0.000041	-0.000009	0.000086	0.1
12	0.000004	0.009505	0.000006	-0.000069	-0.000018	0.000105	0.1
13	0.000005	0.022413	0.000032	-0.000099	-0.000027	0.000122	0.1
14	0.000006	0.042421	0.000053	-0.000128	-0.000031	0.000140	0.1
15	0.000007	0.070496	0.000069	-0.000155	-0.000032	0.000155	0.1
16	0.000008	0.106316	0.000077	-0.000176	-0.000026	0.000169	0.1
17	0.000009	0.147944	0.000078	-0.000191	-0.000013	0.000181	0.1
18	0.000010	0.195059	0.000072	-0.000196	0.000006	0.000192	0.1
19	0.000011	0.244109	0.000061	-0.000192	0.000031	0.000202	0.1
20	0.000012	0.289933	0.000048	-0.000178	0.000058	0.000211	0.1
21	0.000013	0.333175	0.000038	-0.000154	0.000084	0.000220	0.1
22	0.000014	0.365445	0.000031	-0.000123	0.000107	0.000227	0.1
23	0.000015	0.384162	0.000031	-0.000086	0.000123	0.000234	0.1
24	0.000016	0.384807	0.000039	-0.000045	0.000129	0.000239	0.1
25	0.000017	0.363832	0.000054	-0.000004	0.000124	0.000241	-0
26	0.000018	0.316717	0.000076	0.000034	0.000109	0.000238	-0
27	0.000019	0.241528	0.000101	0.000066	0.000084	0.000231	-0

Figure 4.10 – Data saving format of .txt file for Off-line program

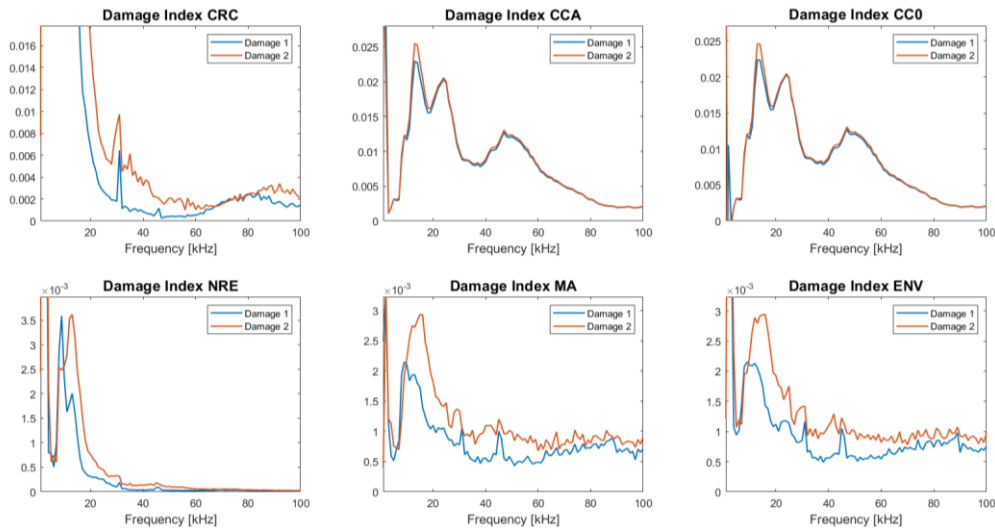


Figure 4.11 – User visualization of each Damage Index of Test 1 and Test 2 configurations respect to the Baseline for the Off-line program

The trend of Damage Index is complex and a uniform methodology to compare them on the entire range of frequency has been chosen. The percentage change of the Damage Index of the Test 2 respect to the Test 1 has been calculated, in order

to relate the sensitivity of the DI algorithms with a percentage increment. An example is reported in Figure 4.12.

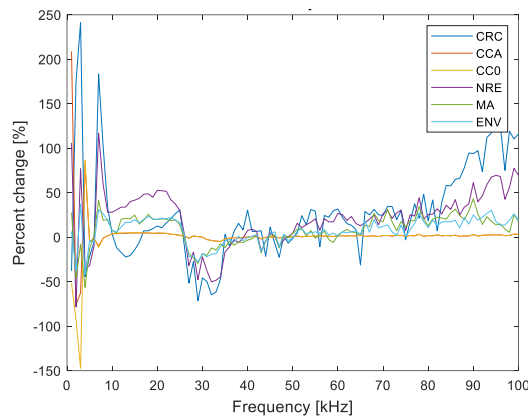


Figure 4.12 – Percentage change of the Damage Index of the Test 2 respect to the Test 1

4.2.3. On-line Monitoring

The Real-Time monitoring, based on the On-line processing program, needs a different type of data saving on .txt files, it is reported in Figure 4.13.

For the data acquired during the test, as already described, the signal is acquired from the same sensor five times in the Baseline configuration, filling the first five columns. Then an average of these measures is calculated and saved in the sixth column. The other columns from the right contain the data acquired in the test configurations and they are used to calculate the Damage Indices. In the first six rows the date and the Absolute Time of the test are registered for each signal. For the Damage Indices saving, another file is compiled referring the DI results to the date of the test and the Absolute Time of the test respect to the Baseline configuration.

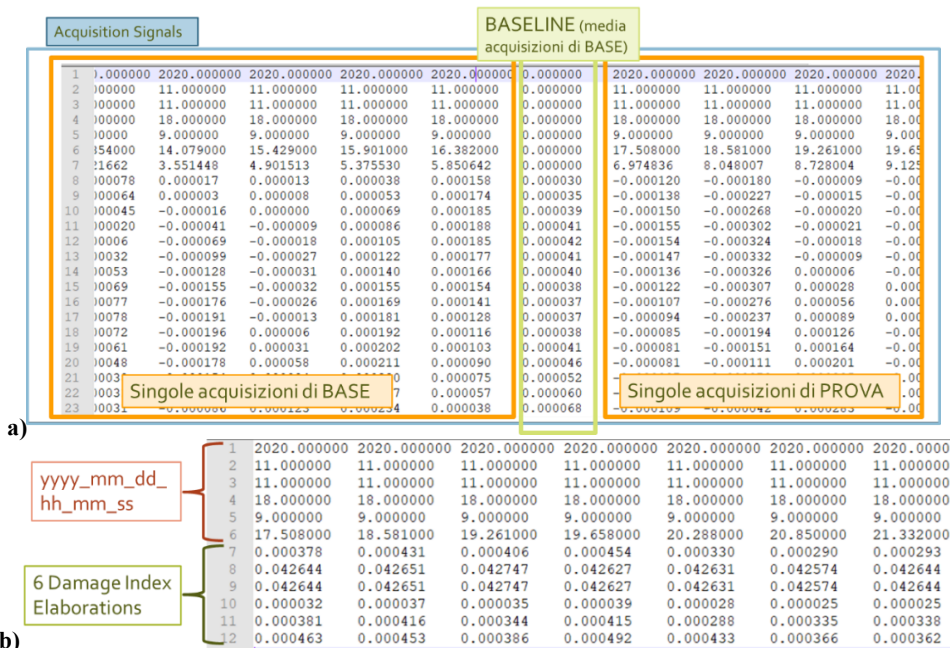


Figure 4.13 – Data saving format of .txt file for On-line program: a) signals, b) Damage Index

In Figure 4.14 are reported the acquired data for each piezo couple overlapped at the same Relative Time. The Baseline signals are plotted in the first column, the Test signals in the second column. In Figure 4.15 is depicted the Real-Time history representing the evolution of the signal, in terms of Voltage and Relative Time, during the test at different Absolute Time values. Looking at the color, it is possible to note important variations in the acquired signal and established the time in which a loss of signal or time shift of peaks occur.

Figure 4.16 permits to evaluate the trend of each Damage Index over the Absolute Time of the test. In addition to the six Damage Index graphs with all the piezo couples' curves, are reported also the trend of the global maximum of the test signal and the maximum standard deviation between the Test and Baseline configurations.

The Voltage scale is set in the range of maximum and minimum values of signal. It is the same for Baseline and Test signals, but varies between piezo couples in order to ease the reading.

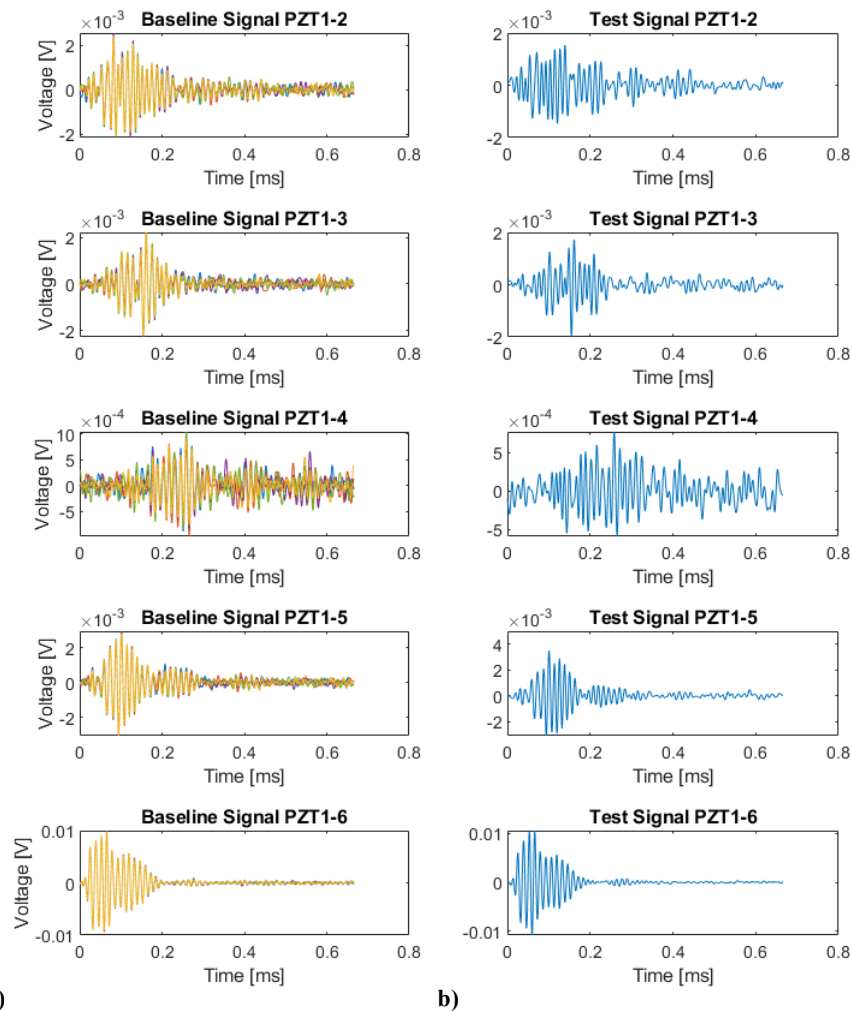


Figure 4.14 – User visualization of the On-line program a) Baseline and b) Test signals for each piezo couple

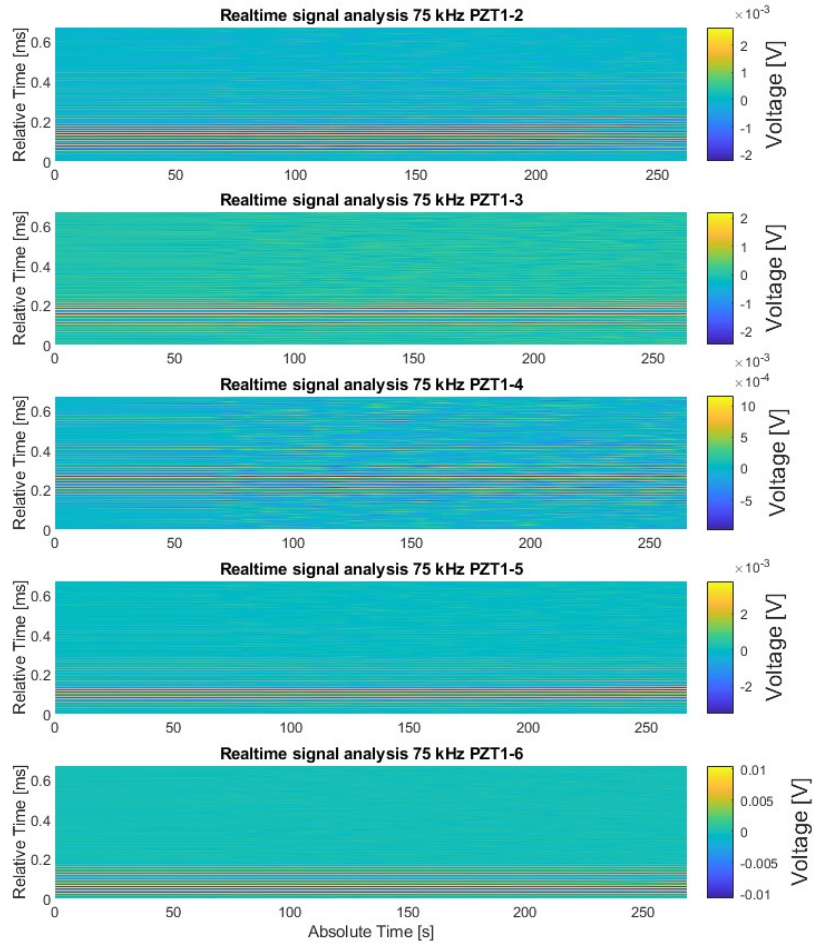


Figure 4.15 – User visualization of the On-line program Realtime signals for each piezo couple

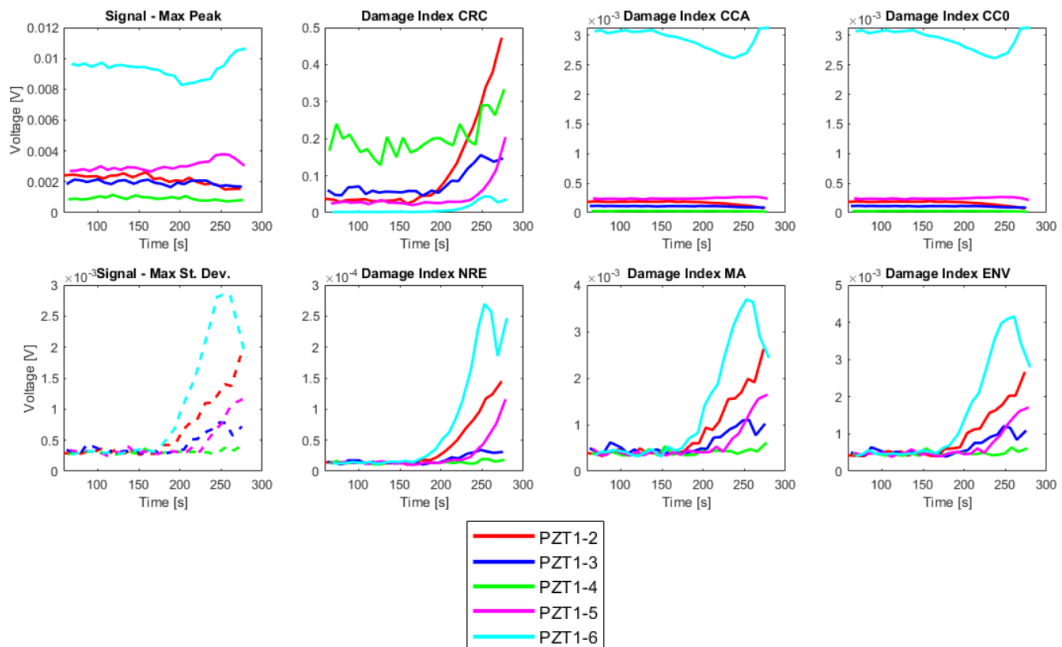


Figure 4.16 – User visualization of the On-line program Damage Index for each piezo couple

Chapter 5

Experimental Results

5.1. Preliminary Tests

5.1.1. Bending Tests on Simulacrum

The four-point bending tests for characterizing the simulacrum specimens have been realized at crosshead speed of 2 mm/min with an inner supports span of 80 mm and an outer span of 160 mm. Figure 5.1 shows the bending fixture and the Simulacrum with the piezoelectric patches and the strain gauges.

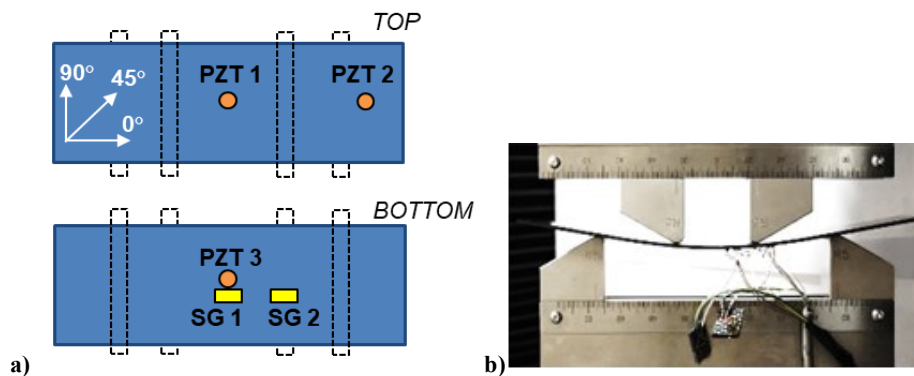


Figure 5.1 – a) Sensors' network on Simulacrum specimen, b) Four-point Bending configuration

The force vs. displacement and force vs. strain curves are reported in Figure 5.2. In correspondence of 1000 N for steel and 500 N for aluminum, it has been identified a deviation from linearity for the second strain gauge, which is placed in lateral position between the upper and lower support. For this reason, to study all the simulacrum specimens in the same elastic behavior, it has been chosen three loading steps at 0 mm, 0.3 mm and 0.6 mm. These configurations of static loading will be reported in the following paragraphs for the validation of SHM methodology on the stressed structures.

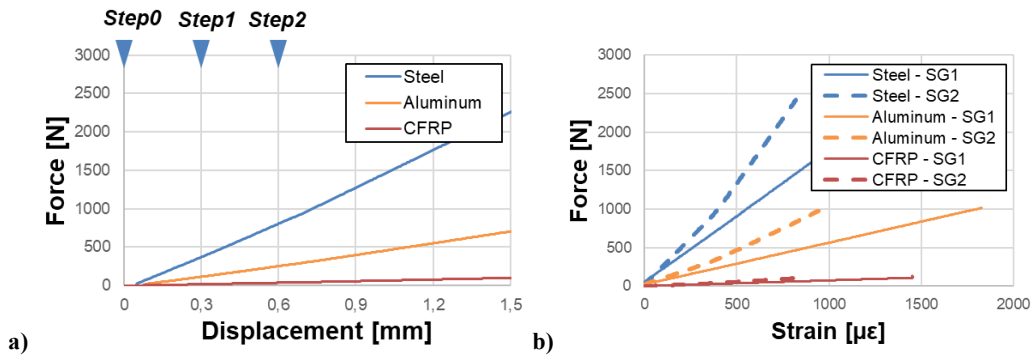


Figure 5.2 – Experimental results of the Bending tests on Simulacrum specimens: a) Force vs. Displacement, b) Force vs. Strain

5.1.2. Bending Tests on Leaf Spring

The bending test on the leaf spring has been conducted with a controlled crosshead speed of 5 mm/min until reaching 50 mm of displacement, the maximum recorded load was 4 kN.

Figure 5.3 shows the representation of the half Leaf Spring component with the piezoelectric patches and the strain gauges. Both strain gauges are placed in the center of the component to monitor the longitudinal strain during the test.

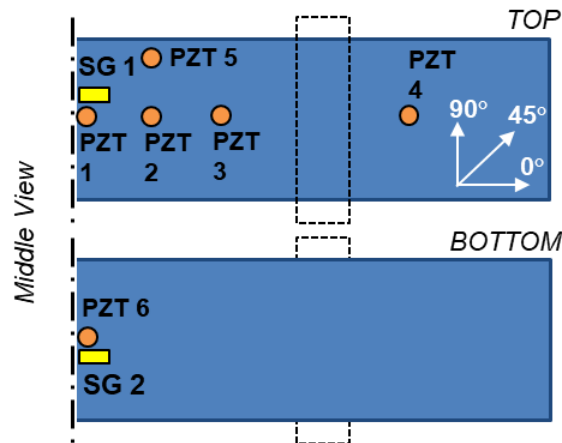


Figure 5.3 – Leaf Spring with the top and bottom faces of the half part with sensors

The component under test has been studied with the force-displacement and the force-strain curves, reported in Figure 5.4. The behavior is linear both for displacement and strain until 4 kN of bending force, without critical signs of yielding and damage. Because in this thesis the SHM methodology has to be validated in the widest range of bending travel for the leaf spring, five steps of load have been considered at 0, 1, 2, 3 and 4 kN.

In Figure 5.5 it is possible to observe the position of the leaf spring at each bending load step. It can be seen that the component changes from curved to flat shape, highlighting the flexible behavior during the working as suspension on vehicle, mainly due to the 45° carbon fiber layers.

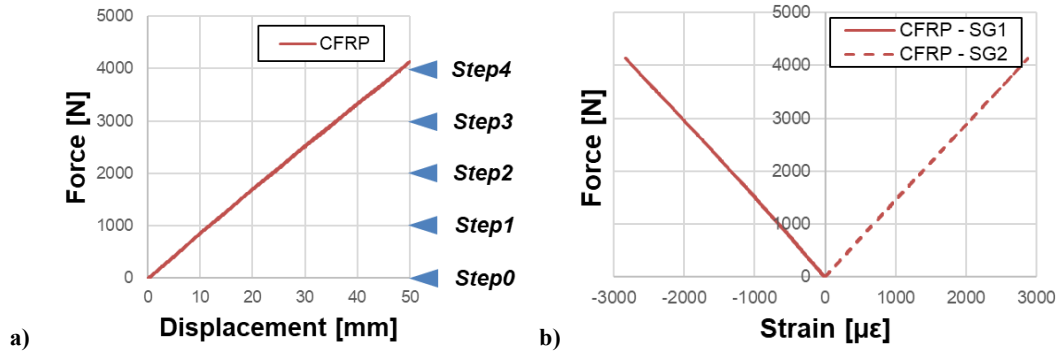


Figure 5.4 – Experimental results of the Bending tests on Leaf Spring component: a) Force vs. Displacement, b) Force vs. Strain

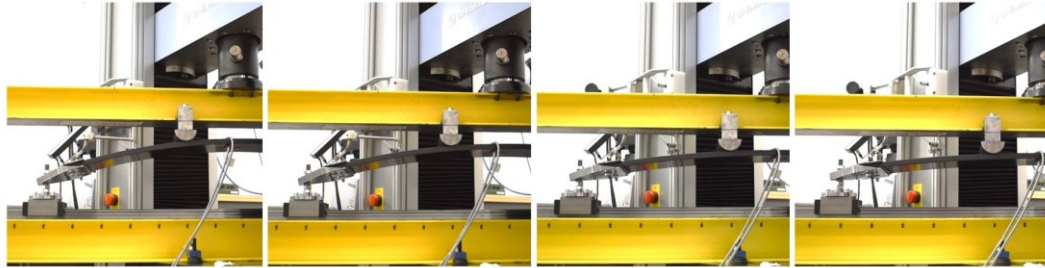


Figure 5.5 – Progression of Bending test on Leaf Spring at 1, 2, 3 and 4 kN

5.2. SHM Off-line Tests

The Off-line Processing of SHM data have been applied on static tests scanning all the PZT couples at 100 frequencies from 1 kHz to 100 kHz with steps of 1 kHz. The PZT 1 remained the actuator for all the iterations and the other piezo patches worked as sensors.

The static configurations for the specimens and the leaf spring have been tested, considering the free condition, the clamping and the bending effects. To identify the influence of the different factors on the SHM system signals, some comparisons have been made, between a Baseline condition and two other configurations.

As described in the Chapter 4 for the Off-line methodology, for each specimen and configuration at 100 frequencies have been realized the representations of:

- raw signal data, as the maximum peak and the maximum standard deviation recorded for the same data series,
- the standard deviation for a Test configuration related to Baseline,
- the trend of Damage Index for Test 1 and Test 2 related to Baseline,
- the percentage variation of Damage Index for Test 2 related to Baseline respect to Test 1 related to Baseline.

To facilitate the reading, in the following paragraphs are reported the percentage variation of Damage Index for each specimen, while the complete representation of acquired data and processing graphs are reported in the Appendix A.

5.2.1. Beam specimen

The Beam specimen is a rectangle of 300x12 mm, it has been tested in the configurations: Appended, On table and Clamped at one edge. Because of the similarities of Appended and On table configurations respect to the Clamped one, only the Appended results are reported. The artificial damage is placed in the center between actuator and sensor. As presented in Figure 5.6, the couple of piezo PZT 1-2 has been monitored to understand the effect of the clamping and the two types of damage on the Piezoelectric response at 100 frequencies in the range 1÷100 kHz.



Figure 5.6 – Piezo couple PZT 1-2 studied for the influence of Damage on the Beam specimen

In Figure 5.7 are reported the Percentage Variations of Damage Index of Damage 2 to No Damage respect to Damage Index of Damage 1 to No Damage for PZT 1-2 piezo couple, for the Beam specimens made of Aluminum, Steel and Carbon Fiber.

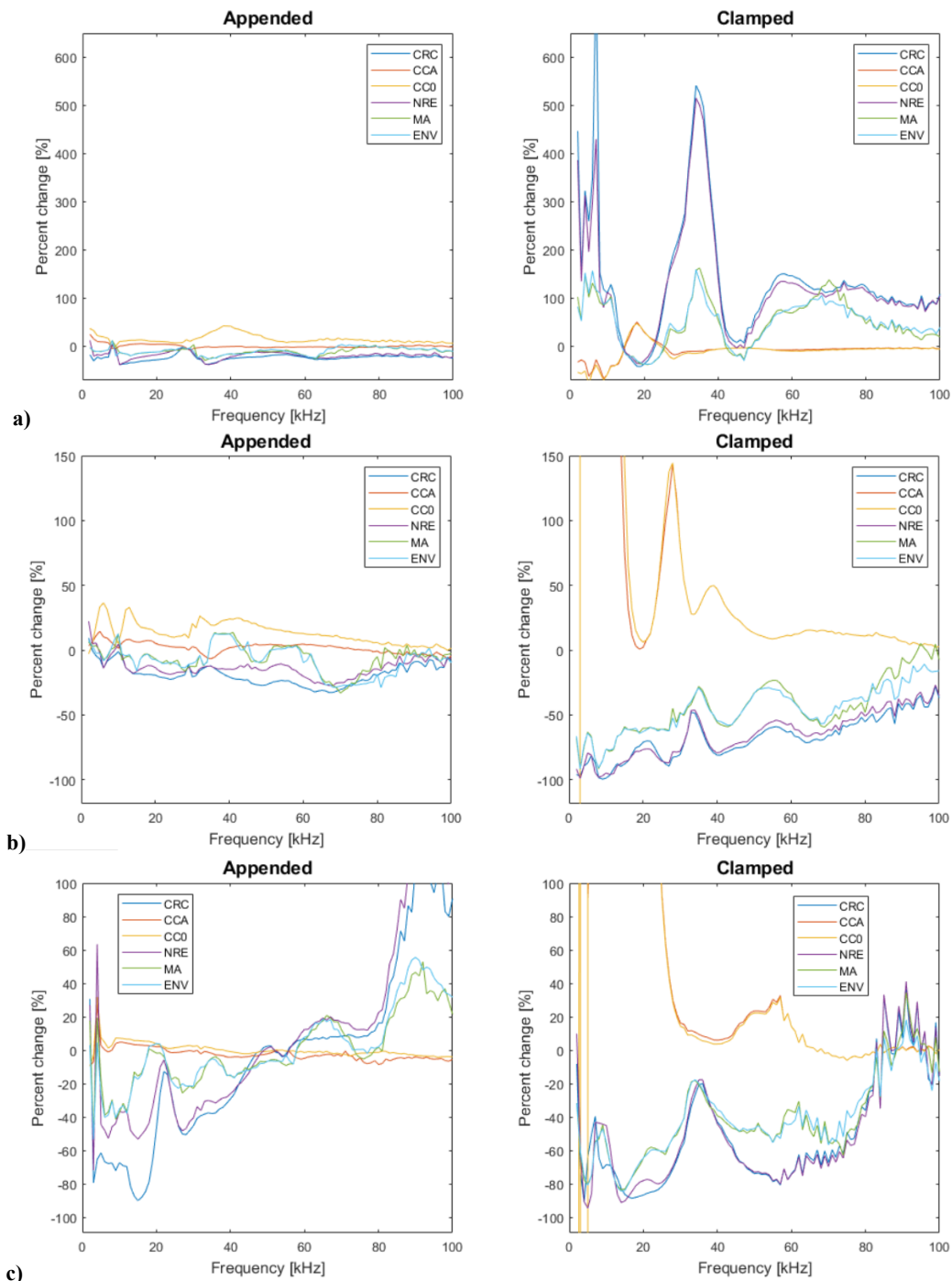


Figure 5.7 – SHM Off-line Test results for the Beam specimens made of a) Aluminum, b) Steel, c) Carbon Fiber

Especially for the Beam specimen made of Steel, it is possible to state that Clamped configuration leads to a general increase of Damage Index value respect to Appended one.

For all the materials investigated, for the Algorithms CRC, NRE, MA, ENV at the frequencies 35 kHz and around 90 kHz, there is a peak related to the detection of the Damage 2 (passing hole diameter 4 mm) respect to Damage 1 (surface indentation diameter 2 mm). For the Algorithms CCA, CC0 there is not a common behavior within the materials.

In other words, the data processing highlights clearly that some frequencies in the range 1÷100 kHz are more sensitive to detect an increasing of the Damage severity.

5.2.2. Plate specimen

The Plate specimen is a square of 250 mm side, it has been tested in the configuration On table. The Appended configuration and the Clamped one have been evaluated, but not applied. The artificial damage is placed on the diagonal of the plate, at 100 mm from each edge in the corner of the piezo couple PZT 1-2. As it is possible to see in Figure 5.8, the damage could interact with the response signal of PZT 2 and consequently of PZT 3. For this reason, the piezo couples PZT 1-2 and PZT 1-3 have been monitored to understand this effect, while PZT 1-4 forecast to be not affected. The influence of two types of damage on the Piezoelectric response has been observed at 100 frequencies in the range 1-100 kHz.

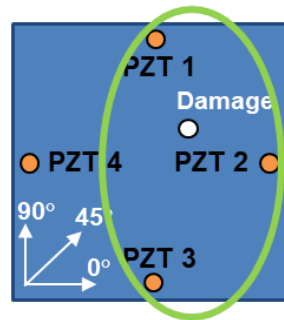


Figure 5.8 – Piezo couples PZT 1-2 and PZT 1-3 studied for the influence of Damage on the Plate specimen

In Figure 5.9 are reported the Percentage Variations of Damage Index of Damage 2 to No Damage respect to Damage Index of Damage 1 to No Damage for PZT 1-2, PZT 1-3, PZT 1-4 piezo couples, for the Plate specimens made of Aluminum, Steel and Carbon Fiber.

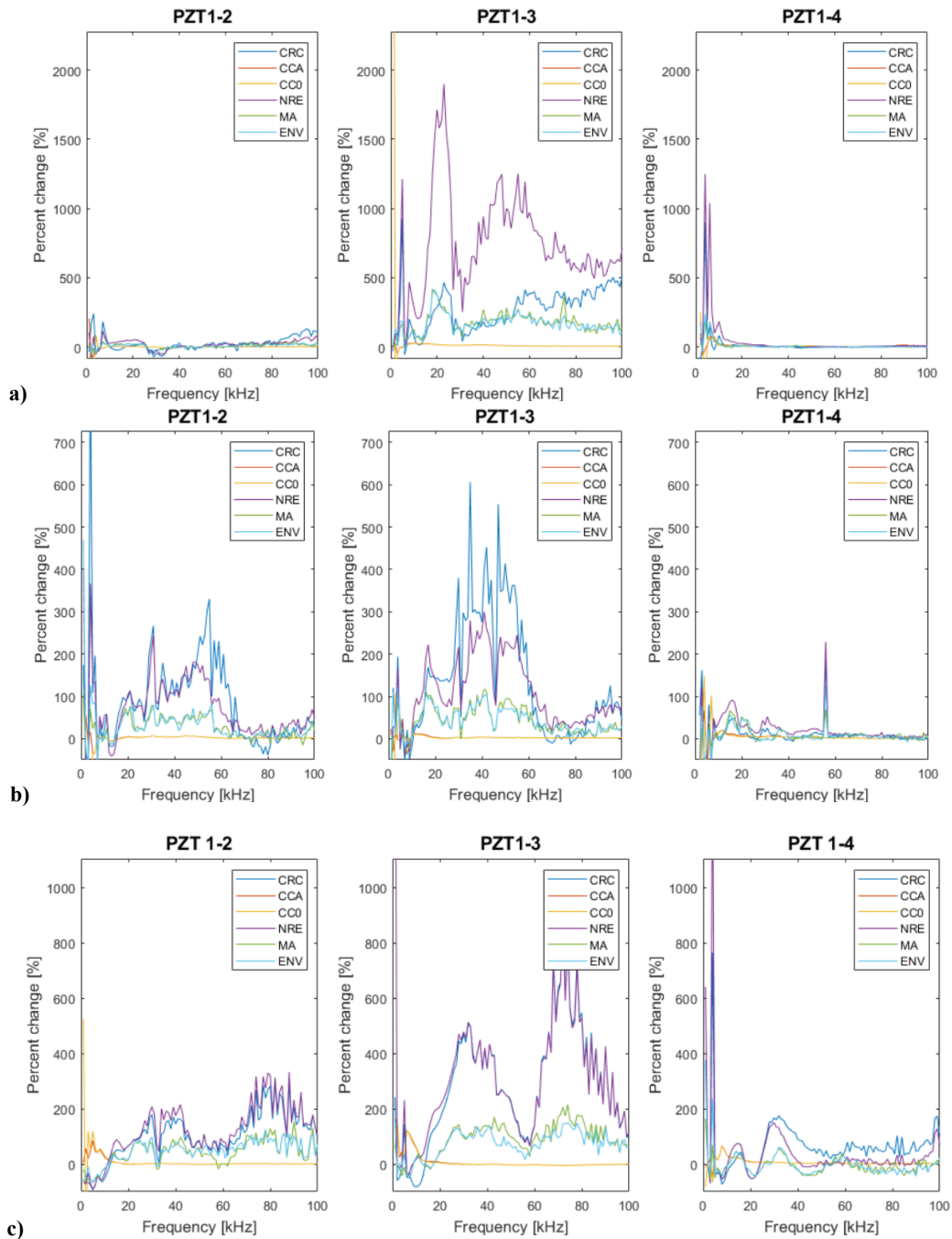


Figure 5.9 – SHM Off-line Test results for the Plate specimens made of a) Aluminum, b) Steel, c) Carbon Fiber

For all the materials investigated, in particular for the Algorithms CRC, NRE, MA, ENV, a great increase of Damage Index has been registered related to the detection of the Damage 2 respect to Damage 1. Especially for the Plate specimen made of Carbon Fiber, it is possible to identify two peaks at about same frequencies found for the Beam, 35÷90 kHz.

Regarding the different Piezo sensors, have a considerable influence of the Damage severity increasing on the Damage Index of PZT 2 and PZT 3 respect to PZT 4. This confirms the initial hypothesis of Damage interaction on the Piezo response when it is on the path of the piezo couple actuator-sensor.

To explain the major Damage Index related to PZT 1-3 respect to PZT 1-2, it is necessary to observe the distance of the two piezo couples. The distance between

PZT 1-3 is 200 mm at 0° direction, while for PZT 1-2 is 140 mm at 45°. The waves from actuator PZT 1 reach first the sensor PZT 2, a part of these reflect to the edge of the plate and reach the sensor PZT 3 together with the waves on the direct path of PZT 1-3. In this way, the influence of the Damage is amplified on the Plate specimen due to reflections of the waves on the edges, leading to a greater Damage Index for couple PZT 1-3 than PZT 1-2.

5.2.3. Simulacrum specimen

The Simulacrum specimen is a rectangle of 250x70 mm, it has been tested in the Bending configuration, with three loading steps at 0 mm (BEND0), 0.3 mm (BEND1) and 0.6 mm (BEND2). The position of PZT 2 has been defined to study the interaction with the upper and lower support cylinders of the bending fixture. The artificial damage is placed in the center of the piezo couple PZT 1-2, in a zone between the upper and lower cylinders, as highlighted in Figure 5.10. In this way, the excitation waves from PZT 1 actuator pass through two cylinders and the damage before to be received from PZT 2 sensor, so the piezo response could be highly influenced.

Another evaluation has been made for PZT 3 sensor, that has been placed exactly under the PZT 1 actuator. In this case, the study has been directed on the transmission of waves through the section of the specimen and how they are influenced from the bending loads. Both the piezo couples PZT 1-2 and PZT 1-3 have been monitored to understand the effect of bending loads and two types of damage on the Piezoelectric response at 100 frequencies in the range 1-100 kHz.

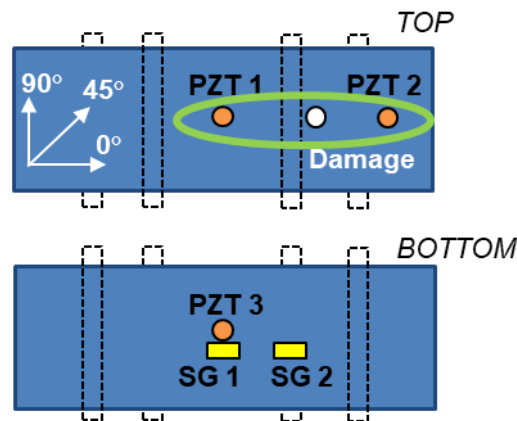


Figure 5.10 – Piezo couple PZT 1-2 studied for the influence of Damage and Bending load on the Simulacrum specimen

In Figure 5.11 are reported the Percentage Variations of Damage Index of BEND2 to BEND0 respect to Damage Index of BEND1 to BEND0 in the three damage conditions, for the Simulacrum specimens made of Aluminum, Steel and Carbon Fiber for PZT 1-2 piezo couple.

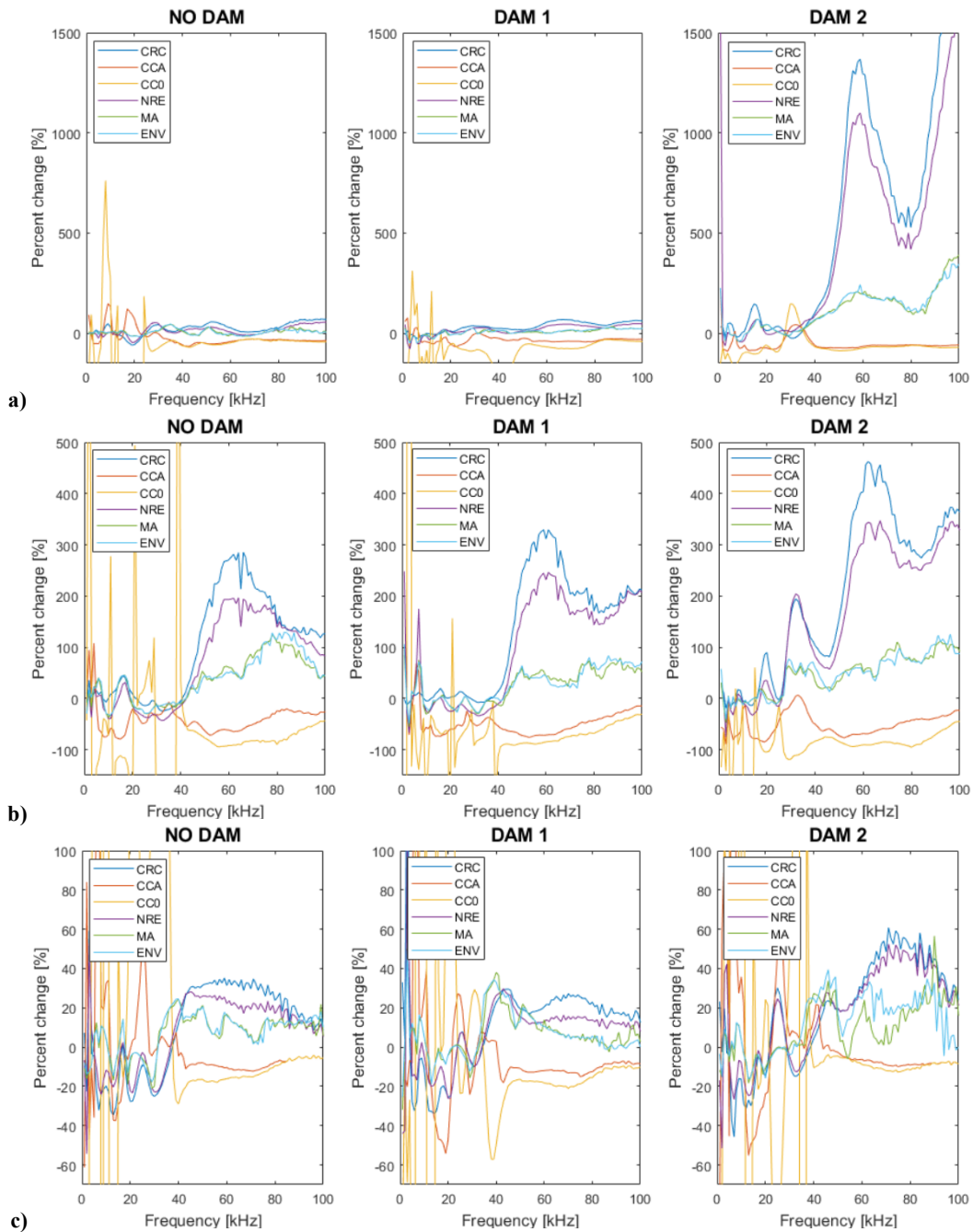


Figure 5.11 – SHM Off-line Test results for the Simulacrum specimens made of a) Aluminum, b) Steel, c) Carbon Fiber for the PZT 1-2 piezo couple

In

Figure 5.12 are reported the Percentage Variations of Damage Index of BEND2 to BEND0 respect to Damage Index of BEND1 to BEND0 in the three damage conditions, for the Simulacrum specimens made of Aluminum, Steel and Carbon Fiber for PZT 1-3 piezo couple.

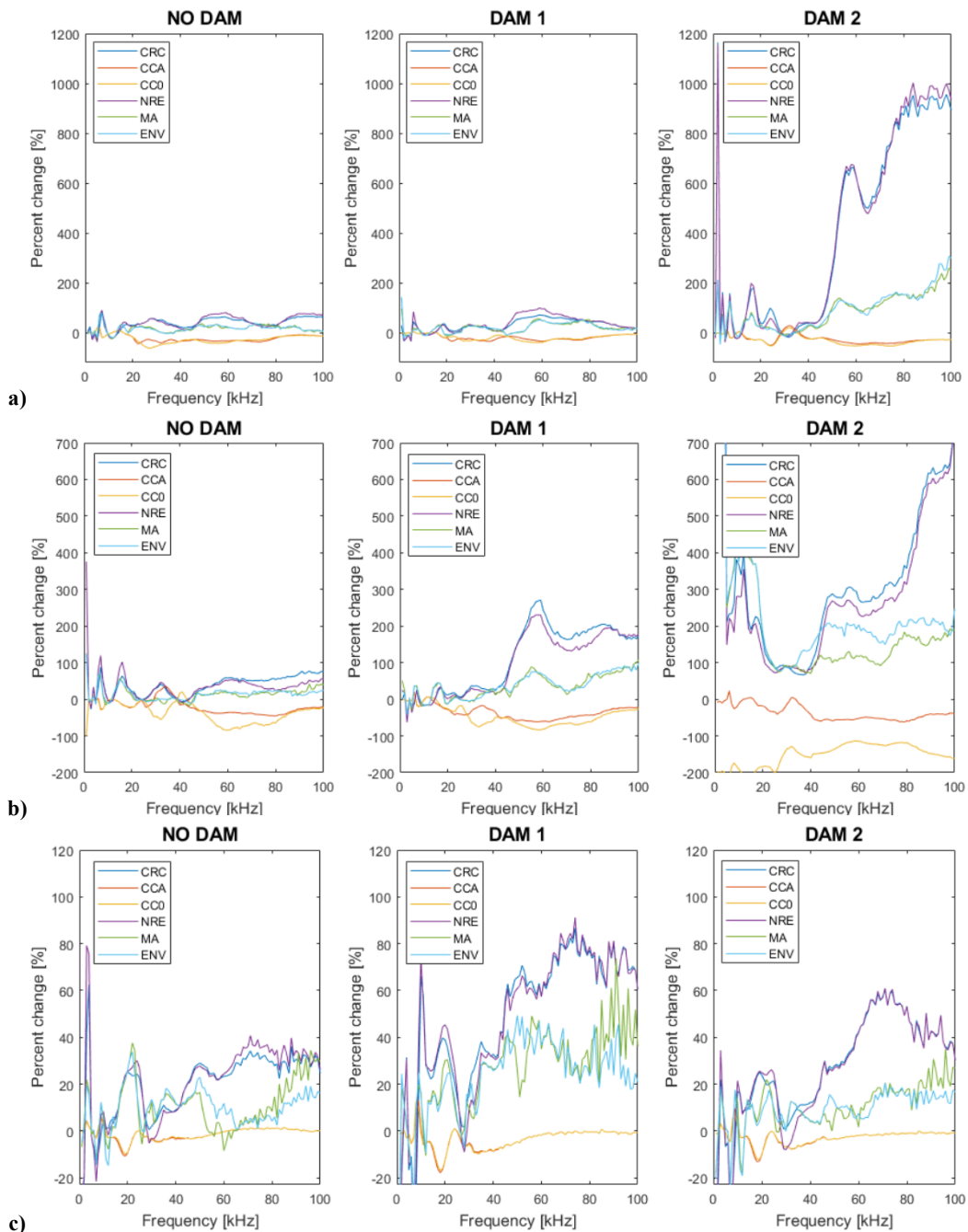


Figure 5.12 – SHM Off-line Test results for the Simulacrum specimens made of a) Aluminum, b) Steel, c) Carbon Fiber for the PZT 1-3 piezo couple

For all the materials investigated, both piezo couples PZT 1-2 and PZT 1-3 showed interesting behavior for Damage Indexes processed with Algorithm CRC and NRE, so hereby are reported the observations only for these two Algorithms.

It can be noted that, for all the configurations and Damage conditions, the Bending step 2 leads to a higher Damage Index than Bending step 1, in fact there is always a positive percentage variation. This demonstrates that the stresses into the structure affect the final results of the SHM system, so they have to be considered for each application.

Furthermore, the Damage condition of the specimen affect the variation of Damage Index between Bending step 2 and step 1, resulting in a progressive growing trend. In the wide range of 1-100 kHz, over 50 kHz some peaks can be

highlighted for all the tests, in particular the frequency of 75 kHz showed the most sensitivity to bending load changes and damage severity increasing.

5.2.4. Leaf Spring component

The Leaf Spring component can be simplified as a curved rectangle of 1000x150 mm, it has been tested in the Bending configuration, with five loading steps (established in the previous paragraph) at 0, 1, 2, 3 and 4 kN. No damage has been applied on the component since it is a unique prototype.

As represented in Figure 5.13, the half Leaf Spring top and bottom views are illustrated to focus the attention on the Piezoelectric patches disposition. The sensors PZT 2, PZT 3 and PZT 4 are aligned at 0° with actuator PZT 1, so they are all on the same carbon fibre bundles. This could produce a better propagation of waves instead of other angulations. To study this effect, the sensor PZT 5 is placed at 45° from PZT 1. The sensor PZT 6 is placed under PZT 1, as already seen for the Simulacrum specimen.

Both the piezo couples PZT 1-2, PZT 1-3, PZT 1-4, PZT 1-5 and PZT 1-6 have been monitored to understand the effect of bending loads on the Piezoelectric response at 100 frequencies in the range 1÷100 kHz.

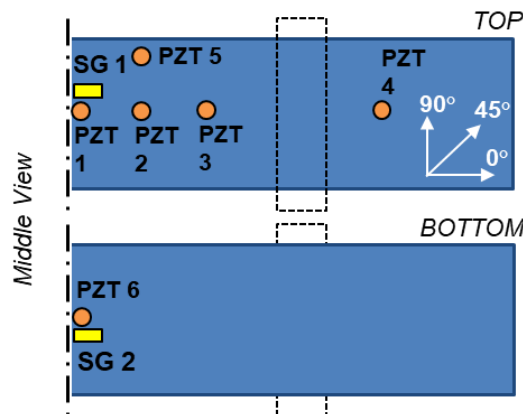


Figure 5.13 – Half part of Leaf Spring component with Piezoelectric patches and Strain gauges

In Figure 5.14 is reported the Percentage Variation of Damage Index of BEND2 to BEND0 respect to Damage Index of BEND1 to BEND0 for each piezo couple on the Leaf Spring.

For all Piezo couples, it is possible to note that Bending step 2 shows a Damage Index higher than Bending step 1, in fact there is always a positive percentage variation. The other comparisons for all piezo couples at the Bending step 3 and step 4 are reported in the Appendix A and showed the same behavior. As for the Simulacrum specimen, it has been found that the stresses into the structure affect the final results of the SHM system, especially for the piezo sensor PZT 6 placed at the opposite face of the actuator PZT 1.

The maximum increasing of Damage Index has been registered for frequency over 50 kHz, around 75 kHz, as for the Simulacrum specimen.

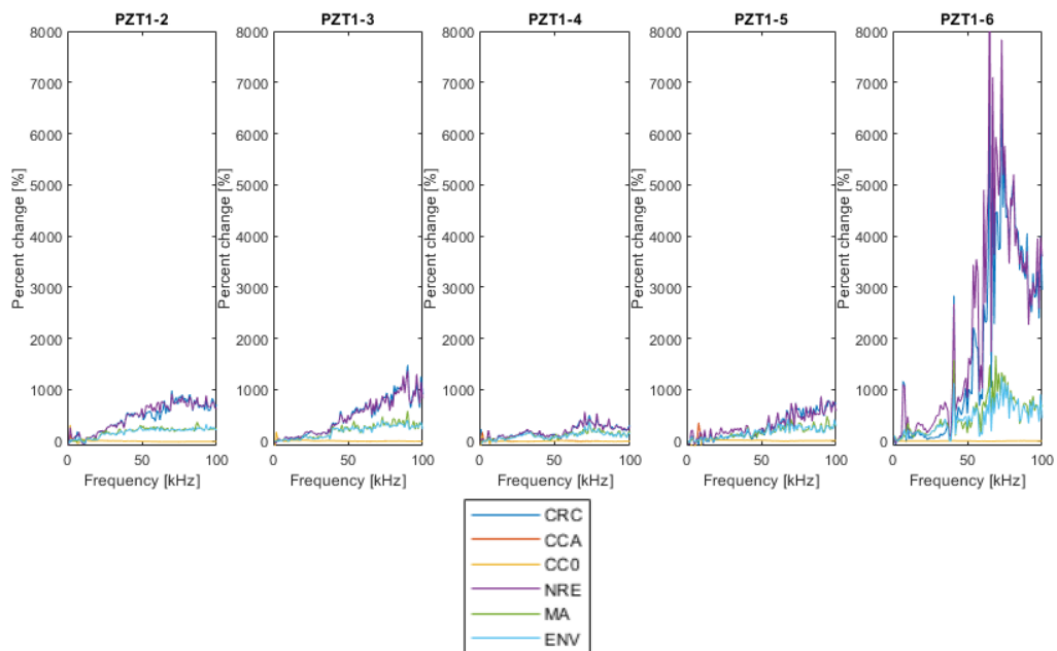


Figure 5.14 – SHM Off-line Test results for each piezo couple on the Leaf Spring

In Figure 5.15 are reported the Percentage Variation of Damage Index of BEND2, BEND3, BEND4 to BEND0 respect to Damage Index of BEND1 to BEND0, for piezo couples PZT 1-2 and PZT 1-4 on the Leaf Spring.

The comparison between all Bending steps respect to Bending step 1 for a single Piezo couple showed definitely the high relation of Damage Index with the stress in the structure, bringing benefit to the analysis. The Damage Index Algorithms CRC and NRE are the most sensitive to the loading variation.

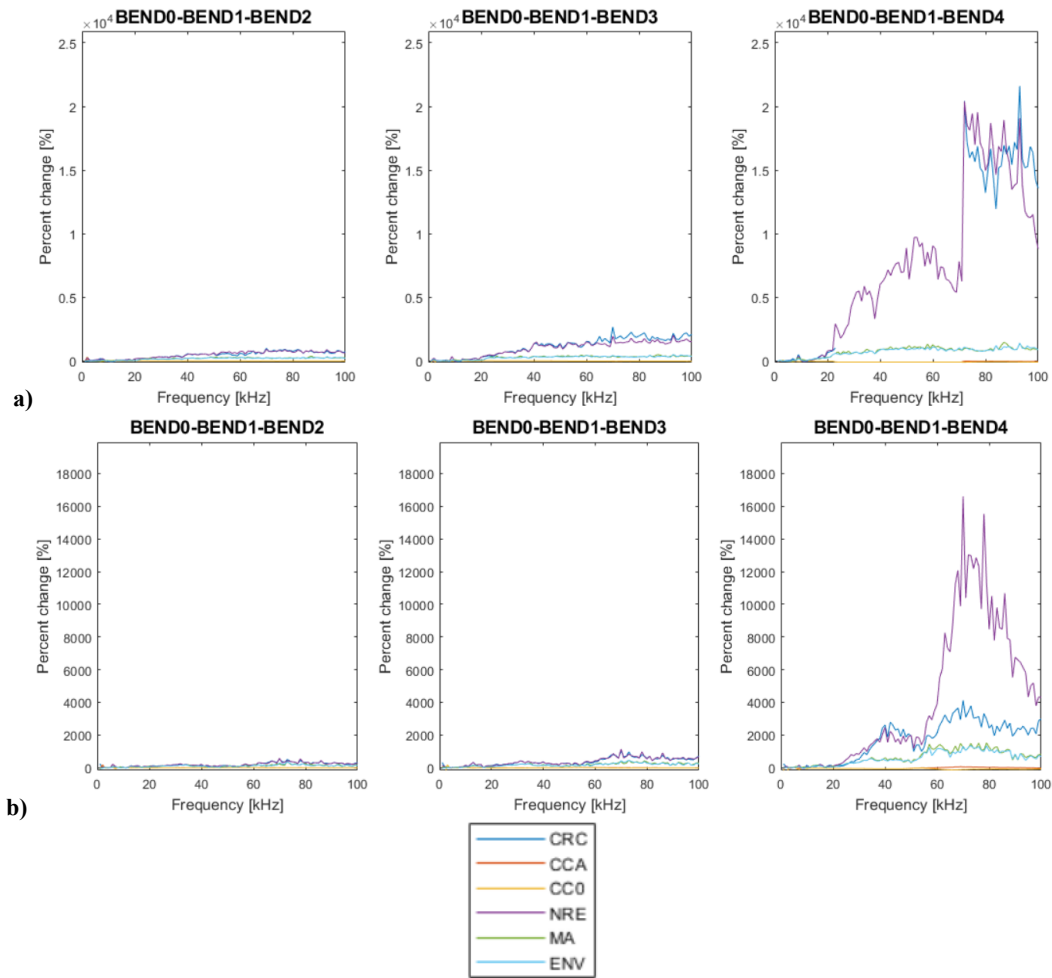


Figure 5.15 – SHM Off-line Test results for a) PZT 1-2 and b) PZT 1-4 on the Leaf Spring

5.3. SHM On-line Tests

The On-line Processing of SHM data have been executed monitoring all the piezo couples of the Leaf Spring component at the frequency of 75 kHz, chosen with the results of the SHM Off-line program. The PZT 1 remained the actuator for all the iterations and the other piezo patches worked as sensors. All the Algorithms have been applied in the study.

Two real cases have been evaluated on the Leaf Spring:

- static condition, mounted on the bending fixture without load
- dynamic condition, with a cyclic bending loading after an initial phase of calibration in static condition at 0 kN

To assess the possibility of the SHM system to detect damages or variation on the component, a clamp has been used to locally increase the stiffness and simulate a damage on a Leaf Spring section.

As described in Chapter 4 for the On-line methodology, the calibration phase requires the acquisition of ten baseline signals in the initial condition.

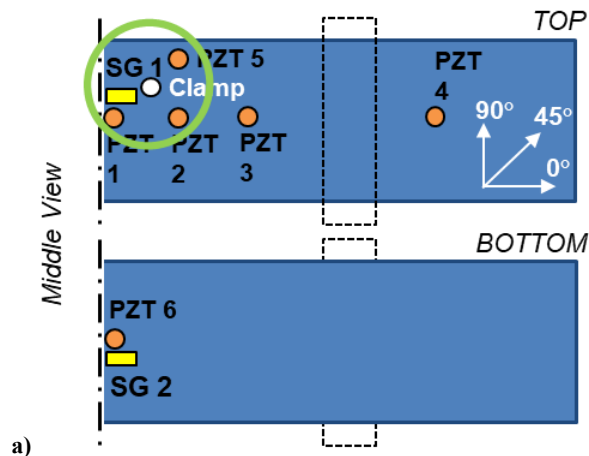
In the static condition, the clamp has been mounted after the calibration and the effect on the Damage Index has been evaluated. In the dynamic condition, two different tests have been carried on under the same bending cycle: one without clamp and one with the clamp mounted after the calibration.

For each test, the On-line program produces the representations:

- raw signal data, comparison of all baseline signals with the actual signal
- raw signal data history, comparison of actual signals from the beginning of the test with the absolute timeline
- the trend of maximum peak and maximum standard deviation for the acquired signals
- the trend of Damage Index for the actual signal related to the average baseline signal acquired in the calibration phase

5.3.1. Leaf Spring in Static condition

Static tests have been carried out on the Leaf Spring mounted on the bending fixture without load. The objective of the test is to evaluate the effect of a clamp on the Damage Index. The Figure 5.16 shows the position of the clamp on the central zone of the Leaf Spring, on the path of the piezo couples PZT 1-5 and PZT 1-2.



a) Figure 5.16 – Piezo couples PZT 1-2 and PZT 1-5 studied for the influence of Clamp and Bending load on the Leaf Spring component

The calibration phase acquired ten signals for baseline average, then the test started at the second 0. The clamp has been applied at second 90 and removed at second 150, the test finished after 170 seconds.

In Figure 5.17 is reported the On-line monitoring graph for all the piezo couples at 75 kHz. As can be seen, the maximum peak of absolute signal and standard deviation showed a significative variation during the phase of placing and removing the clamp. In particular, the maximum peak for the piezo sensors PZT 2 and PZT 6 increased with the clamp, while decreased for PZT 5 at 45°. The values for other

sensors PZT 3 and PZT 4 far from the actuator had no important variations. The maximum standard deviation showed an increase due to the clamp for the sensors PZT 2, PZT 5 and PZT 6, demonstrating an effective potential to study the phenomenon.

All the Algorithms for Damage Index calculation showed a great influence from the clamp introduction. The CRC, NRE, MA and ENV Algorithms had a behavior similar to the maximum of standard deviation, highlighting the influence on piezo couples PZT 1-2, PZT 1-5 and PZT 1-6 where the clamp is placed. In addition, the CRC expressed a particular sensitivity to the Damage Index of piezo sensors far from the clamp, PZT 3 and PZT 4. The CCA and CC0 Algorithms did not show much variation for the Damage Index of all the piezo sensor.

In synthesis, for the static case the majority of Algorithms involved in the SHM On-line Processing program detected a significative influence of the clamp application on the Leaf Spring for the frequency of 75 kHz.

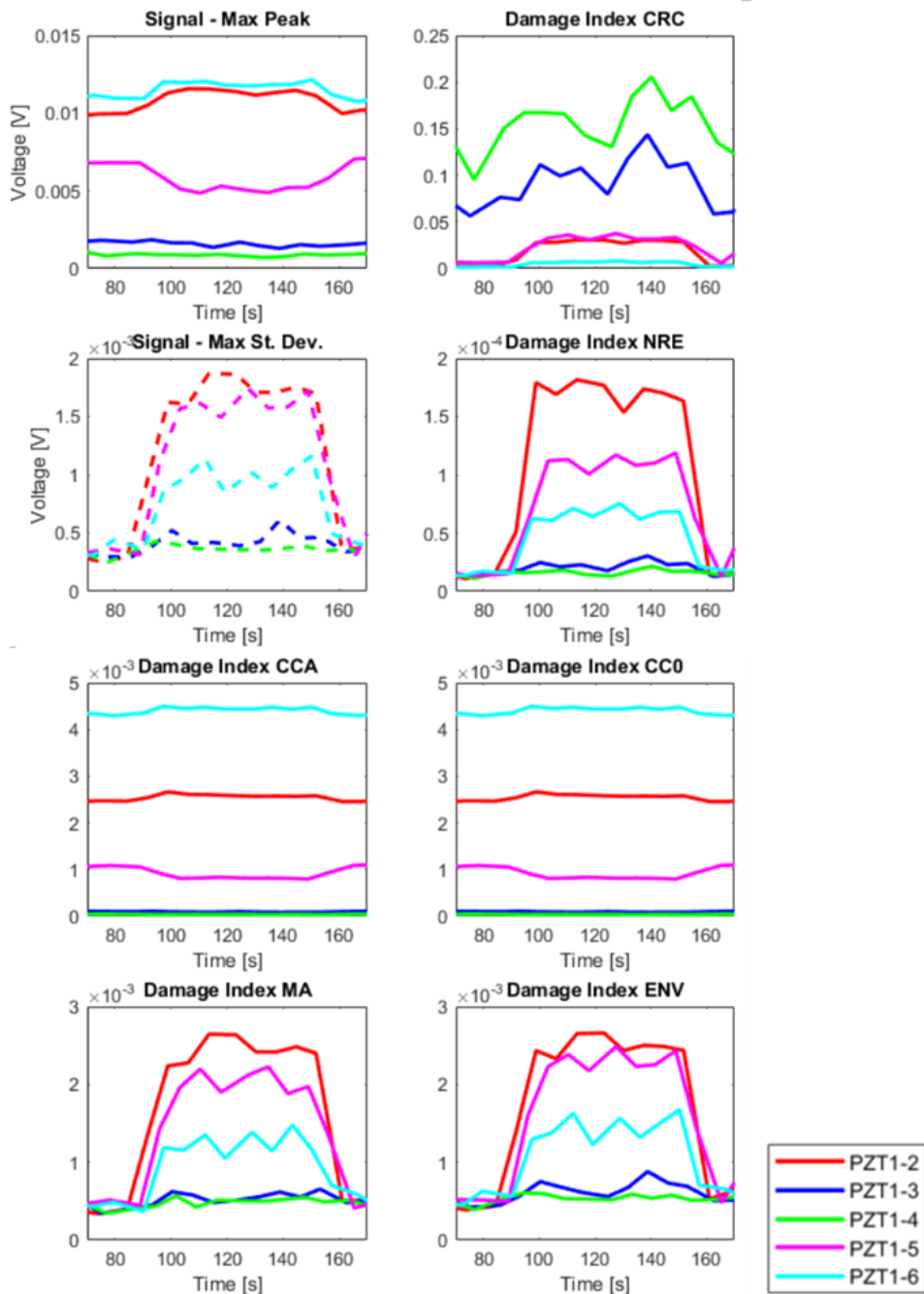


Figure 5.17 – SHM On-line Test results for the Leaf Spring in static condition with clamp

5.3.2. Leaf Spring in Dynamic condition

Dynamic tests have been done during a cyclic bending test monitoring all the piezo couples at the frequency of 75 kHz, chosen with the results of the SHM Off-line program. The objective of the test is to evaluate the effect of a clamp on the Damage Index, considering the bending of the structure in addition to the static condition evaluated in the previous paragraph.

The test followed a specific cycle prepared on Software Trapezium X controlling the Shimadzu dynamometer, to evaluate the repeatability of the SHM system response. The monitoring system composed by HBK QuantumX for Strain gauges and NI USB-6259 for Piezo patches is reported in Figure 5.18, with a detail

of the upper bending support and the clamp on the path of the piezo couples PZT 1-5 and PZT 1-2, as for the static test.

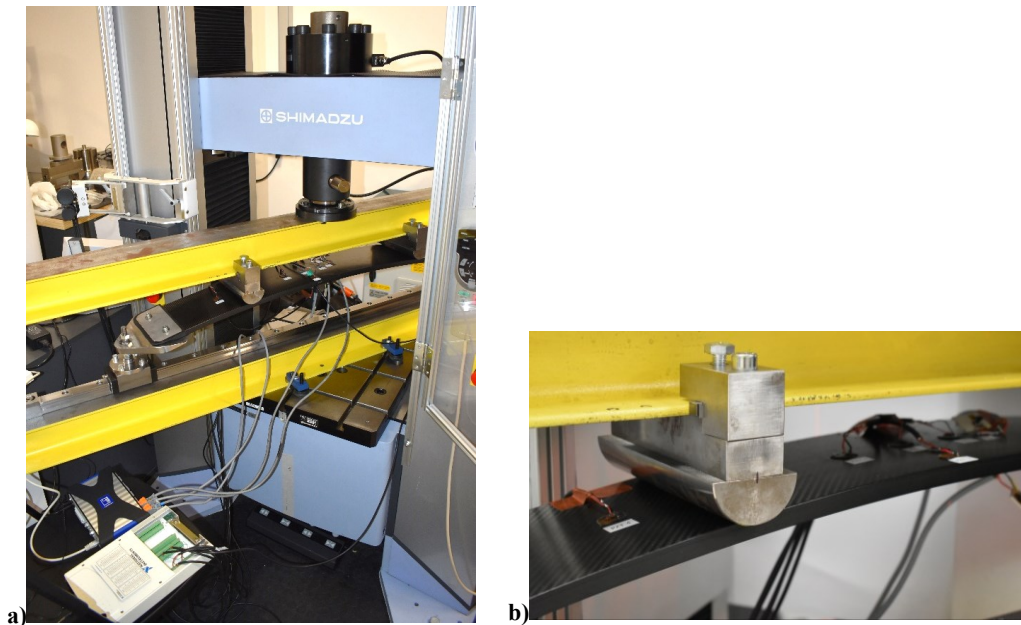


Figure 5.18 – a) Experimental system for the SHM of the Leaf Spring component in Bending configuration, b) detail of the upper bending support

The test cycle in load control is reported in Figure 5.19, in terms of Force-Time. It consists of three loading-unloading at Bending step 1 and three at Bending step 2 with a crosshead speed of 5 mm/min. In the releasing phase the reaching point is 150 N of force to maintain the stability of the structure on the fixture. The Strain measured from the strain gauges during the test is reported in Figure 5.20.

The calibration phase acquired ten signals for baseline average in the initial relaxed condition, then the test started at the second 0. The duration of the test was 3000 seconds (50 minutes). One test has been conducted bending the Leaf Spring without clamp. Another test has been made with the application of the clamp at second 50 and not removed until the end of the experiment.

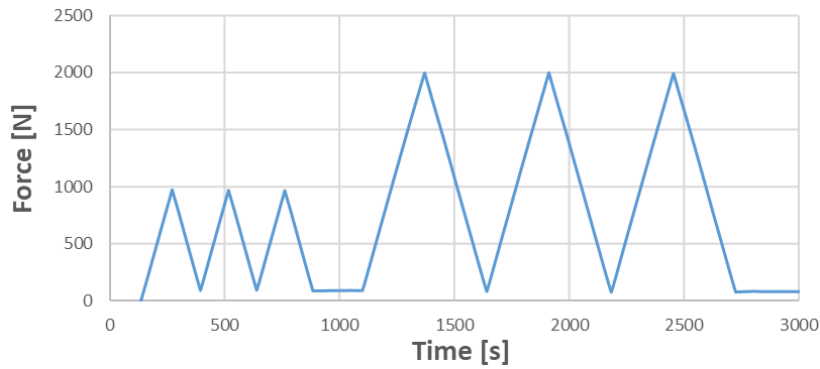


Figure 5.19 – Test cycle in terms of Force vs. Time

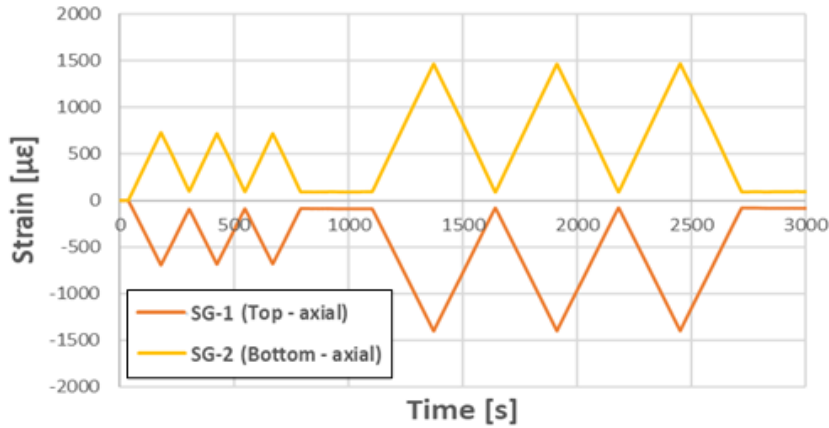


Figure 5.20 – Strain gauges measures during the bending cyclic test on Leaf Spring

The baseline series of signals and the last acquisition of test signals for each piezo couple are reported in Figure 5.21. On the left column, the initial baseline data set remains for all the test duration, while on the right column the raw data of the piezo couples is updating each iteration.

It is possible to see that the signal acquired before and after the bending cycles is similar for all the piezo sensors. This information is important to say that the structure after bending come back approximately to the original state not only for macroscopic load and strain measures, but also at microscopic scale studied with the ultrasonic waves sensed by piezoelectric patches.

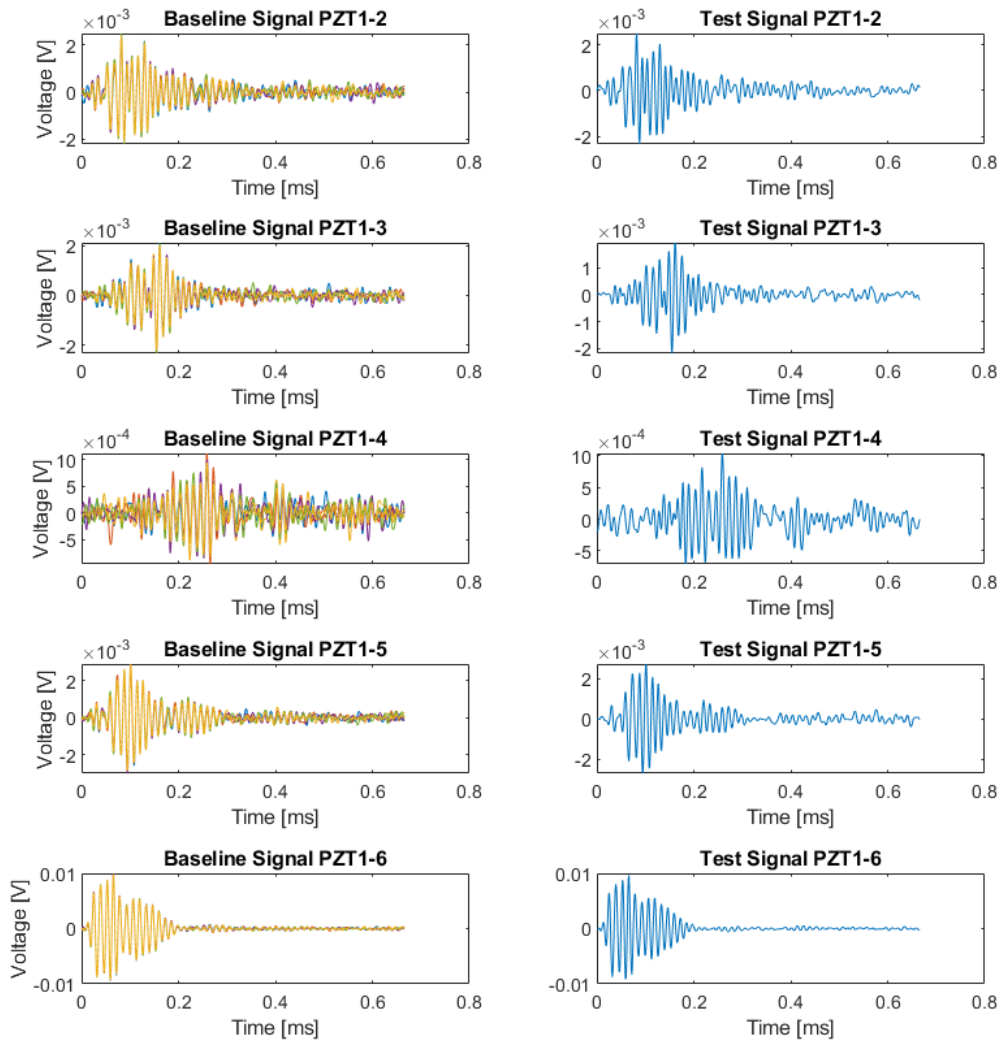


Figure 5.21 – SHM On-line Test results for the Leaf Spring in dynamic condition without clamp

The raw data for the bending test without clamp are reported in Figure 5.22, in which the Absolute time is the test time, while the Relative time is the signal acquisition time. With this visualization it is possible to easily verify the voltage peaks disappearing or shifting in time due to external test events.

It is possible to see that the signals acquired from sensors PZT 2 and PZT 5 near to the actuator PZT 1 are not so much affected from the bending cycles. A little decreasing in the signal amplitude and a time shift for signals at higher relative time have been registered.

For the sensor PZT 6 placed under the actuator, the intensity of signal due to the bending loading was important. For the sensors PZT 3 and PZT 4 the low signal amplitude was highly influenced from the bending, causing loss of signal and time shift of voltage peaks.

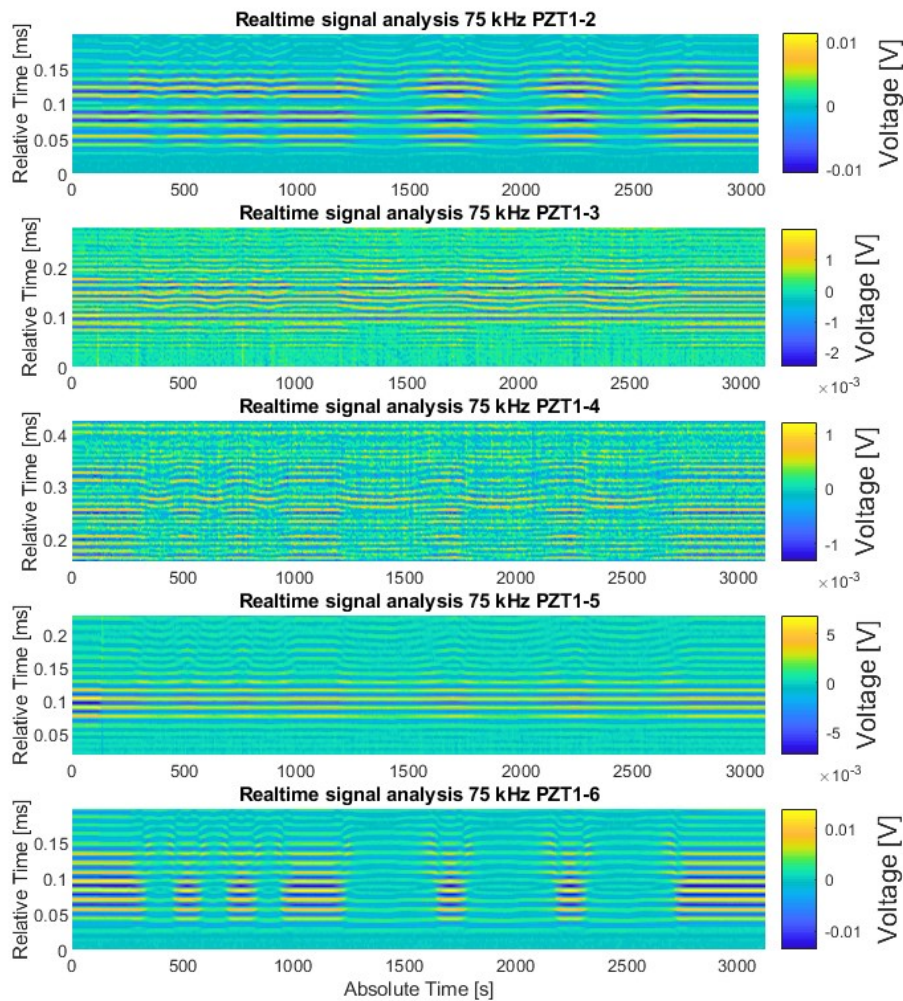


Figure 5.22 – SHM On-line Test results for the Leaf Spring in dynamic condition without clamp

The Figure 5.23 and Figure 5.24 report the On-line monitoring for entire bending cycle test without and with the clamp introduction. The comparison has been made for each piezo couple between the trend of maximum Voltage peak, maximum Voltage standard deviation and the six Damage Index values.

Regarding the maximum peak of voltage signals, the sensors PZT 2, PZT 5 and PZT 6 showed a decrease proportional with the bending load, while the sensor PZT 3 a slight increase. The effect of the clamp at second 50 produced the same behavior seen in the static test, with an increase of signal intensity for PZT 2 and PZT 6 and a decrease for PZT 5. The effect of the clamp in the bending cycles led to an increased drop of voltage signal both for the Bending step 1 and step 2.

Focusing on the maximum standard deviation of the acquired signals, the increases are proportional with the bending load of the cycles. When the clamp is applied all the values of standard deviation increase, in particular for the cycles at the bending step 1.

As observed in the static condition, all the Damage Index values demonstrated a behavior similar to the standard deviation with great variations with the bending cycles. Apart the CCA and CC0, all the Algorithms expressed positive variations specially for the sensors near to clamp PZT 2, PZT 5 and PZT 6. The CRC Algorithm was sensitive also for the sensor far from clamp PZT 4.

In synthesis, for the dynamic case the majority of Algorithms involved in SHM On-line Processing program detected a significant influence of the bending loading and after the application of clamp on the Leaf Spring for the frequency of 75 kHz.

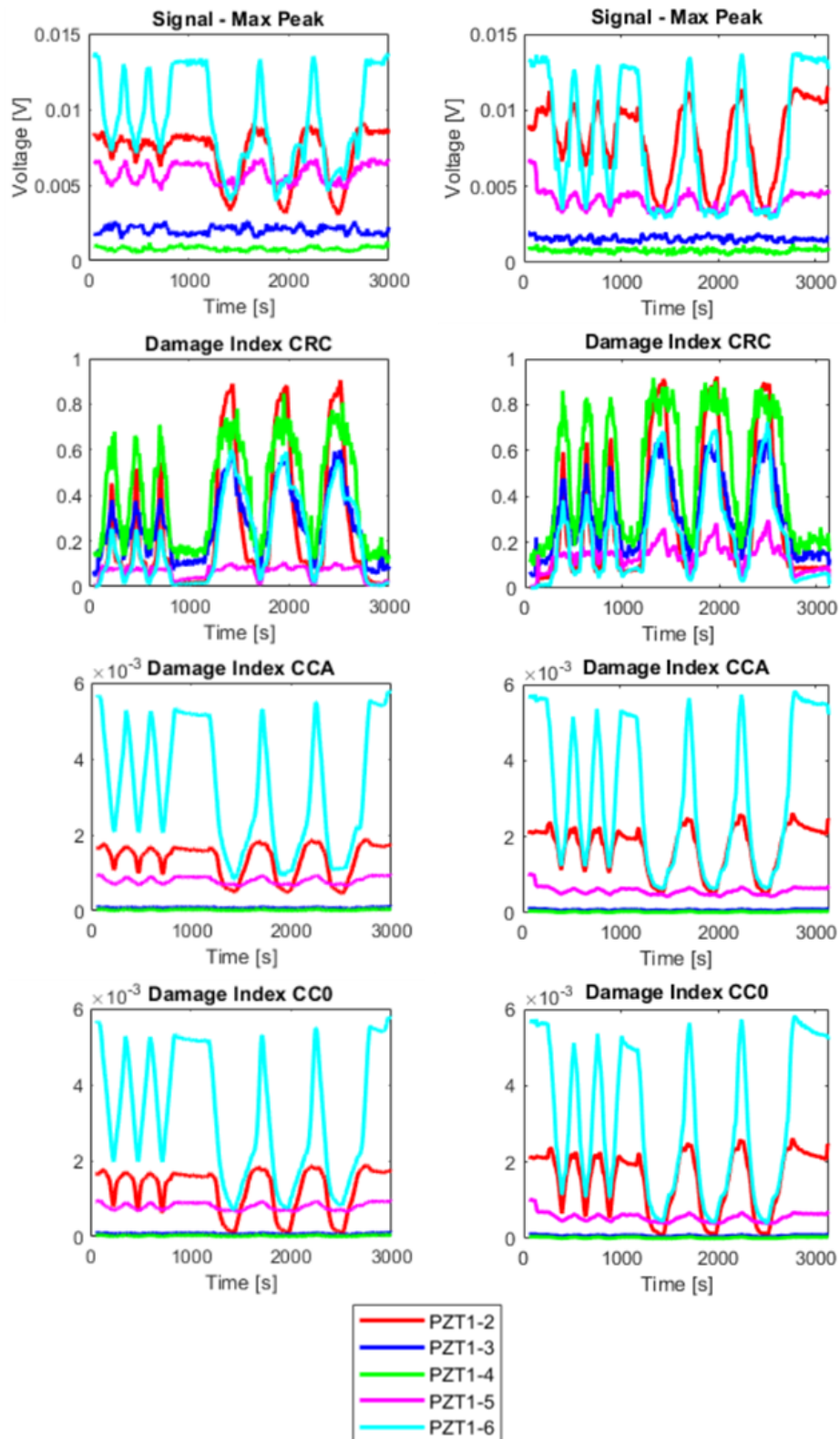


Figure 5.23 – SHM On-line Test results for the Leaf Spring in dynamic condition without (left column) and with clamp (right column) – part 1

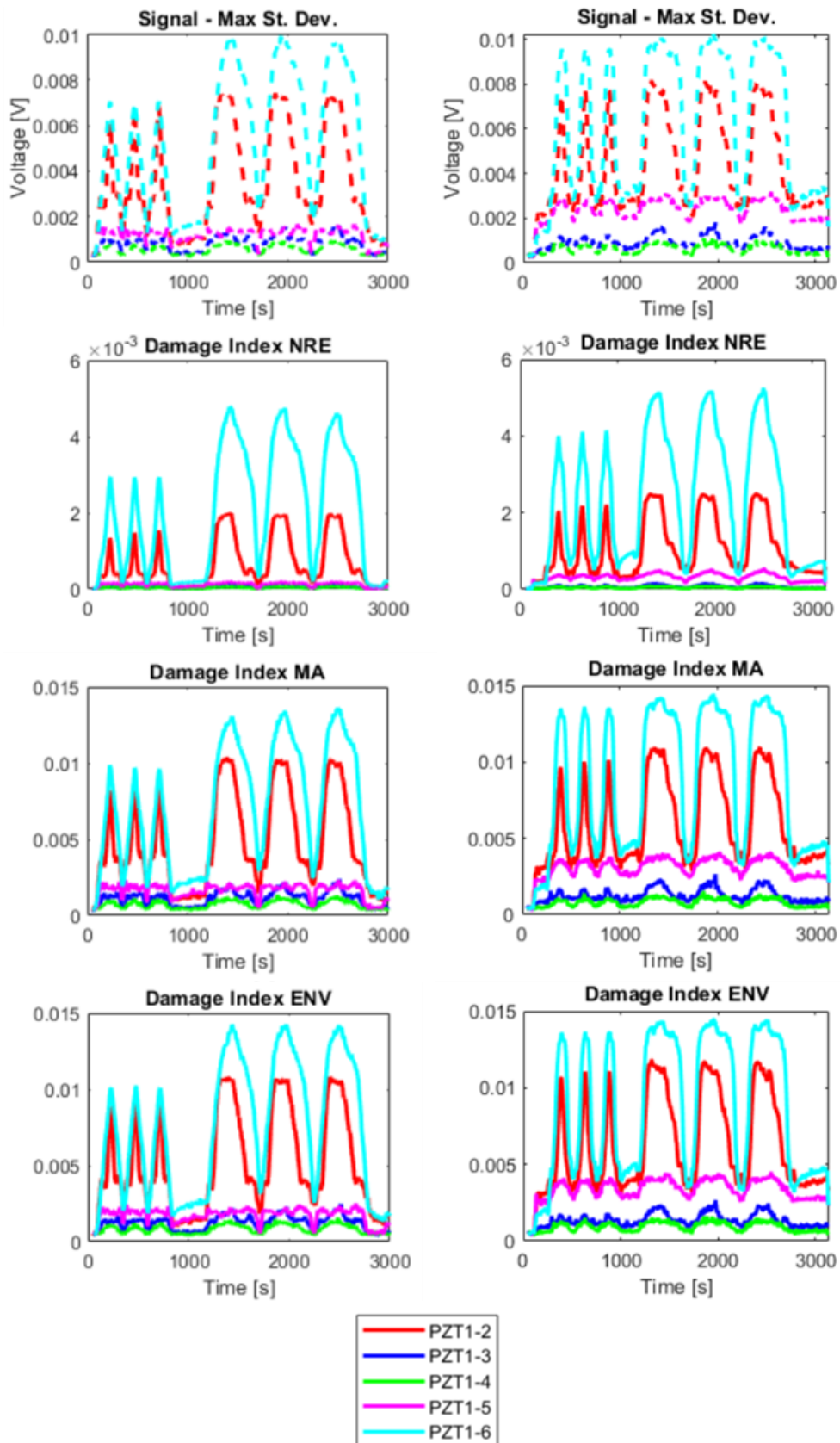


Figure 5.24 – SHM On-line Test results for the Leaf Spring in dynamic condition without (left column) and with clamp (right column) – part 2

Chapter 6

Virtual Simulations

The Structural Health Monitoring is an experimental technique suitable for structures of particular interest, such as for safety requirements, industrial activities, energy production. The basis of the method is the propagation of an ultrasonic vibration in the structure, which behavior is influenced from material, thickness, environmental conditions, possible defects, presence of damages. This last factor is the reason of the application for SHM systems, that monitor the component for a period waiting for the damage detection.

The SHM sensor network is therefore designed according to the structure geometry and the knowledge about the critical zones and the failure criterion of the material. The experience on the correct positioning of sensors is related to the experimental tests made on simple specimens or sections of the structure in order to setup the system. It is not normally taken into account the possibility to design the final sensor network before the practical trial, but for complex or expensive structures this could be an interesting point of development.

The limitations of the Finite Element Analysis (FEA) models in the case of SHM conditions regard the realistic modeling of the damages, the exact simulation of the vibrations combined to the mechanical stresses on the structure, the lack of accounting the imperfect geometry of components and environmental conditions. For all these reasons the virtual tool has not been used in this work to simulate defects or damages on the structure and presence of external or internal stresses. The aim of the research is to understand if the simulations can be a support for the general comprehension of the vibrational phenomenon and give an idea of the possible signals to measure even in a phase precedent to the production.

This Chapter describes the methodology developed to model the real systems composed by specimens and piezoelectric sensors, through a particular electro-mechanical analogy to compensate the absence of specific keywords on LS-DYNA for piezoelectric modeling. The results of the simulations have been compared directly with the Voltage signals acquired in the experimental tests.

6.1. Virtual Methodology

6.1.1. FEA Models

The FEA simulations have been conducted on LS-DYNA, using LS-PrePost to set the models. The Explicit solver has been used because the vibration phenomenon is time-dependent and its velocity is relatively high. The Implicit solver has not been used because it is normally suitable for quasi-static simulations without a dependence from time.

The modelled structures are the same of the experimental tests, as schematized in Table 6.1. The geometries of specimens, the materials, the thicknesses have been respected. All the piezo sensors on the Top face of the specimens have been modelled.

The CAD models of Beam specimen, Plate specimen, Simulacrum specimen and Leaf Spring component are reported in Figure 6.1.

Type	Material	Geometry	Dimension [mm]	N. Piezo Real Test	N. Piezo Modelled
Specimen BEAM	Composite Aluminum Steel	Rectangular	300 x 12	2	2
Specimen PLATE	Composite Aluminum Steel	Square	250 x 250	4	4
Specimen SIMULACRUM	Composite Aluminum Steel	Rectangular	250 x 70	3	2
Component LEAF-SPRING	Composite	Rectangular curved	1000 x 150	6	5

Table 6.1 – List of specimens, materials, geometries, number of piezo simulated with FEA models

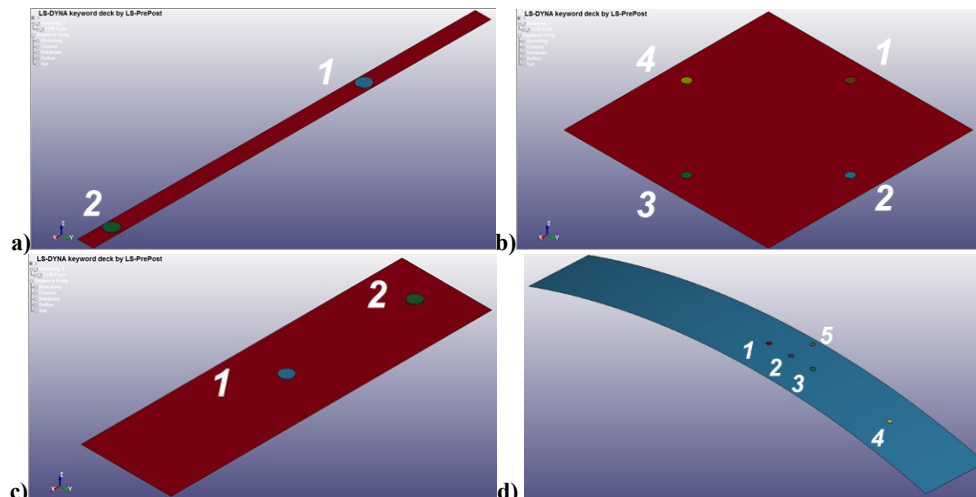


Figure 6.1 – CAD models of a) Beam, b) Plate, c) Simulacrum, d) Leaf Spring

The models of specimens have been designed and meshed using LS-PrePost because of the simple geometry and planarity, while the Leaf Spring component has been meshed in Altair HyperMesh and then imported in LS-PrePost for the FEA

setup in LS-DYNA. Particular attention has been given to the meshing strategy of the specimens, in view to apply in future the methodology on large components, not only the Leaf Spring. The beam specimen has been taken as case study for its simplicity, small dimension and presence of only one piezo couple. Some trials have been carried on using different approaches to model the beam, the piezoelectric, glue and export keywords, as reported in Table 6.2.

Each methodology was studied in order to preserve the adaptability on large models and the sustainability of computation time. The method 1 was the initial approach, considering the Beam specimen as shell 2D and the piezo actuator and sensor as set of nodes, the method 2 with piezo modeled as shell 2D did not work properly, the method 3 with glue as a solid 3D required the glue properties difficult to measure in reality, the method 4 (bold in Table) was chosen for the present work modeling the piezo as solid 3D and glue with Tied contact, the method 5 is a future development for thick structures and can be probably more computationally expensive. The polymeric cover of DuraAct has been considered in the method 3 but rejected in the final release of method 4. The electrodes and cables have not been modeled.

In Figure 6.2 and Figure 6.3 are reported the detailed views of the piezo models respectively for the actuator and sensor.

Method	Beam	Piezo 1	Input	Piezo 2	Output	Glue
1	Shell 2D	Nodes set	Prescribed motion	Central node Nodes set	Nodout Nodfor	None
2	Shell 2D	Shell 2D	Prescribed motion	Shell 2D	Nodout Nodfor Recforc	None
3	Shell 2D	Nodes set	Prescribed motion	Central node Nodes set	Nodout Nodefor Recforc (Glue-Beam)	Solid 3D
4	Shell 2D	Solid 3D	Prescribed motion	Solid 3D	Nodout Nodefor Recforc (Piezo-Beam)	None
5	Solid 3D	Solid 3D	Prescribed motion	Solid 3D	Nodout Nodefor Recforc (Piezo-Beam)	None

Table 6.2 – Methods used to model beam, piezo patches, glue and export keywords

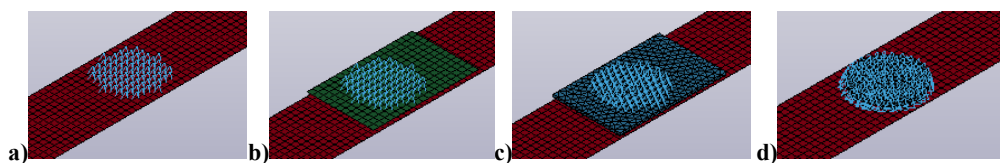


Figure 6.2 – Methods a) 1, b) 2, c) 3, d) 4 used to model beam, glue, piezo actuator

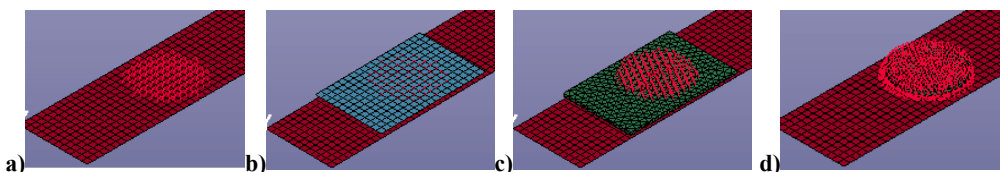


Figure 6.3 – Methods a) 1, b) 2, c) 3, d) 4 used to model beam, glue, piezo sensor

The mesh has been prepared with square 2D elements of size equal to 1 mm for the beam and with tetrahedron 3D elements of size around 1 mm for the piezo. The

dimensions of the piezo disk were thickness of 0.5 mm and diameter of 10 mm. Tied contact is implemented to model the glue between the beam specimen (master) and the bottom set of nodes of piezo (slaves). The details of mesh and set of nodes used for Tied contact are depicted in Figure 6.4.

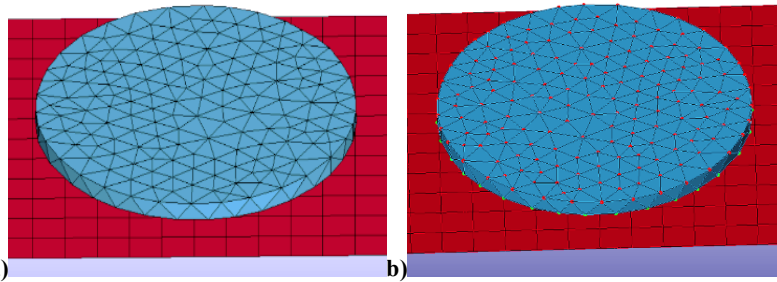


Figure 6.4 – a) Mesh of beam specimen with shell 2D and piezo with solid 3D, b) selection of piezo nodes on bottom (green) and top surfaces (red)

The LS-DYNA keywords mainly used in the FEA models are listed below:

- ***BOUNDARY_PRESCRIBED_MOTION_SET** imposes the motion of the nodes set on bottom surface of piezo actuator, as in Figure 6.5;

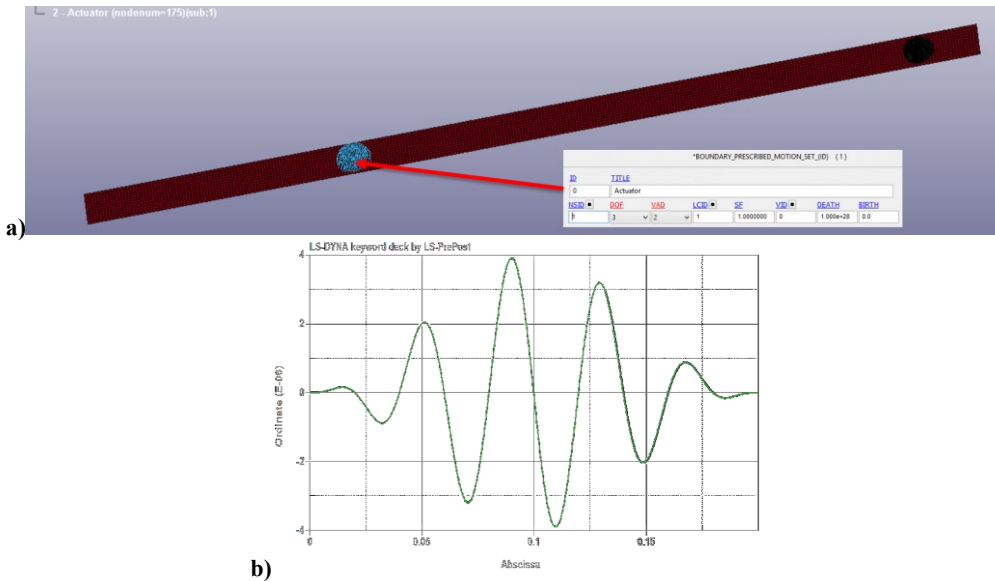


Figure 6.5 – a) Selection of the set of nodes on bottom surface of piezo actuator, b) Displacement signal at 50 kHz imposed using the keyword ***BOUNDARY_PRESCRIBED_MOTION_SET**

- ***DATABASE_NODOUT** exports the nodal displacement of the center node on bottom surface of piezo actuator and sensor in global coordinate system (x,y,z), as in Figure 6.6;

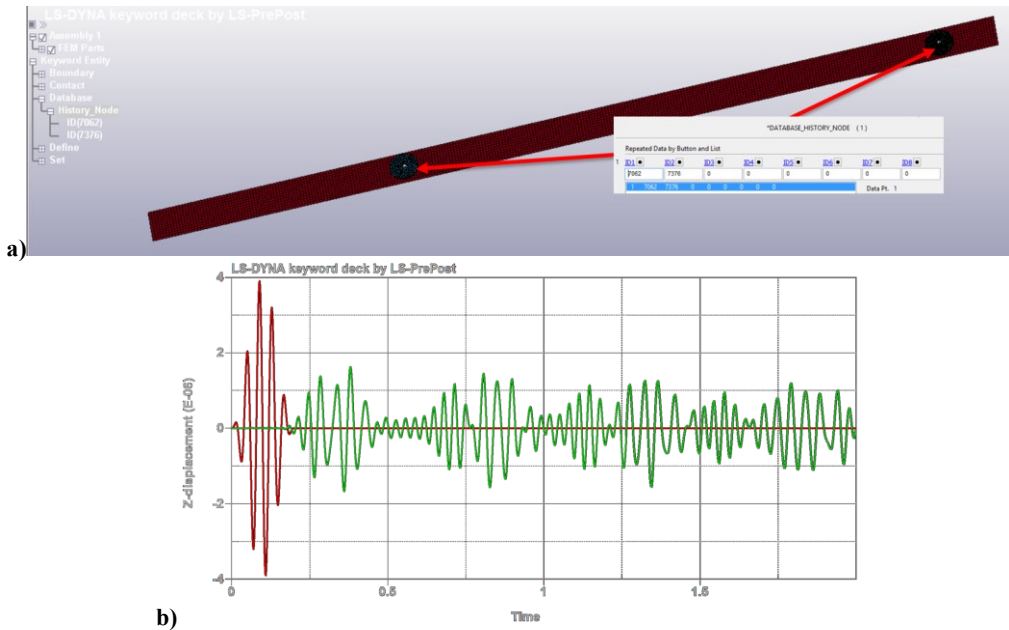


Figure 6.6 – a) Selection of the center nodes on bottom surface for piezo actuator and sensor, b) Example of Displacement for piezo actuator (red) and piezo sensor (green) exported using the keyword `*DATABASE_NODOUT`

- `*DATABASE_NODFOR` exports the nodal forces of the center node on bottom surface of piezo actuator and sensor in global coordinate system (x,y,z);
- `*DATABASE_RCFORC` exports the interface forces between the piezo actuator or sensor and the beam in global (x,y,z) and local coordinate systems, as in Figure 6.7.

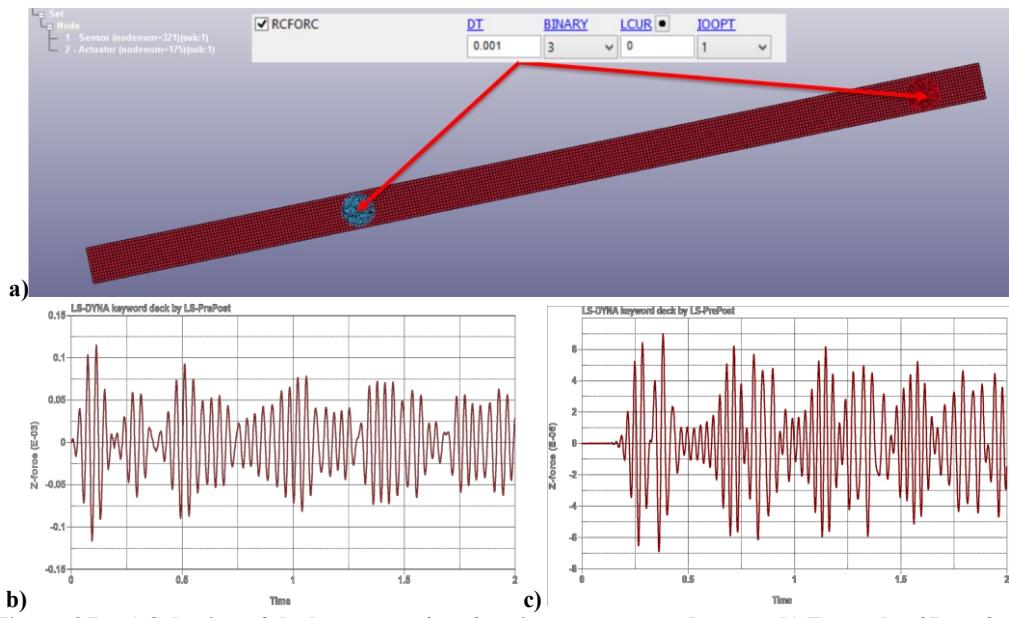


Figure 6.7 – a) Selection of the bottom surface for piezo actuator and sensor, b) Example of Interface Force for piezo actuator and c) piezo sensor exported using the keyword `*DATABASE_RCFORC`

The virtual simulations have been conducted at three different frequencies of displacement signal: 25, 50 and 75 kHz. In order to optimize and automatize the procedure of model setup for the input signal, the Hanning displacement signal with frequency 50 kHz was used as a reference and the time scale function of LS-PrePost

has been set using a MatLab customized program. This code is able to open the .k files with the simulation settings of LS-PrePost, modify specific rows and launch the simulation on LS-DYNA solver for each frequency. The following keywords have been modified iteratively with the MatLab code:

- ***DEFINE_CURVE**
SFA = 1000*50/(*Desired Frequency in kHz*)
- ***CONTROL_TERMINATION**
ENDTIM = 50/(*Desired Frequency in kHz*)
- ***DATABASE_BINARY_D3PLOT**
DT = 0.01*ENDTIM = 0.01*50/(*Desired Frequency in kHz*)

The described modelling methodology make the following approximations:

- Radial mode vibration of the piezo is not taken into account;
- Thickness mode vibration of the piezo becomes entirely displacement on the structure;
- Displacement is measured only in 1 node (central node) with *DATABASE_NODOUT;
- Properties of the glue are neglected;
- Properties of the Kapton cover of the piezo are neglected;
- Real piezo pre-loading due to the Kapton cover is neglected;
- Shell 2D elements are used and the propagation of vibrations in the thickness is neglected.

6.1.2. Electro-Mechanical Coupling

The need of an Electro-Mechanical Coupling is due to the impossibility for LS-DYNA software to evaluate electrical variables, but only mechanical displacement or forces. A specific keyword is under development for the piezoelectric simulation, but it was not available for the use in this work. The theoretical relations of piezoelectricity are based on the properties of piezoceramic material contained in the datasheet of PIC255 material [28] for the DuraAct piezo. The equations for the thickness mode vibration of thin disks reported in Figure 6.8 were used in this work.

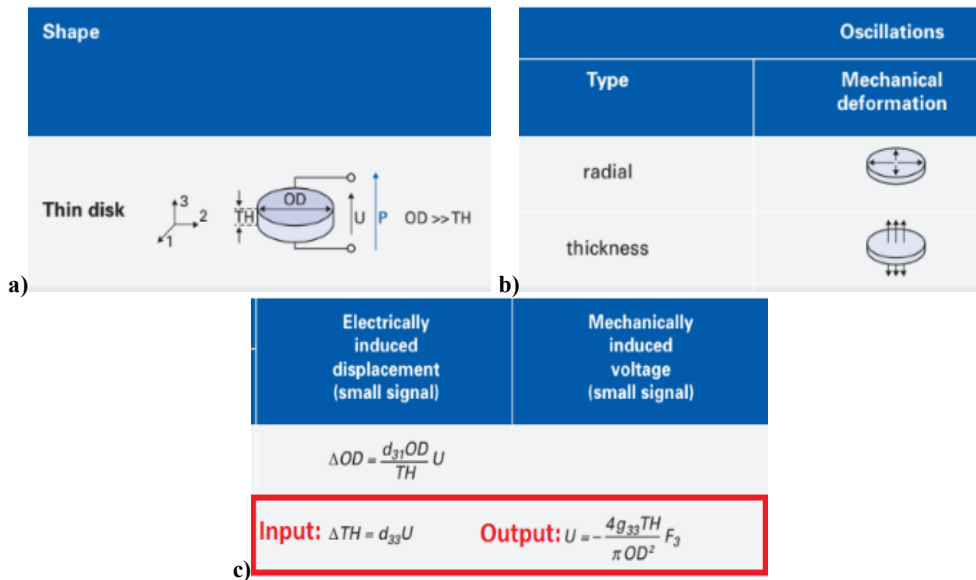


Figure 6.8 – a) Conventions for piezoelectric disks, b) types of oscillation and c) electro-mechanical coupling of inverse and direct piezoelectric effects [28]

The “electrically induced displacement” corresponds to the piezo actuator excitation related to voltage by Equation (4) of inverse piezoelectric effect. The “mechanically induced voltage” corresponds to the piezo sensor response signal related to force by Equation (5) of direct piezoelectric effect.

$$\Delta TH [mm] = d_{33} U \cdot 10^3 \frac{mm}{m} \cdot = 4 \cdot 10^{-7} \cdot U [V] \quad (4)$$

$$U [V] = \frac{4g_{33} TH}{\pi OD^2} \cdot F_3 = -6.37 \cdot 10^{-2} \cdot F_3 [N] \quad (5)$$

Where:

- ΔTH , resulting displacement of the piezo
- $U = [-10:10]$ V, Voltage range used in the experimental tests
- $d_{33} = 400 \cdot 10^{-12}$ C/N, Piezoelectric charge coefficient in direction 33
- $g_{33} = 25 \cdot 10^{-3}$ Vm/N, Piezoelectric voltage coefficient in direction 33
- $TH = 0.2$ mm, thickness of the piezo core
- $OD = 10$ mm, diameter of the piezo core

For the actuation signal with shape of 5 sines Hanning modulation, the Voltage has been converted to Displacement according to Equation (4) and then applied to the model of piezo actuator with the already explained keyword *BOUNDARY_PRESCRIBED_MOTION_SET.

For the sensor response signal, the Voltage has not been obtained from Force as indicated by Equation (5). In fact, the Voltage values from Force exported using the keyword *DATABASE_NODFOR did not correlate with the Voltage values from experimental tests. This could be for one of the approximations of the model listed before. The incongruence has been fixed with an empiric analogy, especially studied for the beam specimen and then validated on the other specimens and Leaf Spring component.

The relation bases on the replacement of Force with Displacement in the electro-mechanical coupling to calculate the electrical Voltage. An example of the calculation steps and a result of the method are reported in Figure 6.9. Two coefficients have been used to scale the amplitude of actuator and sensor signals, while the time scale is conserved. The scale factor SF has been applied to the same Equation (4) of the actuator signal. The coefficient K has been applied to the inverse of Equation (4) for the sensor signal.

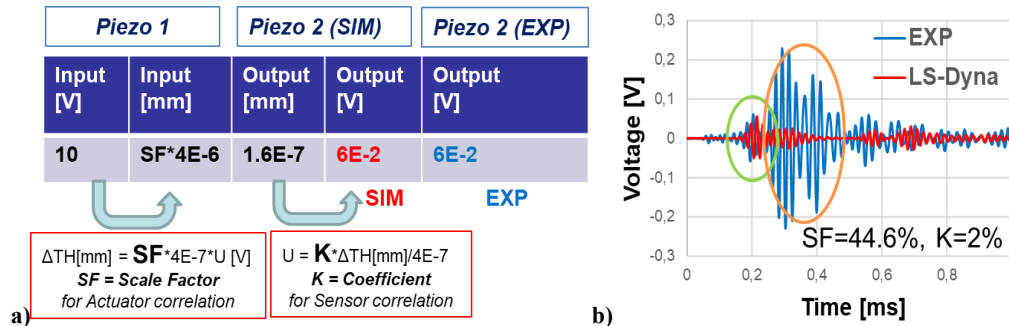


Figure 6.9 – a) Method developed to calculate Voltage from Displacement, b) correlation with real data

Before to discuss the definition of the coefficients, Equation (6) has to be expressed to estimate the dynamic forces from the mass of piezoelectric, the displacement and the frequency for sinusoidal operations [28]:

$$F_{dyn} = \pm 4\pi^2 \cdot m \frac{\Delta L}{2} f^2 \quad (6)$$

Where:

- $F_{dyn}[N]$ is the dynamic force;
- $m[kg]$ is the mass of piezoelectric disk;
- $\Delta L[m]$ is the displacement;
- $f[Hz]$ is the frequency.

The scale factor SF was designed to calibrate the actuation signal, in the transmission of vibration from piezo actuator to the structure. It has been calculated for each specimen, material and frequency, as reported in Figure 6.10. The methodology to obtain the SF value is describe below:

- Run the simulation using the SF=1;
- Check how distant the interface force (between piezo and specimen) is from the dynamic force estimated by Equation (6);
- Iteratively change SF until the interface force is equal to the dynamic force.

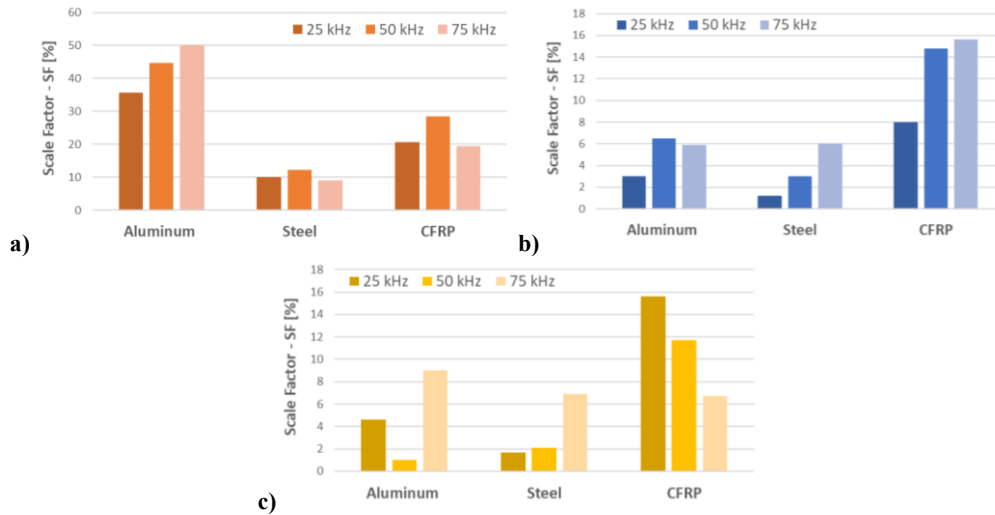


Figure 6.10 – Scale Factors (SF) for a) Beam, b) Plate and c) Simulacrum specimens at 25, 50, 75 kHz

The coefficient K was designed to calibrate the received signal, in the transmission of vibration from structure to the piezo sensor. A special test has been prepared joining two piezoelectric patches together with the same glue used on the beam and maintaining the same thickness. One was the actuator and one the sensor, with the same modulated signal, as reported in Figure 6.11.

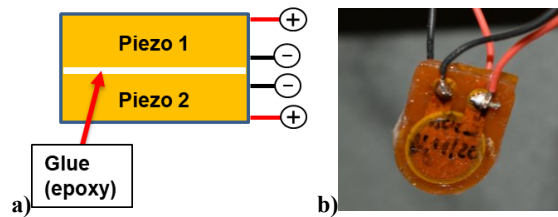


Figure 6.11 – Scheme of the special test, b) detail picture of the piezo joining

A simple LS-DYNA model has been set in order to compare virtual and real results, as can be seen in Figure 6.12. In particular blue curve is the experimental signal, light blue curve is the virtual data, orange curve is the virtual signal corrected changing the coefficient K. The green circle is the zone of best fitting, found in the first sinusoid to avoid reverberances of the vibrations between the two piezo.

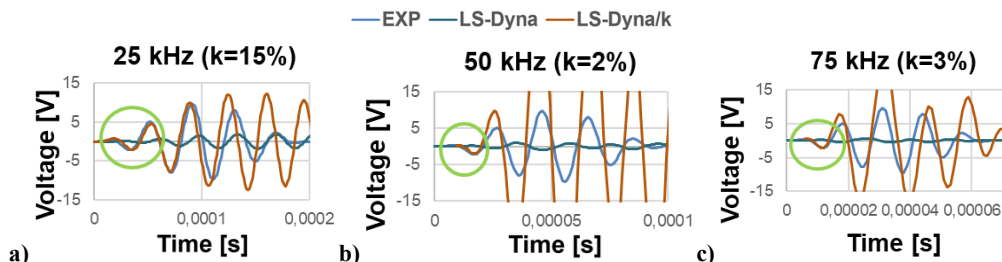


Figure 6.12 – Sensor responses from the special test at frequencies of a) 25 kHz, b) 50 kHz, c) 75 kHz

6.2. SHM Virtual Results

In this section are reported the results of the virtual simulations, set accordingly with the described methodology. All the specimens have been modeled with the

actuation of piezo 1 at the frequencies 25, 50 and 75 kHz, in free conditions without constraints due to clamps or bending equipment, in the health condition without Damage. In fact, the aim was to setup the coupling methodology to correlate the response of piezoelectric transducers both on small and large specimens made of different materials.

The Graphs describe for each specimen the simulation of the displacement for piezo actuator and sensors, and the correlation of displacement for the piezo sensors. To facilitate the reading, only the results for CFRP material are reported, while the results for steel and aluminum are collected in the Appendix.

The Figures describe the evolution of wave propagation on the studied structures at different simulation time. The visualization and the color scales represent for specimens the displacement in the z-axis normal to the piezo plane, while for Leaf spring the 1st principal stress normal to the piezo plane in local coordinate system due to the curvature of the component. Anyway, the stress is quite representative of the wave propagation on the structure. Because of the small values, to visualize a significative wave behavior, the virtual results have been properly scaled up.

6.2.1. Beam Specimen

The Beam specimen has one couple of piezo actuator and sensor, which are placed in asymmetric positions to evaluate possible waves spread at different time.

Figure 6.13 describes the evolution of wave propagation, in particular: a) actuation begins, b) waves spread in two directions, c) wave reflects on the edge opposed to piezo sensor, d) 1st wave reaches the piezo sensor, e) 2nd wave reaches the piezo sensor and constructively interferes with the 1st wave.

Figure 6.14 a) shows that the 1st wave arrives to the piezo sensor 2 at 0.15 ms for the three frequencies, demonstrating a constant velocity of the wave in the range 25-75 kHz for the CFRP material. The last waves are reflections on the edges.

Figure 6.14 b) reports the Voltage correlation, that is affected by an interference in the experimental signal before 0.15 ms for all the frequencies, maybe due to the vicinity of the cables. The FEM model simulates accurately the time of the 1st wave for all the frequencies, but the virtual methodology applied is able to correlate better the Voltage amplitude for the frequency 50 kHz. The last waves are not good correlated, highlighting the capacity of the virtual model to simulate the 1st wave received and not the reflections.

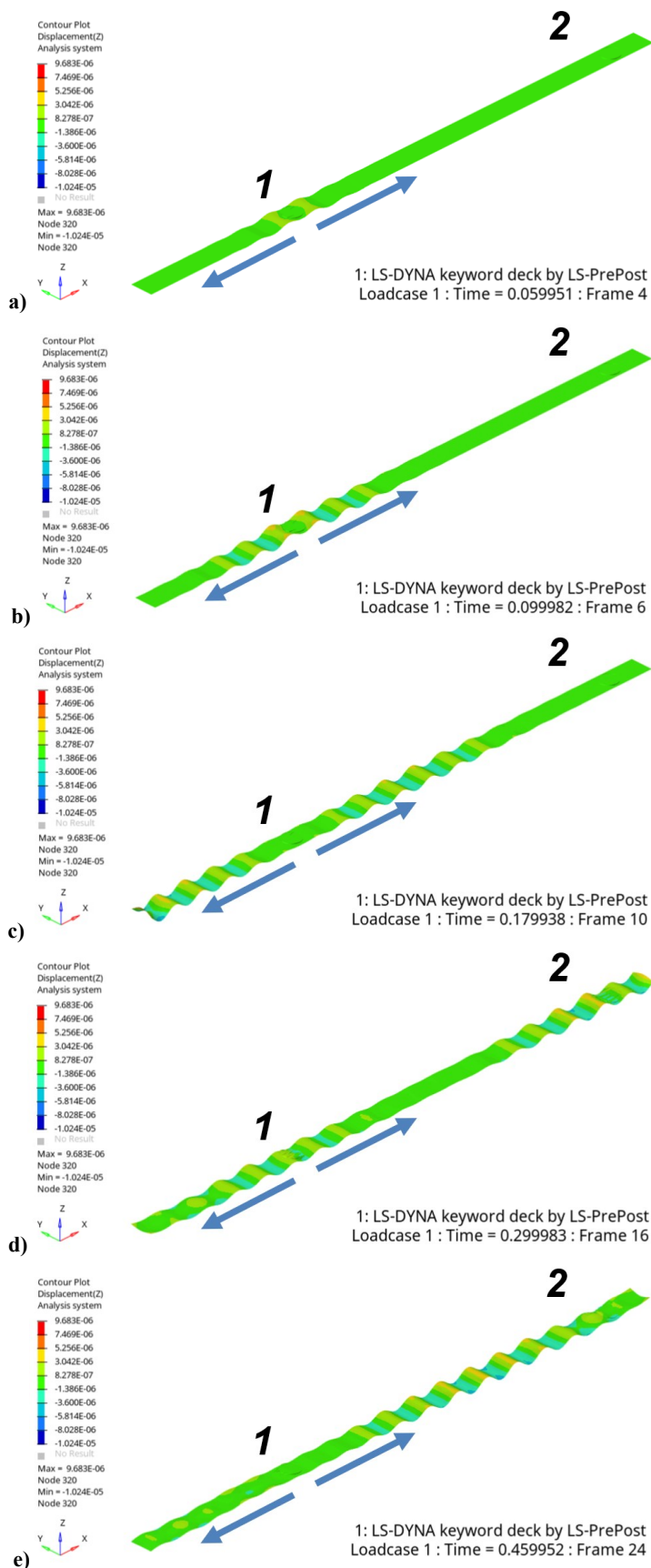


Figure 6.13 – Evolution of the wave propagation on the Beam specimen at 25 kHz, in terms of z-Displacement at different simulation time

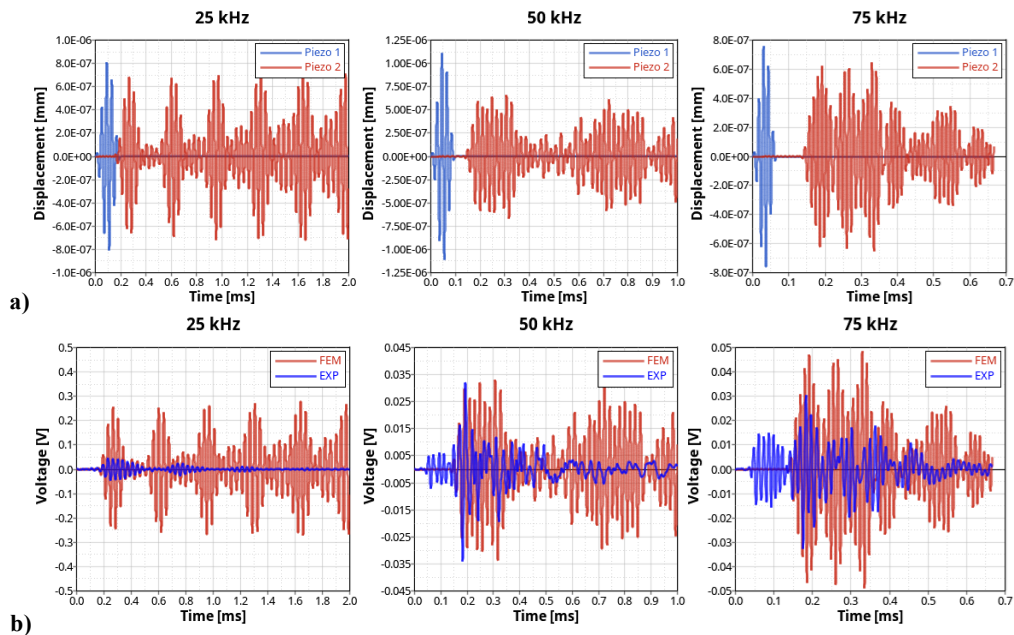


Figure 6.14 – Results at 25, 50 and 75 kHz for Beam specimen made of CFRP: a) virtual Displacement of piezo actuator 1 and sensor 2, b) correlation between virtual and real Voltage signals of piezo sensor 2

2

6.2.2. Plate Specimen

The Plate specimen has three couples of piezo actuator and sensor, which are placed on the centre of each square side to understand the wave propagation on the plane and to evaluate the analogy of response for piezo sensors 2 and 4.

Figure 6.15 describes the evolution of wave propagation: a) actuation begins, b) waves spread uniformly with circular propagation, c) wave reflects on the near edge, d) reflected waves constructively interfere mainly in x direction and at 45° reaching together piezo sensors 2 and 4, e) while the wave in x direction has completely reflected, the waves on piezo 2 and 4 reflect another time at 45° reaching the piezo sensor 3.

Figure 6.16 a) shows that piezo sensors 2 and 4 receive the waves symmetrically at the same time, so their signals are superposed, as expected and seen before. The waves arrive at 0.15 ms on piezo sensors 2, 4 and at 0.20 ms on the piezo sensor 3 for the three frequencies.

Figure 6.16 b) and c) report the Voltage correlations for piezo sensor 2 and 3, that are good for all the frequencies in terms of amplitude and time of arrival of the first waves. For the frequencies 50 and 75 kHz the piezo response is affected by an interference in the experimental signal before 0.15 ms, maybe due to the vicinity of the cables.

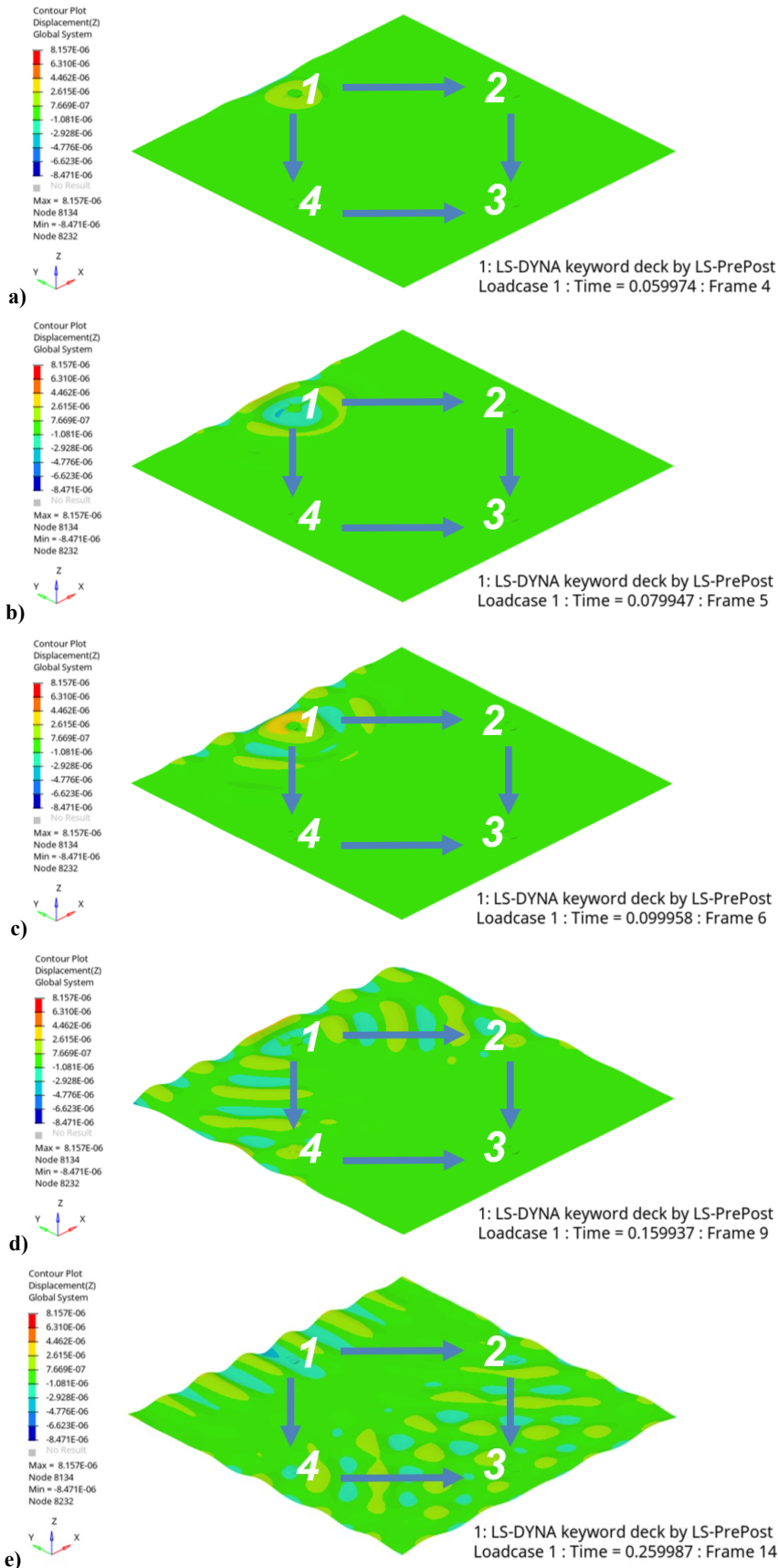


Figure 6.15 – Evolution of the wave propagation on the Plate specimen at 25 kHz, in terms of z-Displacement at different simulation time

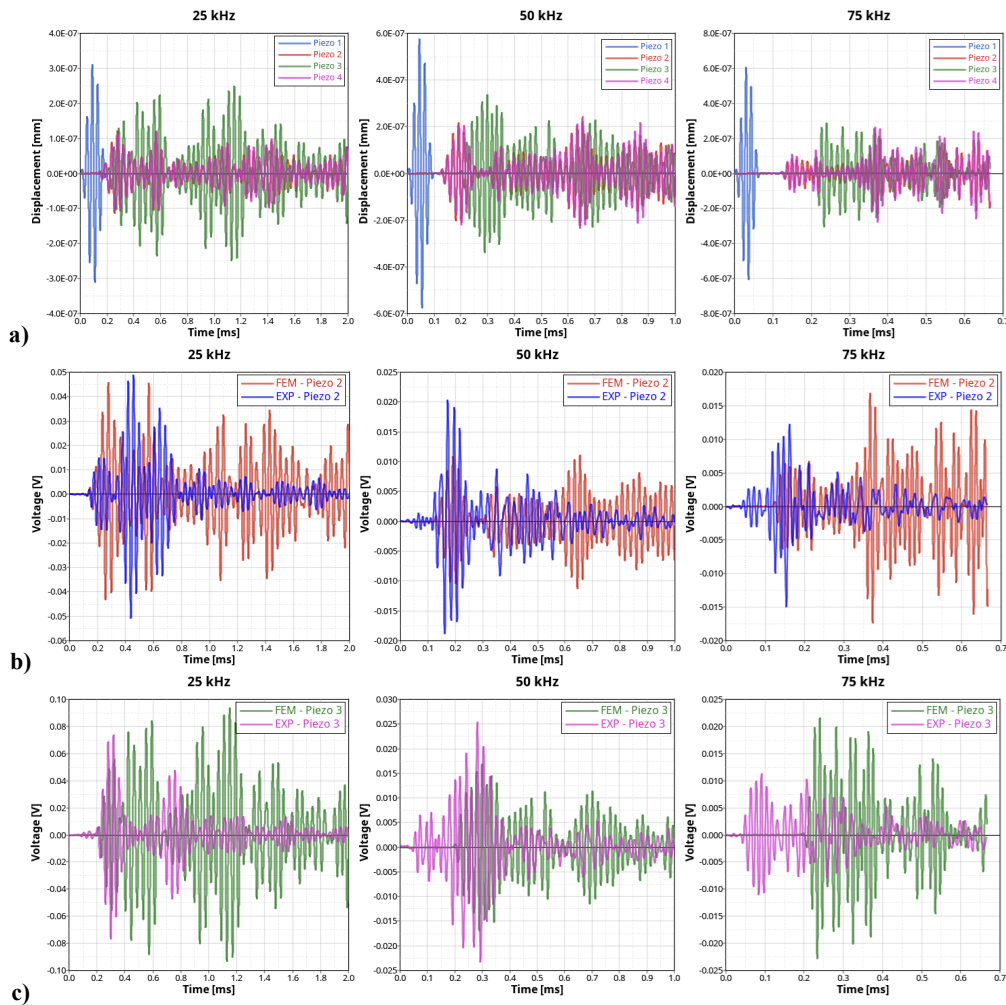


Figure 6.16 – Results at 25, 50 and 75 kHz for Plate specimen made of CFRP: a) virtual Displacement of piezo actuator 1 and sensors 2, 3, 4, correlation between virtual and real Voltage signals of b) piezo sensor 2 and c) piezo sensor 3

6.2.3. Simulacrum Specimen

The Simulacrum specimen has one couple of piezo actuator and sensor, which are placed one in the centre of the surface and one near the edge.

Figure 6.17 describes the evolution of wave propagation: a) actuation begins, b) waves spread uniformly with circular propagation reaching the piezo sensor, then the reflections on the edges produce a superposition of waves visible in c), d), e).

Figure 6.18 a) shows that the 1st wave arrives at 0.10 ms on piezo sensor for the three frequencies. Figure 6.18 b) reports the Voltage correlations, that is affected by an interference in the experimental signal before 0.10 ms, maybe due to the vicinity of the cables. The FEM model simulates accurately the time of the 1st wave for all the frequencies, but the virtual methodology applied is able to correlate better the Voltage amplitude for the frequency 75 kHz.

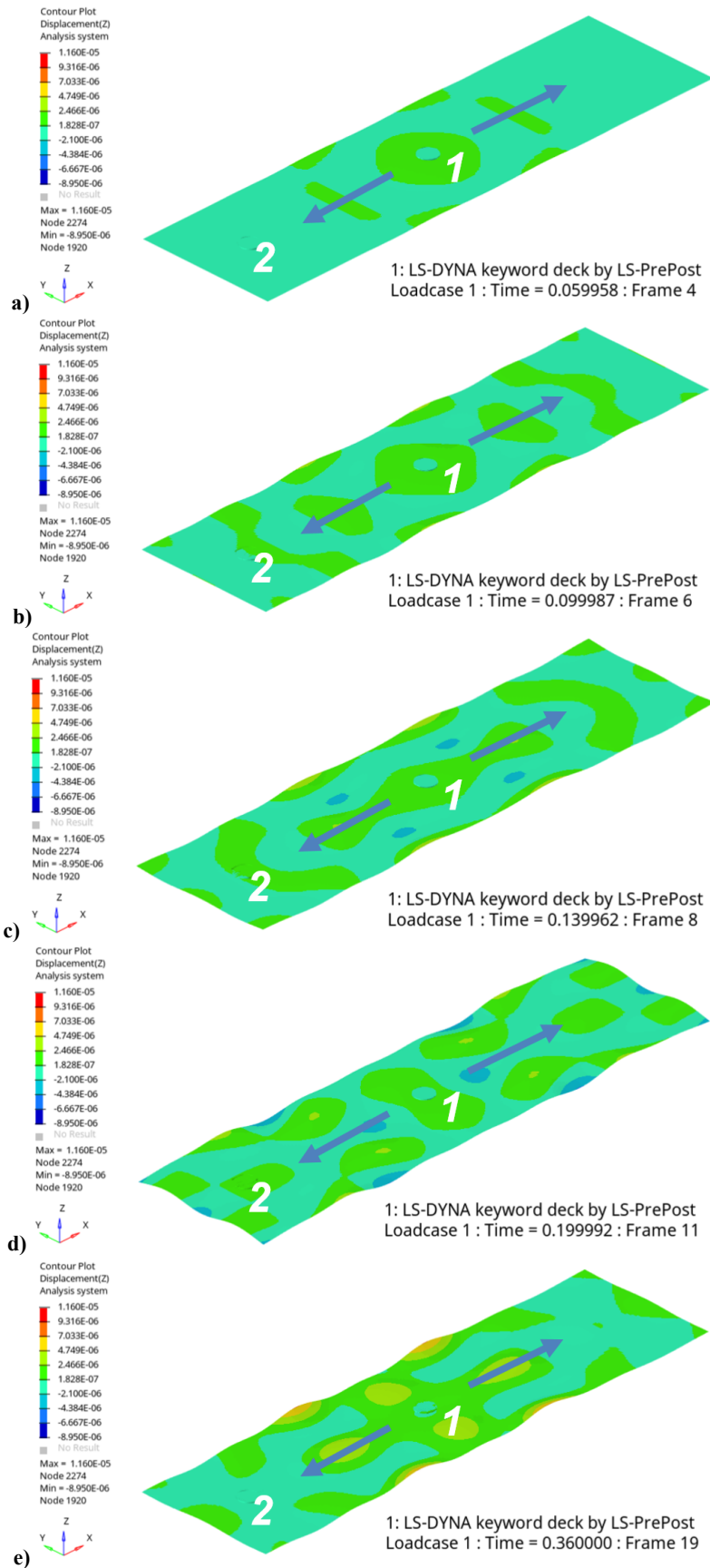


Figure 6.17 – Evolution of the wave propagation on the Simulacrum specimen at 25 kHz, in terms of z-Displacement at different simulation time

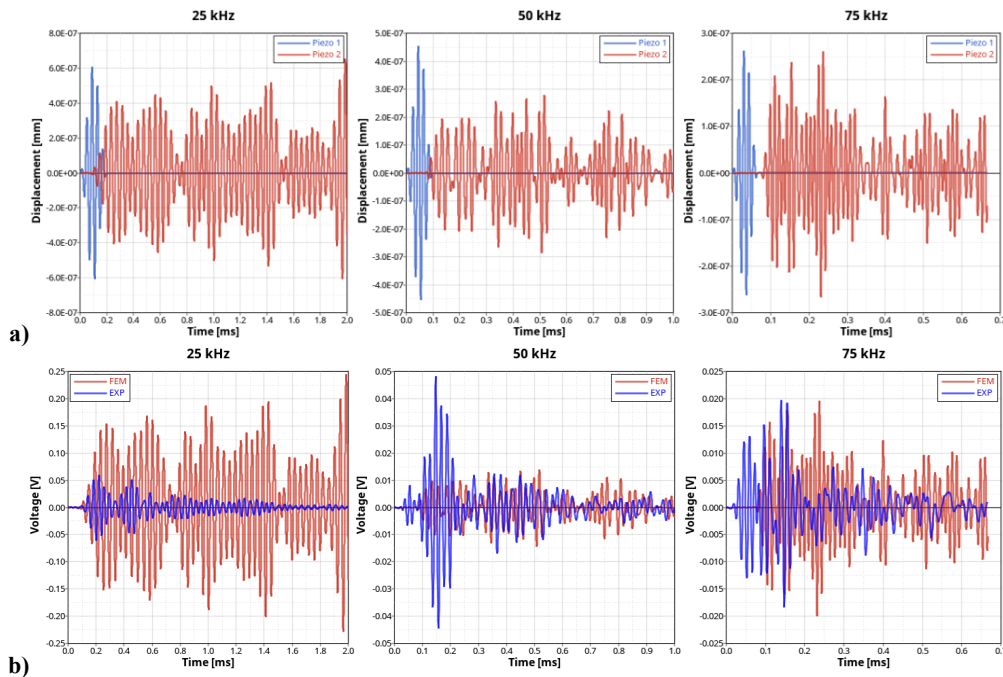


Figure 6.18 – Results at 25, 50, 75 kHz for Simulacrum specimen made of CFRP: a) virtual Displacement of piezo actuator 1 and sensor 2, b) correlation between virtual and real Voltage signals of piezo 2

6.2.4. Leaf Spring Component

The Leaf Spring has four couples of piezo actuators and sensors, which three sensors are placed at various distances in the middle of the component and one at 45° respect to the actuator.

Figure 6.19 describes the evolution of wave propagation, in terms of 1st Principal Stress: a) actuation begins, b) waves spread uniformly with circular propagation reaching the piezo sensors 2 and 5, then the waves propagate on the length of the component reaching the piezo sensors 3 and 4, while on piezo sensors 2, 3, 5 continue to receive the waves reflected from the near edges.

Figure 6.20 a) shows that the virtual displacement for all the piezo sensors has quite the same amplitude and the waves arrive before to piezo sensor 2 then 5, 3, 4 according to their distance from the actuator.

Figure 6.20 b) reports the Voltage correlations, that is is affected by an interference in the experimental signal before 0.25 ms only for the piezo sensor 4. All the real responses are in the order of 1 mV, but the FEM model simulates accurately the Voltage amplitude with the time of the first wave arrived.

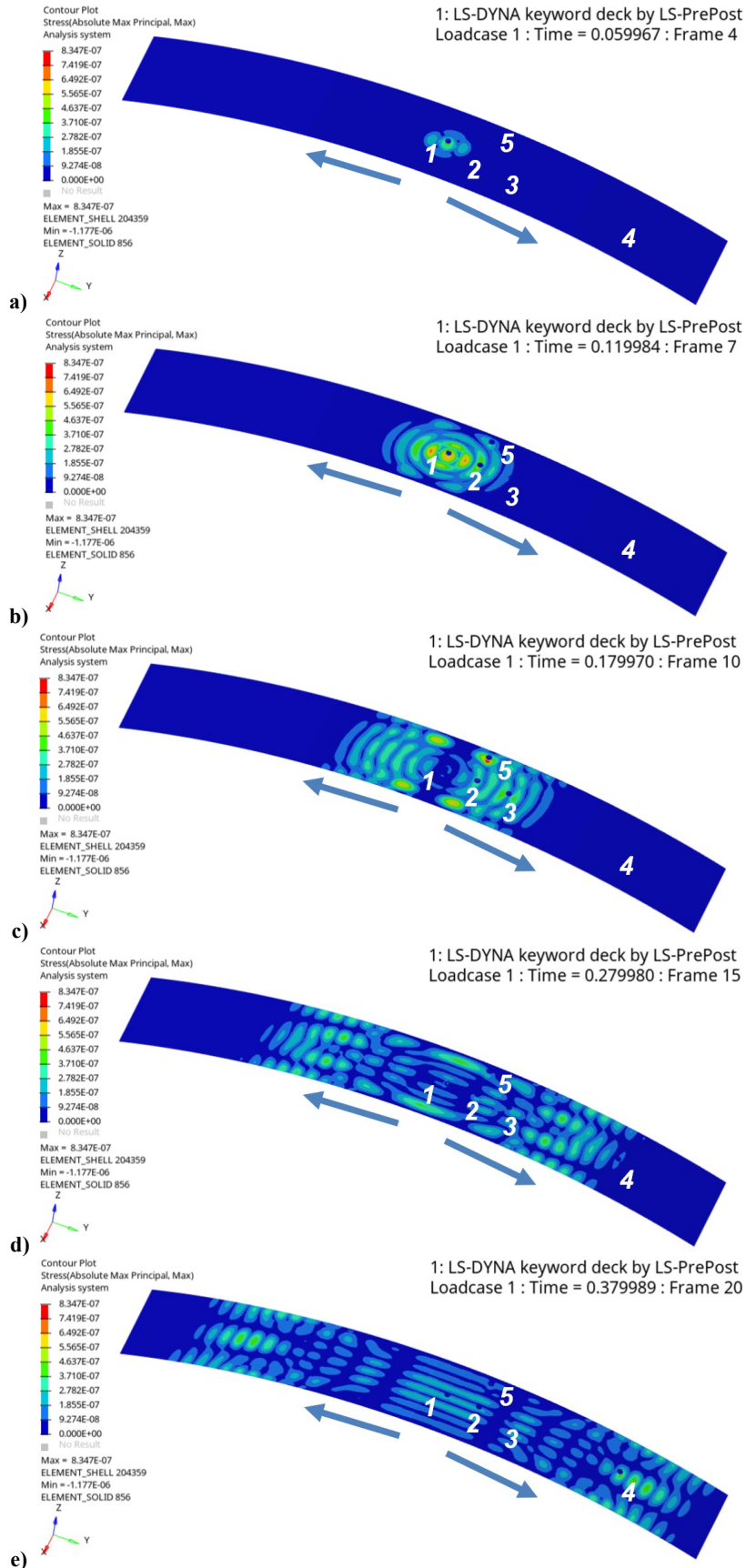


Figure 6.19 – Evolution of the wave propagation on the Leaf Spring at 25 kHz, in terms of 1st Principal Stress at different simulation time

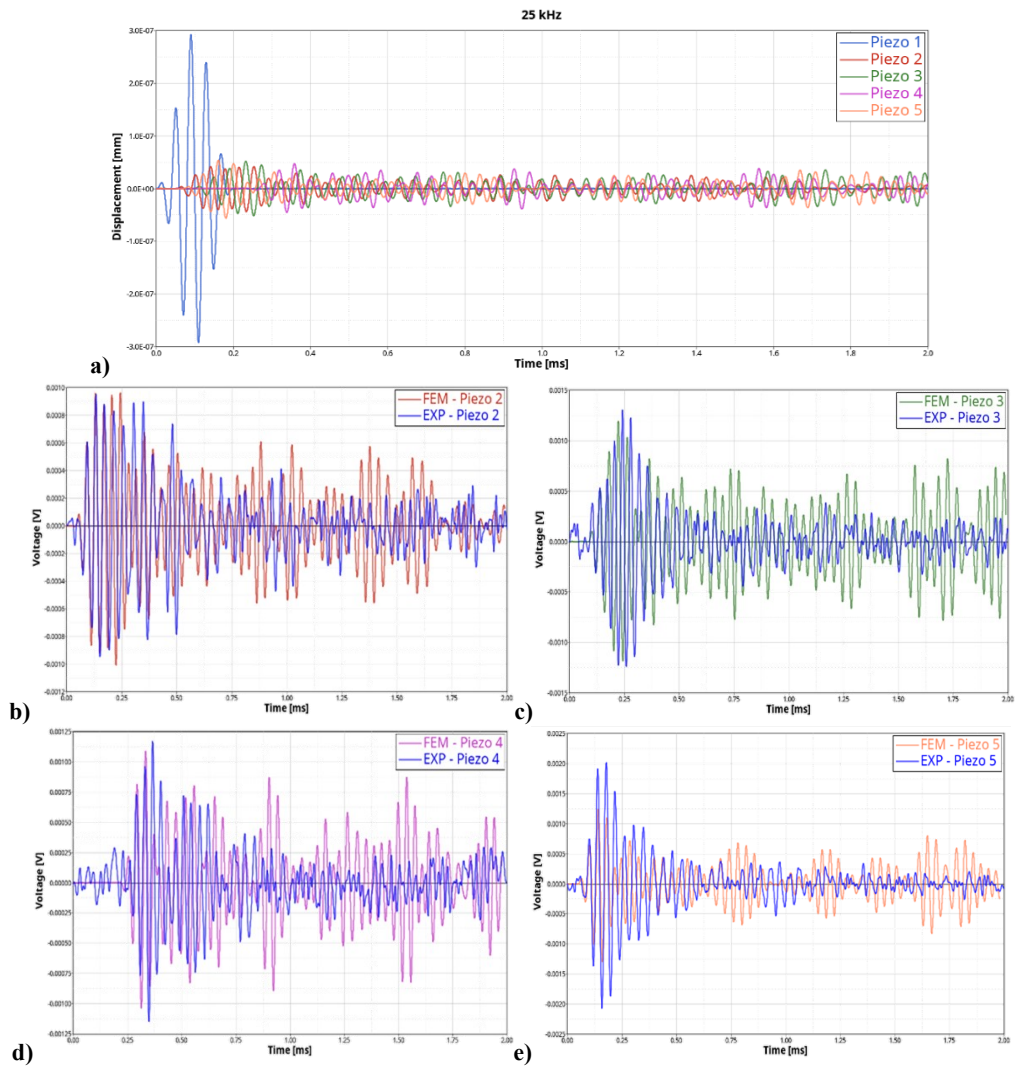


Figure 6.20 – Results at 25 kHz for Leaf Spring: a) virtual Displacement of piezo actuator 1 and sensors 2, 3, 4, 5, correlation between virtual and real Voltage signals of b) piezo sensor 2, c) piezo sensor 3, d) piezo sensor 4, e) piezo sensor 5

Chapter 7

Conclusions

The main goal of this Thesis has been the application of a Structural Health Monitoring (SHM) system based on Piezoelectric transducers to an Automotive carbon fiber suspension component.

The proposed methodology was based on testing simple specimens made of three materials: carbon fiber composite, aluminum, steel. The different geometries, number of piezoelectric transducers used, combination of test configurations and loading cases increased in complexity to reach the wider knowledge of the system response for the final tests on Leaf Spring component.

The definition of the system was original and started from a bibliographic research on the technical specifications of SHM system provided for the Aircraft industry. A National Instruments controller has been used for analog control of piezoelectric patches and data logging. The data processing has been assessed thanks to a properly developed MatLab program, indicating the Health status of the structure as a numerical value, called Damage Index. In particular, a series of six Algorithms that calculate different Damage Index are applied to raw data acquired in this thesis, in order to identify the best in terms of sensitivity to the particular conditions of the structures under test.

The research presented had the aim to combine the electronic validation of the SHM system with the exposure of specimens to loading configurations, in order to investigate the influence of that on the Damage Index calculation.

The six Damage Index algorithms have been applied for the processing analysis of two different programs: the “Off-line” program developed to post-process all the experimental data in a second time respect to the acquisition, and the “On-line” program developed only for the leaf spring component to post-process the experimental data at the moment of acquisition.

The Off-line Processing of SHM data have been applied on static tests scanning all the PZT couples at 100 frequencies from 1 kHz to 100 kHz with steps of 1 kHz. The PZT 1 remained the actuator for all the iterations and the other piezo patches

worked as sensors. The static configurations for the specimens and the leaf spring have been tested, considering the free condition, the clamping, the bending effects.

The main results of the Off-line Monitoring Tests on the specimens are:

- There is a high relation of Damage Index with the stress in the structure; this can be explained with geometry change of loaded structures, that affect the ultrasonic waves captured from piezoelectric sensors;
- In the wide range of 1-100 kHz, at the frequency of 75 kHz the Damage Index Algorithms showed the highest intensity of variation with bending load changes and damage severity increasing;
- Because of the absence in literature indications about the frequency selection for SHM data, the greatest variation of Damage Index has been intended as best sensitivity of system to external conditions;
- The experimental methodology has highlighted the CRC and NRE Damage Index Algorithms as the most sensitive to the loading variation.

The On-line Processing of SHM data have been executed monitoring all the piezo couples of the Leaf Spring component at the frequency of 75 kHz, chosen with the results of the SHM Off-line program. To assess the possibility of the SHM system to detect damages or variation on the component, a clamp has been used to locally increase the stiffness and simulate a damage on a Leaf Spring section.

Two real cases have been evaluated on the Leaf Spring: static condition, mounted on the bending fixture without load, and dynamic condition, with a cyclic bending loading after an initial phase of calibration in static condition at 0 kN. In both conditions the majority of Algorithms detected a significative influence of the bending loading and after the application of clamp on the Leaf Spring for the frequency of 75 kHz.

A Finite Element Analysis (FEA) has been conducted to understand the capability of virtual simulation to support the positioning of sensors on the component to be monitored. The Explicit solver of LS-DYNA has been used because the vibration phenomenon is time-dependent and its velocity is relatively high. The virtual simulations have been conducted at the three different frequencies of displacement signal 25, 50 and 75 kHz, in free conditions without constraints due to clamps or bending equipment, in the health condition without Damage.

An Electro-Mechanical Coupling methodology has been created to correlate the electrical variables to the mechanical displacement or forces. The theoretical relations of piezoelectricity for the thickness mode vibration of thin disks based on the properties of piezoceramic materials were used in this work.

The evolution of wave propagation on the specimens has been studied, in particular the virtual animations helped to understand the reflections on the edges and the preferred direction of waves. The FEM model simulated accurately the time of arrival for the 1st wave for all the frequencies, correlating better the Voltage amplitude for the frequencies 50 and 75 kHz.

Finally, to synthesize the main results of the Thesis, it is possible to state that:

- Piezoelectric Sensors response changes with materials, stress condition and damage type;
- Damage Index values must be linked to other measurements (e.g. Strain) when the structure is stressed;
- Frequency of 75 kHz is the most sensitive to Damage and bending load for Leaf Spring component;
- CRC is the preferred Algorithm to monitor Damage and bending load for Leaf Spring component;
- Waves received from piezo sensors can be simulated in a good manner and can support the design phase of the Sensor Network.

The described Damage Index Algorithms need fine tuning and lots of experiments to ensure reliability of the system for application in the Automotive field, but the results obtained in this Thesis are extremely encouraging.

References

- [1] D. Balageas, C.-P. Fritzen, A. Güemes. *Structural Health Monitoring*. Wiley. 2006.
- [2] J. M. Zanker. *Sensation, Perception and Action - An Evolutionary Perspective*. Palgrave Macmillan. 2010.
- [3] D. Roach, S. Neidigk. *Does the Maturity of Structural Health Monitoring Technology Match User Readiness?*, in: F.-K. Chang. *Structural Health Monitoring 2011 - Condition-Based Maintenance and Intelligent Structures, Volume 1 - 5.1 Introduction of SHM Survey - Background and Motivation*. DEStech Publications. 2011.
- [4] H. Rafik. *Contrôle santé des structures composites: approche expérimentale et statistique*, Ph.D. Thesis. 2012.
- [5] B. Christiansen. *A Complete Guide To Condition Based Maintenance (CBM)*. <https://limblecmms.com/blog/condition-based-maintenance>. (Last website visit on November 2020)
- [6] *Definition of Connected Car – What is the connected car? Defined*. <https://www.autoconnectedcar.com/definition-of-connected-car-what-is-the-connected-car-defined>. (Last website visit on November 2020)
- [7] S.S. Kessler, S.M. Spearing. *Structural Health Monitoring of Composite Materials using Piezoelectric Sensors*. 2002.
- [8] T. Ooijevaar. *Vibration Based Structural Health Monitoring of Composite Skin-Stiffener Structures*, Ph.D. Thesis. 2014.
- [9] M. Mitra, S. Gopalakrishnan. *Guided wave based structural health monitoring: A review*, Smart Materials and Structures. 2016.
- [10] N. Rauter, B. Hennings, M.N. Neumann, A. Asmus, R. Lammering. *Chapter 3 - Wave Propagation in Elastic Solids: An Analytical Approach*, in: R. Lammering, U. Gabbert, M. Sinapius, T. Schuster, P. Wierach. *Lamb-Wave Based Structural Health Monitoring in Polymer Composites*, Research Topics in Aerospace. 2018.
- [11] Y-K. An, M.K. Kim, H. Sohn. *Chapter 4 - Piezoelectric transducers for assessing and monitoring civil infrastructures*, in: M.L. Wang, J.P. Lynch, H. Sohn. *Sensor Technologies for Civil Infrastructures - Volume 1: Sensing Hardware and Data Collection Methods for Performance Assessment*, Woodhead Publishing Series in Electronic and Optical Materials. 2014.
- [12] A. Marzani, S. Salamone. *Numerical prediction and experimental verification of temperature effect on plate waves generated and received by piezoceramic sensors*, Mechanical Systems and Signal Processing. 2012.

- [13] B. Poddar, C.R. Bijudas, M. Mitra, P.M. Mujumdar. *Damage detection in a woven-fabric composite laminate using time-reversed Lamb wave*, Structural Health Monitoring. 2012.
- [14] G. Mook, J. Pohl, Y. Simonin. *Chapter 19 - Lamb Wave Generation, Propagation, and Interactions in CFRP Plates*, in: R. Lammering, U. Gabbert, M. Sinapius, T. Schuster, P. Wierach. *Lamb-Wave Based Structural Health Monitoring in Polymer Composites*, Research Topics in Aerospace. 2018.
- [15] F. Raddatz, A. Szewieczek, M. Sinapius. *Chapter 5 - Experimental Methods*, in: R. Lammering, U. Gabbert, M. Sinapius, T. Schuster, P. Wierach. *Lamb-Wave Based Structural Health Monitoring in Polymer Composites*, Research Topics in Aerospace. 2018.
- [16] L. Wang, F.G. Yuan. *Group velocity and characteristic wave curves of Lamb waves in composites: Modeling and experiments*, Composites Science and Technology. 2007.
- [17] N.D. Boffa. *Structural Health Monitoring (SHM) systems in aircraft: wing damage detection employing guided waves techniques*, Ph.D. Thesis. 2016.
- [18] A. Gianneo, M. Carboni, M. Giglio. *Feasibility study of a multi-parameter probability of detection formulation for a Lamb waves-based structural health monitoring approach to light alloy aeronautical plates*, Structural Health Monitoring. 2017.
- [19] M. Kannusamy, S. Kapuria, S. Sasmal. *Accurate baseline-free damage localization in plates using refined Lamb wave time-reversal method*, Smart Materials and Structures. 2020.
- [20] Acellent Technologies, Inc. <https://www.acellent.com>. (Last website visit on November 2020).
- [21] F. Lionetto, A. Licciulli, F. Montagna, A. Maffezzoli. *Piezoceramics: an introductory guide to their practical applications*, Materials & Processes. 2004.
- [22] C.J. Keulen. *Process and Structural Health Monitoring of Composite Structures with Embedded Fiber Optic Sensors and Piezoelectric Transducers*, Ph.D. Thesis. 2012.
- [23] P. Sadílek, *Structural Health Monitoring of Composites using Piezoelectric Patches*, Ph.D. Thesis. 2013.
- [24] M.S. Salmanpour, Z.S. Khodaei, M.H. Ferri Aliabadi. *Impact Damage Localisation with Piezoelectric Sensors under Operational and Environmental Conditions*, Sensors. 2017.
- [25] X.P. Qing, S.J. Beard, A. Kumar, K. Sullivan, R. Aguilar, M. Merchant, M. Taniguchi. *The performance of a piezoelectric-sensor-based SHM system under a combined cryogenic temperature and vibration environment*, Smart Materials and Structures. 2008.
- [26] F.-K. Chang. *Composite Structures with Built-In Diagnostics*, Stanford University. 1999.
- [27] D.G. Bekas, Z. Sharif-Khodaei, M.H. Ferri Aliabadi. *An Innovative Diagnostic Film for Structural Health Monitoring of Metallic and Composite Structures*, Sensors. 2018.

- [28] A. Otto, P. Schittenhelm, K. Spanner. *Piezoelectric Solutions. Part I – Piezo Components & Materials. Part II – Piezo Actuators & Transducers. Part III – Piezo Actuator Tutorial*. Physik Instrumente (PI) GmbH & Co. 2016.
- [29] S. Bosse, D. Lehmlus, W. Lang, M. Busse. *Material-Integrated Intelligent Systems*, Wiley-VCH. 2018.
- [30] D. Balageas, C.P. Fritzen, A. Güemes. *Structural Health Monitoring*, ISTE. 2006.
- [31] C.J. Keulen, M. Yildiz, A. Suleman. *Damage detection of composite plates by Lamb wave ultrasonic tomography with a sparse hexagonal network using damage progression trends*, Nondestructive Testing and Evaluation. 2012.
- [32] X. Liu, Y. Xu, N. Li, X. Wang, W. Zhang. *Effect of Adhesive Debonding on the Performance of Piezoelectric Sensors in Structural Health Monitoring Systems*, Sensors. 2019.
- [33] O. Putkis, R.P. Dalton, A.J. Croxford. *The influence of temperature variations on ultrasonic guided waves in anisotropic CFRP plates*, Ultrasonics. 2015.
- [34] J.-B. Ihn, F.-K. Chang. *Detection and monitoring of hidden fatigue crack growth using a built-in piezoelectric sensor/actuator network: I. Diagnostics*, Smart Materials and Structures. 2004.
- [35] J. Yan, H. Jin, H. Sun, X. Qing. *Active Monitoring of Fatigue Crack in the Weld Zone of Bogie Frames Using Ultrasonic Guided Waves*, Sensors. 2019.
- [36] L.E. Mujica, F. Gharibnezhad, J. Rodellar, M. Todd. *Considering temperature effect on robust principal component analysis orthogonal distance as a damage detector*, Structural Health Monitoring. 2019.
- [37] N. Mechbal, M. Rebillat. *Damage indexes comparison for the structural health monitoring of a stiffened composite plate*, 8th ECCOMAS Thematic Conference on Smart Structures and Materials. 2017.
- [38] T. Clarke, F. Simonetti, P. Cawley. *Guided wave health monitoring of complex structures by sparse array systems: Influence of temperature changes on performance*, Journal of Sound and Vibration. 2010.
- [39] N.P. Yelve, S. Rode, P. Das, P. Khanolkar. *Some new algorithms for locating a damage in thin plates using lamb waves*, Engineering Research Express. 2019
- [40] X. Zhao, H. Gao, G. Zhang, B. Ayhan, F. Yan, C. Kwan, J.L. Rose. *Active health monitoring of an aircraft wing with embedded piezoelectric sensor/actuator network: I. Defect detection, localization and growth monitoring*, Smart Materials and Structures. 2007.
- [41] K.J. Schubert, A.S. Herrmann. *On the influence of moisture absorption on Lamb wave propagation and measurements in viscoelastic CFRP using surface applied piezoelectric sensors*, Composite Structures. 2012.
- [42] S.T. Daura. *Potentials of guided waves in aircraft CFRP components in terms of damage tolerance and SHM implementation*, Final Project. 2014.
- [43] K. Nakatani, S. Kubo, T. Sakagami, D. Shiozawa, M. Takagi. *An experimental study on the identification of delamination in a composite material by the passive electric potential CT method*, Measurement Science and Technology. 2007.

- [44] H. Xiao, Y. Shen, L. Xiao, W. Qu, Y. Lu. *Damage detection in composite structures with high-damping materials using time reversal method*, Nondestructive Testing and Evaluation. 2018.
- [45] G. Park, C.R. Farrar, F. Lanza di Scalea, S. Coccia. *Performance assessment and validation of piezoelectric active-sensors in structural health monitoring*, Smart Materials and Structures. 2006.
- [46] J.E. Michaels, S.J. Lee, T.E. Michaels. *Impact of Applied Loads on Guided Wave Structural Health Monitoring*, Review of Progress in Quantitative Nondestructive Evaluation. 2011.
- [47] J. Lee, Y. Cho. *Using Lamb Waves to Monitor Moisture Absorption in Thermally Fatigued Composite Laminates*, Journal of the Korean Society for Nondestructive Testing. 2016.
- [48] X. Lu, C.K. Soh, P.V. Avvari. *Lamb wave propagation in vibrating structures for effective health monitoring*, Health Monitoring of Structural and Biological Systems. 2015.
- [49] R. Gorgin, Y. Luo, Z. Wu. *Environmental and operational conditions effects on Lamb wave based structural health monitoring systems: A review*, Ultrasonics. 2020.
- [50] A. Güemes, A. Fernandez-Lopez, A.R. Pozo, J. Sierra-Pérez. *Structural Health Monitoring for Advanced Composite Structures: A Review*, Journal of Composites Science. 2020.
- [51] C.S. Wang, F. Wu, F.-K. Chang. *Structural health monitoring from fiber-reinforced composites to steel-reinforced concrete*, Smart Materials and Structures. 2001.
- [52] Y.-S. Roh. *Built-In Diagnostics for Identifying an Anomaly in Plates using Wave Scattering*, Ph.D. Thesis. 1998.
- [53] C. Fendzi. *Contrôle Santé des Structures Composites: application à la Surveillance des Nacelles Aéronautiques*, Ph.D. Thesis. 2015.
- [54] T. Hajzargerbashi, T. Kundu, S. Bland. *An improved algorithm for detecting point of impact in anisotropic inhomogeneous plates*, Ultrasonics. 2011.
- [55] R. Gorgin, Z. Wu, D. Gao, Y. Wang. *Damage size characterization algorithm for active structural health monitoring using the A0 mode of Lamb waves*, Smart Materials and Structures. 2014.
- [56] Z.S. Khodaei, O. Bacarreza, M.H. Aliabadi. *Lamb-Wave Based Technique for Multi-Site Damage Detection*, Key Engineering Materials. 2013.
- [57] J. Hettler, M. Tabatabaeipour, S. Delrue, K. Van Den Abeele. *Linear and Nonlinear Guided Wave Imaging of Impact Damage in CFRP Using a Probabilistic Approach*, Materials. 2016.
- [58] M. Carello, A. G. Airale, A. Ferraris, A. Messana, L. Sisca. *Static Design and Finite Element Analysis of Innovative CFRP Transverse Leaf Spring*. Applied Composite Materials. 2017.
- [59] T.H. Loutas, P. Charlaftis, A. Airoidi, P. Bettini, C. Koimtzoglou, V. Kostopoulos. *Reliability of strain monitoring of composite structures via the use of optical fibre ribbon tapes for structural health monitoring purposes*, Composite Structures. 2015.

Appendix A

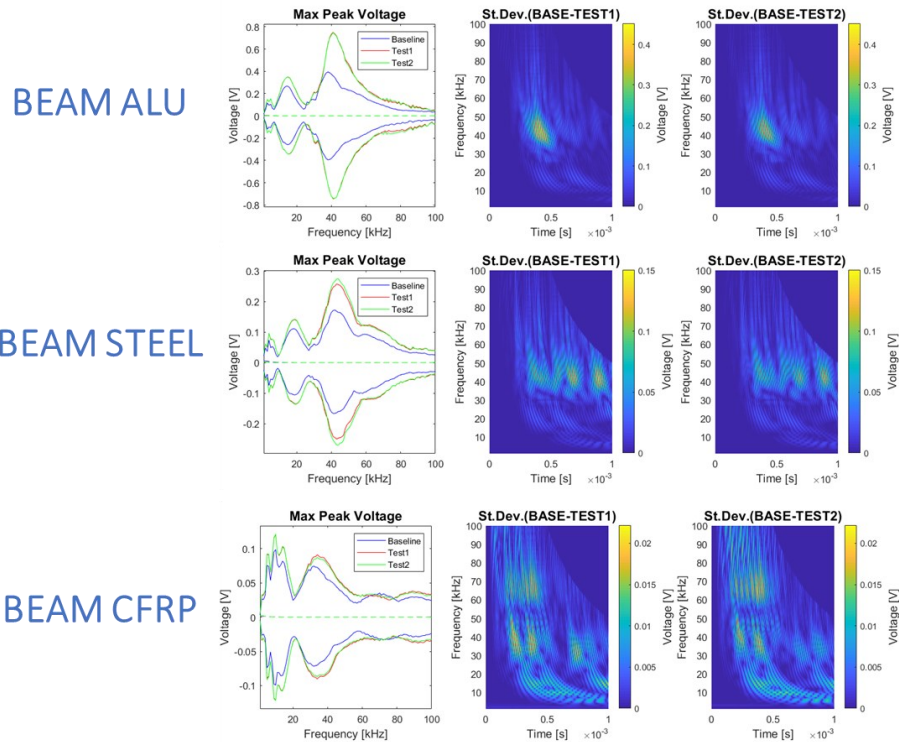
SHM Off-line Data & Results

As described in Chapter 3 for the Off-line methodology, for each specimen and configuration at 100 frequencies have been realized the representations of:

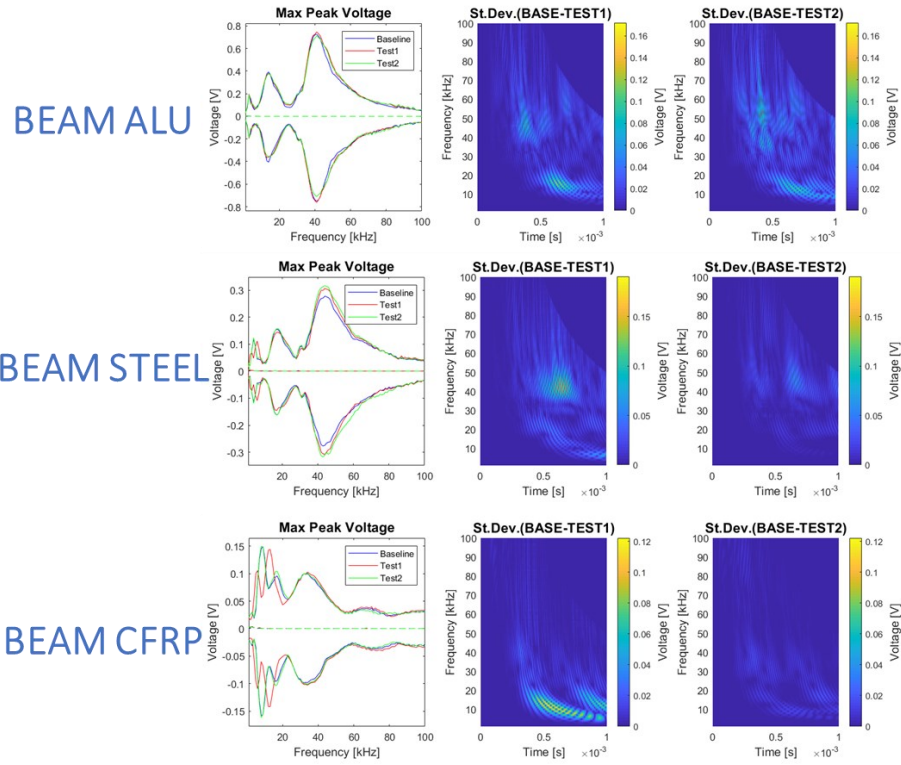
- raw signal data, as the maximum peak and the maximum standard deviation recorded for the same data series,
- standard deviation for a Test configuration related to Baseline,
- trend of Damage Index for Test 1 and Test 2 related to Baseline,
- percentage variation of Damage Index for Test 2 related to Baseline respect to Test 1 related to Baseline.

Beam specimen

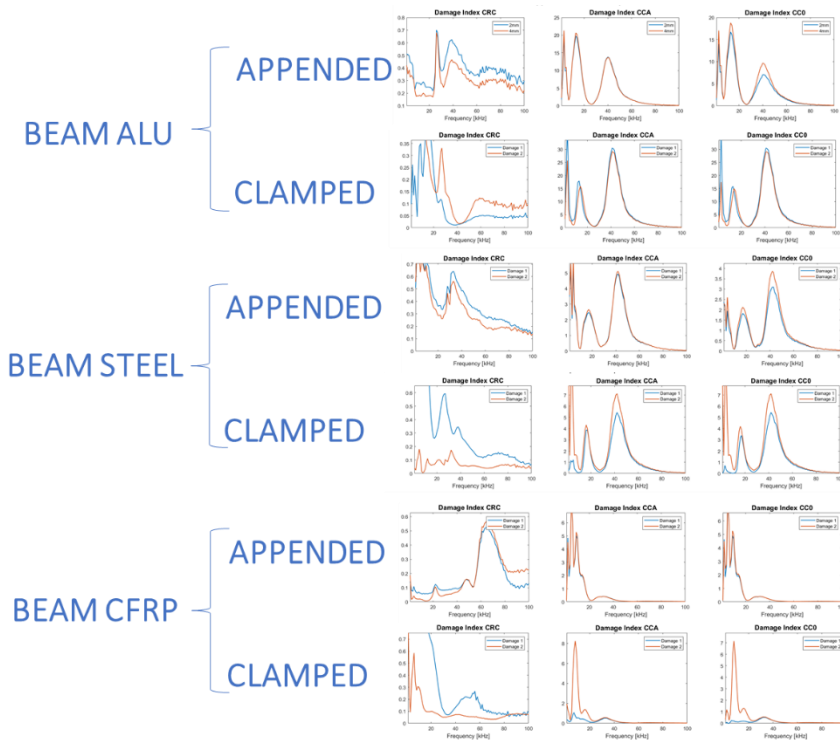
PZT 1-2 Appended:



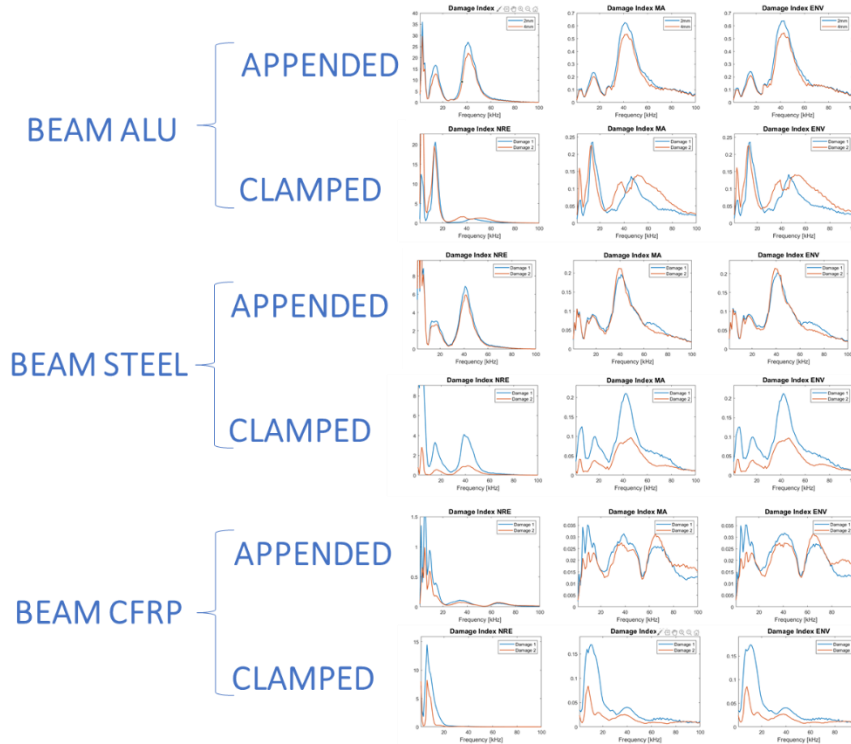
PZT 1-2 Clamped:



PZT 1-2 CRC, CCA, CCO:



PZT 1-2 NRE, MA, ENV:



Beam Specimen PZT 1-2 Percentage Variation of Damage Index of Damage 2 to No Damage respect to Damage Index of Damage 1 to No Damage:

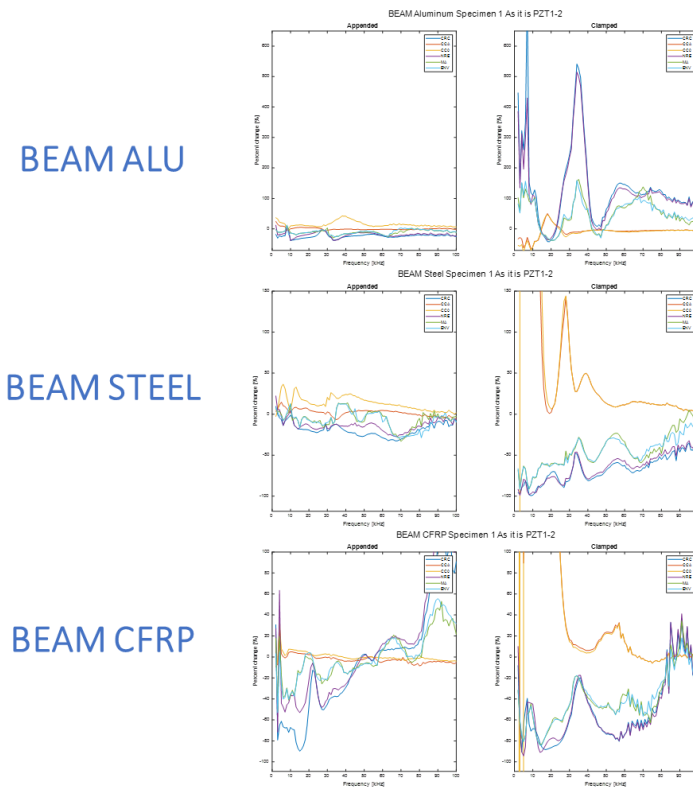
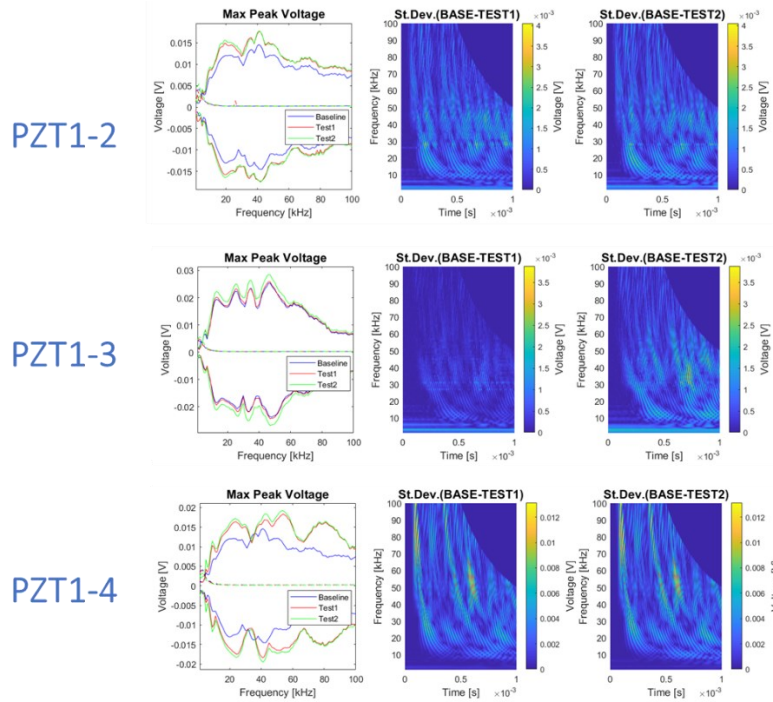
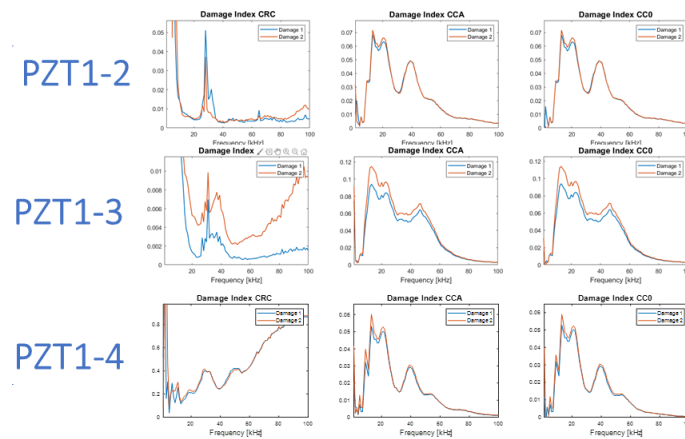


Plate specimen

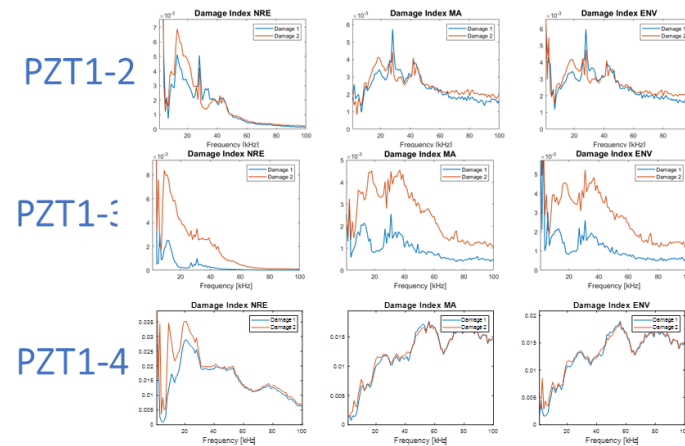
Aluminum on table:



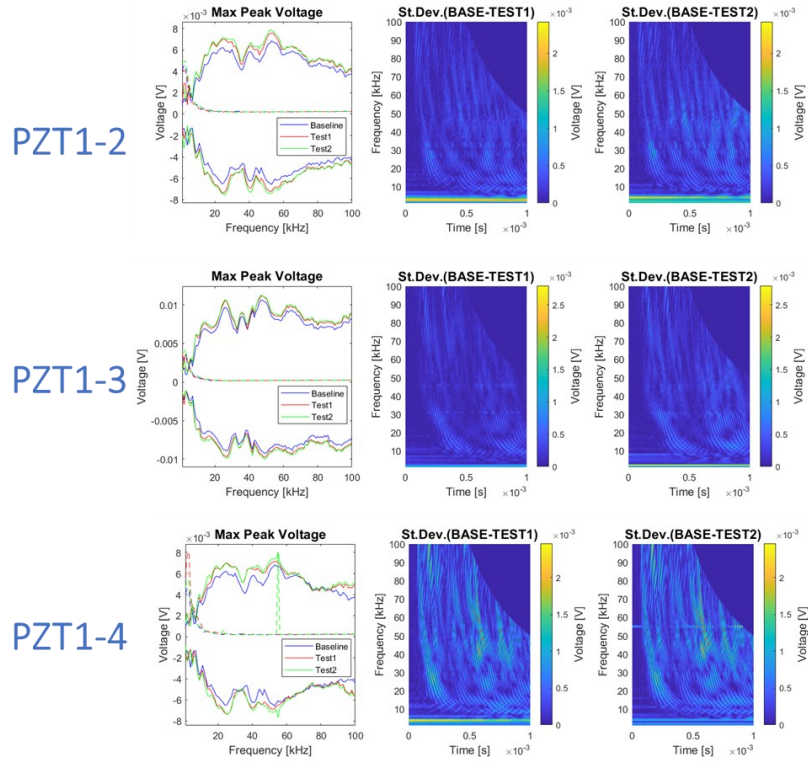
Aluminum on table CRC, CCA, CCO:



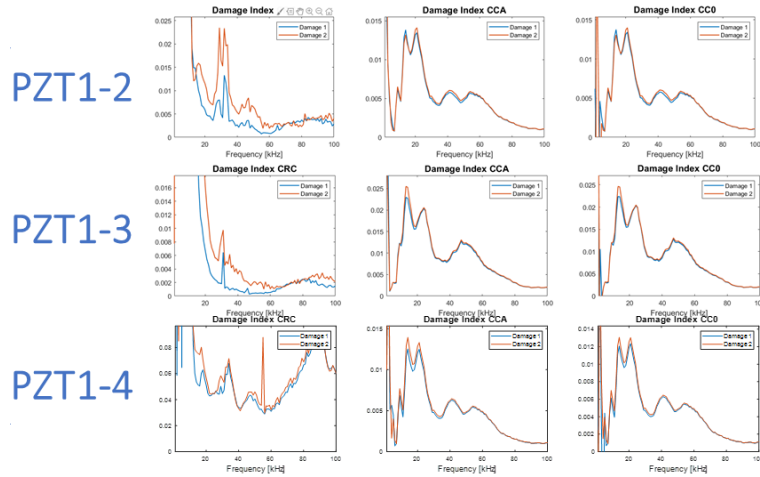
Aluminum on table NRE, MA, ENV:



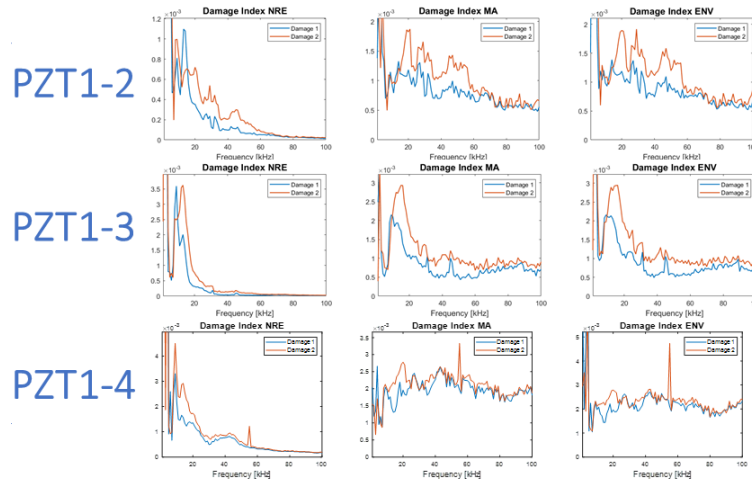
Steel on table:



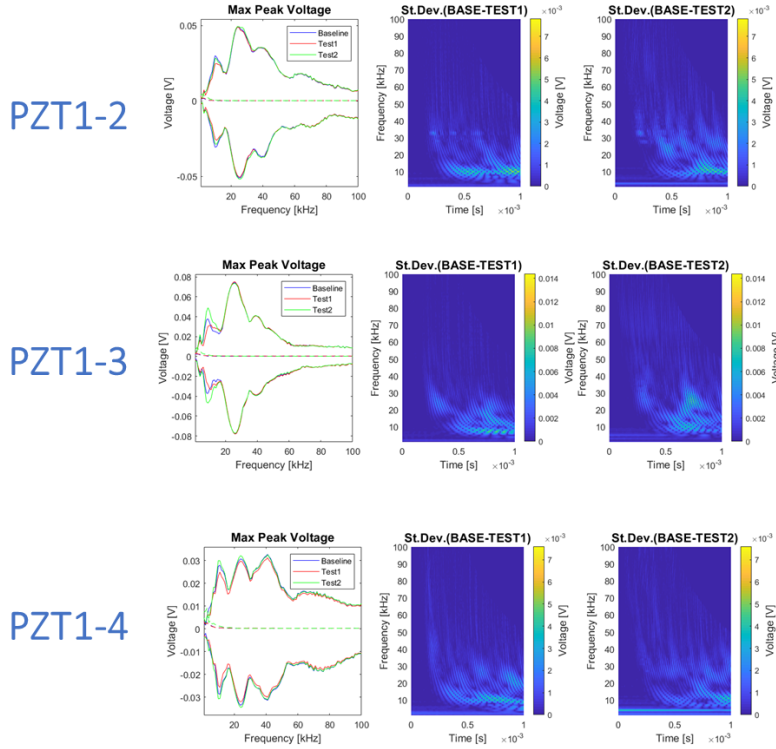
Steel on table CRC, CCA, CCO:



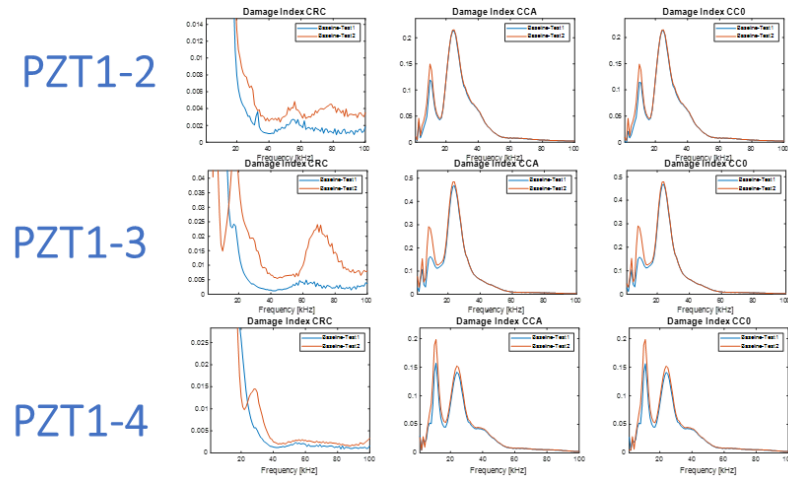
Steel on table NRE, MA, ENV:



CFRP on table:



CFRP on table CRC, CCA, CCO:



CFRP on table NRE, MA, ENV:

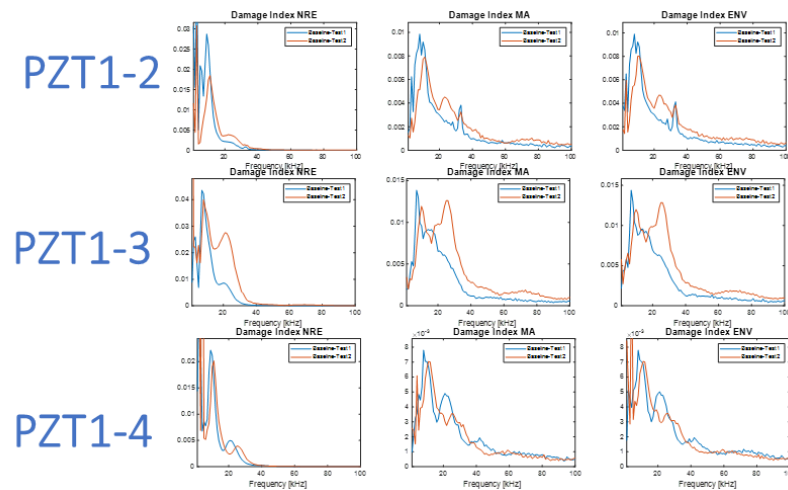


Plate Specimen PZT 1-2, PZT 1-3, PZT 1-4 Percentage Variation of Damage Index of Damage 2 to No Damage respect to Damage Index of Damage 1 to No Damage:

PLATE ALU

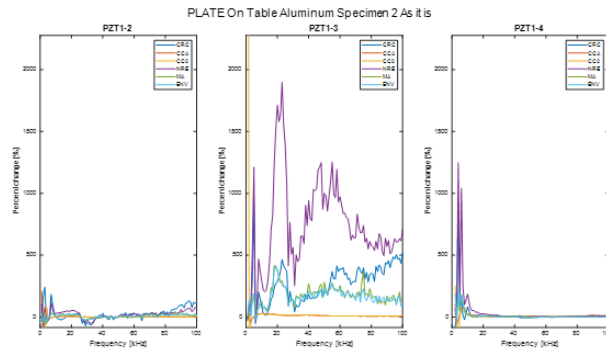


PLATE STEEL

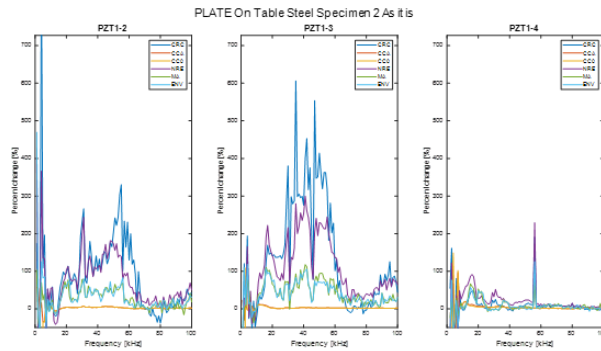
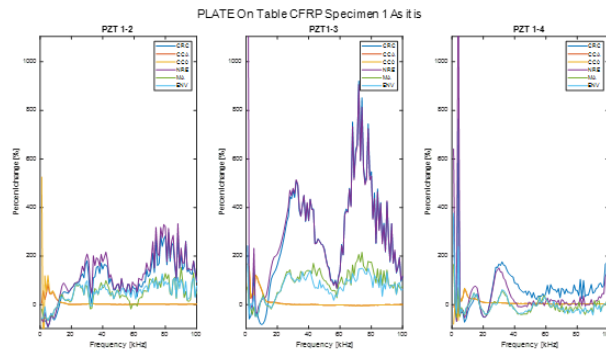


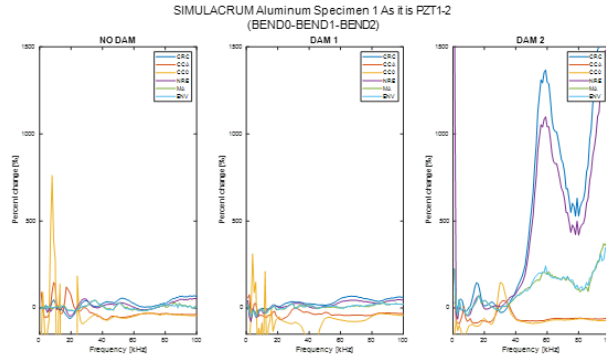
PLATE CFRP



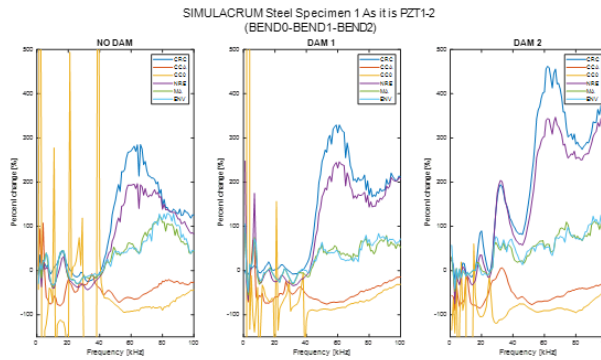
Simulacrum specimen

Simulacrum Specimen PZT 1-2 Percentage Variation of Damage Index of BEND2 to BEND0 respect to Damage Index of BEND1 to BEND0 in the three damage conditions:

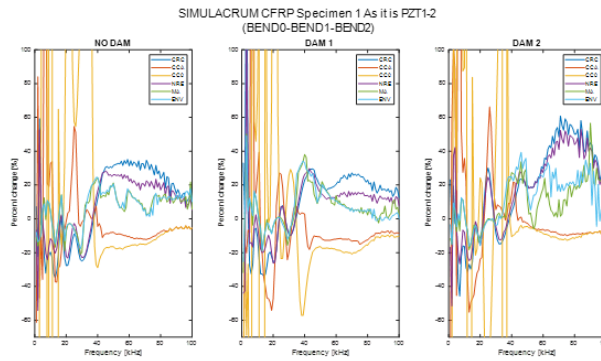
SIMULACRUM
ALU



SIMULACRUM
STEEL

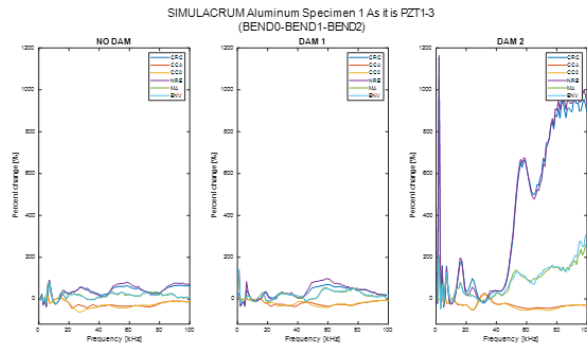


SIMULACRUM
CFRP

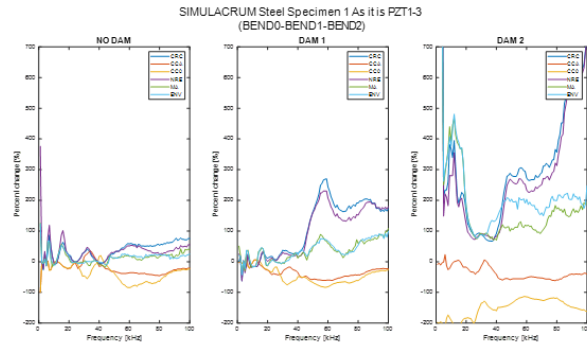


Simulacrum Specimen PZT 1-3 Percentage Variation of Damage Index of BEND2 to BEND0 respect to Damage Index of BEND1 to BEND0 in the three damage conditions:

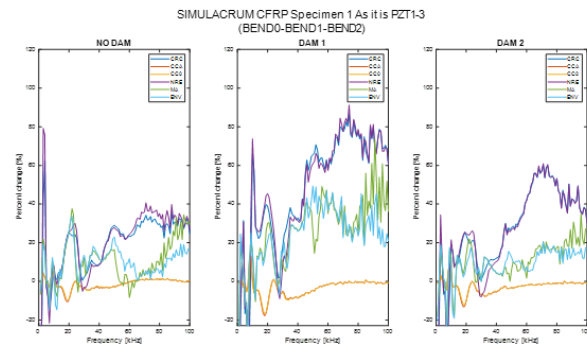
SIMULACRUM
ALU



SIMULACRUM
STEEL

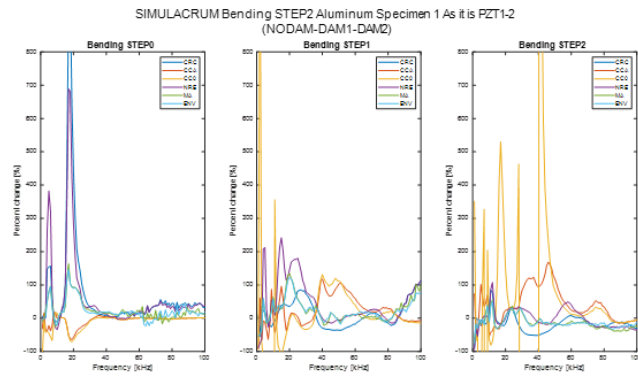


SIMULACRUM
CFRP

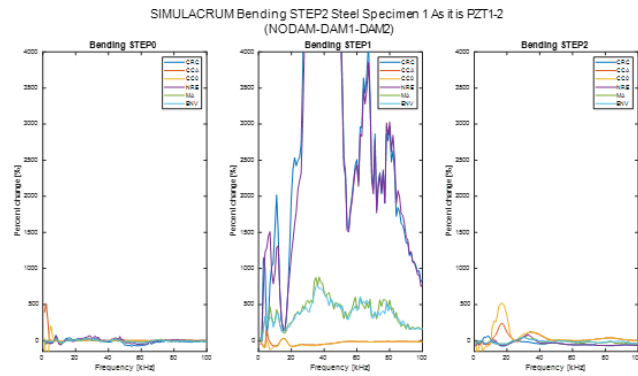


Simulacrum Specimen PZT 1-2 Percentage Variation of Damage Index of Damage 2 to No Damage respect to Damage Index of Damage 1 to No Damage in the three Bending steps:

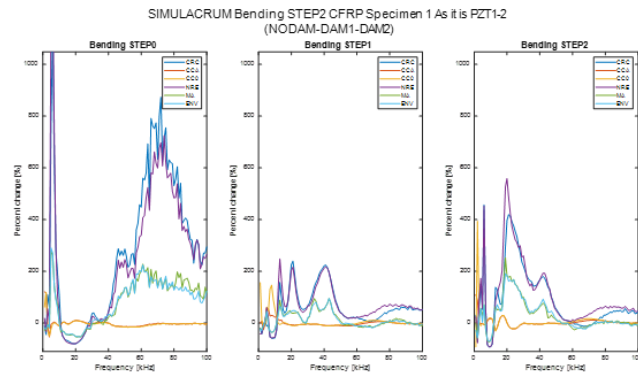
SIMULACRUM ALU



SIMULACRUM STEEL

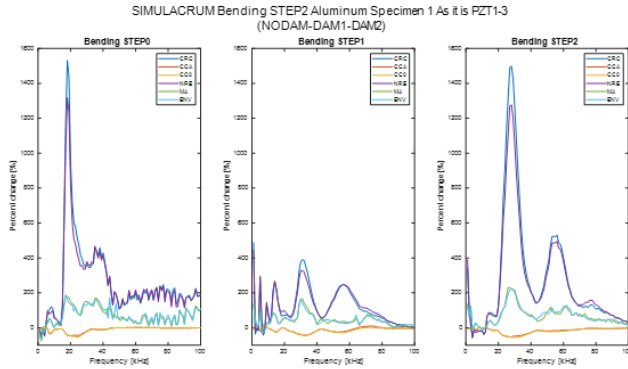


SIMULACRUM CFRP

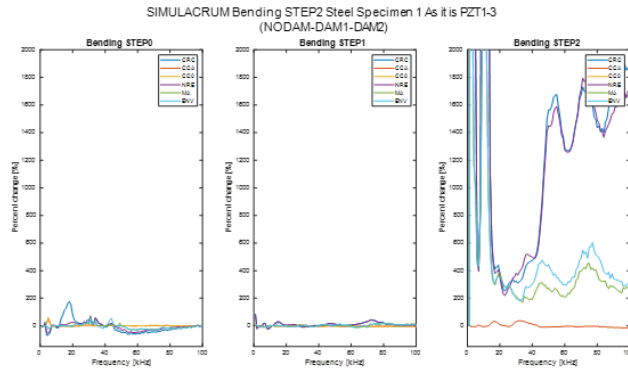


Simulacrum Specimen PZT 1-3 Percentage Variation of Damage Index of Damage 2 to No Damage respect to Damage Index of Damage 1 to No Damage in the three Bending steps:

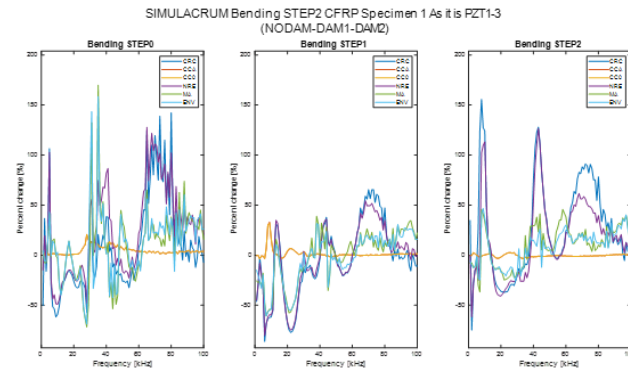
SIMULACRUM
ALU



SIMULACRUM
STEEL

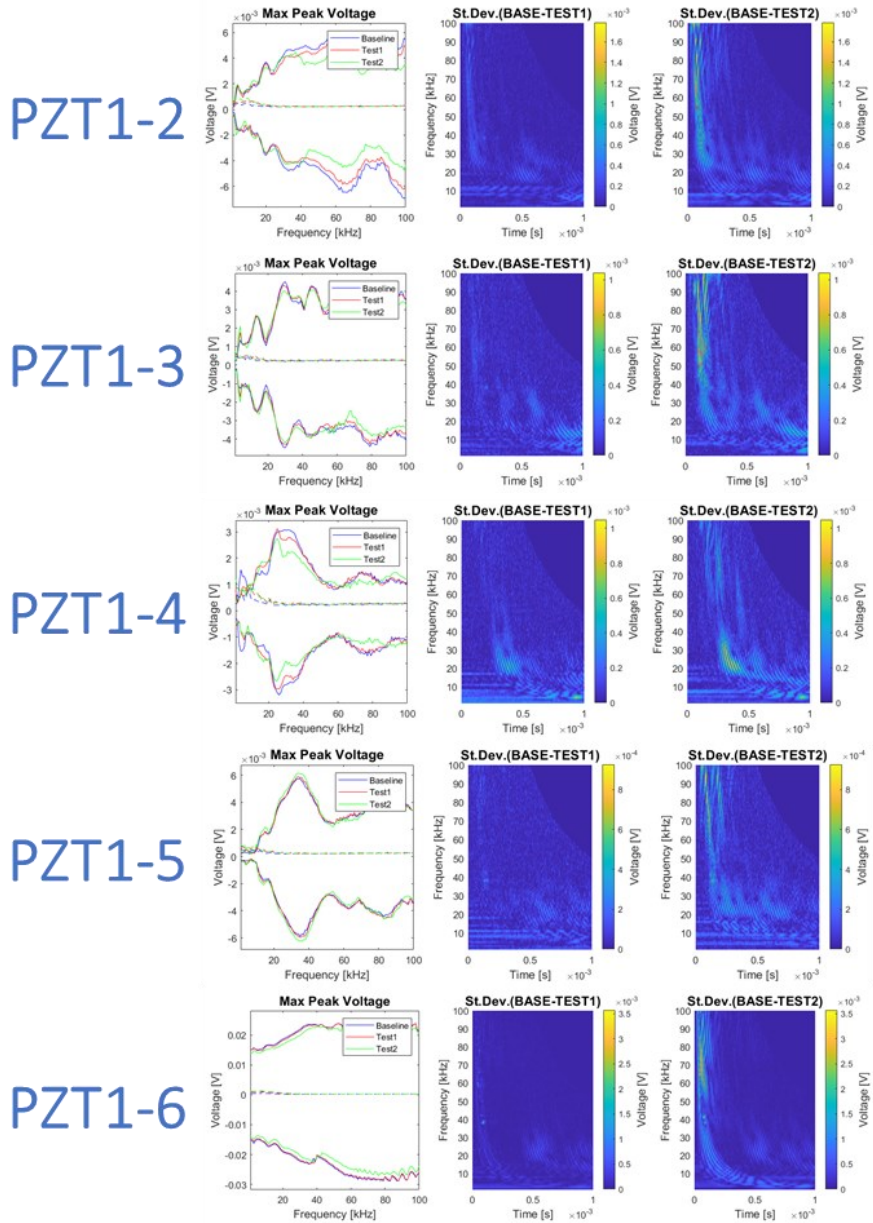


SIMULACRUM
CFRP

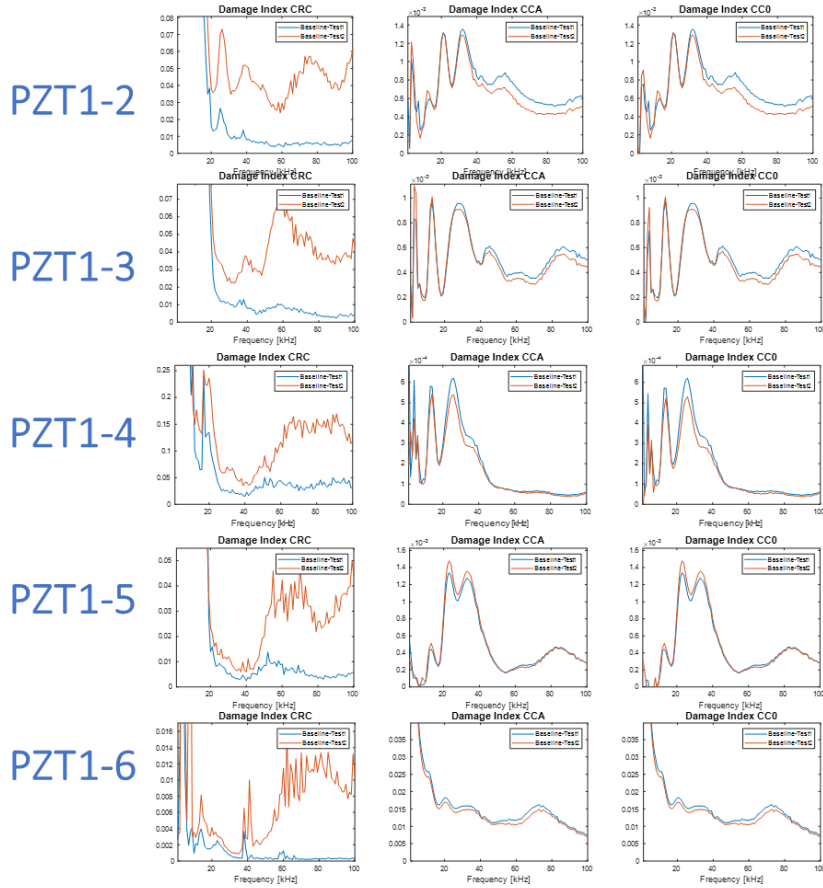


Leaf Spring component

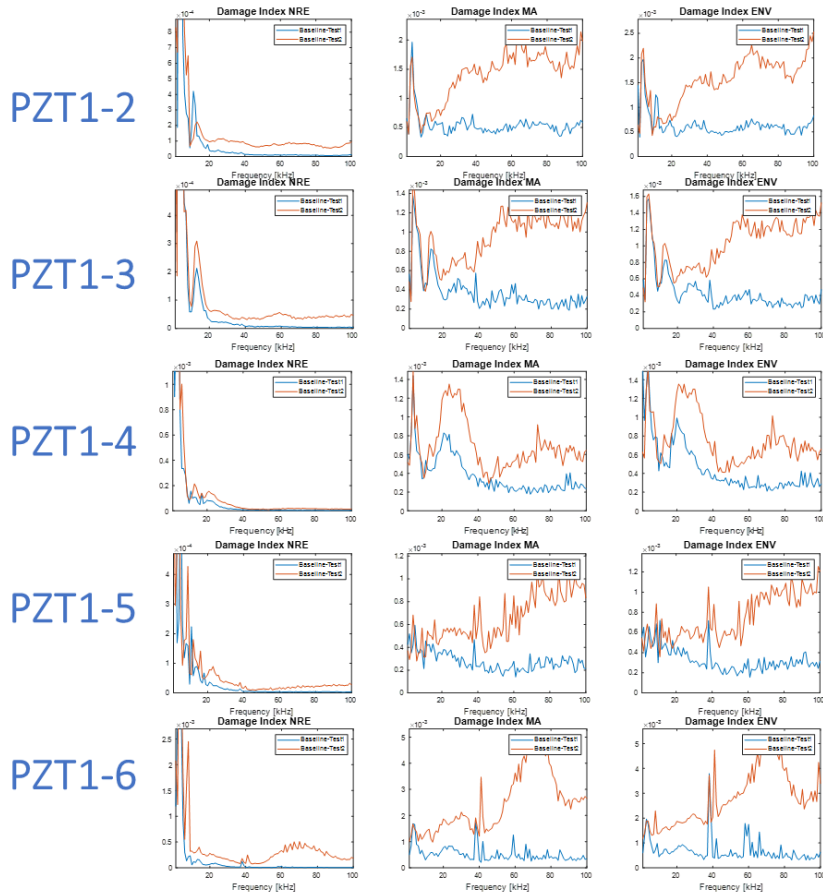
Leaf Spring BEND0-BEND1-BEND2:



Leaf Spring BEND0-BEND1-BEND2 CRC, CCA, CCO:

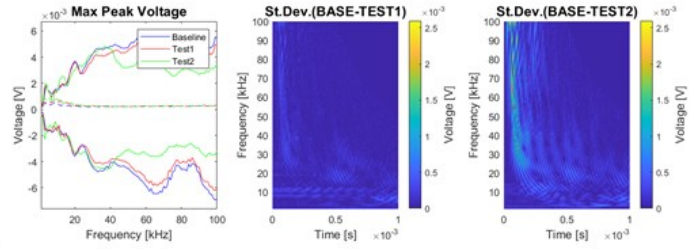


Leaf Spring BEND0-BEND1-BEND2 NRE, MA, ENV:

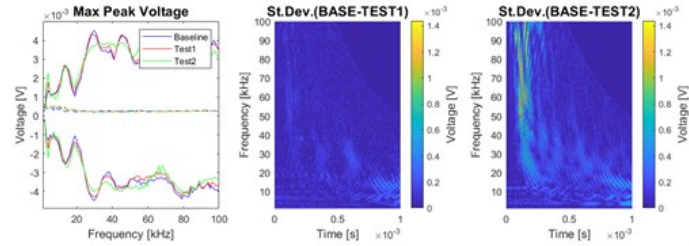


Leaf Spring BEND0-BEND1-BEND3:

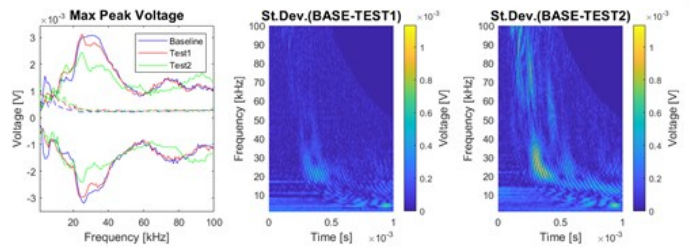
PZT1-2



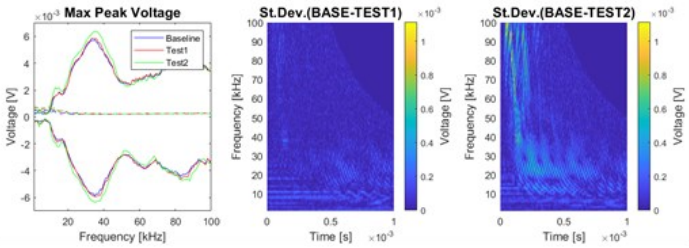
PZT1-3



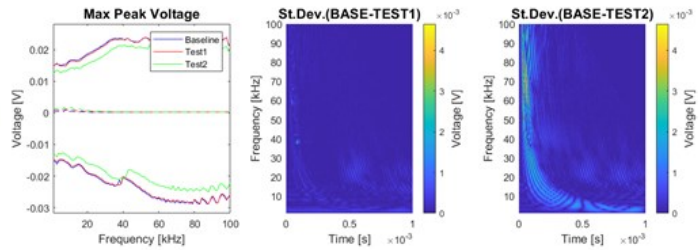
PZT1-4



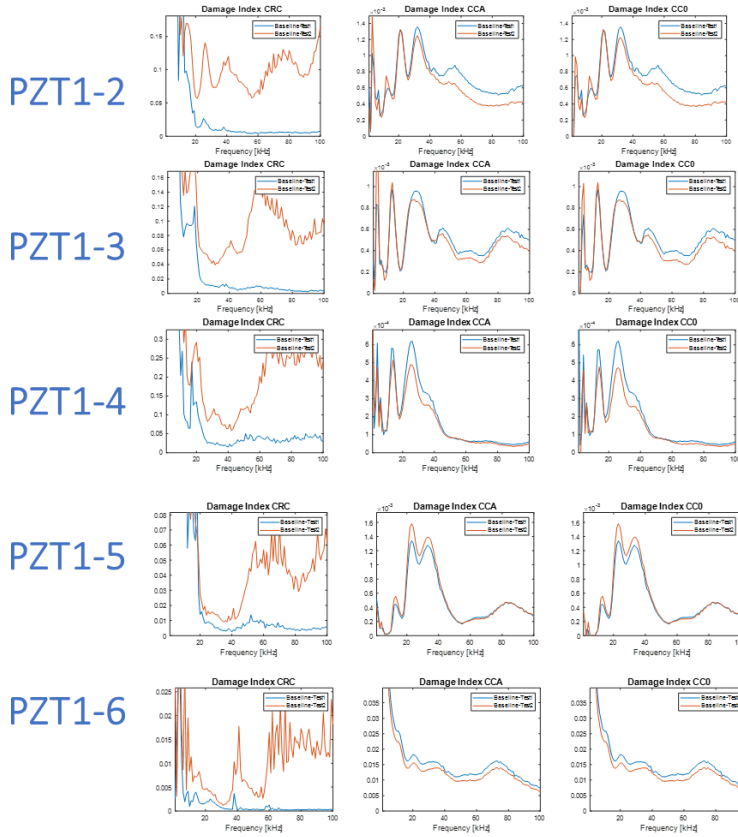
PZT1-5



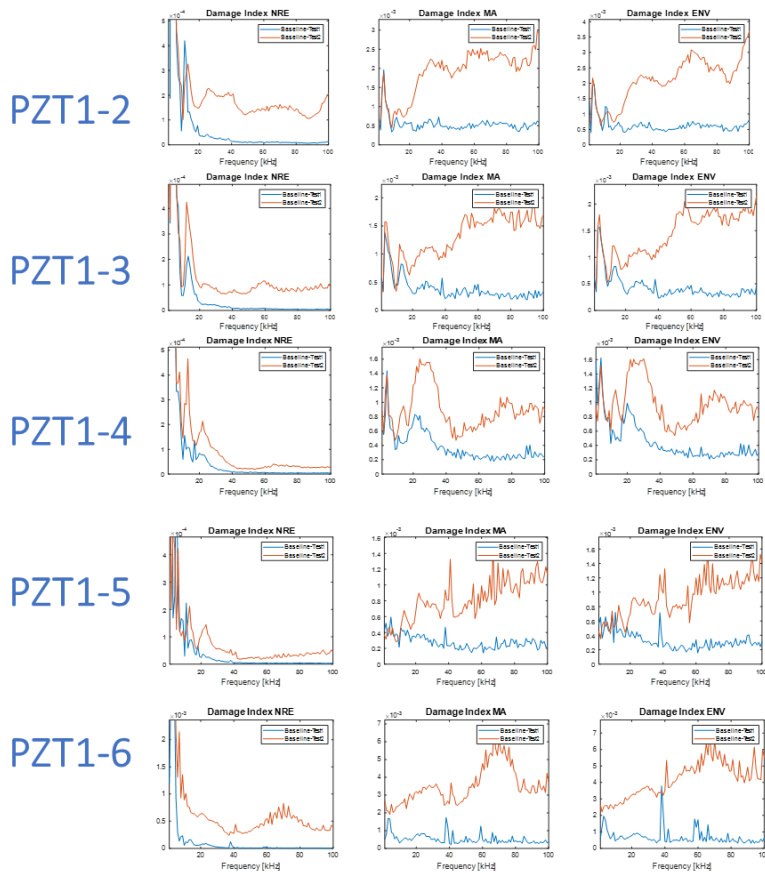
PZT1-6



Leaf Spring BEND0-BEND1-BEND3 CRC, CCA, CCO:

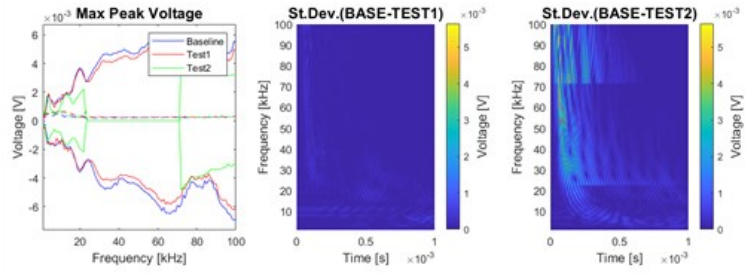


Leaf Spring BEND0-BEND1-BEND3 NRE, MA, ENV:

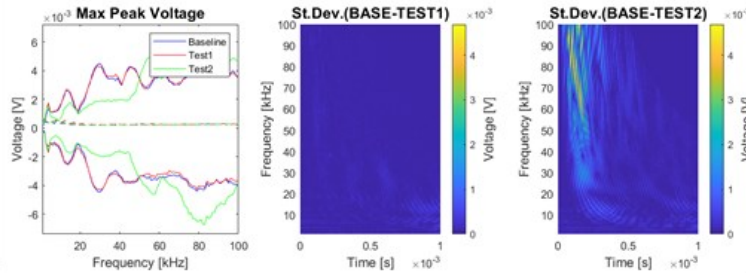


Leaf Spring BEND0-BEND1-BEND4:

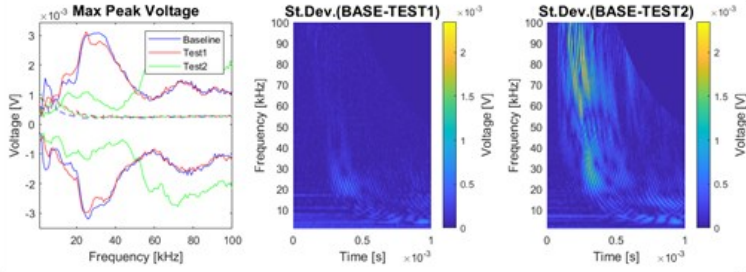
PZT1-2



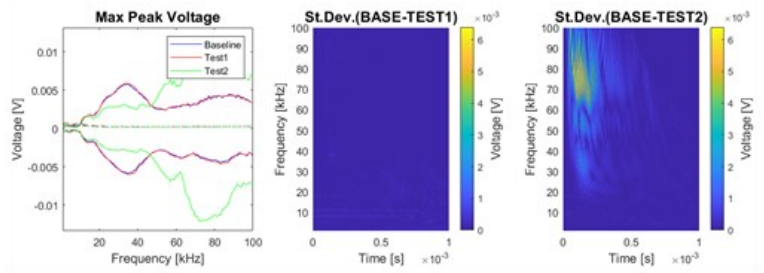
PZT1-3



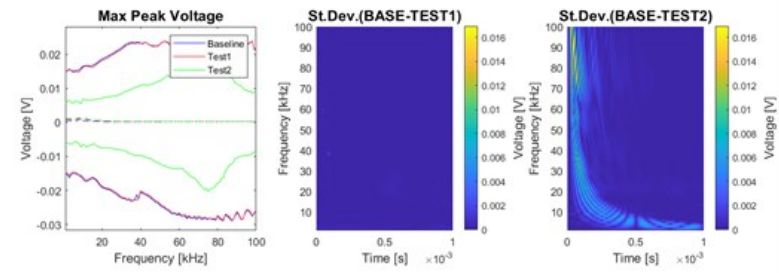
PZT1-4



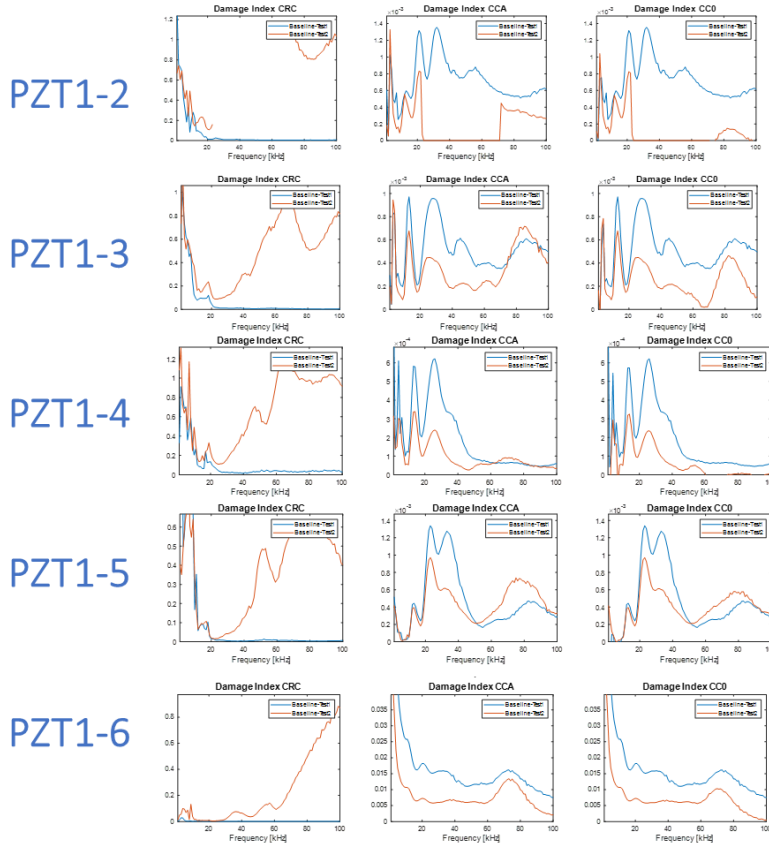
PZT1-5



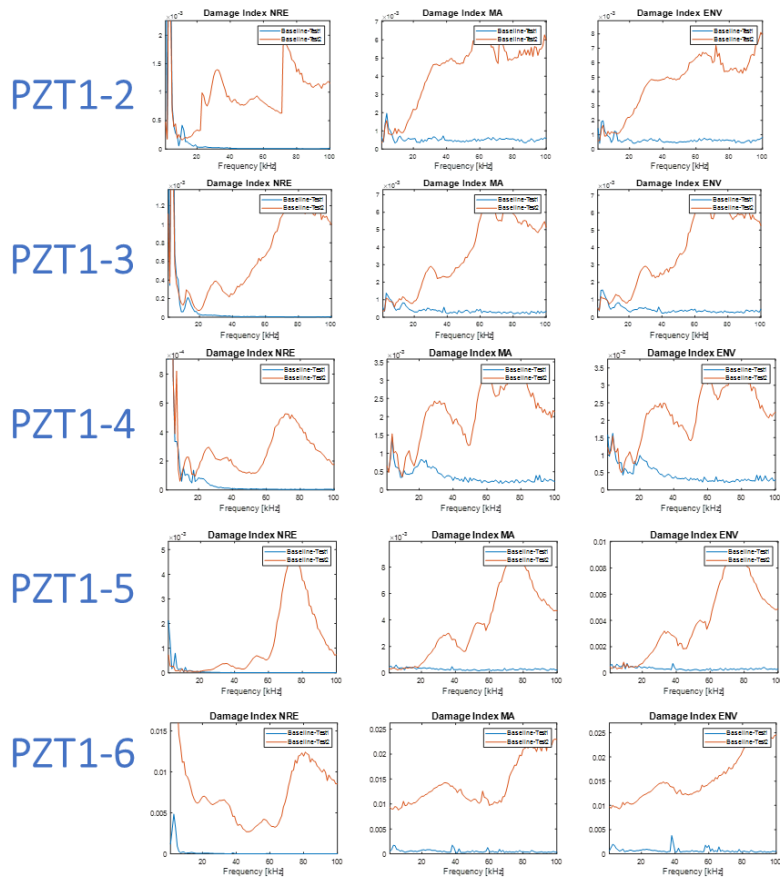
PZT1-6



Leaf Spring BEND0-BEND1-BEND4 CRC, CCA, CCO:

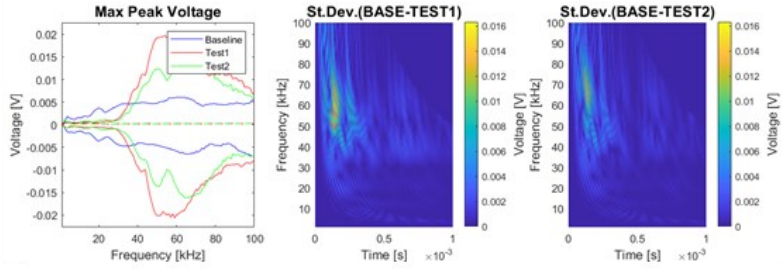


Leaf Spring BEND0-BEND1-BEND4 NRE, MA, ENV:

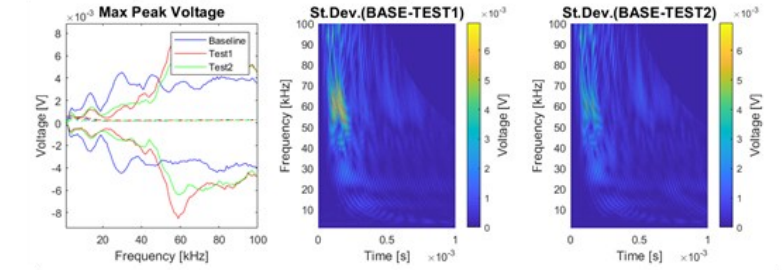


Leaf Spring BEND0-BEND0-APPEND:

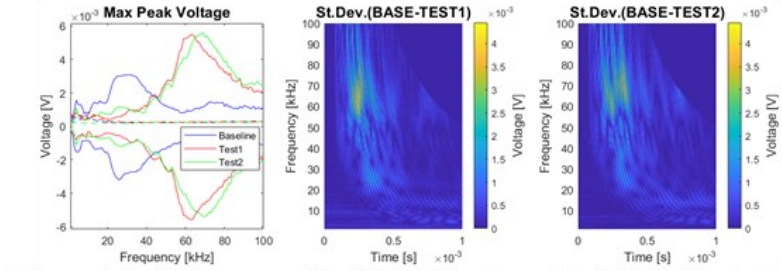
PZT1-2



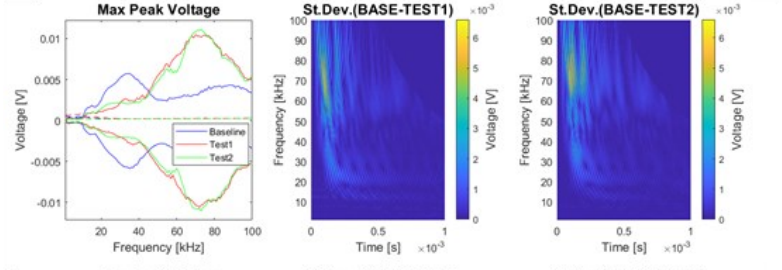
PZT1-3



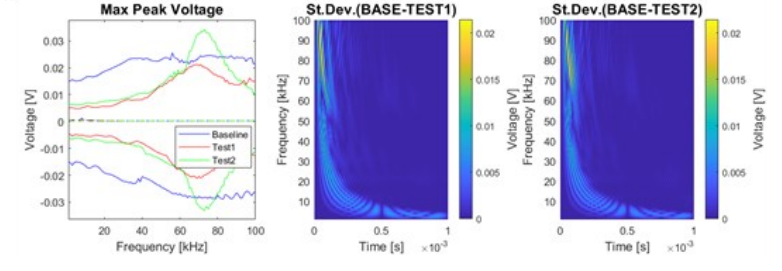
PZT1-4



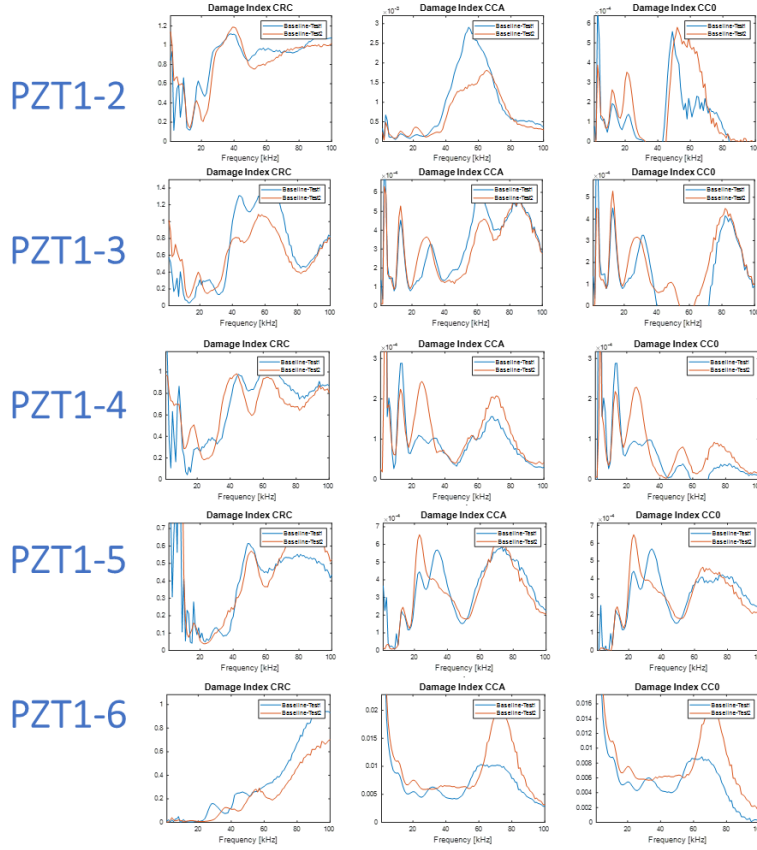
PZT1-5



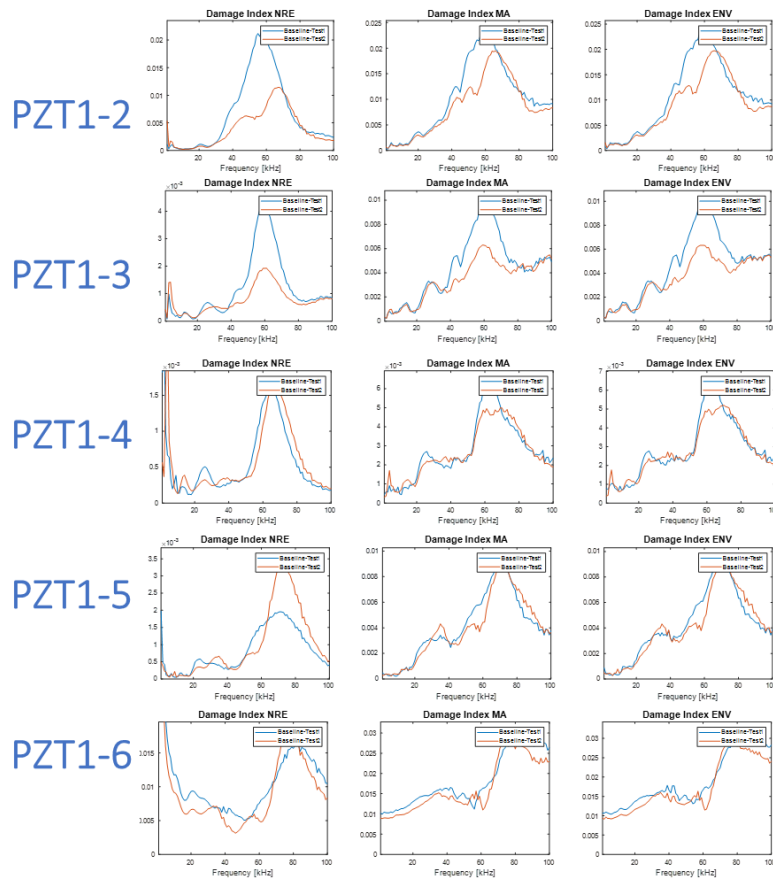
PZT1-6



Leaf Spring BEND0-BEND0-APPEND CRC, CCA, CCO:

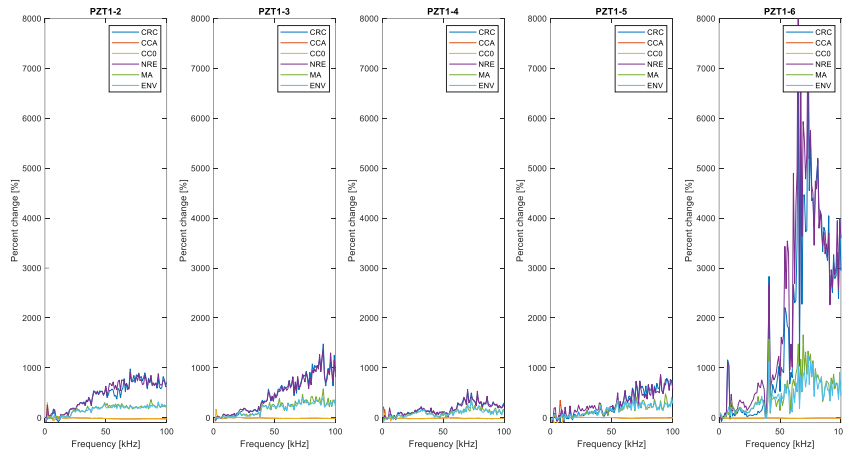


Leaf Spring BEND0-BEND0-APPEND NRE, MA, ENV:



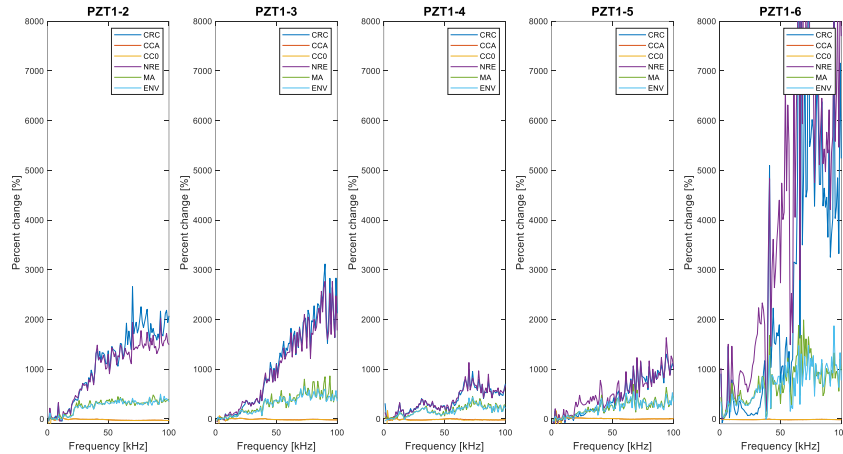
Leaf Spring Percentage Variation of Damage Index of BEND2 to BEND0
 respect to Damage Index of BEND1 to BEND0 for each PZT couple:

LEAF SPRING CFRP Specimen 1 As it is
 (BEND0-BEND1-BEND2)



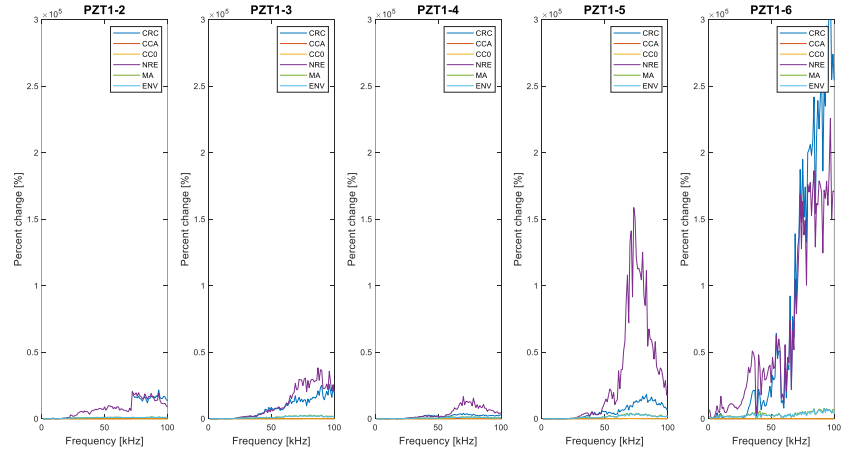
Leaf Spring Percentage Variation of Damage Index of BEND3 to BEND0
 respect to Damage Index of BEND1 to BEND0 for each PZT couple:

LEAF SPRING CFRP Specimen 1 As it is
 (BEND0-BEND1-BEND3)

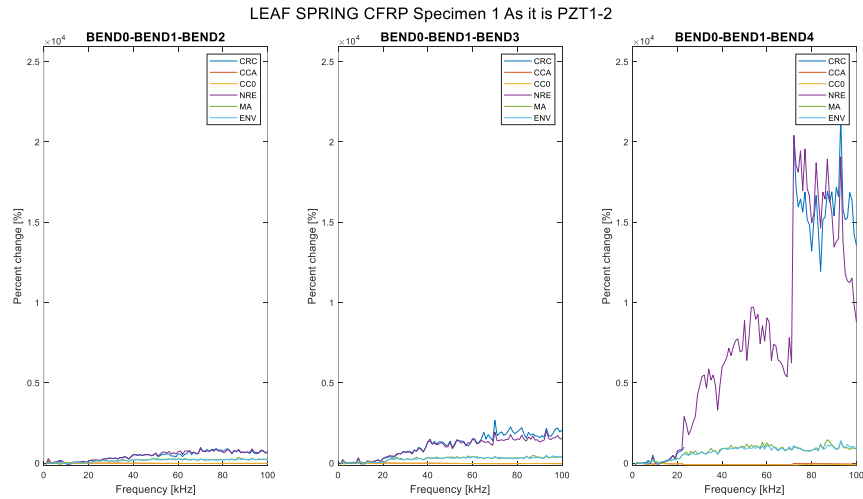


Leaf Spring Percentage Variation of Damage Index of BEND4 to BEND0
 respect to Damage Index of BEND1 to BEND0 for each PZT couple:

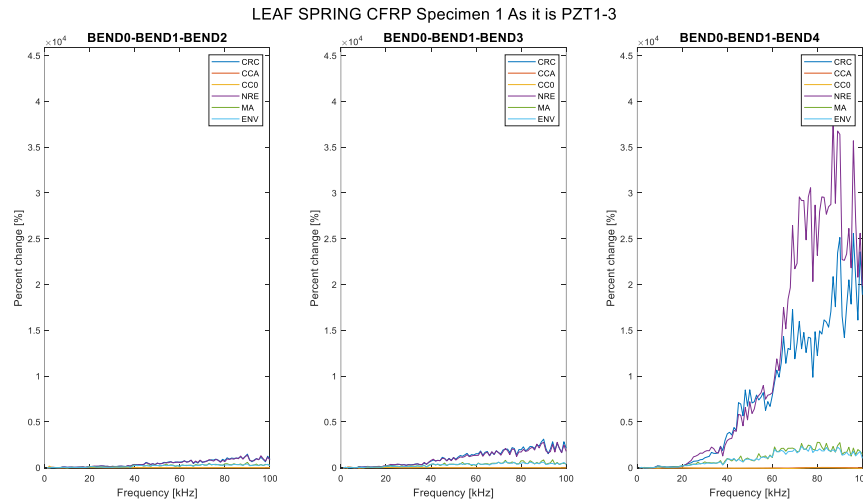
LEAF SPRING CFRP Specimen 1 As it is
 (BEND0-BEND1-BEND4)



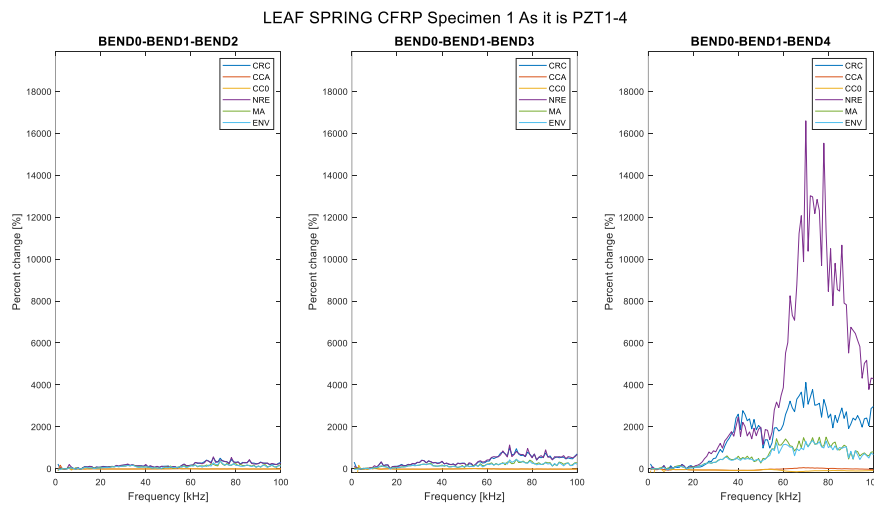
Leaf Spring Percentage Variation of Damage Index of BEND2, BEND3, BEND4 to BEND0 respect to Damage Index of BEND1 to BEND0 for PZT 1-2:



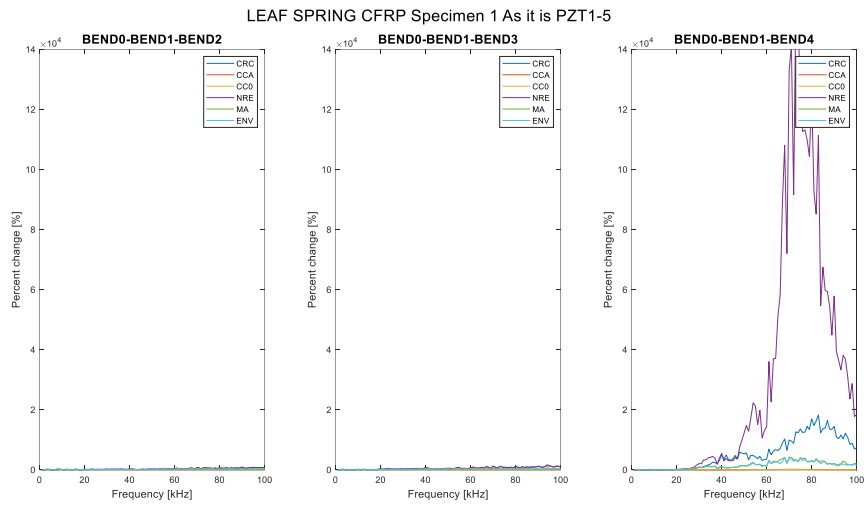
Leaf Spring Percentage Variation of Damage Index of BEND2, BEND3, BEND4 to BEND0 respect to Damage Index of BEND1 to BEND0 for PZT 1-3:



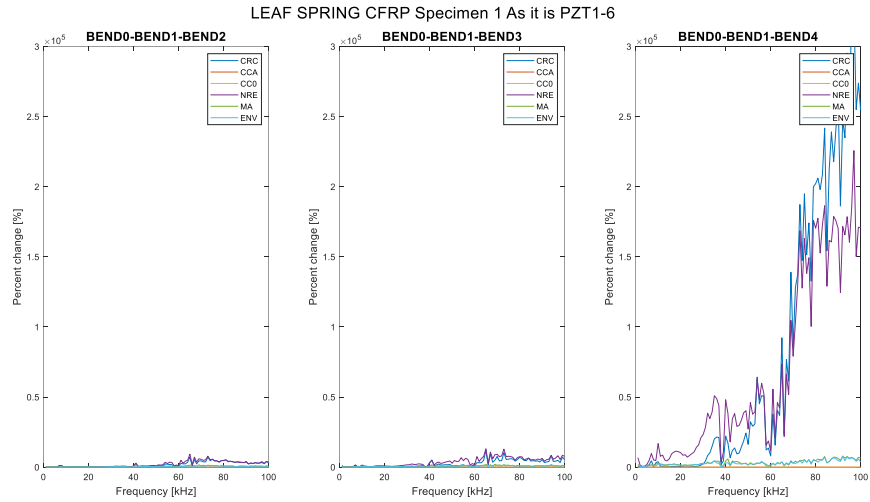
Leaf Spring Percentage Variation of Damage Index of BEND2, BEND3, BEND4 to BEND0 respect to Damage Index of BEND1 to BEND0 for PZT 1-4:



Leaf Spring Percentage Variation of Damage Index of BEND2, BEND3, BEND4 to BEND0 respect to Damage Index of BEND1 to BEND0 for PZT 1-5:



Leaf Spring Percentage Variation of Damage Index of BEND2, BEND3, BEND4 to BEND0 respect to Damage Index of BEND1 to BEND0 for PZT 1-6:



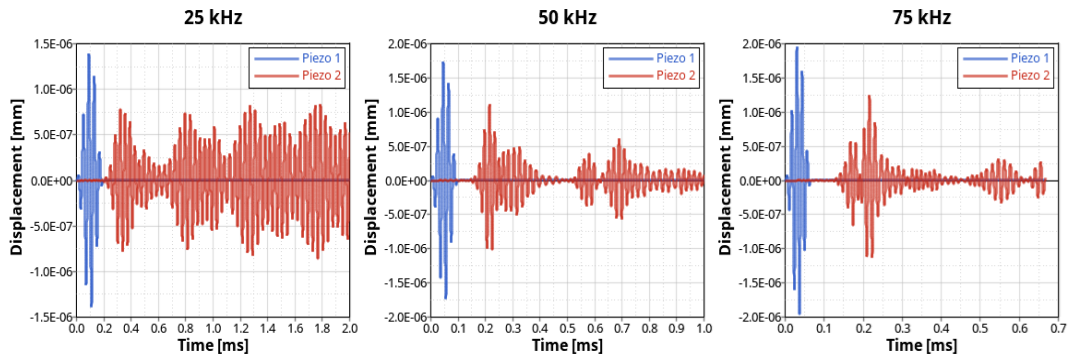
Appendix B

SHM Virtual Results & Correlation

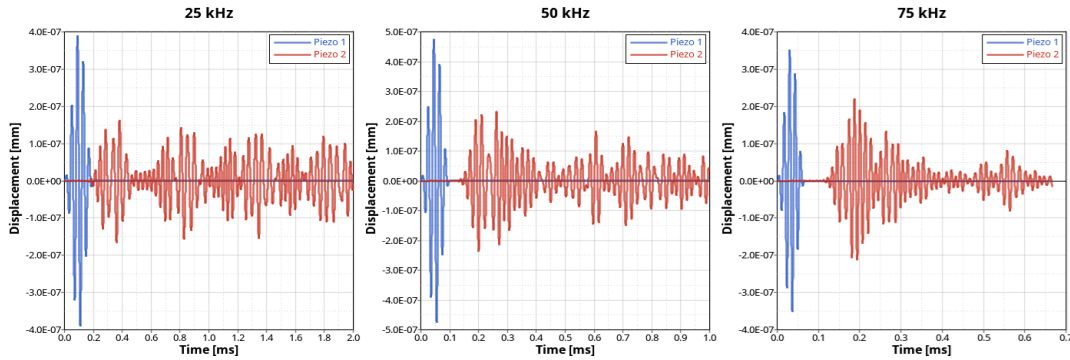
Beam Specimen

Beam Virtual Results

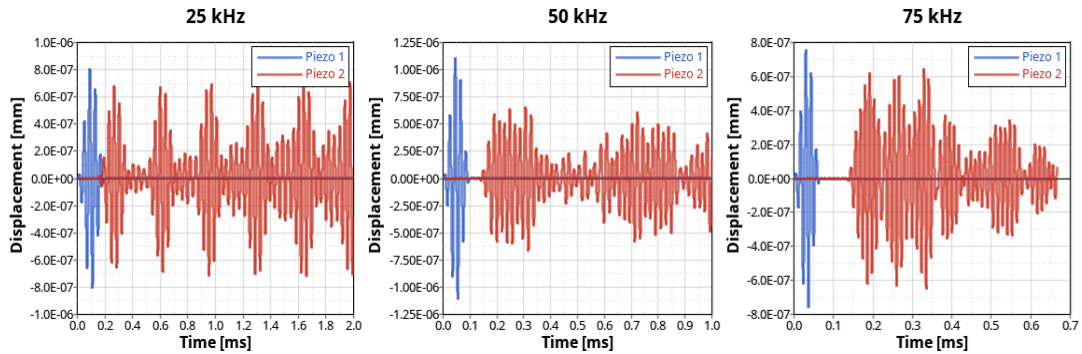
Aluminum



Steel

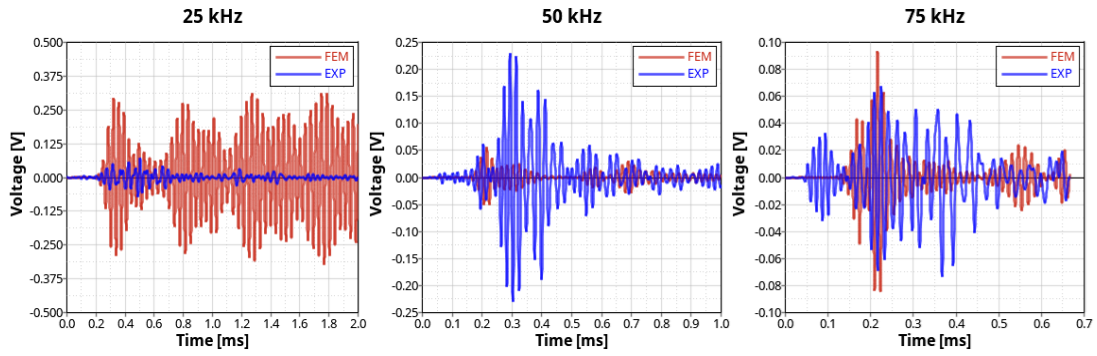


Composite

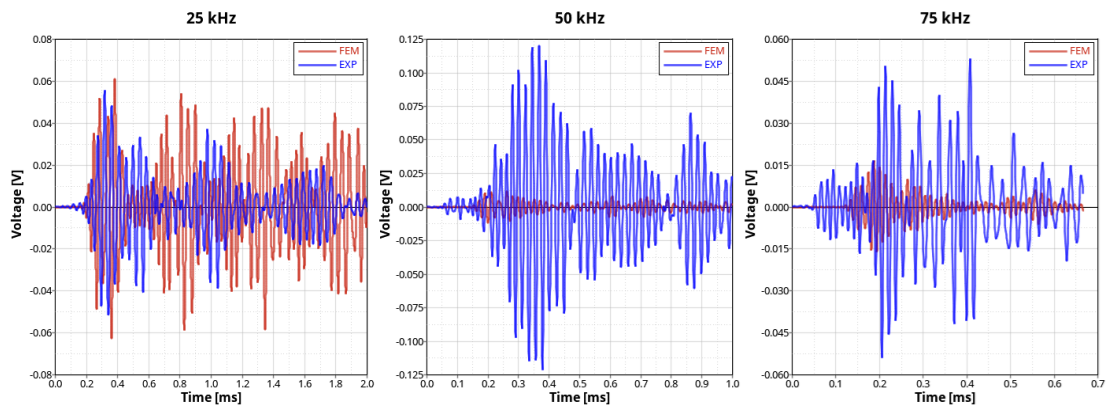


Beam Correlation

Aluminum



Steel



Composite

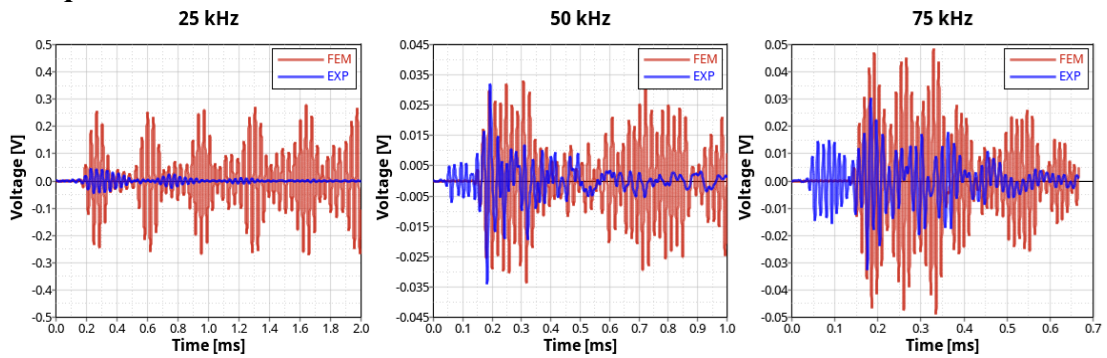
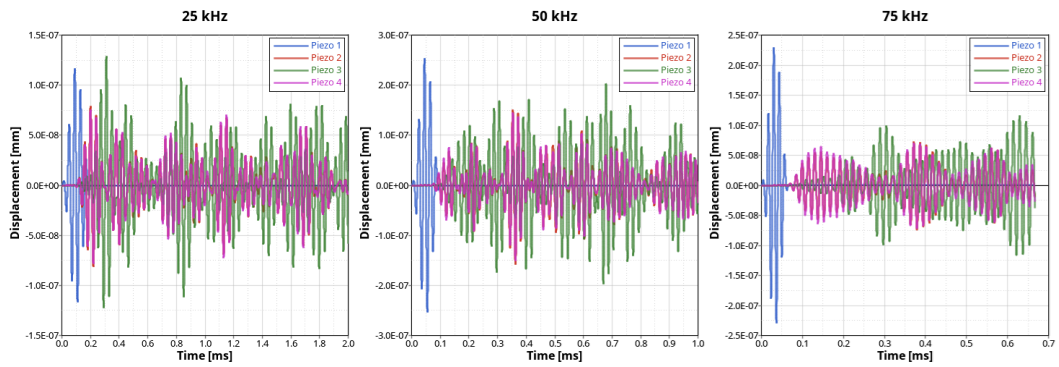


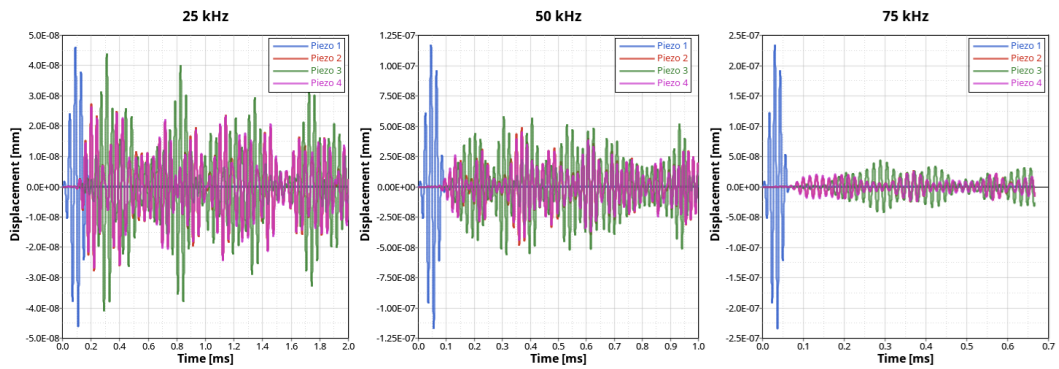
Plate Specimen

Plate Virtual Results

Aluminum



Steel



Composite

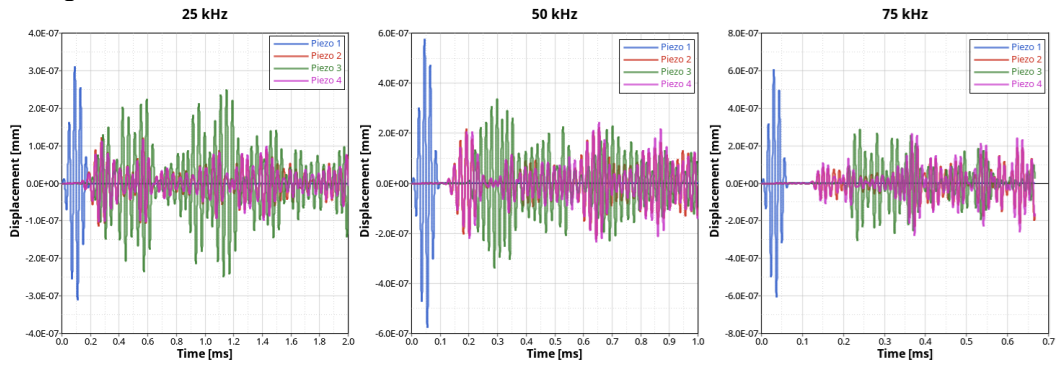
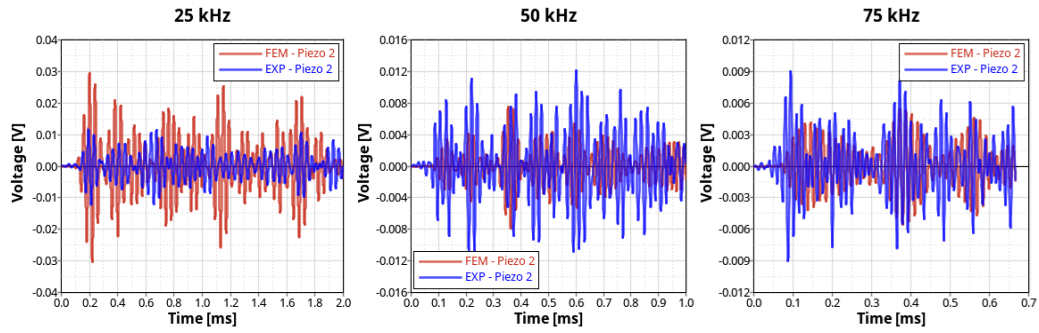
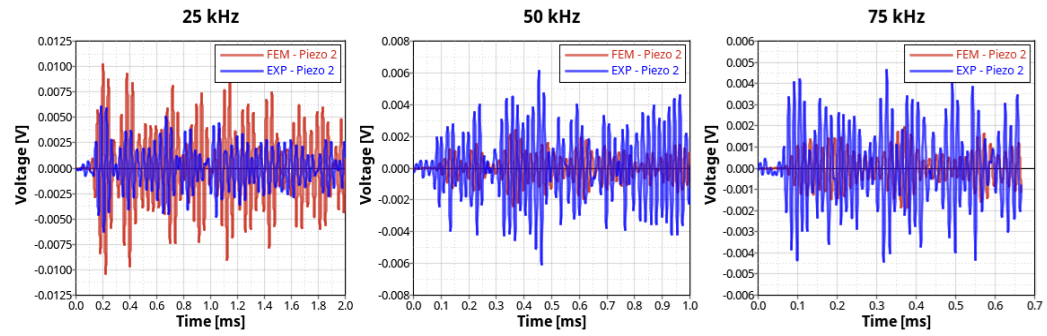


Plate Correlation

Aluminum



Steel



Composite

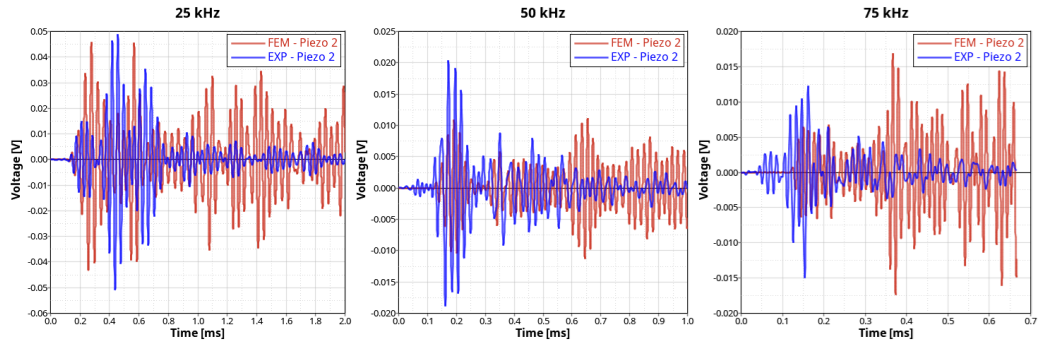
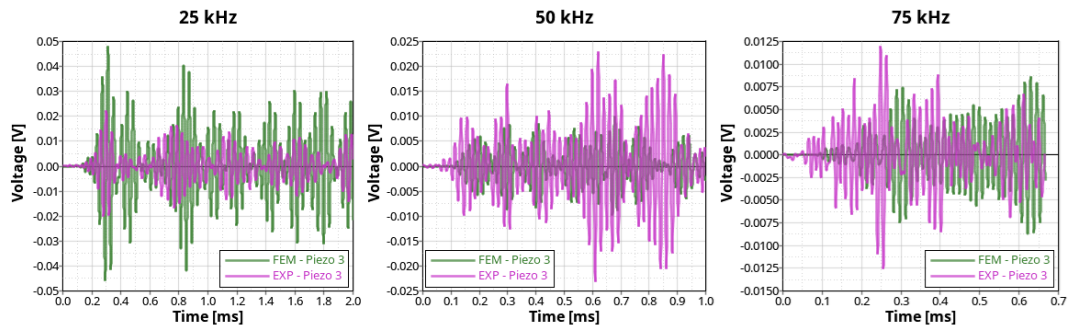
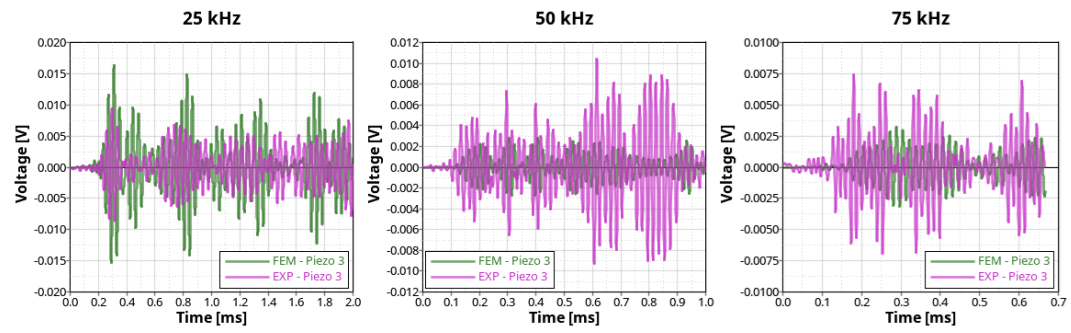


Plate Correlation

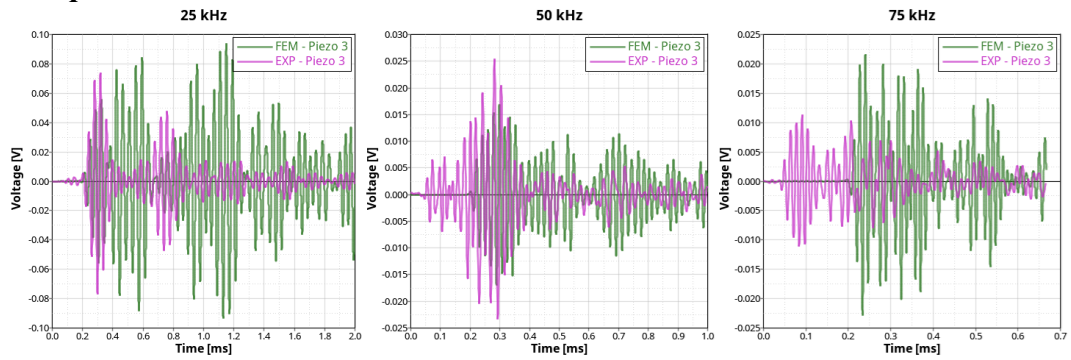
Aluminum



Steel



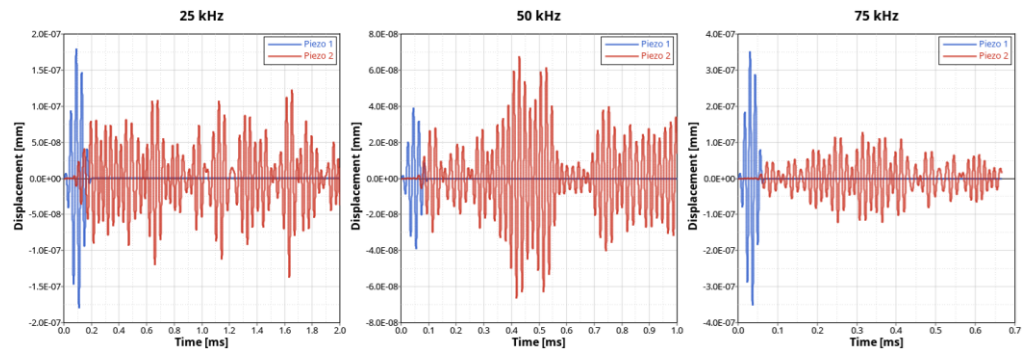
Composite



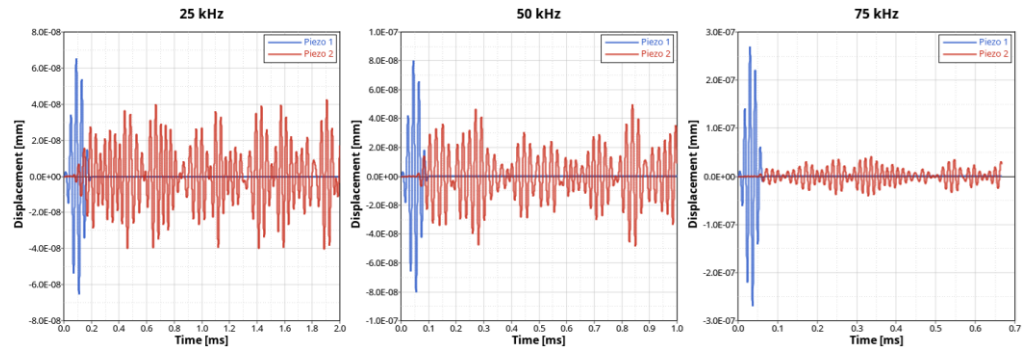
Simulacrum Specimen

Simulacrum Virtual Results

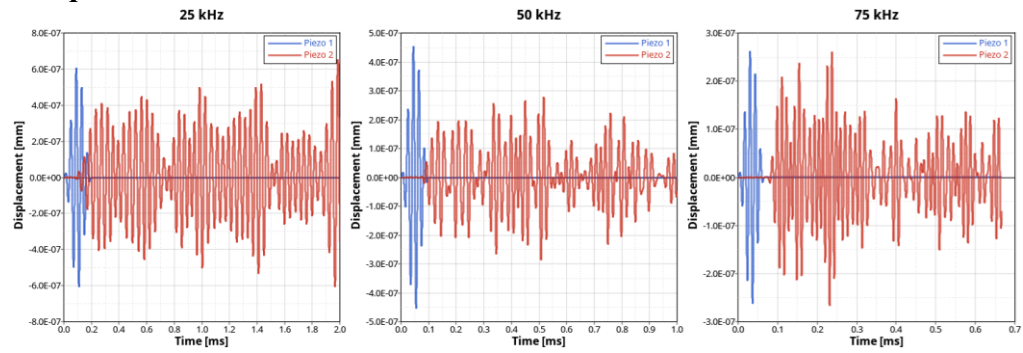
Aluminum



Steel

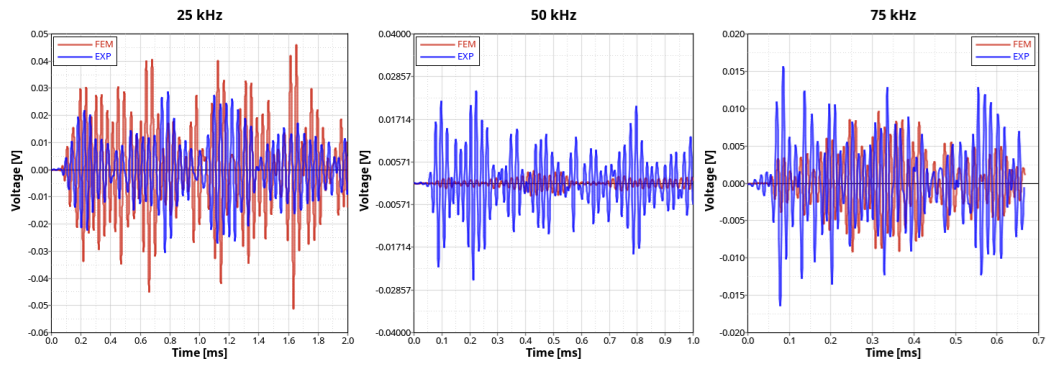


Composite

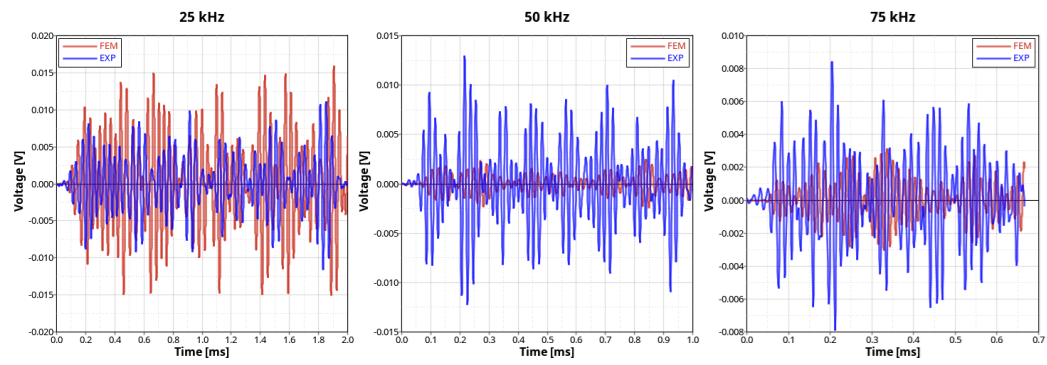


Simulacrum Correlation

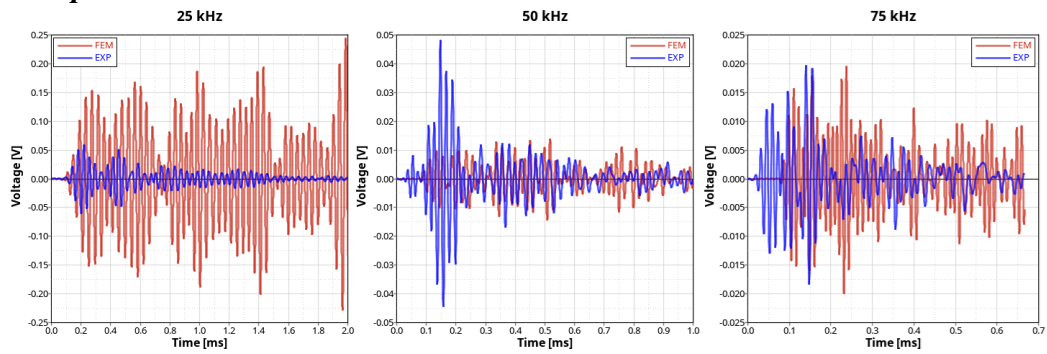
Aluminum



Steel

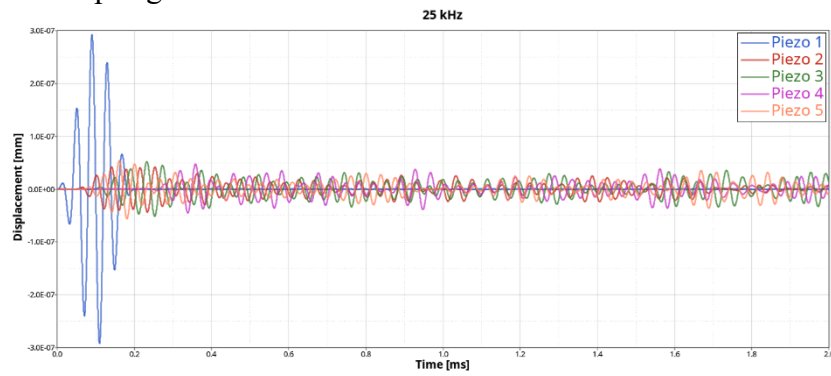


Composite

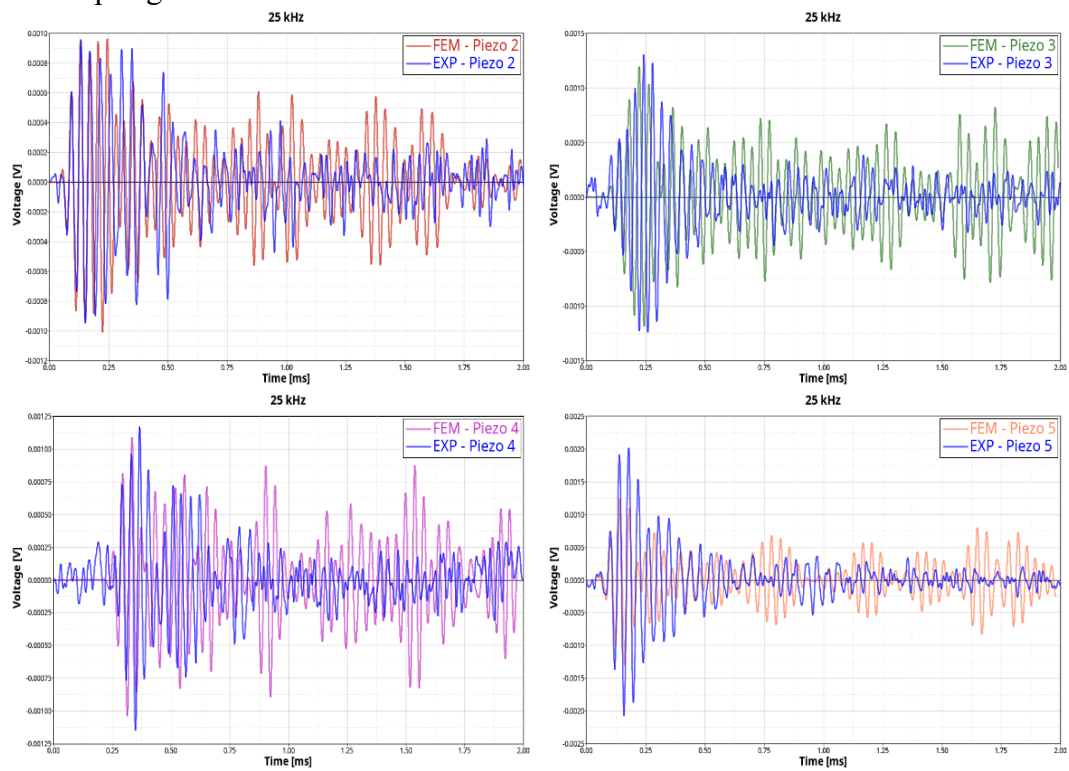


Leaf Spring Component

Leaf Spring Virtual Results



Leaf Spring Correlation



Own Publications

1. Carello, M., Ferraris, A., Airale, A.G., Messana, A., **Sisca, L.**, de Carvalho Pinheiro, H., Reitano, S., 2020. *Experimental Characterization of Piezoelectric Transducers for Automotive Composite Structural Health Monitoring*. Presented at the WCX SAE World Congress Experience. <https://doi.org/10.4271/2020-01-0609>
2. **Sisca, L.**, Messana, A., de Carvalho Pinheiro, H., Ferraris, A., Airale, A.G., Carello, M., 2021. *Validation of a Numerical-Experimental Methodology for Structural Health Monitoring on Automotive Components*. Presented at the ASME 2021 Conference on Smart Materials, Adaptive Structures and Intelligent Systems SMASIS2021. (*submitted and waiting for revision*)
3. Messana, A., **Sisca, L.**, de Carvalho Pinheiro, H., Berti Polato, D., Ferraris, A., Airale, A.G., Carello, M., 2021. *Feasibility Study on Piezoelectric Actuated Automotive Morphing Wing*. Presented at the ASME 2021 Conference on Smart Materials, Adaptive Structures and Intelligent Systems SMASIS2021. (*submitted and waiting for revision*)
4. Carello, M., Airale, A. G., Ferraris, A., Messana, A., **Sisca, L.**, 2017. *Static Design and Finite Element Analysis of Innovative CFRP Transverse Leaf Spring*. Applied Composite Materials 24(6). <https://doi.org/10.1007/s10443-017-9596-6>
5. **Sisca, L.**, Airale, A., Massai, P., Xu, S., Ferraris, A., 2017. *Function integration concept design applied on CFRP cross leaf spring suspension*. International Journal of Automotive Composites 3, 276. <https://doi.org/10.1504/IJAUTO.2017.10012546>
6. **Sisca, L.**, Locatelli Quacchia, P.T., Messana, A., Airale, A.G., Ferraris, A., Carello, M., Monti, M., Palenzona, M., Romeo, A., Liebold, C., Scalera, S., Festa, A., Codrino, P., 2020. *Validation of a Simulation Methodology for Thermoplastic and Thermosetting Composite materials considering the effect of Forming process on the Structural performance*. MDPI, Special Issue Polymers, 12(12), 2801. <https://doi.org/10.3390/polym12122801>
7. Carello, M., Airale, A. G., Ferraris, A., **Sisca, L.**, Messana, A., Amirth Jayasree, N., 2017. *Process analysis for structural optimisation of thermoplastic composite component using the building block approach*. Composites Part B: Engineering 126, pp. 119–132. <https://doi.org/10.1016/j.compositesb.2017.06.007>
8. Amirth Jayasree, N., Airale, A.G., Ferraris, A., Messana, A., **Sisca, L.**, Monti, M., Romeo, A., Carello, M., 2018. *Complete material characterisation of thermoplastic composite laminate at forming state*. Presented at the International Symposium on Dynamic Response and Failure of Composite Materials, Ischia, Naples, Italy.
9. Messana, A., **Sisca, L.**, Ferraris, A., Airale, A.G., Carello, M., 2020. *Lightweight Design of a Multi-Material Suspension Lower Control Arm*.

- Presented at the Proceedings of the ASME IDETC/CIE 2020, Virtual, Online. <https://doi.org/10.1115/DETC2020-22323>
10. Sangermano, M., Antonazzo, I., **Sisca, L.**, Carello, M., 2019. *Photoinduced cationic frontal polymerization of epoxy–carbon fibre composites*. Polymer International 0. <https://doi.org/10.1002/pi.5875>
 11. Messana, A., Airale, A. G., Ferraris, A., **Sisca, L.**, Carello, M., 2017. *Correlation between thermo-mechanical properties and chemical composition of aged thermoplastic and thermosetting fiber reinforced plastic materials: Korrelation zwischen thermomechanischen Eigenschaften und chemischer Zusammensetzung von gealterten thermo- und duroplastischen faserverstärkten Kunst.* Materialwissenschaft und Werkstofftechnik 48(5). <https://doi.org/10.1002/mawe.201700024>
 12. Virgillito, E., Airale, A.G., Ferraris, A., **Sisca, L.**, Carello, M., 2019. *Specific Energy Absorption Evaluation on GFRP Laminate Plate by Optical, Thermographic and Tomographic Analysis*. Exp Tech 43, 15–24. <https://doi.org/10.1007/s40799-018-0257-y>
 13. Ferraris, A., Messana, A., **Sisca, L.**, Santoro, F., Airale, A.G., Carello, M., 2019. *Statistical Energy Analysis SEA: A Correlation Between Virtual and Experimental Results*, in: Carbone, G., Gasparetto, A. (Eds.), Advances in Italian Mechanism Science. Springer International Publishing, Cham, pp. 211–220. https://doi.org/10.1007/978-3-030-03320-0_23
 14. Messana, A., **Sisca, L.**, Ferraris, A., Airale, A.G., de Carvalho Pinheiro, H., Sanfilippo, P., Carello, M., 2019. *From Design to Manufacture of a Carbon Fiber Monocoque for a Three-Wheeler Vehicle Prototype*. Materials 12, 332. <https://doi.org/10.3390/ma12030332>
 15. Messana, A., **Sisca, L.**, Getti, C., Malvindi, A., Ferraris, A., Airale, A., Carello, M., 2019. *Design, Optimization and Manufacturing of an Aluminum Wheel Rim for the IDRakronos Vehicle Prototype*. Computer-Aided Design and Applications 16, 733–741. <https://doi.org/10.14733/cadaps.2019.733-741>
 16. Messana, A., **Sisca, L.**, Getti, C.M., Malvindi, A., Ferraris, A., Airale, A.G., Carello, M., 2018. *Design, Optimization and Production of Aluminum Alloy Rim for the Vehicle Prototype IDRakronos*. Presented at the Proceedings of CAD'18, Paris, France, pp. 112–116. <https://doi.org/10.14733/cadconfP.2018.112-116>
 17. de Carvalho Pinheiro, H., Russo, F., **Sisca, L.**, Messana, A., De Cupis, D., Ferraris, A., Airale, A.G., Carello, M., 2020. *Advanced Vehicle Dynamics through Active Aerodynamics and Active Body Control*. Presented at the Proceedings of the ASME IDETC/CIE 2020, Virtual, Online. <https://doi.org/10.1115/DETC2020-22290>
 18. de Carvalho Pinheiro, H., Castro dos Santos, P.G., **Sisca, L.**, Scavuzzo, S., Ferraris, A., Airale, A.G., Carello, M., 2020. *Dynamic Performance Comparison between In-Wheel and On-Board Motor Battery Electric Vehicles*. Presented at the Proceedings of the ASME IDETC/CIE 2020, Virtual, Online. <https://doi.org/10.1115/DETC2020-22306>
 19. de Carvalho Pinheiro, H., Russo, F., **Sisca, L.**, Messana, A., De Cupis, D., Ferraris, A., Airale, A.G., Carello, M., 2020. *Active Aerodynamics through Active Body Control: Modelling and Static Simulator Validation*. Presented at the Proceedings of the ASME IDETC/CIE 2020, Virtual, Online. <https://doi.org/10.1115/DETC2020-22298>

20. Carello, M., Bertipaglia, A., Messina, A., Airale, A.G., **Sisca, L.**, 2019. *Modeling and Optimization of the Consumption of a Three-Wheeled Vehicle*. Presented at the WCX SAE World Congress Experience. <https://doi.org/10.4271/2019-01-0164>
21. de Carvalho Pinheiro, H., Ferraris, A., Galanzino, E., **Sisca, L.**, Carello, M., Airale, A., Messina, A., 2019. *All-wheel drive electric vehicle modeling and performance optimization*. SAE TECHNICAL PAPER SERIES. <https://doi.org/10.4271/2019-36-0197>
22. de Carvalho Pinheiro, H., Messina, A., **Sisca, L.**, Ferraris, A., Airale, A.G., Carello, M., 2019. *Torque Vectoring in Electric Vehicles with In-wheel Motors*, in: Uhl, T. (Ed.), *Advances in Mechanism and Machine Science, Mechanisms and Machine Science*. Springer International Publishing, pp. 3127–3136. https://doi.org/10.1007/978-3-030-20131-9_308
23. de Carvalho Pinheiro, H., Messina, A., **Sisca, L.**, Ferraris, A., Airale, A.G., Carello, M., 2019. *Computational Analysis of Body Stiffness Influence on the Dynamics of Light Commercial Vehicles*, in: Uhl, T. (Ed.), *Advances in Mechanism and Machine Science, Mechanisms and Machine Science*. Springer International Publishing, pp. 3117–3126. https://doi.org/10.1007/978-3-030-20131-9_307
24. Ferraris, A., Messina, A., Airale, A.G., **Sisca, L.**, de Carvalho Pinheiro, H., Zevola, F., Carello, M., 2019. *Nafion® Tubing Humidification System for Polymer Electrolyte Membrane Fuel Cells*. *Energies* 12, 1773. <https://doi.org/10.3390/en12091773>
25. Ferraris, A., Messina, A., Multari, D., **Sisca, L.**, Airale, A.G., Carello, M., 2019. *Steering System of a Low-Consumption Vehicle: From the Dynamics Analysis to the Design of the Wheel Assembly*, in: Carbone, G., Gasparetto, A. (Eds.), *Advances in Italian Mechanism Science*. Springer International Publishing, Cham, pp. 91–99. https://doi.org/10.1007/978-3-030-03320-0_10
26. Ferraris, A., De Cupis, D., de Carvalho Pinheiro, H., Messina, A., **Sisca, L.**, Airale, A.G., Carello, M., 2020. *Integrated Design and Control of Active Aerodynamic Features for High Performance Electric Vehicles*. SAE TECHNICAL PAPER SERIES. <https://doi.org/10.4271/2020-36-0079>
27. **Sisca, L.**, Virgillito, E., Ferraris, A., Airale, A.G., Carello, M., 2020. *Influence of Freeze-Thaw Aging on the Impact Performance of Damped CFRP Materials for Automotive applications*. *Journal of Sandwich Structures and Materials*, SAGE Publications. (*submitted and waiting for revision*)

Curriculum Vitae

Name: Lorenzo Sisca

Date of Birth: July 4, 1992

Nationality: Italian

Address: Via Domenico Giraudo, 8 – 12100 Cuneo, Italy

Email: lorenzo.sisca@polito.it

- - -

Doctor of Philosophy (Ph.D.) - Mechanical Engineering 11/2017 – 05/2021

Politecnico di Torino

thesis “*Structural Health Monitoring based on Piezoelectric transducers: a Carbon Fiber Automotive Component Application case*”

Supervisor Carello M.

Master’s Degree - Materials Engineering

09/2014 – 07/2017

Politecnico di Torino

thesis “*Study on a Two-Component Epoxy Resin reinforced with Carbon Fibers for Automotive Applications*”

Supervisor Carello M., Sangermano M.

Bachelor’s Degree - Materials Engineering

09/2011 – 03/2015

Politecnico di Torino

thesis “*Injection Moulding of Thermoplastic Polymers*”

Supervisor Sangermano M.

High School Diploma - Chemical Laboratory Technician 09/2006 – 06/2011

Istituto Tecnico Industriale Statale “Mario Delpozzo” di Cuneo

thesis “*The Energy and the Organic Photovoltaic*”

Supervisor Voerzio S.